Development and Implementation of a Redundant Process Control Strategy in Pharmaceutical Continuous Manufacturing

Inaugural-Dissertation

zur Erlangung des Doktorgrades
der Mathematisch-Naturwissenschaftlichen Fakultät
der Heinrich-Heine-Universität Düsseldorf

vorgelegt von

Victoria Isabell Pauli

aus Leipzig

Düsseldorf, Juli 2019

aus dem Institut für Pharmazeutische Technologie und Biopharmazie
der Heinrich-Heine-Universität Düsseldorf

Gedruckt mit der Genehmigung der
Mathematisch-Naturwissenschaftlichen Fakultät der
Heinrich-Heine-Universität Düsseldorf

Berichterstatter:

1. Prof. Dr. Dr.h.c. Peter Kleinebudde, HHU Düsseldorf

2. Prof. Dr. Jörg Breitkreutz, HHU Düsseldorf

3. Prof. Dr. Karl Wagner, Uni Bonn

Tag der mündlichen Prüfung: 01. Juli 2019

I am among those who think that science has great beauty

- Marie Curie -

Table of contents

List of publications

1. *Methodology for a Variable Rate Control Strategy Development in Continuous Manufacturing Applied to Twin-Screw Wet-Granulation and Continuous Fluid-Bed Drying.*
   V. Pauli, F. Elbaz, P. Kleinebudde, M. Krumme.
   Journal of Pharmaceutical Innovation. Volume 13 (2018), pp: 247-260.
   DOI: 10.1007/s12247-018-9320-6
   Personal contribution: 60 %
   VP planned and performed all related trials. She completed and the majority of the subsequent data analysis, wrote the main body of the manuscript independently, and illustrated all graphs and figures. She contributed to the idea and design of the project.

2. *Real-Time Monitoring of Particle Size Distribution in a Continuous Granulation and Drying Process by Near Infrared Spectroscopy*.
   Victoria Pauli, Yves Roggo, Peter Kleinebudde, Markus Krumme.
   European Journal of Pharmaceutics and Biopharmaceutics. Volume 141 (2019), pp: 90-99.
   DOI: 10.1016/j.ejpb.2019.05.007
   Personal contribution: 90 %
   VP planned and performed all related trials. She completed the majority of the data analysis, illustrated all graphs and figures, and wrote the main body of the manuscript independently. She had the idea for the publication and contributed to the study design.

3. *Process Analytical Technology for Continuous Manufacturing Tableting Processing: A Case Study*
   Victoria Pauli, Yves Roggo, Laurent Pellegatti, Nhat Quang Nguyen Trung, Frantz Elbaz, Simon Ensslin, Peter Kleinebudde, Markus Krumme.
   Journal of Pharmaceutical and Biomedical Analysis. Volume 162 (2019), pp: 101-111.
   DOI: 10.1016/j.jpba.2018.09.016
   Personal contribution: 40 %
   VP and YR contributed equally as first authors to the published manuscript. VP planned and performed the majority of all related trials and wrote most of the main body of the manuscript. She contributed more than a third to the idea, the study design, and the data evaluation each.

4. *Orthogonal Redundant Monitoring of a New Continuous Fluid-Bed Dryer for Pharmaceutical Processing by Means of Mass and Energy Balance Calculations and Spectroscopic Techniques.*
   V. Pauli, F. Elbaz, M. Krumme, P. Kleinebudde.
   Journal of Pharmaceutical Sciences. Volume 108 (2019), pp: 2041-2055.
   DOI: 10.1016/j.xphs.2018.12.028
   Personal contribution: 60 %
   VP planned and performed almost all related trials. She completed the majority of the data analysis, illustrated all graphs and figures, and wrote the main body of the manuscript independently. She contributed to the idea for the publication and was responsible for the majority of the study design.

5. Manuscript in preparation: *From-powder-to-tablets: investigation of material residence time distributions in a continuous manufacturing process line for control strategy development*.
   V. Pauli, M. Krumme, P. Kleinebudde.
   Anticipated Journal: European Journal of Pharmaceutics and Biopharmaceutics.
   Personal contribution: to be defined
   VP planned and performed almost all related trials. She completed the majority of the data analysis and illustrated all graphs and figures, up to this date. She contributed to the idea for the publication and to the study design.

6. Manuscript in preparation: *Pharma manufacturing of the future: fully automated, PAT-based DoE process development in an integrated GMP-qualified continuous manufacturing process plant.*
   V. Pauli, M. Krumme, P. Kleinebudde.
   Anticipated Journal: International Journal of Pharmaceutics.
   Personal contribution: to be defined
   VP planned and performed almost all related trials. She completed the majority of the data analysis and illustrated all graphs and figures, up to this date. She contributed to the study design and the functional design of the developed software tool that enables automated process development.

7. Manuscript in preparation: *Predictive model-based process ramp-up in pharmaceutical continuous manufacturing to achieve state-of-control production from the start.*
   V. Pauli, M. Krumme, P. Kleinebudde.
   Anticipated Journal: Pharmaceutical Science and Technology Today
   Personal contribution: to be defined
   VP planned and performed almost all related trials, to generate predictive process models and to demonstrate their applicability during process ramp-up. She completed the majority of the data analysis and illustrated all graphs and figures, up to this date. She contributed to the study design and the functional design of the developed software tool required for the experiments.

Conference contribution

1. *Application of CUSUM-Quality Control Charts in Pharmaceutical Continuous Manufacturing* - oral presentation -
   V. Pauli, F. Elbaz, S. Ensslin, P. Kleinebudde, M. Krumme.
   PBP Word Meeting, Granada, Spain. March 21st, 2018.
   Personal contribution: 90 %
   VP planned and performed all related trials and data analysis, had the idea for the presentation, and prepared more than ninety percent of the submitted abstract as well as the presentation slides.

List of Abbreviations

API	active pharmaceutical ingredient
BT	barrel temperature
BU	blend uniformity
CCP	commercializing continuous processing summit
CFR	code of federal regulation
cGMP	current good manufacturing practices
CM	continuous manufacturing
CMA	critical material attribute
CMAC	United Kingdom Centre for Continuous Manufacturing and Crystallization
COST	changing one factor setting at a time
CPP	critical process parameter
CQA	critical quality attribute
CS	compression speed
CU	content uniformity
DAV	drying air-flow
DIA	dynamic image analysis
DoE	design of experiment
DP	drug product
DRS	dryer rotation speed
DS	drug substance
DT	drying temperature
EMA	European Medicines Agency
EPT	event propagation time
EWMA	exponentially weighted moving average
FBD	continuous fluid-bed drying
FBRM	focused beam reflecetance measurement
FDA	US Food and Drug Administration
FMEA	failure mode effect analysis
FTA	fault tree analysis
GMP	good manufacturing practices
HAZOP	hazard operability analysis
HIV	human immunodeficiency virus
HPLC	high pressure liquid chromatography
HPMC	hydroxypropyl methylcellulose
i	intermediate
ICA	independent component analysis
IPC	in-process control (reference analysis)
ISPE	International Society for Pharmaceutical Engineering
KF	karl fischer titration
LC	label claim
LD	laser diffraction
LFR	liquid feed rate

LOD	loss-on-drying
MCC	microcrystalline cellulose
MEB	mass and energy balance
MR	microwave resonance technology
MRT	mean residence time
MSPC	multivariate statistical process control
nCPP	not critical process parameter
NIRS	near infrared spectroscopy
NME	new molecular entity
OOS	out-of-specification
PAT	process analytical technology
PC(A)	principal component (analysis)
pCMA	potentially critical material attribute
pCPP	potentially critical process parameter
PLSR	partial least squares regression
PMDA	Japanese Pharmaceuticals and Medical Devices Agency
PP	process parameter
PRL	prediction error to laboratory error
PSD	particle size distribution
PTS	powder transfer system
PVP	polyvinylpyrrolidon
QbD	quality by design
QTPP	quality target product profile
R&D	research and development
RER	range error ratio
RMSECV	root mean square error of cross validation
RMSEP	root mean square error of prediction
RPD	ratio of prediction to deviation
RTD	residence time distribution
RTRT	real time release testing
SFR	solid feed rate
SNV	single number variance
SP	setpoint
SS	granulator screw speed
SWM	single wavelength monitoring
T_{EX}	exhaust temperature
TSG	twin-screw wet-granulation
$X_{IN/OUT}$	specific humidity in inlet/outlet air (= mixing ratio in g/kg)

1. Introduction

1.1. Continuous manufacturing: changing a traditional mindset[1]

For the past decades, the vast majority of pharmaceutical drug products have been manufactured by batch processing, a method where all starting materials are charged into the equipment at the beginning of a process and the product is discharged once the process is completed. Sequential unit operations are performed one after the other and the size of the used equipment limits the batch-size. Typically, each step follows an empirically determined recipe and quality is tested by off-line analysis. Batches of material that do not meet their pre-defined quality expectations, for instance caused by unexpected variations in starting material characteristics or process conditions, are discarded or reworked [1, 2]. Production and product release can last for several weeks to months, due to long equipment lag times between different batches and unit operations, global outsourcing of individual process steps and intermediate analyses, as well as extensive post-production release-testing. As a result, supply-chains in batch production are complex and asset utilization is often inefficient [3, 4].

In contrast, continuous manufacturing (CM) is a rather new advancement in the pharmaceutical industry with the potential to increase flexibility, agility, efficiency, and safety of pharmaceutical manufacturing processes. In CM, all process units are directly connected to each other; starting materials are charged at the beginning of the line while final product is simultaneously discharged at the end (*first-in-first-out principle*). Transportation and hence "dead-time" between process steps is eliminated, waste production, manual handling hazards, and environmental impact are reduced. Batch size is determined by throughput and run-time, thus equipment can be significantly smaller, especially for commercial productions. It enables process intensification with harsher and better controlled conditions, if required. The implementation of process analytical technologies (PAT) in the widest sense, allow real-time monitoring of the product and process. PAT and other sensors enable implementation of control loops which allow the manipulation of process parameters dynamically in response to the current process and ingoing material conditions, rather than following a fixed recipe. Material that does not meet its specifications at the outlet can be precisely diverted from the line, eliminating the risk of pockets of defect product making it into the collected batch or even complete batch-failure. It also makes the process amenable for real-time release testing approaches. Therefore, CM facilitates the production of quality drugs by process design rather than by repeated analysis of samples of the final product; a principle also referred to as quality-by-design (QbD) in contrast to quality-by-testing (QbT). Also, since equipment scale-up between early-phase, late-phase, and commercial manufacturing is not necessary, product- and process development in CM can be done with significantly smaller amounts of material in less time [2, 4-9].

Despite of its apparent benefits, the adaption of CM by the pharmaceutical industry has been much slower than expected due to numerous risks and challenges like regulatory uncertainties and anticipated high capital investments. The following sections reflect on economic considerations, expected benefits and potential risk, the authorities' point of view, as well as the

[1] Parts of this section have been previously published in Publication 1 (see page v)

current market situation. Furthermore, available equipments and methods for production and process analysis will be introduced.

In general, the concept of CM can be applied to any pharmaceutical production process (e.g. semi-solids, injectables, capsules, etc.). Nevertheless, the following introductory chapters are focused on downstream continuous manufacturing of tablets, as other pharmaceutical CM processes are not relevant to this thesis. Figure 1 illustrates a conceptual overview of a typical continuous manufacturing process of tablets, compared to a traditional downstream batch manufacturing process.

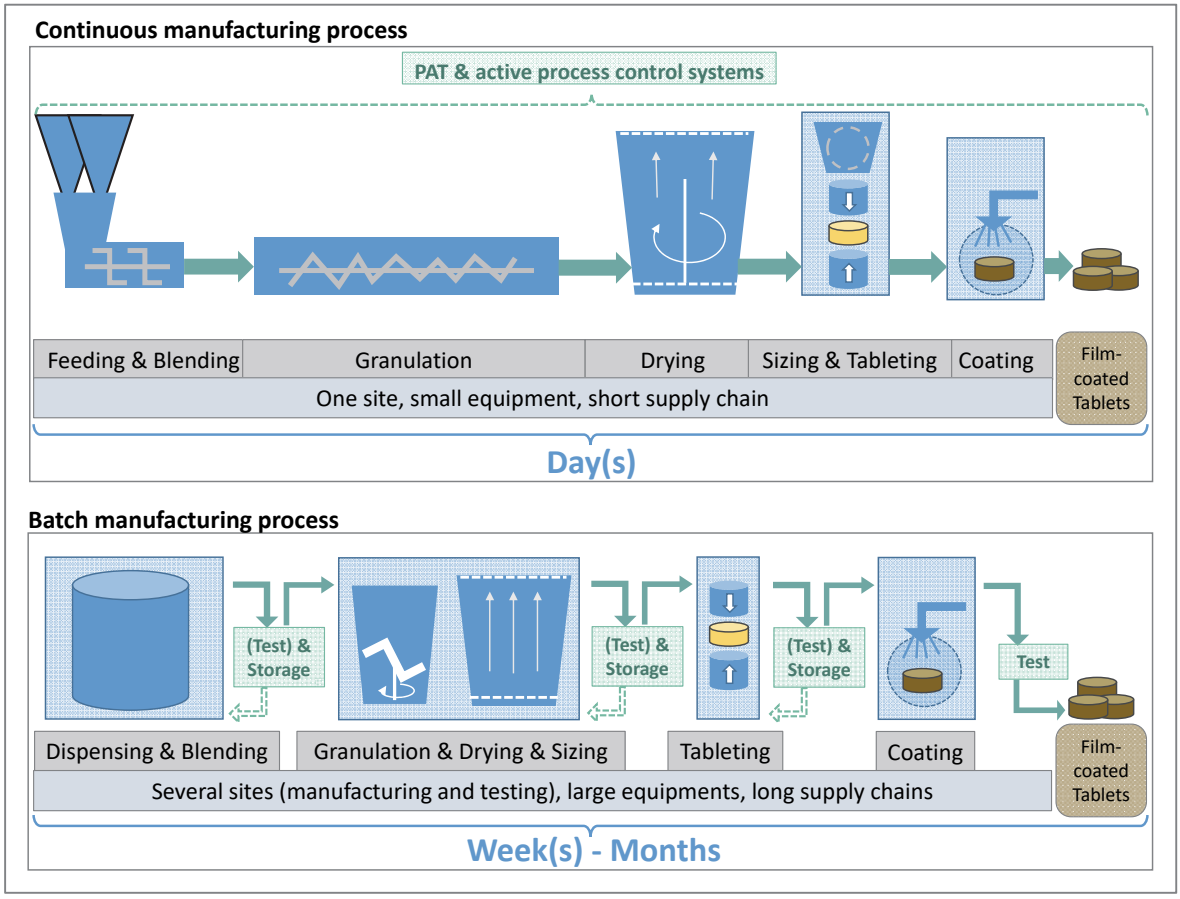

Figure 1: Conceptual overview of a typical downstream continuous manufacturing process (CM) and a typical batch manufacturing process. In CM, process units are connected to form an integrated manufacturing process. Process Analytical Technology (PAT) systems can be utilized to provide real-time data for process control. In batch manufacturing, materials from one step are usually tested offline after the process step is finished. If quality is not met, the material is discarded or reprocessed, prior to the following step (Figure adapted from [2] and [10]).

1.2. Economic considerations and expected benefits

The pharmaceutical industry's combined annual spending on research and development (R&D) efforts has increased at an average compounded rate of 12.3 % in the past half century, while the total amount of United States Food and Drug Administration (FDA)-approved new molecular entities (NMEs) has remained fairly constant at around 20 NMEs per year. The main reasons for escalating R&D costs were the industry's shifting focus to increasingly complex and rare

diseases with equally complex drugs, stricter requirements on clinical studies demanded by the authorities before approval is granted, and the high failure potential of NMEs in various stages of (pre-) clinical trials. With R&D costs doubling roughly every 9 years since the 1970s, the average cost per newly approved NME has increased to an estimated $ 1.4 billion US Dollar today; when considering the money spend on NMEs that did not make it to the market, cost estimations range from $4 - $11 billion [11-14].

Since the biggest portion of R&D expenditure has to be compensated for while patent protection is still granted, market prices of newly approved drug products (DP) have skyrocketed in the past few years. In the meantime, politicians and health-care representatives have increased pressure on the pharmaceutical industry to reduce costs, since the current pricing regime, together with the ageing population, and increasing cases of chronic illnesses pose a serious threat to the sustainability of national health care systems [15-19]. Generally, DP market prices are calculated from research expenditures, process development costs, regulatory approval charges, and manufacturing costs, as well as the estimated patient population and expected sales. Manufacturing costs account for the smallest portion in this calculation, but also offers a relevant opportunity for cost-reduction, as pharmaceutical manufacturing processes have not been subject to vast improvement in the past decades. This was mainly due to perceived regulatory uncertainties and the industry's fear of high capital investments into new unproven technologies, while well-known, validated, and potentially written-off manufacturing facilities are available and operational on top of the already very significant risk of the clinical survival of the experimental molecules. However, the paradigm changes in R&D and health care politics have raised the demand for new, better ways of pharmaceutical manufacturing. In this context, continuous manufacturing is a promising strategy to achieve cost reduction, as it offers various saving opportunities during development as well as during commercial manufacturing [13, 20].

During development, any potential variations in processing conditions and their impact on product quality need to be thoroughly investigated by producing a batch of material at each of these varying factors. These studies are commonly done by Design of Experiment (DoE), a method for statistical experiment planning [21]. In a classic batch process, multi-factorial DoE-trials in small- and large-scale batches are time- and material consuming, as the generation of one data point in a multi-step process can take several days or even weeks and requires one full batch per point. In contrast, the same DoE could be performed in only few days with substantially less material, when applying CM technology, as processing conditions can be changed "on the fly" while the process is running. The required amount of material per setpoint is no longer defined by the equipment size, but by the transient time it takes for the process to reach steady-state. Process scale-up and validation requires correspondingly little material, since the equipment in early- and late phase development can be the same. This is particularly beneficial, as availability of active pharmaceutical ingredient (API) typically is limited and hence expensive in early stages of development [8, 22].

During commercial manufacturing, CM has the potential for cost reduction in both, large- and small- scale productions. In large-scale blockbuster production, integrated process chains shorten lag-times and thus enable more responsive supply-chains, improve asset utilization, and decrease human to human hand-offs, managerial oversight, regulatory oversight, as well as inventory [8]. The implementation of comprehensive real-time process control strategies can lead to quality improvements and the amount of out-of-specification material that has to be

wasted can decrease. Also, the option for real-time-release is introduced, which would make time-consuming post-manufacturing testing obsolete and reduces losses for in process- and quality control [8, 9].

Apart from blockbuster production, CM is a suitable manufacturing method for products that require smaller or more flexible production volumes, since the technology allows to flexibly tailor the batch size to current demand, by adapting production run-time instead of equipment size. This is especially beneficial, since the focus of many pharmaceutical companies has shifted to low-volume or even personalized medicine, niche-markets, and orphan-drugs, after it was recognized that the impact of smaller patient populations can be compensated by a higher price demanded. Also, a broader portfolio for smaller target groups can ensure a steadier cash flow and avoid impactful patent-cliffs. Volume options for "minimum order quantities", which is a common criterion in supply chain design can become obsolete and the implementation of patient-centered dose flexibility becomes more feasible. Production forecasts can be "demand-driven" rather than the current, but often inefficient, long-term forecasting [8, 23-26].

Overall manufacturing-costs savings of up to 40 % are predicted for CM once the capital investment paid off and sufficient experience in CM-process development has been collected; other sources claim even higher savings [27]. In conclusion, efficient small-scale development and production of DP is a very important matter of the post-blockbuster era and demands for the implementation of CM into standard production processes.

1.3. Expected challenges[2]

While CM promises numerous economical and quality advantages, also various challenges or even disadvantages have to be considered and addressed, before the filing and approval of drugs manufactured in a continuous manner can become the new standard.

For once, continuous processes that run over extended periods of time are susceptible to unforeseen incidents like equipment wear-out, clogging of transfer pipes, or fouling of PAT-probes. Further, common and uncommon variations in process conditions can cause deviations that might be critical for product quality. For example, lot-to-lot variability in excipients can influence product and process quality and hence needs to be considered and the impact on the process performance needs to be understood [2, 5-7, 28]. Additionally, process ramp-up (until state of control is reached) can result in out-of-specification (OOS) material that needs to be retested or even discarded; the same is valid for ramp-down once a campaign is finished, or in the case of unforeseen process disturbances. This issue can be especially critical for low-volume products with costly APIs. Consequently it needs to be assured, that the benefits of CM are not outweighed by poor yields at this scale. Risk mitigation can be achieved by smart and dynamic, variable rate control strategies with early warning systems, the possibility to temporarily decouple single unit operations via buffer elements, and by establishing thorough knowledge of the process in relation to runtime and potential sources of process variability [22, 29].

Furthermore, clear batch- or lot- definitions need to be agreed upon, for example via production time or outlet volume instead of feed volume. This is highly important, as all corresponding

[2] Parts of this section have been previously published in Publication 1 (see page v)

documents during manufacturing, release, and distribution are linked to a batch- or lot number. Since a batch is defined as "[...] a specific quantity of a drug or other material that is intended to have uniform character and quality within specified limits, and is produced according to a single manufacturing order during the same cycle of manufacture" [30], it becomes clear that this definition can also be transferred to CM processes.

Additionally, while CM-equipment can be significantly smaller compared to conventional batch production units, it is usually also rather complex. Hence, if complex, time-consuming dismantling and cleaning is necessary during product changeover, the cost advantage gained from increased productivity could be significantly diminished. Smart solutions for cleaning-in-place and disassembly are therefore desired [9]. Also, the implementation of PAT requires development and validation of new methods in accordance to common guidelines, which requires time and resources. The application of real-time PAT during development and manufacturing generates vast amounts of data for each production run. Such data needs to be handled, processed, stored, and analyzed in a systematic way. When using the data for release purposes, data integrity according to title 21, part 11 of the code of federal regulations (CFR) needs to be ensured [31-34].

While the idea of real-time release testing (RTRT) is promising, its implementation is still a major challenge, even though an EMA guideline on the topic is available since 2012 [35]. For once, RTRT-strategies need to ensure representative, robust, and accurate process control on all DP critical quality attributes (CQAs), like content uniformity, dissolution rate, and aspect at all times. Particularly, RTRT-methods for dissolution testing impose vast challenges on the concept. Predictive models that can forecast the physical and chemical interactions that govern in-vitro dissolution from measured process parameters, material attributes, and (intermediate) CQAs have been developed, but their accuracy is still limited. Additionally, precise rejection of OOS material needs to be guaranteed, which is especially challenging when running on full production speed. Validated procedures to handle deviations need to be established. RTRT implementation is encouraged in a data rich environment of PAT-empowered CM, but not mandatory [35, 36].

Since regulatory guidelines require a precise link between the final drug product and its corresponding starting material batches, in case a product recall is required, the traceability of material needs to be investigated and understood. Also, precise process control, ejection of OOS material, and RTRT of quality product is only feasible when the material's residence time distribution (RTD) is known. RTD is defined as "the probability distribution of time that a solid or liquid material stays within one or more sequentially connected unit operations in a continuous flow system" [30]. Consequently, material velocities and front- or back mixing processes in dependence of process parameters and material attributes need to be known and understood. Ideally, sharp and short RTDs caused by ideal plug flow without large axial mixing effects would be desired, however material characteristics and required process parameters might not always allow such an ideal case. Consequently, the RTD for each new product and process needs to be studied [6, 30, 37-39].

1.4. Authorities view

The FDA, the European Medicines Agency (EMA) and the Japanese Pharmaceuticals and Medical Devices Agency (PMDA) all agree that the benefits of CM are expected to outweigh

the initial obstacles, once a solid ground of experience in this field has been established. Guidelines, committees, and an active support network was established, in order to reassure the pharmaceutical industry in investing in promising technologies and promoting change. For example, a recent FDA-guidance from 2017 offers detailed advice on the implementation of continuous manufacturing. Highly specialized teams like the FDA's Emerging Technology Team, the EMA's PAT Team, or the Innovative Manufacturing Technology Work Group from PMDA were established to form the link between industry and health authorities. Since dossiers for filing might require more complex explanations if regulators are still unfamiliar with new concepts, an early dialogue with the regulating bodies is encouraged [2, 5, 40-42].

1.5. Current market status

Major pharma companies like Novartis, GlaxoSmithKline, Johnson&Johnson, Lilly, and Vertex have invested into the development of downstream CM processes in the past decade. Nevertheless, only three companies have received authority approval for CM-produced drug products up to this date. US-based Vertex Pharmaceuticals was the first company to receive approval for the cystic fibrosis drug Orkambi® (lumacaftor/ivacaftor) in July 2015. In February 2018, the company also received FDA-approval for Symdeco® (tezacaftor/ivacaftor), making it their seconds continuous manufacturing-based product on the market. EMA approval is expected by the end of 2018 [43-45]. Likewise, in 2016 the FDA allowed the first switch from a previously approved batch production process to a continuous manufacturing process for Janssen's human immunodeficiency visurs (HIV) treatment Prezista® (darunavir). The company is expected to file a post-approval change in the near future, to include RTRT-approaches into the manufacturing license. Also, Janssen's mother company Johnson&Johnson, pledges to produce 70 % of its high-volume products through continuous manufacturing within less than a decade, to reduce manufacturing and testing cycle time by 80 % [36, 44-47]. Finally, Eli Lilly Pharmaceuticals received FDA-approval in September 2017 for Verzenio® (abemaciclib), used for the treatment of Metastatic Breast Cancer [48].

Other major pharma companies are expected to follow soon. Furthermore, numerous global collaboration-initiatives between academia and industry are sharing efforts to further establish the CM technology within the pharmaceutical sector. Examples are the *United Kingdom Centre for Continuous Manufacturing and Crystallization* (CMAC), the *US Centre for Structured Organic Particulate Systems*, or the *Irish Synthesis and Solid State Pharmaceutical Centre* [8, 49]. Furthermore, various international conferences with a focus on Continuous Manufacturing in pharma provide platforms for knowledge exchange and collaboration, like the *International Society for Pharmaceutical Engineering (ISPE) Continuous Manufacturing Workshop*, the *CMAC-Massachusetts Institute of Technology-CM-Symposium*, or the *CCP Summit* focusing on commercializing continuous processing in pharma [50-52].

1.6. Manufacturing modes

Generally, three main manufacturing modes are available for continuous pharmaceutical downstream manufacturing of tablets: direct compression, dry granulation/compression, and wet-granulation/drying/compression.

Direct compression, a process where the individual formulation ingredients (drug substance and excipients, see section 1.9, page 16 for details on formulation) are fed into a continuous blender

and then transferred directly to a tableting machine, is the simplest CM method. Processing of a batch-blended product is also feasible. Direct compression is the production process of choice for heat- and moisture sensitive materials, but applicability is limited with dusty or poorly flowing powders or if blend components tend to segregate [53, 54].

In continuous dry granulation and compression, a dry granulation unit is inserted between the feeding/blending and tableting steps. Granulation is required, if raw powders show too poor processing behaviors for direct compression. Dry granulation is achieved either through the application of force, or by addition of melt-binders in combination with high shear forces and elevated temperatures. Feasibility of the former option depends highly on powder characteristics, the latter is only applicable for temperature-resistant materials [55-57].

In wet-granulation and subsequent drying, soluble binders are added to the formulation and the powder is agitated while a granulation liquid (usually water) is added. Resulting granules are then dried in different ways. Wet granulation is the most popular method to improve bulk powder properties like flow and compressibility; drawbacks are the high energy consumption during drying. Also, it is only suitable for materials that are stable in aqueous (or organic solvent) environments and at elevated temperatures [33, 58].

In this regard, Vertex's film coated tablet Orkambi® is produced by a continuous twin-screw wet-granulation/fluid-bed drying/compression-process, Janssen's Prezista® and Eli Lilly's Verzenio® are manufactured via direct compression [45, 48] (see section 1.5, page 6 for details on the named products).

1.7. Process units[3]

1.7.1. Connected process line

Figure 2 shows a flow-chart of a typical "from-powder-to-tablets" continuous manufacturing process line. The individual equipment units will be discussed in detail in the following sections.

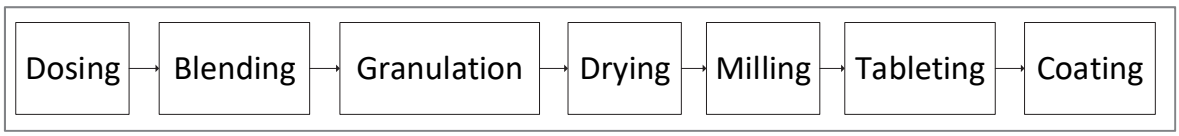

Figure 2: Flow-chart of a typical continuous manufacturing process line from powder to film coated tablets

1.7.2. Feeding

Feeders can either supply a pre-blend at a defined mass flow rate to the next unit operation, or multiple feeders can supply individual formulation components in fixed stoichiometric relationships into a continuous blender (see section 1.9, page 16 for details on formulation).

[3] Parts of this section have been previously published in Publication 2 and 4 (see page v)

Reliable and robust dosing is crucial for the quality and robustness of all subsequent unit operations and hence the final drug product.

Most common powder feeding systems are screw-controlled loss-in-weight feeders (also called gravimetric feeders), where one rotating screw or two co-rotating screws continuously dispense powder from a hopper into the next unit operation. Scrapers or vibrating units can aid with poor flowing powders. A weighting-cell monitors the actual feed rate, a corresponding control unit adjusts the screw-speed according to the weight-cell readings. Throughput-ranges between few grams per hour and several kilograms per hour are available. Gravimetric feeders can also operate in volumetric mode by fixing the screw rotation speed, however this option is considered less reliable than gravimetric mode, due to complex, unpredictable flow properties of bulk powders [59-62].

1.7.3. Blending

The different tablet ingredients need to be thoroughly blended, to ensure content uniformity or general property uniformity (such as dissolution) in the final drug product. If multiple dosing units supply individual formulation components (see section 1.9, page 16 for details on formulation), continuous blending systems need to be installed. Examples are fluidized bed mixers, rotating drum blenders, or convective continuous mixers. In fluidized bed mixers, particles are blended by the random movement that is induced from traveling through a linear fluid-bed. In rotating drum mixers, the particles mix and move forward due to frictional stress induced by a rotating cylinder and the fill level gradient. Convective continuous mixers contain impellers fixed on a rotating shaft inside a horizontal cylinder, that induces particle movement and hence blending, while the material travels through the cylinder. Designs of impellers and cylinders vary greatly in available equipment, depending on the intended process and product. Suitable process control systems should be in place to monitor and control blend uniformity (Examples will be given in chapter 1.11.2 - Process analytical technology) [63-65].

Blending can also be done in batch mode by weighing all ingredients into a suitably large container and blending by mechanical agitation over a suitable period of time. Although, batch blending could be considered conflictive to CM philosophy, it might be the preferred unit operation ensuring uniformity of properties with poor flowing powders and/or complex formulations.

1.7.4. Granulation

Granulation is a process of particle enlargement by different agglomeration techniques, to improve the processability of fine powders, by increasing bulk density and flowability, reducing the risk for segregation, and increasing dispensing performance. The mechanism that agglomerates powder particles encompasses a series of steps: wetting and nucleation, coalescence/growth, consolidation, and attrition/ breakage [66]. After successful granulation, the ratio of API and excipients is locked on a microscopic scale and hence ensures blend uniformity, which is especially helpful in low strength dosages. Wet or dry granulation techniques are available; the preferred method is highly product dependent. The resulting granule characteristics can highly influence the final drug products quality attributes [59, 67, 68].

Common continuous wet-granulation techniques are spray drying, fluid-bed granulation, or continuous twin-screw wet-granulation. In spray drying, solutions or suspensions of powders are sprayed through a nozzle into a hot-air chamber in order to produce small, dry droplets. High energy consumption, issues with nozzle blockage, and comparably small granules with poor processability for tableting are drawbacks on this method [33]. In fluid-bed granulation, the granulating liquid is sprayed onto a fluidized powder bed where nuclei are formed to initiate particle agglomeration. Most CM systems are based on linear rectangular fluid-beds where the material travels by either vibrational or gravimetric forces while being granulated and subsequently dried. The concept is rarely used in the pharmaceutical industry, due to broad residence time distributions, long processing times, and high energy consumption for granulation and subsequent drying [33, 69, 70]. In continuous twin-screw wet-granulation (TSG), the powder blend of active pharmaceutical ingredients and excipients together with the granulation liquid is continuously fed into a barrel containing a set of co-rotating screws [59]. The high-shear forces applied by the rotating screws result in thorough mixing and formation of wet granules in a microscopic scale while the material travels through the barrel [22]. TSG will be discussed in more detail in section 1.8.2 (page 13 ff.), as it was the granulation technique of choice in the presented thesis.

A typical continuous dry granulation method is roller compaction. The powder blend is densified into flat, band-shaped ribbons by passing through a gap between two counter-rotating rollers. This forms ribbons of densified material, which are then milled into granules. The size of the screen defines their size, together with formulation, feed rate, compaction force, and gap width. The advantage of this procedure is the absence of moisture; drawbacks are the creation of high amounts of fines and decreased compactibility compared to the pure blend [56, 71, 72]. Another dry granulation option is melt granulation. In CM, twin-screw melt granulation is a typical application where accelerated temperatures and the presence of high shear forces plasticize the added melting binder and hence, aid in granule formation [57, 73, 74].

1.7.5. Drying

For wet-granulation processes without integrated drying, an external drying step is required, since excess water can interfere with subsequent process steps (e.g. sticking on the tablet press) and negatively influence the final drug products quality (e.g. stability and dissolution rate). Over-drying should be avoided, as it can cause processability issues (e.g. dust formation or electrostatics) or influence the DP quality (e.g. disintegration time) [67, 68].

Drying of particulate, porous materials happens in two main drying phases called primary and secondary drying. In primary drying, the free moisture at the particle surface or within large pores is evaporated at a constant rate. The evaporation rate is limited by the rate of heat being added to the granules and capacity of the surrounding air to carry away moisture. Consequently, drying rate can be increased by increasing heat, agitation, or the surrounding air flow rate, and/or by decreasing pressure. In secondary drying, the process is controlled by slow diffusion of water from the fine pores to the particle surface. Drying rate decreases over time, as the diffusion path increases. The break point between the two drying phases is called the critical moisture content. This typical drying behavior of porous, granular materials has been investigated and confirmed extensively for numerous bulk materials and was recently also demonstrated on single, levitating particles [75-78]. Figure 3 illustrates the two drying phases.

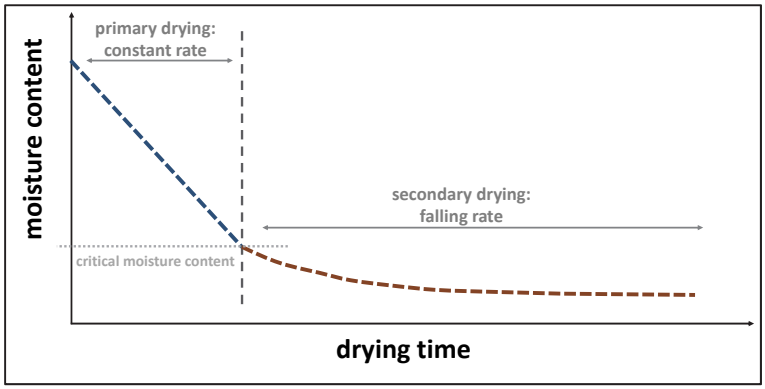

Figure 3: Main drying phases of particulate porous materials (Figure adapted from [77, 78]).

The most common continuous drying method for wet granular materials is fluid-bed drying (FBD), a method where a pre-heated air stream is passed upwards through the product. The resulting gas-solid mixture enables excellent interphase contact and uniform bed temperatures, which results in relatively high heat- and mass transfer rates and hence high drying rates (within the constraints of the generally low heat transfer rates from gas to solids). Early approaches to continuous FBD function on the basis of a static or vibrating horizontal fluid-bed, where wet granules are dried while they move horizontally through the (potentially semi-compartmentalized) rectangular dryer, either by gravitational flow or vibration. Residence time distributions (RTD) of these designs are wide [70, 79]. New approaches in continuous FBD attempt to tighten the RTD with the introduction of compartmentalized, semi-continuous drying systems. The two most prominent pieces of equipment on the market are the GEA ConsiGma^{TM} and the Glatt GPCG2 CM continuous fluid-bed dryers. The GEA system functions on the basis of a segmented fluid-bed dryer containing six separated, identical, static drying chambers operated in a semi-batch mode. Wet granules emerging from the granulator are sequentially filled into the chambers by a rotating inlet valve; the filling time and mass flow rate define the chamber fill mass [29, 80, 81]. The Glatt system has been developed on the basis of a star-shaped rotor that is inserted into a static drying chamber to create ten rotating process compartments that are subsequently but continuously filled with wet granules. The granules are conveyed clock-wise 8/10th of a full rotation through the fluidizing chamber to the outlet port, while being dried at the desired temperature, air flow rate, and rotation speed [82, 83]. More details on this system will be discussed in section 1.8.2 (page 13 ff.), as it was the drying technique of choice in the presented thesis.

1.7.6. Milling, tableting, and coating

If necessary, a milling step can be inserted between drying and tableting, in order to avoid oversized particles entering the press, as they might hinder uniform filling of the die and cause poor tablet content uniformity. Examples for continuous milling systems are air jet, disk, or hammer mills [84, 85]. Pulverization of granules should be avoided, as formation of too many fines can cause sticking on the tablet press, or influence the tablets dissolution profiles [86].

Tablets are one of the most popular dosage forms, whenever the active pharmaceutical ingredient and the targeted disease allow oral intake, as tablets allow easy dosing, administration, transport,

and storage. Despite its apparent simplicity, compression of bulk materials into tablets is a complex and irreversible dynamic process that requires thorough process understanding and expertise. The process consists of the steps die filling, compaction, and ejection. A feed shoe deposits the powder blend or granules in the die before the material is compacted between an upper and lower punch that apply pressure. Material bonding occurs through van der Waals forces, mechanical interlocking, and formation of solid bridges. Tablet quality depends highly on formulation properties and tableting process parameters like compression pressure and speed [87, 88].

The two main systems for tablet compression, are eccentric presses and rotary tablet presses. Eccentric presses are commonly equipped with only one die and a set of two punches; tableting speed is limited to approximately 60-100 tablets/minute [88]. In a rotary press, a variable number of dies and punches are installed on a circular die table (turret). Filling, compression, and ejection are completed in a circular motion at variable rotation speed. Many systems allow a pre-compression step to release air from the powder bed. The force is applied by both, upper and lower punch movement. Rotary presses have a considerable dwell time, which allows further deformation visible in stress relaxation of plastic components and leads to porosity reduction. Depending on the equipment design, up to one million tablets can be produced per hour in double rotary presses [87, 88].

The resulting tablet should be free from functional or visual defects. Functional defects arise from faulty formulations. Visual defects are usually caused by inadequate formulations, moisture contents, or machine settings [87]. If desired, tablet cores can be coated for aesthetic appearance, to mask bad taste or odor, to protect against UV or moisture, or to achieve modified release tablets. Coating is commonly achieved in rotary drum coaters, where a liquid coating preparation is sprayed on a tablet bed while heated air is circulated through the coating drum to evaporate the solvent [89].

1.7.7. Powder transfer system

To achieve a fully connected from-powder-to-tablet CM production line, powder transfer systems (PTS) are required to continuously transfer wet or dry materials between the different unit operations and to refill the hoppers of the dosing systems, especially in cases where gravity fed flow is not feasible. If the transfer distance is fairly short, blowing material by a pressured air stream might be sufficient. In the case of longer transfer distances or upward transfer, vacuum based PTS can be required.

1.8. Equipment Focus[4]

1.8.1. Twin-screw wet-granulation by Thermo Fisher Scientific Pharma 16

Generally twin-screw wet-granulation (TSG) offers a high level of flexibility, compact design, and is applicable to continuous manufacturing. TSG requires less granulation liquid than conventional batch high shear granulators [90]. Equipments from different suppliers function on

[4] Parts of this section have been previously published in Publication 1 and 4 (see page v)

similar bases with only minor differences in design and setup. The Pharma 16 twin-screw granulator from Thermo Fisher Scientific (Karlsruhe, Germany), was the granulation unit of choice in the presented work. It consists of a barrel, a gear-box connected to two screws with modular screw elements, a heating and cooling unit, a feeding unit to supply granulation liquid, and a HMI. The stainless steel barrel is divided into an upper and lower half that is further horizontally segmented into eight zones of equal size. Different temperature settings can be applied to each zone individually. Different ports can be inserted into the upper half of the barrel, e.g. powder or liquid inlet ports. The granulation liquid is continuously pumped with a rotary peristaltic pump from a tank into the barrel at a given feed rate (Corresponding feeding units for the powder blends were discussed in chapter 1.7.2, see page 7).

The screw configuration can be adapted by assembling different screw elements on a hexagonal shaft. The length of the individual elements is commonly given in multiples of the screw diameter D (here: D = 16 mm). Conveying elements transport the material between inlet and outlet, while imparting low mechanical energy. Depending on the elements axial distance between two adjacent flights ("pitch"), transport speed can be varied. Between transport sections kneading sections can be inserted to facilitate mixing, densification and granulation of the material. Kneading elements come with different staggering angles (30°, 60°, or 90°). The number of elements per kneading section, the staggering angle, and the total number of kneading sections defines the shear forces that act on the granules. Mixing elements (also called distributive flow elements) can aid in mixing the powder blends, or distributing the granulation liquid in the blend. When placed at the end of the screw they can aid in homogenizing the granule size distribution by inducing milling effects. Screw speed can be set between 10 – 1000 rpm [90, 91]. See Figure 4 for details on the most common screw elements and an example of a screw setup.

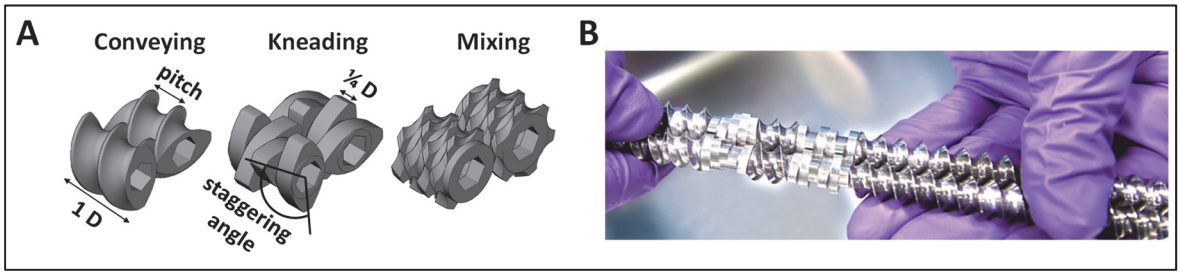

Figure 4: A: Most common screw elements in twin-screw wet-granulation (D = screw diameter). B: Example of a finished screw setup (Figure A adapted from [91]).

The screw design and the formulation ingredients are the most important factors to define the granule characteristics. In addition, the total material mass flow, the liquid-to-solid ratio (L/S), and the screw speed play an important part in the granulation behavior, as they all influence the granule critical quality attributes (CQAs), like particle size distribution or bulk/tapped density, as well as the final tablets characteristics tensile strength or disintegration time [41, 92]. Besides, higher L/S ratios improve the nucleation and agglomeration mechanism required for granulation, too wet material however can cause process issues due to paste formation [90, 91].

The screw speed has an impact on TSG fill-level, shear stress, and the material residence time distribution (RTD), which in turn can influence mixing efficiency and water distribution [41]. Barrel temperature demonstrated to be correlated to particle size with certain formulations, due to increased solubility of solids and/or altered moisture absorption of excipients at elevated temperatures [93, 94].

Since most of the mentioned factors can have confounded effects on granule characteristics and are highly formulation dependent, it is not possible to define generalized models on TSG processes. To ensure robust continuous twin-screw wet-granulation, the effect of each potential critical process parameter (pCPP) and potential critical material attribute (pCMA) on the intermediate and drug product CQAs, has to be investigated during formulation and process development.

1.8.2. Continuous fluid-bed drying via Glatt GPCG2 CM FBD

The Glatt GPCG2 CM FBD (Glatt GmbH, Binzen, Germany) was the drying unit of choice in the presented thesis. It consists of a star-shaped rotor, divided into ten process compartments, that is inserted into a static drying chamber. The dividing walls of the rotor extend over the whole height of the fluidizing chamber and seal off the process compartments against the outer jacket of the drying chamber and each other. This avoids crosstalk (spillover) of material between the chambers during operation and effectively works similar to a rotary star valve in a forced feed mechanism. An exchangeable air permeable bottom plate is screwed to the bottom of the star-shaped rotor. A connected drive unit generates the clock-wise rotation of the rotor within the static drying chamber. The process compartments are subsequently but continuously filled through an inlet port with wet granules emerging from a twin-screw wet-granulation unit (see 1.8.1). The granules are conveyed clock-wise $8/10^{th}$ of a full rotation through the fluidizing chamber to the outlet port, while being dried at the desired temperature and air flow rate. The rotation speed defines the effective drying time of the material inside the fluidizing chamber and can be adjusted according to the process needs. Figure 5 shows a cut-away perspective representation of the drying chamber and rotor [82, 83].

The amount of water remaining in the granules at the end of the drying process (determined as loss-on-drying, LOD), is an intermediate critical quality attribute (CQA) of the final drug product, as it could directly influence several DP CQAs (e.g. stability, aspect, dissolution rate), or negatively affect long-term stability. Furthermore, deviations from the targeted LOD can have a negative impact on subsequent processing steps (e.g. sticking in the tablet press). Hence, a tight monitoring- and control system of the drying unit efficiency needs to be in place, in order to keep the LOD of the dried granules within its predefined quality limits at all times [67, 68].

A detailed overview of the whole granulation and drying process-line, including sensors and process data available for process control is shown in Figure 6. Humidity of the inlet air stream is measured at room temperature, before the air is conditioned to the desired drying temperature by a heating unit. The generated total air flow rate is divided at variable proportions between the fluidizing chamber and a bypass pipe by a flap valve, to allow appropriate control of the air flow rate in the fluidizing chamber. Flow-sensors measure total air flow rate and bypass air flow rate, in order to determine the air flow rate in the fluidizing chamber.

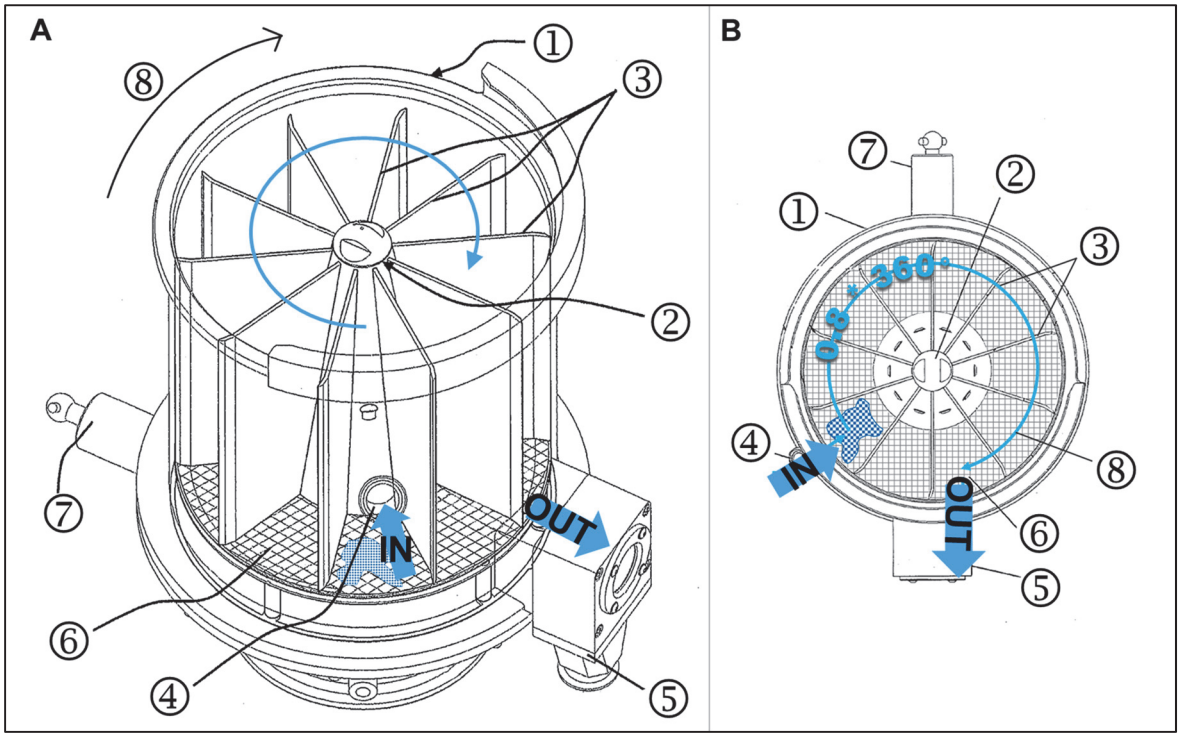

Figure 5: A: front-view-, B: top-view cut-away perspective representation of the Glatt GPCG2 CM drying chamber (1), containing the star-shaped rotor (2) with dividing walls (3), the inlet and outlet port for granules (4)&(5), the air flow-receiving base made of a steel-sieve (6) and the connection to drive unit (7) that generates rotation of the rotor in direction (8). The granules travel 8/10th of a full rotation between the inlet and outlet port while being dried (Drawing adapted from [82, 83]).

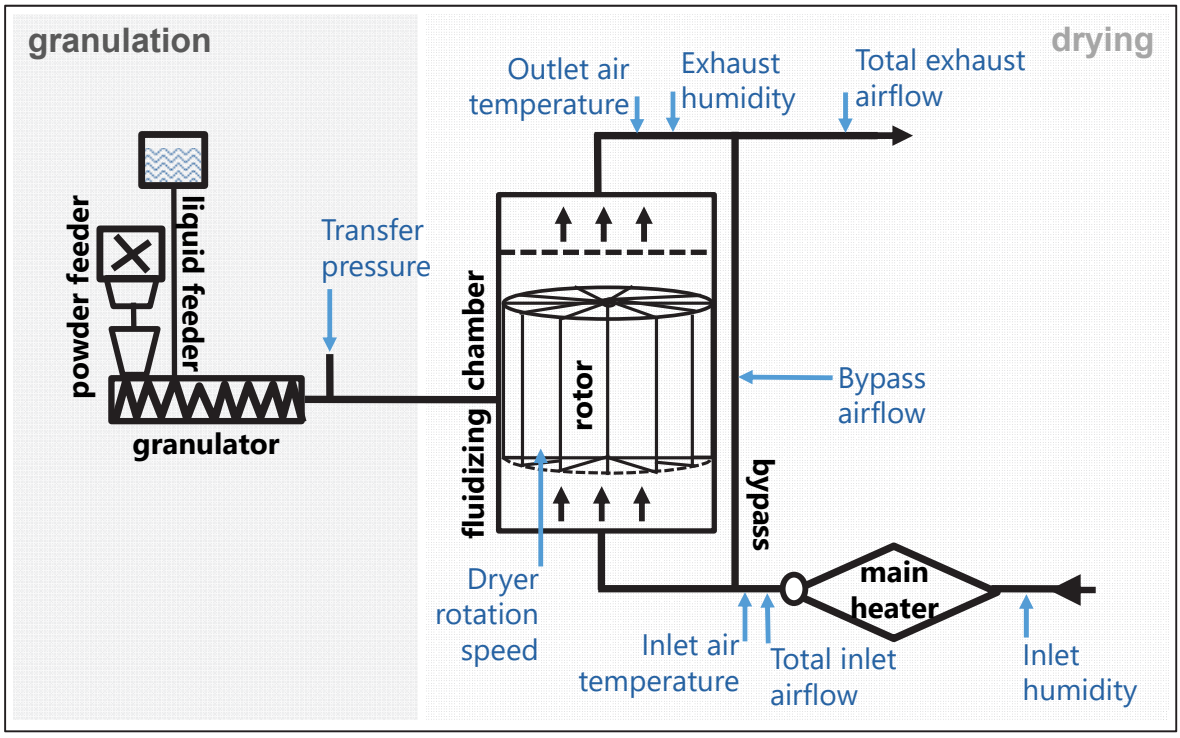

Figure 6: A twin-screw wet granulating (TSG) unit is connected to the Glatt GPCG2 CM continuous fluid-bed dryer. The fluid-bed dryer contains air flow rate-, temperature- and humidity- sensors at the indicated positions. Process parameters of both units are continuously logged every ten seconds (Figure adapted from [95]).

As a consequence of this design, all ten process compartments are exposed to the same inlet air humidity, temperature, and air flow settings. Once the air flow exits the fluidizing chamber, it is passed through a filter unit and merged with the bypass to a single exhaust air flow stream. Exhaust humidity and temperature are measured before the merge, total exhaust air flow rate is measured after the merge. Since pressurized dry air is introduced into the dryer to transfer the wet material from the granulating unit to the inlet port, to blow out dried material through the outlet port, and to regularly clean the filters of the outlet air, the total exhaust air mass increases compared to the inlet air mass.

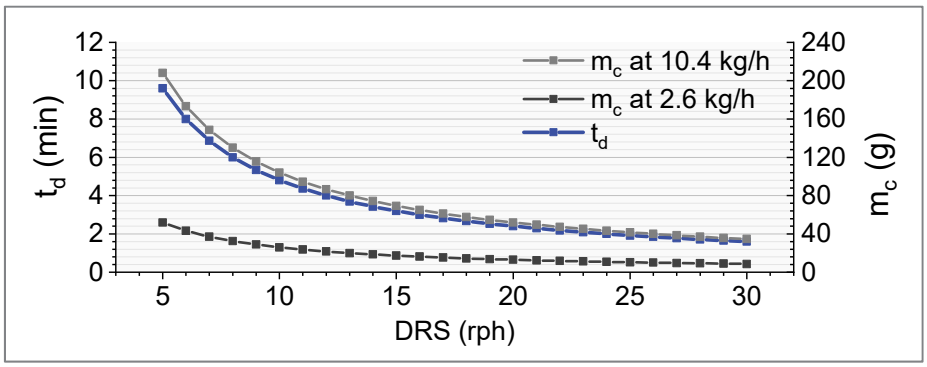

Figure 7: Correlation between drying time t_d and chamber fill mass m_c in relation to the dryers rotation speed DRS at different material mass flow rates.

Generally, the drying efficiency of the Glatt GPCG2 continuous dryer can be adapted through three process parameters: drying air flow (DAV), drying temperature (DT), and dryer rotation speed (DRS). However, adaption of DT is not suitable as a fast responding process control action, due to long thermal-equilibration times of the stainless-steel drying chamber. DAV is correlated in a negative relationship with LOD [22].

DRS simultaneously influences the rotation time t_r *[min]*, and hence the granules' drying time t_d *[min]*, and fill mass of wet granules per drying chamber m_c *[kg]*. Explicitly, the lower the rotation speed, the longer the drying time and the higher the chamber fill mass (at constant mass flow rate $\dot{m}$ [kg/h]; see Figure 7 and eq. 1-eq. 3 for details).

eq. 1 $$t_r = \left(\frac{60}{DRS}\right)$$

eq. 2 $$t_d = \left(\frac{60}{DRS}\right) * 0.8$$

eq. 3 $$m_c = \frac{0.1 * \dot{m}}{DRS}$$

As both factors influence the drying efficiency in a contrary manner, it depends on the material characteristics and process parameters DAV and DT, if the correlation between DRS and LOD is positive or negative [22].

1.9. Formulation

Next to the API, a tablet commonly contains numerous additional substances with specific and crucial functions, so called excipients. Excipients can improve processability, performance, and also stability of the final drug product. They can be classified into the five main categories diluents (e.g. *microcrystalline cellulose (MCC) or Calciumhydrogenphosphate anhydrous*), binders (e.g. *Hydroxypropyl methylcellulose (HPMC) or Polyvinylpyrrolidon (PVP)*), disintegrants (e.g. *Sodium starch glycolate or Crospovidone*), lubricants (e.g. *Sodium stearyl fumarate or Magnesium stearate*), and flowability enhancers (e.g. *Colloidal siliciumdioxide*). Additionally, coating-related excipients, colorants, pH modifiers, antioxidants, and flavor additives can play a role in tablet formulation. Excipients can be derived from either natural, synthetic, or semisynthetic sources. Physicochemical compatibility between the different excipients and the API can limit the available choices during formulation development [96-99]. Overall, formulation approaches for traditional batch manufacturing and CM-processing do not differ qualitatively, but potential variations in quantity might be expected.

1.10. Pharmaceutical development[5]

1.10.1. Quality-by-Design

In conventional batch manufacturing, product quality is usually ensured by end-product testing once production is completed, a concept also referred to as Quality-by-Testing. Nowadays, due to numerous technological advancements in the past decades, significant opportunities for improvement in pharmaceutical development and manufacturing exist. Quality is built into the product from the start; a concept referred to as Quality-by-Design (QbD). QbD embodies a systematic approach to pharmaceutical development with an emphasis on product- and process understanding as well as process control that is based on sound science and quality risk management principles [100]. QbD-based development is applicable to continuous manufacturing; the individual components of QbD-based pharmaceutical development will be discussed in more detail in the following sections.

1.10.2. Critical Quality Attributes of solid oral dosage forms

A general guideline for pharmaceutical development of drug products (DP), independent of the manufacturing process, is provided by ICH Q8. According to the guideline, the drug product's desired characteristics and level of quality, required to ensure the patient's safety and the drug's efficacy, should be defined in the *Quality Target Product Profile* (QTPP), prior to starting any commercial form development activity. Based on the QTPP, the DPs critical quality attributes (CQAs) can be defined. CQAs are physical and chemical product characteristics that have to remain within appropriate, pre-defined limits throughout manufacturing, in order to guarantee the desired level of DP performance. The QTPP of film-coated tablets for immediate release generally includes assay, aspect, dissolution rate, content uniformity, and stability as the drug products CQAs, as they can sufficiently ensure the product safety and efficacy for the patient,

[5] Parts of this section have been previously published in Publication 1 (see page v)

when they meet their pre-defined limits. Corresponding intermediate CQAs of a CM wet-granulation and drying process are dried granules' content uniformity (CU), moisture content determined as loss-on-drying (LOD), and particle size distribution (PSD), as they directly influence DP CQAs. CQAs can be controlled through their corresponding *critical process parameters* and *critical material attributes* of input materials (CPPs and CMAs). Since CPPs & CMAs are highly dependent on the investigated product- and process, they need to be determined for each new product or process by a combination of quality-risk-management methodologies and systematic experimental analysis [21, 101-103].

1.10.3. Quality Risk Management

According to the ICH, risk is defined "as the combination of the probability of occurrence of harm and the severity of that harm" [104]. Regarding pharmaceutical drug products, risks differ between the different stakeholders, from industry, government, medical practitioners, and patients. However, the protection of the patient should always be considered as the prime importance [104].

Quality risk management procedures for a pharmaceutical manufacturing process need to evaluate three aspects: first, all potential quality-critical risks that could occur during manufacturing and could negatively impact the product's (intermediate-) CQAs need to be identified (*risk identification*). Second, the probability of occurrence of each identified risk needs to be evaluated (*risk analysis*). And third, the consequences of the occurrence for DP quality need to be quantified, in order to judge its severity (*risk evaluation*).

The first two steps are commonly done in a rather theoretical approach. All process parameters and material attributes that could potentially vary in the production line are *identified*, based on historical data, theoretical analysis, as well as individual experiences from numerous involved cross-functional stakeholders (further summarized as *variables*, e.g. temperatures, equipment specifications, process settings, etc.). Even the most unlikely risks or concerns have to be considered during this step. Possible tools like flowcharts, check sheets, or fishbone diagrams can be beneficial in the process [105].

While all identified variables are potentially critical in theory, some are not likely to vary significantly during production. Therefore, probability of occurrence of each variable should be judged during *risk analysis*. Judgement should be done with a standardized procedure, based on experience and logic reasoning from all involved stake-holders, if possible backed up with historical data or other means of proof. Prominent standard methodologies are for example the Failure Mode Effects Analysis (FMEA), Fault Tree Analysis (FTA), Hazard Operability Analysis (HAZOP), or criticality matrix ratings. Numerous guidelines on such tools are available [104, 106-109]. All variables that are identified with a low probability of occurrence in this process, can be disregarded as not-critical. All remaining variables are defined as potentially critical process parameters and material attributes (pCPPs/pCMAs, summarized as *factors*), and their effects on (intermediate) CQAs need to be evaluated in detail, to judge and quantify their severity [104].

1.10.4. Design of Experiment

Design of Experiments (DoE) is the preferred method for empirical risk evaluation, especially when complex processes are investigated. Compared to the traditional COST approach (changing one single variable at a time), DoE enables testing a large number of factors with optimal efforts and permits the identification of factor-interactions. By systematically varying factor settings between their respective low and high limits, the quantitative effects of pCPPs and pCMAs on (intermediate) CQAs (also referred to as *responses*) can be assessed. Statistical analysis of results allows to maximize information content, while the number of experiments is minimized [21, 101, 102, 105].

By fitting a regression model to the empirically determined factor-response dataset, the coefficients of main effects can be quantified; depending on the design, also interaction and quadratic effects can be described. The goodness of a fitted regression model can be summarized by the model performance indicators R^2, Q^2, model validity, and reproducibility. R^2 is the fraction of the response-variation that is explained by the fitted model, Q^2 estimates the predictive ability of the model by generalized cross-validation, validity judges the model appropriateness in a general sense, based on ANOVA lack of fit test, and reproducibility considers the variation in center points compared to overall variability. Generally, for a model to be judged as good, model performance indicators should be $(R^2\text{-}Q^2) < 0.3$; $Q^2 > 0.5$; validity > 0.25; reproducibility > 0.5. Relevant equations to calculate these parameters can be found in [105].

The resulting regression models then allow to predict responses for any factor combination that lies within the investigated factor space. This ability builds the foundation for a comprehensive science-based control strategy of the manufacturing process, since the descriptive, statistical process models can be applied in regulating process control loops. The accuracy of the prediction depends on the models confidence interval and the process robustness [105].

Generally, DoE can be applied to three objectives: screening, optimization, and robustness testing. The objective defines the complexity of the design and the number of trials; decreasing the number of trials, decreases the experimental effort at the cost of reduced resolution [105]. A more detailed description on the different DoE objectives and corresponding designs, as well as details on the analysis of results, model interpretation, and possibilities for model refinements, was previously published in publication 1 (see page v).

1.11. Process Control Strategies[6]

1.11.1. General principle and aim

CM promises unrestricted scale-up of production volumes at consistent product quality within specified limits. This promise however can only be kept, if a comprehensive, real-time process control strategy is in place. This strategy needs to consider all possible sources of process variability. The aim is reduced risk for complete operation shutdown while ensuring, that the finished batch of drug product has consistent, uniform character and quality within pre-defined limits at all times [2, 5-7]. Such a control strategy is commonly based on the implementation of suitable Process Analytical Technologies (PAT) and statistical process control tools. When product quality is found to be out-of-specification, automatic control-actions can adapt critical process parameters and/or divert material from the line in real-time.

In the following chapters, the most common PAT-tools for the monitoring of CQAs water content in dried granules (commonly specified as loss-on-drying, LOD), active pharmaceutical ingredient (API) content in powders, tablets, and granules, and particle size distribution (PSD) of dried granules will be introduced; PATs relevant to the presented thesis will be discussed in detail. Furthermore, common available tools for statistical process control will be presented. (See section 1.10.2, page 16, for details on the selection of LOD, PSD, and API content as relevant CQAs for continuous manufacturing of tablets via twin-screw wet granulation and fluid-bed drying).

1.11.2. Process analytical technology

Process analytical technologies (PATs) are defined as systems “for designing, analyzing, and controlling manufacturing through timely measurements of critical quality- and performance attributes of raw and in-process materials and processes, with the goal of ensuring final product quality” [5]. Fast, non-destructive measurement techniques that scan the product in-line or on-line are preferred, but also regular sampling of small amounts for a (potentially destructive) at-line measurement is a feasible PAT approach, as long as the economic benefit (i.e. reduced risk for complete batch failure) outweighs the economic loss from sampling. An available FDA Guidance on PAT implementation describes the regulatory framework for PAT-tools, with the aim to encourage the inclusion of innovative beneficial techniques into pharmaceutical manufacturing processes [5].

1.11.3. PAT for API content, LOD, and PSD

API content

Common PAT-tools to monitor a drug products content uniformity, or intermediate blend uniformity in downstream CM, are Raman spectroscopy and near infrared spectroscopy (NIRS). Raman spectroscopy is a type of vibrational spectroscopy that is based on the Raman effect: an inelastic scattering effect of electromagnetic radiation that can be observed when the radiation

[6] Parts of this section have been previously published in Publication 1-4 (see page v)

and molecular vibrations exchange energy. In detail, the sample to be analyzed is exposed to monochromatic laser light. Upon interaction with molecular vibrations, the energy in the laser photons shifts, which can be analyzed by a detector collecting the scattered light. Since the shifts in energy are specific for different molecules, calibration of Raman spectra to certain chemical sample characteristics like API content is feasible for amenable molecules. NIRS is also a spectroscopic method that investigates the vibrational properties of a given sample. Absorption intensities in characteristic API-bands are calibrated to the sample's API content (as determined by reference analysis). Details on NIRS calibration are discussed in more detail in section 1.11.4, as it was applied in the presented thesis (see page 22 ff.). Raman and NIRS can be utilized individually or simultaneously, as the resulting information of the two techniques is similar, but complementary. Both measurements can be done in a very fast non-destructive manner, making them amenable for real-time release purposes [110, 111].

Calibration of both spectroscopic methods is most commonly done via high pressure liquid chromatography (HPLC) as reference analytics; also UV-spectroscopy is a feasible alternative.

Moisture content (LOD)

Most prominent PAT-tools to measure moisture content during drying of granules are microwave resonance technology (MR) and NIRS. Furthermore, the implementation of Mass- and Energy balances (MEB), based on the physical measurement of process conditions can facilitate the prediction of dried granules moisture content.

In MR, microwave resonances are calibrated to material moisture contents. Early tools calibrate single resonances in the range of 2-3 GHz which limited the applicability to moisture contents below approximately 8 %, newer tools apply multiple frequencies over a wider range, which allows to widen the feasible measurement range [112, 113]. In NIRS, absorption intensity in spectral water bands is calibrated to the sample moisture content (as determined by a suitable reference analysis). Details on NIRS calibration are discussed in more detail in section 1.11.4, (see page 22 ff.). MEB calculations allow to predict a samples moisture content after drying, based on available process values logged from installed humidity, temperature and air flow rate sensors, together with the knowledge on the materials that entered the dryer. Since MEB is solely based on physical measurement principles, it allows direct calculation of LOD, independent of the used materials and hence without the need of product specific calibration. The derivation of MEBs has been thoroughly described for various FBD equipment; since the calculations are highly equipment specific, they are not directly transferable between equipment types [114-116]. Other applications for moisture monitoring include triboelectric probes and electrical capacitance tomography. The former measures the exchange of electrons between an earthed metallic surface and the fluidized granules, which is influenced by the water content; the latter correlates water content to the permittivity value between adjacent electrode pairs. So far, these methods have only been applied to batch fluid-bed drying processes [117, 118].

Common available reference methods for moisture content are *Karl-Fischer titration (KF)* or *loss-on-drying measurement (LOD)*. KF is a quantitative titration method that determines trace amounts of water based on its reaction with sulfur dioxide and iodine in a buffered ethanol solution [119]. In LOD, sample moisture is analyzed by analyzing its weight-loss upon heating. Once the weight stabilizes over a defined time period, the initial moisture content is calculated.

Since the weight loss is not specific, thorough knowledge of the sample constitution and reaction to heat is required [120].

Particle size distribution (PSD)

Prominent options to monitor granule particle size in-line, at-line, or on-line, include imaging techniques, focused beam reflectance measurements (FBRM), spatial filter velocimetry, or laser-diffraction (LD) [121-123].

An example for a direct imaging, non-product-contact, on-line PAT-tool is the Eyecon2™ Particle Characterizer (Innopharma Labs, Dublin, Ireland). It uses a combination of LED-illumination sources coupled with an image capturing device and particle sizing algorithms that acquire size distribution profiles in real-time [124]. FBRM uses a focused laser beam that scans across particles passing the probe window. The instrument measures the time the laser beam is reflected and propagated back while a particle passes, in order to calculate chord length distribution based on time and velocity. The technique is commonly applied in the chemical or petroleum industry but applications as at-line PAT tool during fluid-bed granulation have been reported [125]. Spatial filter velocimetry also projects a laser beam onto the moving particles, but measures the generated shadow, in order to calculate chord length distribution. The granules need to pass through the probe head for the optical sensor to analyze shadow time and particle velocity. An internal compressed air supply system ensures the granule dispersion and keeps the measurement window clean [122]. In LD, a dispersed sample passes through a beam of monochromatic light, where it causes light diffraction. The angular variation in intensity of light diffracted is measured by a detector and can be correlated to particle size. Large particles cause light diffraction at smaller angles relative to the laser beam, and small particles cause light diffraction patterns at larger angles. The correlation between diffraction pattern and particle size is generally based on the Mie theory of light scattering for smaller particles or the Fraunhofer approximation for larger particles. The latter is a simplified approach that requires little to no knowledge about the sample's optical properties, but reliable utilization is limited to opaque particles larger than 50 μm [126, 127]. Also, monitoring of particle size related information by NIRS has been described in several literature sources [128-130], details will be provided in section 1.11.4 (page 22 ff.).

General issues to in-line or on-line PSD measurements that occur with almost all techniques, are probe fouling and formation of large granule clusters due to sticking. They can be partially addressed by installing cleaning and dispersion systems based on compressed air or scrapers, the application of anti-static sprays, or polished probe windows [122, 124].

Common off-line analyzing techniques that can be applied as reference methods to determine granule's PSD, are dynamic image analysis and sieve analysis. In dynamic image analysis, a sample's particle size distribution is calculated via digital image analysis of dispersed particles passing a camera setup [131]. In sieve analysis, a certain amount of sample is classified and quantified by a sieve tower that contains numerous sieves in ascending degrees of coarseness [132]. Generally, PSD measurements of anisometric particles (most relevant cases) are questionable methods, as the definition of the "true" value cannot be defined theoretically: every method produces its own typical (ideally correct) values as per definition of the particle property they assess. Effectively, comparison of PSD's measured by different methods is telling equally as much about the method as about the particles.

1.11.4. Near-Infrared spectroscopy & chemometric calibration

NIRS has become one of the most prominent qualitative and quantitative PAT-tools in pharmaceutical development and manufacturing, as it is a safe, fast, and non-destructive method which does not require sample preparation. The integration of NIRS into pharmaceutical manufacturing is endorsed by all major authorities. Numerous guidelines on NIRS method development and validation have been published in the past [6, 33, 133-137].

Instrumentation

NIRS is a spectroscopic method that investigates the vibrational properties of a given sample by exposing it to light in the near-infrared region of the electromagnetic spectrum, which ranges from approximately 780 nm to 2500 nm (4000 – 12800 cm^{-1}). When a molecule absorbs infrared radiation, its individual bonds start to vibrate. NIR spectra are dominated by C-H, N-H, O-H, and S-H overtones, and combinations of fundamental mid-infrared vibrations. Either the attenuation of the reflected beam or the intensity of the transmitted beam is measured by a detector. The resulting spectra are rather complex, making it difficult to assign certain features to specific chemical components. However, since absorption/transmittance patterns are very specific for individual molecules, the spectra contain composite chemical and physical information that can be extracted and calibrated by suitable chemometric (multivariate) data treatment. In contrast to mid-infrared radiation, NIR radiation can penetrate several millimeters into the analyzed materials, since absorptions in this range are rather low. Generally, the environment, the samples physical (morphology, density, temperature, etc.) and chemical properties (material composition, water content, etc.), and the sample presentation to the NIR probe (direct, through glass, etc.) can influence the absorption pattern and need to be considered during application [110, 111, 135].

PAT applications

When properly calibrated, NIRS can be applied for the identification of raw materials, for in-line monitoring of process steps like blending (API blend uniformity), wet-granulation and drying (moisture content measurement), and tableting (API content uniformity) [42, 138-146]. Generally, sample water content can be calibrated to its specific NIR-absorption spectrum, because the regions between 1400 – 1450 nm and 1900 – 2000 nm are highly correlated to water absorption [121, 147]. API content can be best calibrated, if the drug substance to be analyzed shows good NIR-activity in specific wavelength regions that do not overlap with the water bands. Both applications are considered as PAT standard with numerous examples available in literature [31, 42, 111, 121, 128-130, 139-141, 144, 145, 147-151]. Aside from the potential to quantify chemical sample features, physical sample properties like granule morphology, density, shape, and size are thought to cause changes in the baseline and slope of a spectrum, which also allows calibration against these various material properties. The functional principle of these calibrations is thought to be rather complex, as physical properties can influence the absorption patterns in many ways. Bottom line is that the extraction of information about the various material properties in a calibration exercise, is a purely numerical extraction of information contained in the spectra that is hidden to direct physical interpretation of the spectra, but can produce reproducible and accurate predictions of these various material properties. It is basically a fingerprinting approach. Numerous examples on the topic have been reported in literature [31,

110, 121, 123, 128-130, 147, 152-155]; a review of available publications was previously published in Publication 2 (see page v).

Spectra pre-treatment

Physical sample variations can cause unwanted spectral effects (e.g. slope changes and baseline offsets), that can mask desired chemical information contents. Preprocessing of raw data by different algorithms can help to mitigate such impacts, with the aim to separate light scattering effects from light absorbance. Most prominent preprocessing methods are baseline corrections, standard normal variate (SNV), multiplicative scatter correction (MSC), and/or application derivatives. Baseline-correction is performed by subtracting a linear or polynomial baseline from the original spectrum. SNV is an effective scatter correction algorithm, where each spectrum is centered around zero, by subtracting the mean and dividing each signal value by the spectrums standard deviation. In MSC, spectra are shifted and scaled to fit a given target spectrum, usually taken from a previously established library. Derivatives are applied to remove constant background signals and to enhance the visual resolution, especially for weak peaks. With each subsequent derivation, a constant offset is removed. Spectral pre-treatment during calibration and validation is commonly applied by combining sound experience with a try-and-error approach, as no standard algorithm is the solution to all problems. However, their application should be done with care, as they could also remove desired analyte signals. Likewise, to correlate physical properties to absorption patterns, raw spectra have to be analyzed, since slope offsets and baseline shifts are the desired information source [110, 156, 157].

Chemometric analysis and calibration

Chemometrics are defined as a "a chemical discipline that uses mathematics, statistics, and formal logic to (1) design or select optimal experimental procedures; (2) to provide maximum relevant chemical information by analyzing chemical data; and (3) to obtain knowledge about chemical systems" [158]. The main tool in chemometrics is multivariate data analysis (MVDA), a method that is essential for quantitative and qualitative assays based on NIRS. In detail, MVDA is the observation and analysis of more than one statistical input and outcome variable at the time, with the aim to extract the most important data. Prominent qualitative MVDA methods are principal component analysis (PCA), and independent component analysis (ICA). The most prominent quantitative method is partial least squares regression (PLSR).

In detail, PCA is an unsupervised method that allows to highlight similarities and differences in a set of observations, by transforming them into a set of new linearly uncorrelated variables called Principal Components (PCs). This procedure permits a visualization of the data distribution, without requiring any prior knowledge about the data. PCs account for the majority of variability in the dataset: the first PC is the vector through the data that explains the most variability, the next PC is orthogonal to the previous and describes the maximum amount of the remaining variability in the data, and so on. This procedure allows to describe the contained information with considerably fewer variables than the original dataset and removes noise from the analysis. It aims to discover and display object-clusters of related characteristics for exploratory data analysis. In NIRS, PCA is commonly applied to qualitative process monitoring and to get a first overview of the sample distribution prior to quantitative calibration. More details on the mathematics behind PCA can be found in [110].

Independent Component Analysis (ICA) is special case of blind source separation with the aim to decompose a multivariate signal into independent non-Gaussian components (also called latent variables or sources). Like PCA, ICA performs a decomposition of spectra, by assuming that the components are statistically independent. However, while PCA cannot recover the original signals from a multivariate one, ICA can apply information on statistical independence to recover the original sources. There are numerous algorithms available that do ICA, all differing in the way independence is defined. The two most prominent ones define it by either minimizing mutual information in the data set or by maximizing non-Gaussianity. Details on the mathematics behind ICA can be found in [159-162].

The most popular algorithm for quantitative, multivariate regression in NIRS is PLSR, a method that combines PCA with multiple linear regression. The aim of PLSR is the prediction of a set of dependent variables Y (i.e. API content in a tablet) from a set of independent variables X (i.e. NIRS absorption over a certain wavelength range), by extracting a set of orthogonal factors (latent variables) from X and Y datasets simultaneously, while maximizing the covariance structure between these blocks. The mathematics are based on two simultaneous PCA analysis of X and Y, where the structure of the Y-data is used to find the PCs in X. The amount of data that is explained by each PC is maximized; the more PCs are included into a model, the more variation is explained, which in turn might increase the predictive power but also might cause over-prediction of noise effects. Hence, a developed model should be systematically validated according to common guidelines, to ensure that the right amount of PCs has been selected for robust model performance. PLSR is especially useful, when the number of independent variables is high compared to the number of observations [110, 163-165].

Calibration assessment and model validation

Several guidelines on validation of NIRS analytical methods have been published by the major authorities that summarize a number of standard parameters suitable for NIRS method validation. For once, the adequacy of selected number of PCs and degree of overfit can be investigated via root mean square error of prediction and -cross validation (RMSEP and RMSECV) and permutation analysis. RMSECV/RMSEP is a common resampling statistic, calculated based on the calibration- or validation data set by the leave-one-out method. The models predictive power can be evaluated by plotting RMSECV and RMSEP as a function of the number of selected PCs, each selected PCs should result in a significant decrease in both parameters. Permutation analysis is a statistical resampling method that investigates a model's degree of overfit. The datasets y-variables are randomly rearranged for a specified amount of times. Separate models are fitted to all new x-y combinations, containing the same number of PCs as the original model. R^2 (coefficient of determination) and Q^2 (predictive ability) of permuted models should be significantly lower than of the original model to demonstrate a low degree of overfit [166, 167].

Linearity, accuracy and robustness of the developed method should also be evaluated. Coefficient of determination R^2, bias (calculated as the residual average), and slope of the correlation plot between predicted and reference values, allow to judge the model's linearity; good linearity is indicated by R^2 and slope as close as possible to 1, and bias and intercept as close as possible to 0. A NIR-specific guideline scale classifies $R^2 < 0.7$ as inadequate [33, 134, 148]. Repeatability of NIRS spectral acquisition (and thus, repeatability of NIRS-predictions) can be analyzed by examining the standard deviation between predictions based on spectra

acquired from the same sample. Furthermore, the ratio of prediction to deviation (RPD), the ratio of prediction error to laboratory error (PRL), and the range error ratio (RER) are useful parameters for model assessment. RPD represents the relationship between the variation in sample population and the models prediction error, calculated as the ratio of reference standard deviation and RMSECV or RMSEP. RPD > 3 is considered successful and RPD < 1.75 inadequate. PRL represents the ratio of RMSEP or RMSECV to the standard error laboratory SEL. PRL should be ≤ 2 for excellent models. RER is calculated as the ratio of calibration sample range (based on reference analytics) and RMSECV or RMSEP. RER ≥ 10 indicates high model utility, 3 < RER < 10 indicates that practical utility is limited [32, 33, 134-136, 148, 168].

1.11.5. Statistical process control[7]

Statistical process control (SPC) allows to identify deviations in process performance by comparing the current variation statistics of real-time process data (i.e. sensor data, process variables, PAT-data, etc.), to a previously established base-case performance, also called common variation. Common variation is caused by numerous (small) disturbances and sensor noise that is considered to be unavoidable but not critical for product quality. Statistics are based on empirical process data from previous campaigns that demonstrated to be under control and yielded product of acceptable quality. Deviations from the common variation statistics indicate an uncommon disturbance that needs to be investigated [169].

While traditional SPC can only monitor one process parameter at a time, multivariate SPC (MSCP) allows to monitor and control complex processes (several parameters at once), through chemometric methods, for example principal component analysis (PCA). PCA evaluates the largest variabilities within a data matrix and summarizes them into principal components (PCs = latent variables). This reduces the number of variables to monitor, separates systematic information from unsystematic variation, and enables the detection of variable-relationships. By comparing PC statistics of the current process to a former *state-of-control* process (i.e. the *common variation*), unusual process-shifts and deviations can be detected. Contribution plots (also called loading plots) can indicate, how each of the original variables contributed to the calculation of the PCs [167, 170]. More details on PCA are provided in section 1.11.4 (page 22 ff.).

Various types of quality control charts are available to visualize the results of (M)SPC analyses. Such charts usually plot numerical values of relevant variables over time and compare them to historical average and standard deviation statistics [167]. Typical examples of process control charts are Shewart charts, CUSUM charts, or EWMA charts. The Shewart chart simply plots process- or latent variables against time together with indications of the target and control limits. Unless stated otherwise, the target is equal to the process average, warning and control limits are set at the 95 % and 99 % limits (i.e. ± 2 and ± 3 standard deviations). Shewart charts have limited ability to detect small process drifts or shifts. An example of a Shewart chart is shown in Figure 8. The CUSUM (*cu*mulative *sum* of differences) chart allows to detect weak and moderate process disturbances, by plotting cumulative deviations from target, instead of individual observations. [158, 167, 171]. The EWMA (*e*xponentially *w*eighted *m*oving *a*verage)

[7] Parts of this section have been previously published in Conference Contribution 1 (see page vi)

chart can be applied to model a dynamic process. By taking memory and drift into account, the detection of memory patterns becomes feasible [167].

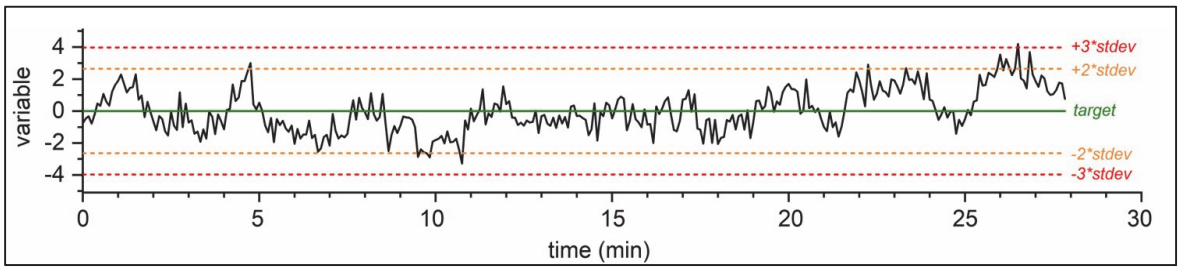

Figure 8 Example of a Shewart control chart with typical warning and control limits in the 95 % and 99 % ranges (i.e. ±2 and ±3 standard deviations).

The appropriate selection of a control chart and process parameters to observe highly depends on the observed process and intended use of the chart. While process control charts are already well-established in other manufacturing industries (e.g. petrol, chemical) and also in clinical trial analysis, their application to downstream pharmaceutical continuous manufacturing is rather new [172, 173].

1.11.6. Orthogonal, redundant process control

In analytics, orthogonal methods refer to two individual procedures that use different principles to analyze the same sample characteristic, for example IR spectroscopy and mass-spectrometry for sample identification, or the utilization of different columns with different bonded phases in HPLC. The aim of using such orthogonal methods can be the ongoing evaluation of the primary method, to assure its constant specificity and accuracy, even if other sample characteristics change over time [174].

Likewise, the principle of orthogonality can be transferred to manufacturing process control. When applying several orthogonal PATs to monitor one critical quality attribute or critical process parameter, the level of security can be increased. This is especially important in continuous manufacturing, where constant fast and accurate process monitoring is essential in order to maintain continuous production with minimal process downtimes and high yields of product, at a pre-defined quality standard. When relying on just one analytical method (e.g. NIRS for water content determination), probe fouling or other unforeseen incident like lamp-failure can require a temporary process shutdown, since quality requirements and a potential real-time-release strategy do not allow the process to be running “blind”. However, if a second, orthogonal method is implemented, it can be feasible to keep the production running while the primary analyzer is fixed. To the author’s best knowledge, the concept of orthogonal process control in pharmaceutical continuous manufacturing has not yet been discussed in literature, up to this date.

2. Aims of the Thesis

Continuous manufacturing (CM) facilitates the design of manufacturing systems that introduce time-dependent processes and hence process controls that can respond to external disturbances in real-time through the appropriate adaption of process conditions. Contrary to traditional batch manufacturing, the CM-approach is much more applicable for real world uncertainty conditions with regard to raw material properties and equipment related imperfections, since no process ever operates in a 'true' steady-state, where all time-derivatives are exactly zero. External variables will vary uncontrollably within a certain range and the introduction of the time-dependent process offers options to react to them dynamically. Furthermore, the intentional variation of certain process conditions (e.g. total material throughput) could increase process design flexibility [28, 169, 175]. Accordingly, CM introduces a new degree of freedom to pharmaceutical manufacturing: the possibility of dynamic operation.

Nonetheless, adaption of process conditions is only worthwhile, if acceptable product quality can be ensured at any time. Therefore, dynamic CM requires a suitable process control strategy in place. Such control strategy needs to consider all relevant sources of variation, monitor product quality in real-time, and facilitate accurate model-based adaption of process conditions in case of quality deviations. In brief, three critical questions need to be answered, to design such a control strategy: *what* to control, *how* to control, and *when & where* to control?

The presented thesis aims to answer these three questions in depth, in order to develop a comprehensive, redundant, variable rate control strategy for downstream CM that enables the production of quality product at all times. In detail, the three main objectives of the presented thesis are as follows:

- To answer *what* to control, the process has to be understood. Therefore, the first part of the thesis aims to identify and quantify critical factor-response relationships between process conditions and product quality attributes, with the intention to generate statistical descriptive process models that form the basis for predictive adaptive control mechanisms. Such mechanisms should be able to cope for uncontrolled process variations and external disturbances, as well as intended variations in total material throughput. Furthermore, the potential for automated process development in CM should be explored.

- To answer *how* to control the process, suitable process analytical technologies (PAT) have to be identified and implemented, to monitor all critical quality attributes (CQAs). Orthogonal process analyzers can ensure the collection of redundant information and hence can avoid 'blind spots' due to unforeseen incidents. Therefore, the second part of the thesis aims to implement, develop, and validate suitable orthogonal PAT methods for CQAs of intermediates or the final product. Further, an appropriate method for data reconciliation should be developed that allows to manage the redundant orthogonal process information, in case of deviations.

- To answer *when & where* to control the process, the system dynamics have to be understood. Therefore, the third part of the thesis aims to investigate the materials' residence time distribution in the manufacturing line at varying process conditions, to allow accurate application of adaptive control mechanisms and precise ejection of out-of-specification product.

While the project focusses on continuous tablet production via twin-screw wet-granulation and continuous fluid-bed drying, the developed strategies and methods intend to act as a general framework for control strategy development that is transferable to other CM processes in the future.

3. Results and Discussion

3.1. Outline

Three main objectives were completed in the presented thesis to develop a thorough and redundant control strategy for pharmaceutical continuous manufacturing (CM) of tablets via twin-screw wet-granulation and continuous fluid-bed drying.

First, the intention of the control strategy was defined, to know *what* to control. Hence, critical quality attributes (CQAs) and corresponding critical process parameters and critical material attributes (CPPs, CMAs) that require close monitoring and control were identified. Empirical quantification of each CPP's and CMA's effects on respective CQAs, generated thorough process understanding and allowed to define descriptive statistical model-based control-actions that can steer the process at variable rates and also in case of quality events. Furthermore, it was demonstrated that automated process development at minimal operator involvement is feasible in CM.

Second, the analytical basis of the control strategy was defined, to know *how* to control the process. Therefore, suitable process analytical technologies (PAT) that can monitor identified CQAs were selected and implemented; accurate and robust methods for each PAT were developed and validated. At least two orthogonal PATs for the monitoring of one CQA were selected, to ensure the collection of redundant information that prevents 'blind spots' due to unforeseen incidents like probe fouling. In order to manage the orthogonal redundant process data in case of disagreement, a method for data reconciliation through multivariate statistical process control was developed.

Third, the system dynamics in regard to the material's residence time distribution (RTD) in the line were investigated, to know *when and where* to control the process. By analyzing how variations in process conditions impact the materials RTD in the line, the materials RTD in future productions can be predicted. Therefore, accurate, predictive adaption of process parameters and precise diversion of OOS material, in case of quality incidents, can be facilitated in the future.

The following sections reflect on each of the described steps in detail and discuss the obtained results. The main focus of the thesis was put on controlling CQAs water content and particle size distribution of the dried granules, as they have the largest influence on drug product quality in the investigated CM process. A minor focus was put on controlling the active pharmaceutical ingredients blend uniformity and content uniformity in the processed blends, granules, and tablets.

All trials were performed with Diclofenac Sodium as a model drug compound, formulated with standard excipients for the production of tablets via wet granulation (see 6.2, page 117 for details). While some of the results are highly product specific (e.g. the developed NIRS methods, the developed statistical descriptive process models, etc.), the general methodology for control strategy development as it is presented, is applicable to any other drug product processed on the investigated CM-line.

3.2. Intention of the control strategy: what to control?[8]

3.2.1. Concept

Figure 9 visualizes the methodology that was applied to define the intention of the process control strategy. A combination of quality-risk-management practices and systematic experimental process analysis allowed to develop statistical process models. The models were then applied to implement compensatory process control actions into the manufacturing plant.

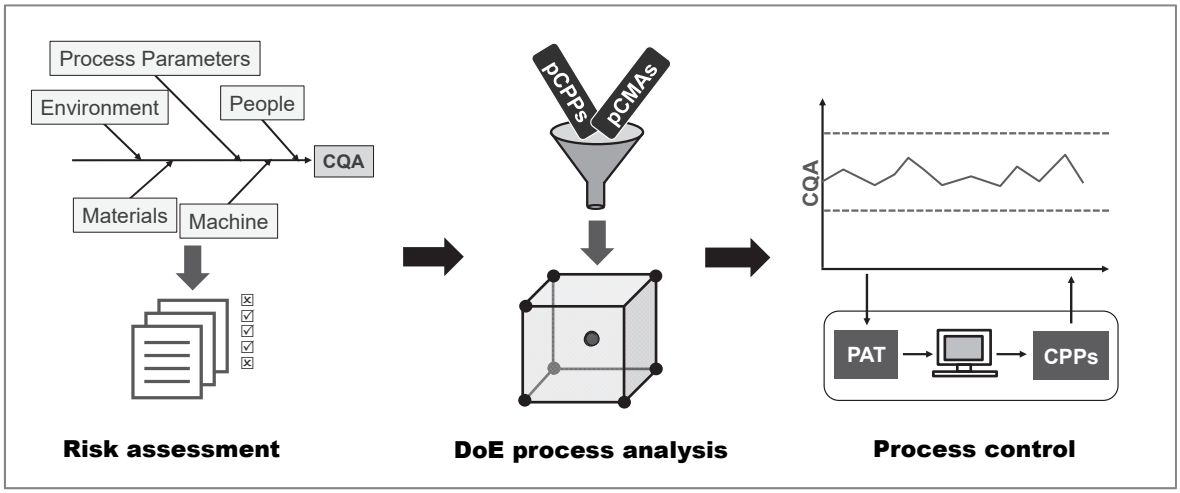

Figure 9: First, identification of critical quality attributes (CQAs) and corresponding potentially critical process parameters and material attributes (pCPPs/pCMAs) through methodological risk assessment was performed. Second, identification of CPPs & CMAs and quantification of their effects on CQAs via DoE-based process analysis was done. Third, statistical process models were implemented to facilitate variable rate control of the process within pre-defined quality limits (PAT = process analytical technology; figure adapted from [22]).

3.2.2. Critical quality attributes

In the case of a continuous wet-granulation - drying - compression process, intermediate CQAs to be controlled are dried granules' water content (specified as loss-on-drying, LOD), particle size distribution (PSD), and active pharmaceutical ingredient (API) content uniformity, as they all directly influence the final drug product CQAs assay, aspect, dissolution rate, content uniformity, and stability [22].

3.2.3. Risk assessment

Since the main focus of the thesis was put on controlling LOD and PSD of dried granules, control of API content uniformity was not considered in this part of the project. However, the same methodology could be applied. To identify all potentially critical process parameters and

[8] Parts of this section have been previously published in Publication 1 (see page v)

material attributes (pCPPs and pCMAs) that could possibly influence intermediate CQAs LOD and PSD, a thorough process risk assessment was performed in two subsequent steps.

First, fishbone analysis of the two process units twin-screw wet-granulation (TSG) and continuous fluid-bed drying (FBD) was completed, as they have the largest influence on LOD and PSD [22]. Consideration of the five sub-categories environment, materials, process parameters, machine, and people in a multi-stakeholder team-exercise, exposed 44 variables in TSG and 23 variables in FBD that could hypothetically influence intermediate CQAs LOD and PSD. The created fishbone diagram of the two process steps is shown in Figure 10.

Theoretically, all of the identified variables are pCPPs or pCMAs. However, as some are not likely to vary significantly during production, each variables' probability of occurrence was judged in a criticality matrix rating in the second step of the risk analysis. Variables with low probability of occurrence were classified as not critical (nCPPs).

In the criticality matrix rating, ten factors were identified to be potentially critical for LOD and/or PSD: seven quantitative pCPPs and three uncontrolled pCPPs/pCMAs. Quantitative factors are process parameters that can be directly manipulated to a precise setting to investigate their influence on CQAs (e.g. liquid feed rate, granulator screw speed). Uncontrolled factors are common variations during production that cannot be set to a desired value (e.g. dryer inlet humidity, which is defined by the room relative humidity, or pre-blend LOD) [22].

All identified pCPPs and pCMAs are listed in Table 1, together with abbreviations for future reference. Detailed justifications for classifying each variable as potentially critical or not critical is included in the supplementary data (see 10.1, Table S 1, page I); more details on the performed risk assessment can also be found in the original publication (see Publication 1, page v).

Table 1: Summary of potentially critical factors in continuous twin-screw wet-granulation and fluid-bed drying as identified during risk assessment.

#	Factor	Abbreviation	Classification	Factor type
01	Solid feed rate	SFR	pCPP	Q
02	Liquid feed rate	LFR	pCPP	Q
03	Granulator screw speed	SS	pCPP	Q
04	Barrel temperature	BT	pCPP	Q
05	Dryer rotation speed	DRS	pCPP	Q
06	Drying temperature	DT	pCPP	Q
07	Drying air flow rate	DAV	pCPP	Q
08	Dryer inlet humidity*	X_{IN}	pCPP	U
09	Pre-blend LOD	LOD_0	pCMA	U
10	Equipment runtime	N/A	pCPP	U

*Q=quantitative factor, U= uncontrolled factor, pCPP= potentially critical process parameter, pCMA= potentially critical material attribute. *dryer inlet humidity corresponds to the room relative humidity, and is controlled by the room monitoring system in the range of 30 – 70 % rH.*

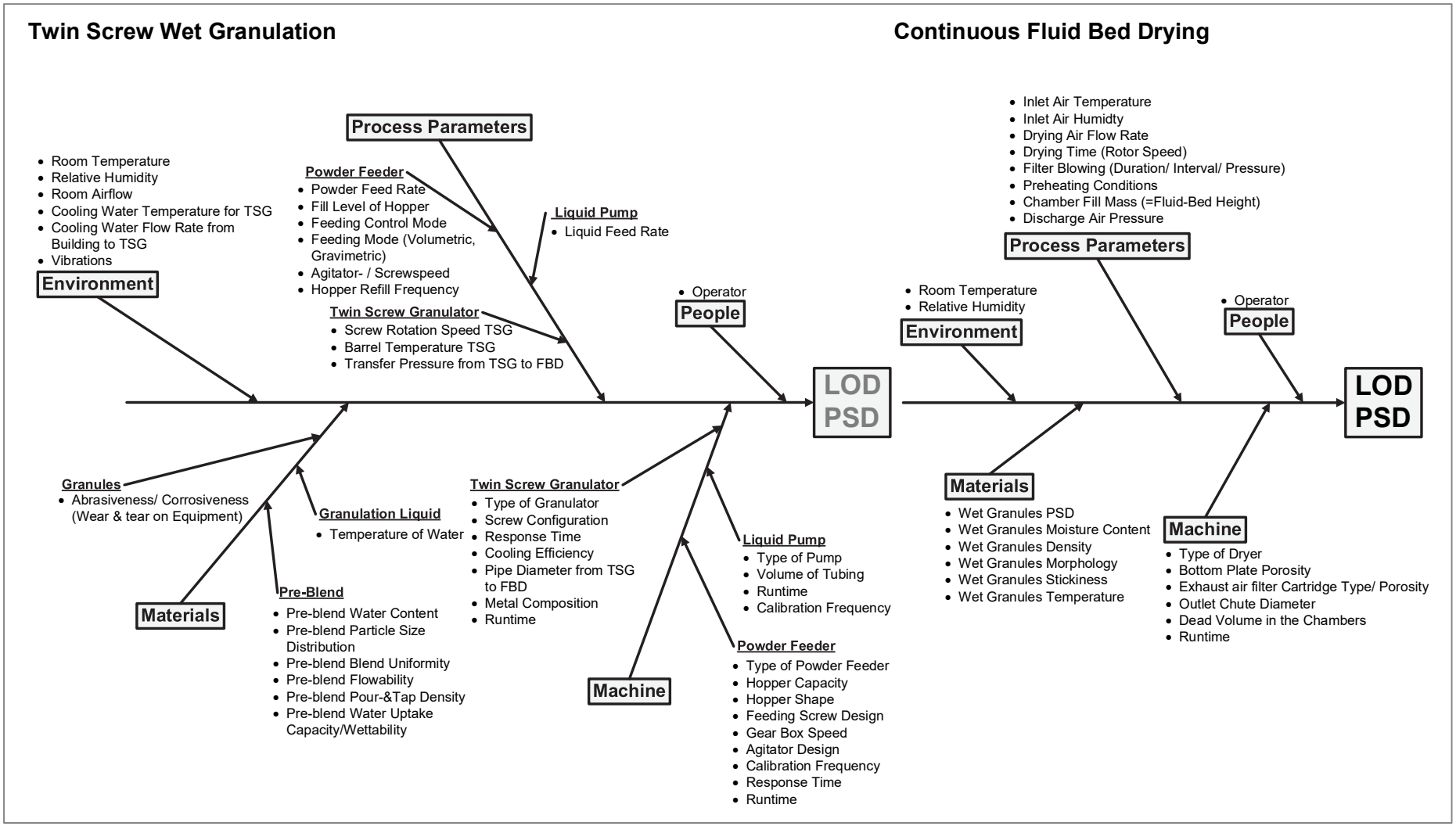

Figure 10: Fishbone analysis of twin-screw wet-granulation and continuous fluid-bed drying in regard to intermediate CQAs LOD and PSD (Figure adapted from [22]).

3.2.4. DoE-based process analysis to identify and quantify CPPs and CMAs

Based on the ten identified pCPPs and pCMAs (see 3.2.3, above), thorough empirical process analysis was performed by means of a screening-DoE and selected follow-up trials. The aim was to identify CPPs and CMAs and to quantify their effects on CQAs LOD and PSD.

Details on the planning, design, process parameter settings, investigated ranges, execution, and analysis of performed experiments were extensively discussed in Publication 1 (see page v), and hence will not be discussed again in detail. In summary, comprehensive understanding of qualitative and quantitative CPP/CMA-to-CQA relationships was established. All tested quantitative factors (see Table 1) demonstrated criticality for either LOD, or PSD, or both; with the exception of barrel temperature, which was hence denoted as not critical. Uncontrolled factors pre-blend LOD and dryer inlet humidity, demonstrated uncritical in the observed range of common variation. They should still be monitored in future experiments, in case the common variation deviates (e.g. due to seasonal changes, new excipient batches, etc.). Equipment runtime was found to be critical within the first twenty minutes after starting a granulation and drying experiment. This was true for experiments starting on clean equipment, as well as experiments starting on "dirty" equipment that was emptied but not cleaned on the previous day. Based on these observations, a transient phase of 20 minutes was defined as standard equilibration time after a setpoint change and before sampling, to ensure statistically significant response-variations are observed in all trials.

Additionally, quantitative process models were fitted from the resulting dataset for all critical factor-response relationships. Their prediction accuracy was demonstrated through four independent test experiments. Control actions for variable rate control of LOD, based on the resulting statistical process models, were implemented and successfully tested.

In summary, a systematic methodology for variable rate control strategy development was established in the presented publication (Publication 1, see page v), that could be applied to other CM-processes in the future.

The concept of variable rate process control will be discussed in more detail in section 3.2.6 (page 42 ff.).

3.2.5. Automated DoE-based process analysis

One of the repeatedly claimed benefits of CM technology is the reduced material consumption in early and late-phase development [2, 10], as process parameters can be changed 'on-the-fly' during a DoE investigation. Hence, in CM the amount of material used per DoE setpoint-combination is defined by the transient time it takes for the process to reach steady-state after a setpoint change, rather than the equipment size, as it is the case in batch development [8, 22]. However, changing parameters simultaneously 'on-the-fly' in a manual manner becomes nearly impossible for operators, when numerous parameters on different process units are investigated, as it was done in the above mentioned screening-DoE experiment (see 3.2.4, above). For example, adapting liquid feed rate 'on-the-fly', is only feasible if it is ensured that solid feed rate is adapted precisely at the same time. Otherwise, too wet or too dry material could enter the dryer and cause sticking in the transfer tubes or clog the dryer air-filters. Furthermore, an

operator manually changing numerous parameters several times in a row, presents a high risk for human error.

To offer a solution to this problem, the "Sequencer"[9] was developed and implemented into the CM-plant process automation system DeltaV. The Sequencer is a software tool that was designed to facilitate the simultaneous adaption of up to ten process parameters from up to eight different process units in up to thirty pre-defined time intervals. A screenshot of the Sequencer's appearance in DeltaV and its functionalities is shown in Figure 11.

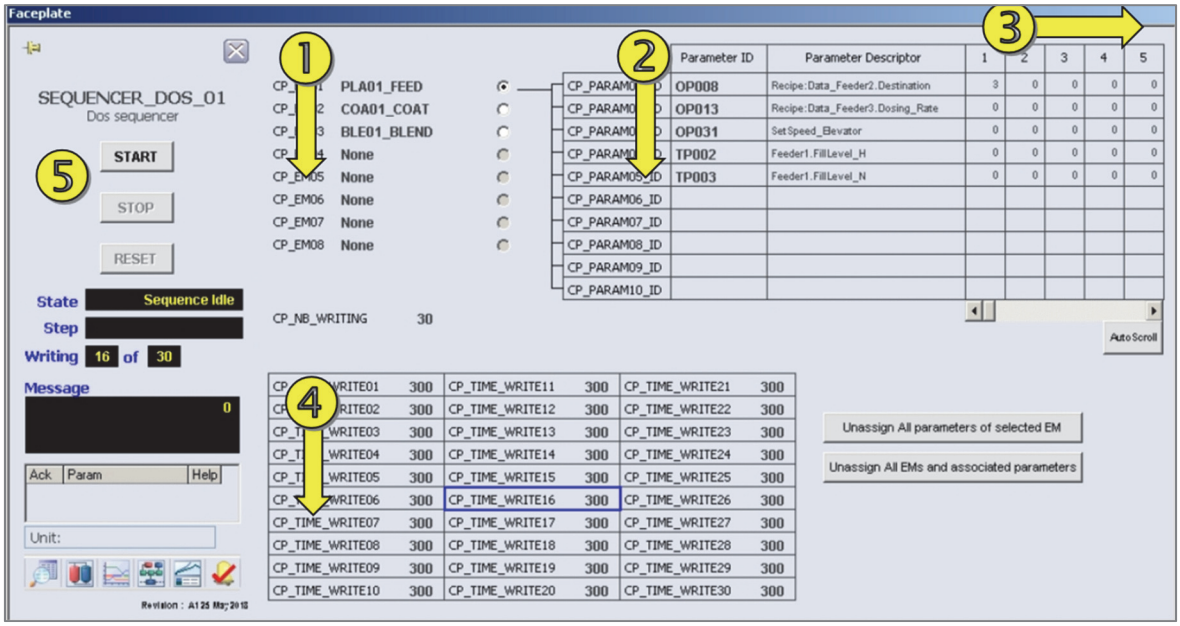

Figure 11: Sequencer for automated DoE-based process development in CM, implemented into DeltaV (example screenshot). Up to eight different process units (1) can be selected and for each process unit, up to 10 process parameters (2) can be defined. For each process parameter, up to 30 setpoint steps (3) can be defined prior to starting the experiment. For each combination of process parameters (called a "writing") a time interval (4) can be defined. Once the Sequencer is started (5), it automatically applies the pre-defined settings to conduct the planned set of experiments.

Based on its design, the Sequencer supports the regularly claimed CM-benefits of reduced material throughput during development and additionally can reduce operator involvement. Hence, it can decrease development costs and the potential for human error, since all experimental steps can be cautiously selected and checked beforehand.

To demonstrate the legitimacy of these claims, the earlier described DoE-based investigation on identified pCPPs/pCMAs (see section 3.2.4, page 34 ff.) was repeated in a fully automated approach through the Sequencer. To allow higher material throughputs in this 'auto-DoE' trial, the investigated factor levels of DAV were slightly increased and the investigated range on DRS and SS was widened, compared to the initial screening-DoE design. Barrel temperature and runtime were not investigated again.

[9] Programming and implementation of the designed Sequencer into DeltaV was executed by CM-Unit internal automation engineers.

Accordingly, a fractional factorial DoE-design with 2^{6-2} =16 experiments plus three repetitions at center point settings was designed from six quantitative factors and two uncontrolled factors. Center point settings matched the standard process parameters as listed in section 6.4.6 (page 121), an overview of the investigated ranges is shown in Table 2. One additional trial at 80 m^3/h drying air volume, and two additional trials at 11 & 23 rph dryer rotation speed were added to increase the resolution on both factors (all other CPPs were kept constant at center point settings during these additional trials). Furthermore, three test-trials were performed to evaluate the prediction accuracy of the resulting process models. Process parameters for these test trials were selected from within the factor space of the auto-DoE (i.e. from between the +/- limits).

Table 2: Overview of investigated ranges in the automated DoE trial ('auto-DoE')

Factor	Factor	Abbreviation	Range (+/-)	Unit
Solid feed rate	Q	SFR	3.0 to 5.0	kg/h
Liquid feed rate	Q	LFR	1.0 to 1.4	kg/h
Granulator screw speed	Q	SS	300 to 600	rpm
Dryer rotation speed	Q	DRS	5 to 29*	rph
Drying temperature	Q	DT	70 to 90	°C
Drying air flow rate	Q	DAV	100 to 140 and 80**	m^3/h
Dryer inlet humidity	U	X_{IN}	monitored	g/kg
Pre-blend LOD	U	LOD_0	monitored	%

*Q=quantitative factor, U= uncontrolled factor; *additional trial at 11 & 23 rph added to increase resolution; ** additional trial at 80 m^3/h added (remaining CPPs kept constant at center point settings)*

The duration of each DoE-trial was defined by the previously specified standard equilibration time of 20 minutes [22] plus the respective rotation speed, as one full rotation of granules (i.e. 10 process chambers) was sampled for IPC analysis after equilibration was finished and before the next setpoint combination was applied by the Sequencer (e.g. 20 + 3.5 minutes = 23.5 minutes trial duration for a trial at 17 rph DRS). Trials were split between two consecutive days, test-trials were performed on a third day.

A detailed overview of all trials, run order, heating- & cooling steps, process times, and IPC results of the collected samples is added in the supplementary data (see 10.2, Table S 2, page IV). Data transformation (log_{10} transformation of response data), DoE-analysis, and model refinement were done in analogy to the initial screening-DoE as described in [22], to generate four independent process models for LOD, PSD X10, PSD X50, and PSD X90.

The summary of fit of the four models is illustrated in Figure 12, with all model performance indicators being in the range for good models (i.e., (R^2-Q^2) < 0.3; Q^2 > 0.5; validity > 0.25; reproducibility > 0.5, according to [105]). The low model validity in LOD is caused by the high model reproducibility (> 0.99) and hence of no concern. Uncontrolled factors pre-blend LOD and inlet humidity X_{IN} (= roomy relative humidity) were found to be not critical in the investigated range. Coefficient plots of the final models are included in the supplementary data (section 10.2, Figure S 1, page III).

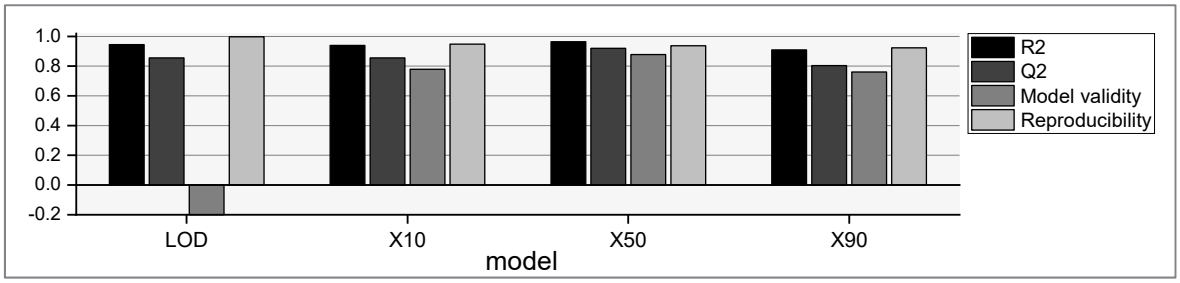

Figure 12: Summary of fit for LOD and PSD process models. All models demonstrate good model performance (defined as (R^2-Q^2)< 0.3; Q^2 > 0.5; validity > 0.25; reproducibility > 0.5, according to [105]). Observed low model validity in LOD is caused by the very high model reproducibility (> 0.99) and hence of no concern.

Furthermore, all models demonstrated good prediction accuracy, as shown in Figure 13, where predicted responses from the three test trials are compared to observed responses based on IPC measurements.

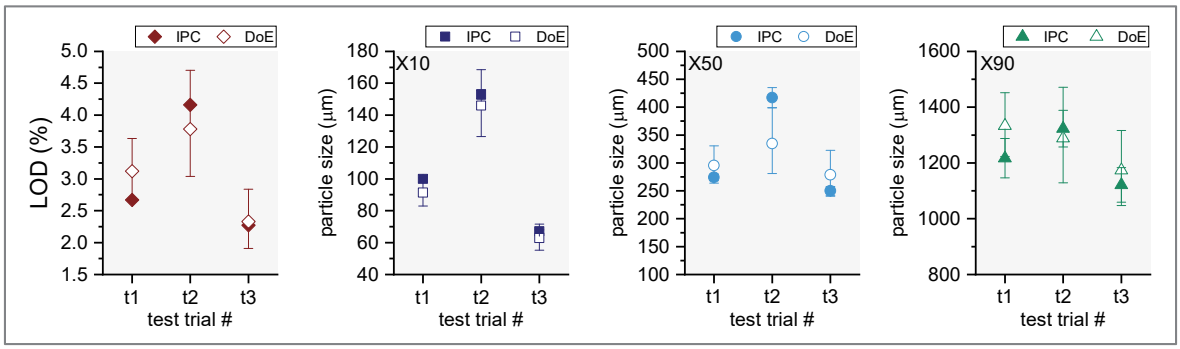

Figure 13: Observed responses in the three performed test trials, compared to predicted responses to evaluate the auto-DoE models predictions accuracy. The error bars indicate the models prediction accuracy.

In summary, a total runtime of 17.6 h was required to perform 22 automated DoE experiments, during which good process models with acceptable prediction accuracy were generated. The total calculated runtime includes heat-up and cool-down phases and equilibration times after changing process parameters. Overall, less than 40 kg of powder blend were consumed with all trials, corresponding to less than 10 kg of API. In contrast, batch processing times of a similar trial can take several days to weeks, and the material consumption is usually much larger, as it has to be adapted to the equipment size [2, 10]. Consequently, the performed auto-DoE successfully demonstrated that automated development in CM can minimize the overall process time and material consumption. Good experimental results were found, while less than 10 kilograms of API were consumed.

Nevertheless, the described automated setup still required regular operator attention for manual sampling and offline IPC analysis. Whereas, when combining Sequencer-driven automated DoE process analysis with suitable online PAT-technologies for CQA monitoring, this could be avoided.

To evaluate this approach, IPC results were compared to the analysis results from different available PAT-methods. For LOD, corresponding PATs NIR spectroscopy (NIRS) and mass- and energy balance (MEB) calculations were considered; for PSD, NIRS was considered as a feasible on-line PAT. Details on the development and validation of these PAT-methods are provided in section 3.3 (page 49 ff.).

Accordingly, Figure 14 A illustrates the comparison between IPC LOD results, NIRS predictions, and MEB calculations from each performed auto-DoE experiment. PAT-results are plotted as the observed average and standard deviation of the method, during the respective IPC-sampling time. To allow a more systematic comparison, Figure 14 B plots the measured vs. predicted correlation for IPC-NIR and IPC-MEB.

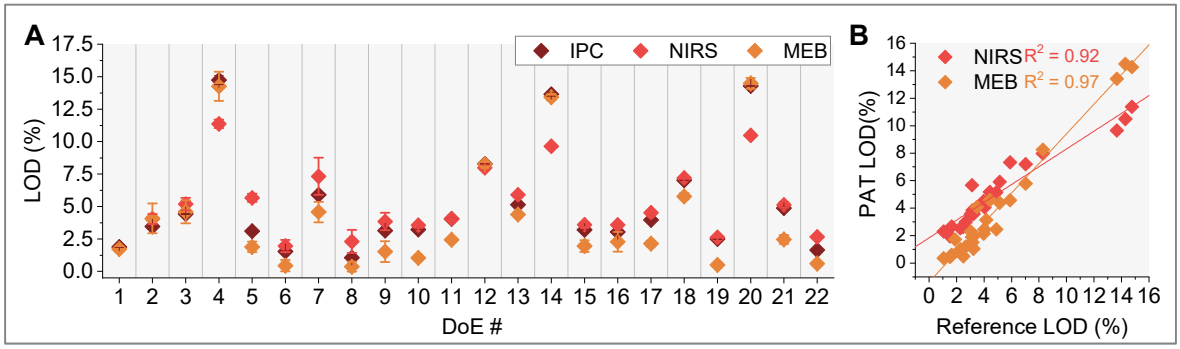

Figure 14: A: Direct comparison between IPC LOD measurement and PAT for each DoE-trial. B: Observed (IPC) vs. predicted (PAT) plots. For NIRS-IPC correlation, $R^2 = 0.92$, Bias = -0.05, Slope = 0.65, Intercept = 1.83; for MEB-IPC correlation, $R^2 = 0.97$, Bias = 0.99, Slope = 1.08, Intercept = -1.38.

Overall, good agreement between IPC and the two PAT methods NIRS ($R^2 = 0.92$) and MEB ($R^2 = 0.97$) was found. Since the NIRS method was developed for LOD ≤ 11 %, deviations above 11 % moisture content are expected (see DoE trial # 4, 14, and 20 in Figure 14). For samples ≤ 11 % LOD, the average absolute difference NIRS-IPC was ± 0.7 % LOD, the maximum observed difference was + 2.6 % (see DoE # 5). Potential reasons, for those deviations can be probe fouling, too short spectral filtering times, or poor sample presentation (see section 3.3.2.2, page 57 ff. for details). For MEB, the average absolute difference to IPC was ± 1.0 % LOD, the maximum difference was - 2.4 % (DoE # 21 in Figure 14). Potential reasons for MEB's tendency to report too low LOD values in some cases will be discussed in more detail in the next chapter (see 3.3.2.1, page 50 ff.).

The same comparison was conducted for PSD. Figure 15 compares IPC PSD results with NIRS predictions (No IPC results are available for DoE# 7, 14, and 20, as granules were too coarse). When considering the overall trends, good agreement between IPC PSD and NIRS was found (see Figure 15 A). However, when considering the direct correlation between observed (IPC) and predicted (PAT) results, correlation is poor with $R^2 = 0.53$, 0.45, and 0.01 for PSD X90, X50, and X10, respectively (see Figure 15 B). Those observed deviations in NIRS prediction might be due to the calibration range of the NIRS methods and the sample presentation in front of the probe. This will be discussed in more detail in section 3.3.3.1 (page 64 ff.).

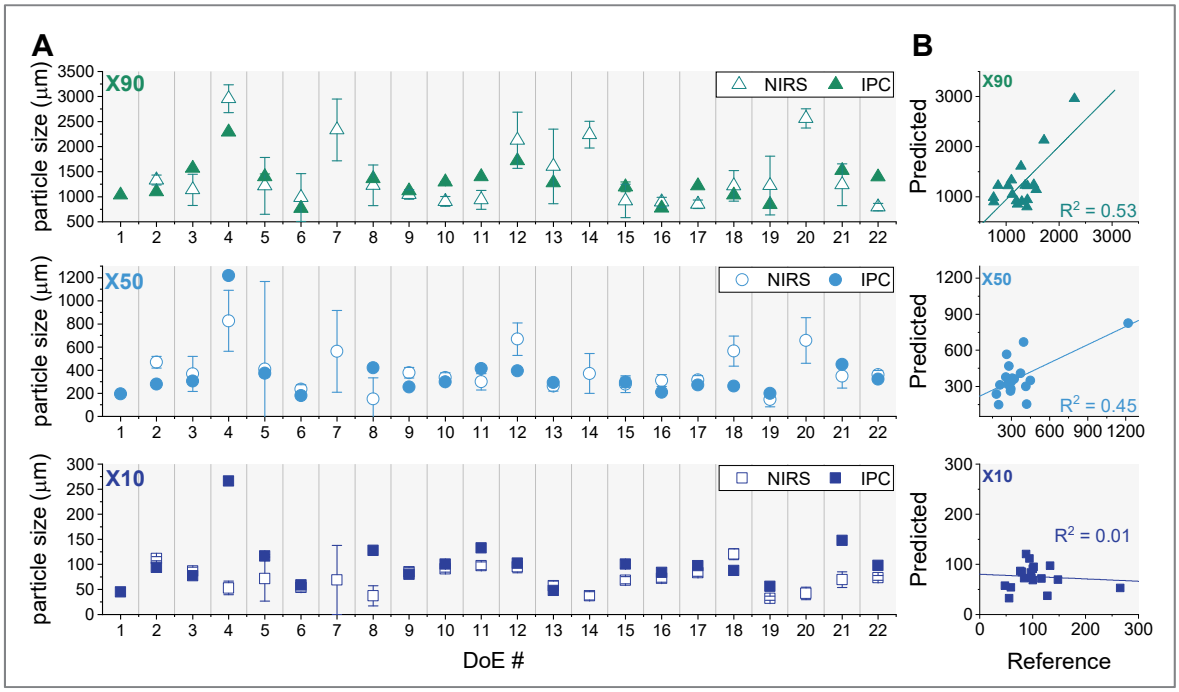

Figure 15: A: Direct comparison between IPC PSD measurements and PAT (No IPC results available for DoE# 7, 14, and 20, as granules were too coarse; no NIRS data available for DoE# 1, due to technical issues). B: Observed (IPC) vs. predicted (PAT) plots. For PSD X10: Bias=28, R^2=0.01, Slope=-0.05, Intercept=80; for PSD X50: Bias=-16, R^2=0.45, Slope=0.50, Intercept=194; for PSD X90: Bias=37, R^2=0.53, Slope=1.06, Intercept=-117.

To further investigate, if it is feasible to generate accurate process models from the PAT-based LOD and PSD X10, X50, and X90 results, regression models were fitted to each corresponding factor-response dataset. Each model contained the same model terms as the original IPC-model, and the response datasets were also $\log_{10}$-transformed (see Figure 12, page 37, for the IPC-based summary of fit). The resulting PAT-based model coefficients and confidence intervals are summarized and compared to the IPC-based models in Figure 16; model performance indicators for each fitted model are listed in Table 3.

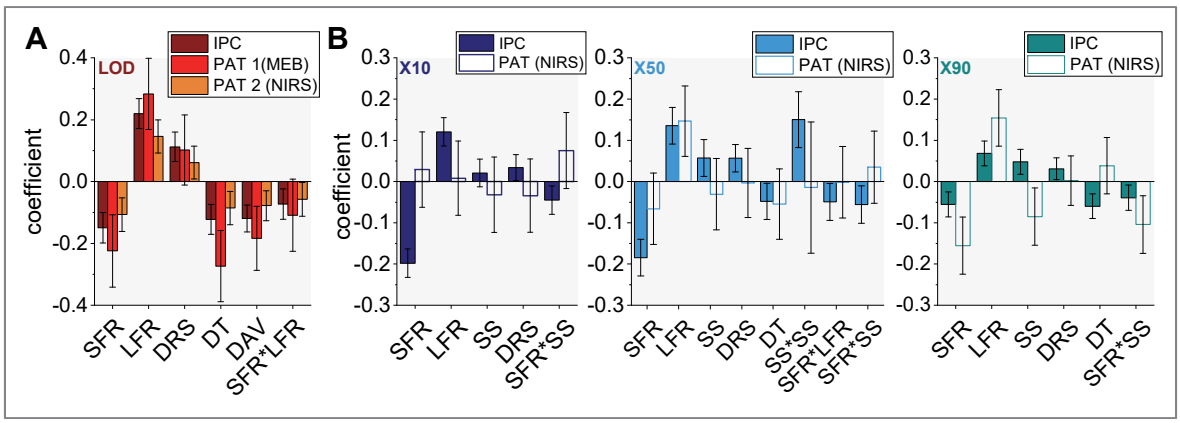

Figure 16: Comparison of coefficient plots for each regression model (coefficients were scaled and centered). Good comparability was found between IPC and PAT-based models for LOD. No significant models could be fitted to PSD NIRS-data for X10 and X50. For PSD X90, an acceptable model was fit (according to the model performance indicators, see Table 3), but results contradict the IPC model terms in the case of SS, DRS, and DT.

Regarding LOD, the coefficient plots show good comparability between the three models (see Figure 16 A). Even though the model terms' coefficients and significance levels vary between IPC and PATs, model performance indicators demonstrate good performance for both PAT models (see Table 3).

Regarding PSD X10 and X50, no significant correlation was found between DoE-settings and NIRS results. Regarding PSD X90, the fitted model is acceptable according to the performance indicators R^2=0.75, validity=0.75, and reproducibility=0.82. Nevertheless, Q^2=0.34 is out of the acceptance range and the coefficients for screw speed, dryer rotation speed, and drying temperature contradict the IPC-based model (see Figure 16 B). Consequently, NIRS-based PSD control is not accurate enough for automated PAT-based process model development. Its applicability for routine process monitoring, to observe trends and sudden changes in PSD (as demonstrated by Figure 15) will be discussed in more detail in section 3.3.3.1 (page 64 ff.).

Table 3: Summary of fit for each of the fitted IPC and PAT models on LOD and PSD (Good model performance being defined as (R^2-Q^2)< 0.3; Q^2 > 0.5; validity > 0.25; reproducibility > 0.5, according to [105]).

	LOD			PSD X10		PSD X50		PSD X90	
	IPC	NIRS	MEB	IPC	NIRS	IPC	NIRS	IPC	NIRS
R^2	0.94	0.86	0.88	0.94	0.24	0.97	0.64	0.91	0.75
Q^2	0.86	0.65	0.67	0.86	-0.20	0.92	-0.20	0.80	0.34
Model validity	-0.20	0.93	0.78	0.78	0.52	0.88	0.64	0.76	0.75
Reproducibility	1.00	0.71	0.89	0.95	0.82	0.94	0.81	0.92	0.82

To further analyze the three obtained LOD-models (IPC vs. NIRS vs. MEB), each CPP's average effect on LOD was assessed; calculated as the inverse of the ratio between DoE-examined CPP-range ($CPP_{high/low}$) and the predicted LOD span at these high and low CPP-setpoints ($LOD_{highCPP/lowCPP}$), as shown in eq. 4.

eq. 4 $$\frac{LOD_{highCPP} - LOD_{lowCPP}}{CPP_{high} - CPP_{low}} = average\ effect\ \left[\frac{\%LOD}{CPP\ unit}\right]$$

Since the regression models were fit to $\log_{10}$-transformed y-datasets and contain interaction terms and/or quadratic terms, the calculated average effect is not equal to the respective CPPs model coefficient. Nevertheless, it allows suitable approximation of the average quantitative CPP-to-LOD relationship in the investigated range.

This hypothesis was confirmed by a COST-approach trial (changing one factor setting at a time, in contrast to DoE) on DRS, DT, and DAV. In this trial, parameter settings were varied individually and sequentially within their respective high and low setpoints to analyze the individual effect on LOD. The results from the COST-approach trial are summarized in Figure 17; calculated average effects (according to eq. 4) from all three DoE-based LOD models (IPC, NIRS, and MEB) and observed average effects (calculated as observed effect-span over analyzed CPP-range, in analogy to eq. 4) from the COST-approach trials are summarized in Table 4.

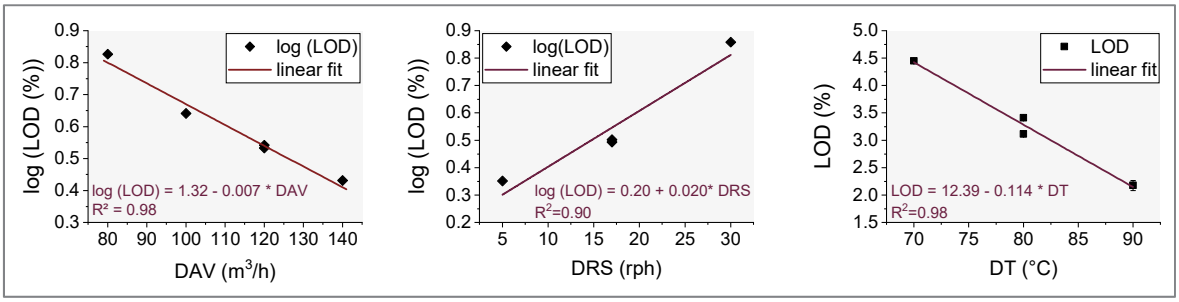

Figure 17: Summary of the performed COST approach trial, where process parameters DRS, DT, and DAV were varied individually and sequentially within their respective high and low setpoints, to analyze their individual effect on LOD.

Table 4: Comparison of average factor effects in %LOD per CPP-unit, based on the three different process models

CPP	Range	DoE by IPC	DoE by NIR	DoE by MEB	COST	unit
SFR	3 – 5 kg/h	-1.37	-1.13	-1.27	N/A	%LOD/(kg*h^{-1}) SFR
LFR	1.0 – 1.4	10.31	7.81	8.23	N/A	%LOD/(kg*h^{-1}) LFR
DRS	5 – 29 rph	0.09	0.05	0.05	0.09	%LOD/rph
DT	70 – 90 °C	-0.11	-0.09	-0.16	-0.11	%LOD/°C
DAV	100 – 140	-0.05	-0.04	-0.05	0.04	%LOD/(m^3*h^{-1})

The comparison in Table 4 demonstrates that, no matter the experimental approach, or the analytical method (i.e. DoE vs. COST and IPC vs. PAT), the resulting average effects are comparable. The COST-approach confirmed that fractional factorial DoE-investigations are suitable to generate reliable and accurate process models.

Hence it was established that a fully automated DoE-based process analysis by the Sequencer in combination with PAT-based CQA analysis in real-time is feasible, in the case of LOD. While NIRS methods are highly product specific and need to be developed beforehand, MEB is merely equipment specific and hence can aid in process development from the start (Different possibilities to improve the two selected PAT methods for LOD control will be discussed further in the next chapter; e.g. improved sample presentation for NIRS or improved heating/cooling procedures of the FBD to minimize the effect of thermal equilibration times on MEB).

Regarding PSD, other online or at-line PAT-options need to be investigated in the future. Laser diffraction was initially selected as a second, orthogonal PAT-method in this project. However, the instruments applicability is restricted to samples with particle sizes < 1700 µm. Hence, DoE-analysis based on LD was not possible, as samples' PSD exceeded this limit. LD could be a feasible PAT-option for PSD monitoring after a milling step. Other possible examples for online or at-line PAT that could be applied in the future for automatic DoE-analysis, include dynamic image analysis, focused beam reflectance measurement, or spatial filtering velocimetry [121-123].

To further increase development efficiency, the performed auto-DoE on granulation and drying could also be combined with the successive process-units milling, tableting, and coating. Automatic on-line and at-line PAT tools for tablet quality are already commercially available (e.g. NIRS for API content uniformity, analysis of compression force for tablet weight, or auto-sampling devices that frequently analyze tablet hardness, weight, and thickness [176-180]). This will be assessed in more detail in the future.

Altogether, many of the frequently claimed CM-benefits were confirmed to be true by the presented data: reduced development times at lower material consumption (here: 2 days and less than 10 kg of API for a full scale development campaign), reduced lag-times and cleaning efforts between process steps (here: none), and minimal manual handling hazards for operators (here: API dispensation at the beginning and granule sampling at the end for PSD and LOD analysis). Those benefits provide a strong argument for CM: even though PAT method development and validation might consume time and resources prior to starting the automated process development; the reduced API consumption, and overall reduced need for time and resources will outweigh these drawbacks in the future.

Consequently, CM-process development in a fully automated "lights-out"-operation seems feasible and highly beneficial for the future. The process models established from such an autonomous development campaign could then be adapted and improved in a next step through a model-predictive control algorithm (MPC) that learns from current data and guides the process within its quality limits during routine production.

3.2.6. Application of statistical descriptive models for process control

The previous sections described and established a systematic methodology to identify and quantify critical process parameters, with the aim to generate descriptive, DoE-based, statistical process models. These models for once increase process understanding. Furthermore, they form the basis for compensatory control actions in a process control strategy. Compensatory control actions can ensure consistent product quality within specified limits at all times, when combined with adequate PAT instruments that monitor the process state in real-time.

To demonstrate the implementation of such model-based compensatory control actions, three separate experiments were performed: first, predictive variable rate process control was demonstrated; second, controlled process-ramp-up was demonstrated; and third, automated PAT-based predictive feedback-control of the dryer in real-time was demonstrated. The results are summarized below. Details on the selected PAT analyzers are provided in the next section (see 3.3, page 49 ff.).

Predictive variable rate process control

Predictive process control at variable rates of material throughput is of high interest in CM, as it can improve overall runtime of a chain of unit operations. Unplanned production breaks can generate transient conditions, potentially leading to out-of-spec (OOS) material; hence, they are not desired. In reality however, fouling of probes, wear-out of equipment-pieces, or other unforeseen incidents are not preventable at all times. A feasible alternative to stopping the whole line is the implementation of decoupling elements (buffers) that allow to temporarily decouple a certain unit operation from the continuous process, while other unit operations are kept running in controlled state. To avoid overfilling of the buffers during incident-management, decreasing the total material throughput rate $\dot{m}_{tot}$ might be necessary. Likewise, briefly increasing $\dot{m}_{tot}$ for rapid filling of a decoupling-element could facilitate preventive cleaning of certain equipment at pre-defined time points (e.g. the transfer tube between TSG and FBD).

However, scaling $\dot{m}_{tot}$ during continuous production is only worthwhile, if dried granules' CQAs will remain within their specification limits at all times. Since LOD demonstrated to be a linear function of $\dot{m}_{tot}$ with a slope of +1.2 %LOD/(kg/h) [22], 'simply' scaling the production

throughput at constant process parameters is not feasible. Instead, predictive compensatory control actions of CPPs have to be applied, to keep LOD constant at varying throughput rates.

To demonstrate this approach a set of experiments was performed. A detailed description of conducted trials and results has been previously published in Publication 1 (see page v). In summary, predictive (model-based) adaption of dryer rotation speed (DRS) and drying air flow (DAV) could successfully compensate the influence of varying throughput rates on LOD. By varying DRS between 5 – 29 rph and DAV between 85 – 150 m^3/h, LOD was controlled within pre-defined quality limits (target ± 0.5 % LOD), even though material throughput was varied between 2.6 – 7.8 kg/h. In contrast, LOD deviated by ± ~3 % LOD from target, when $\dot{m}_{tot}$ was scaled without compensatory control. The results are summarized in Figure 18. The applied DRS- and DAV-model terms as listed in Figure 18, are based on the initial DoE-trials published in Publication 1 [22].

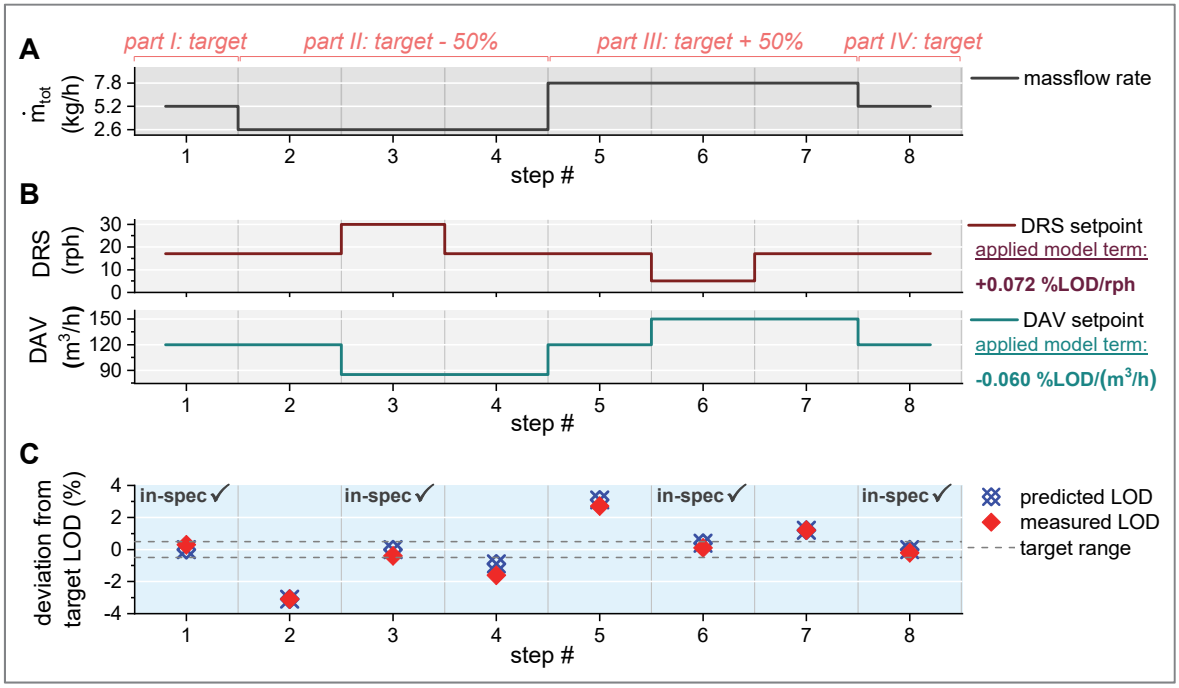

Figure 18: demonstration of variable-rate model-based control of LOD via DAV and DRS: when total massflow rate $\dot{m}_{tot}$. (A) is decreased by 50% from target, at constant DRS and DAV (B), LOD (C) decreases accordingly (see part II: step #2). Through model-based adaption of CPPs DRS and DAV, it was possible to control LOD back to the initial target range (see part II: step #3), while solitary adaption of DAV without DRS was not sufficient (see part II: step #4). Similar results were obtained when increasing massflow rate (see part III: step #5-#7. Figure adapted from [22].

Demonstration of controlled process start-up

The current internal standard procedure for process start-up consists of pre-heating the empty FBD for 2 hours at the intended drying temperature, before granulation and drying is started with constant process parameters. This procedure results in over-dried granules within the first few rotations. This is due to the stainless-steel drying chamber approximating the set inlet air temperature during pre-heating, and subsequently dropping down to the real process temperature once compensatory evaporative heat loss cools down the process temperature equilibrium. Hence, once granulation and drying is started, the dryer requires a certain time for this

thermodynamic equilibration, until the chamber heating and the evaporative heat loss are balanced, and granule LOD remains stable over time. This dynamic behavior is illustrated in Figure 19, which shows the dried granule's LOD in regard to process run-time (at constant process parameter settings). LOD was found to be outside of its acceptance limits during the first fifteen minutes of process time and continued to increase slightly for approximately 2 hours, before thermal equilibration between the heated stainless-steel chamber and the evaporation-based cooling was achieved.

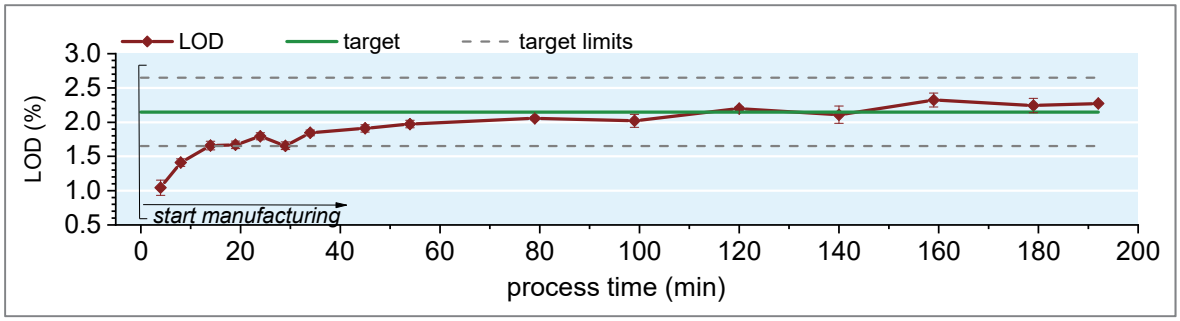

Figure 19: LOD-dynamics during process start-up after 2 hours of FBD pre-heating, according to the current internal standard protocol (t = 0 min being the manufacturing start). Acceptance limits are defined as target ± 0.5%, with target = dry-blend LOD = 2.15%.

Model-based adaption of dryer rotation speed (DRS) should allow to compensate this excessive heat-capacity in the drying chamber during start-up: at higher DRS, the granule's drying time is shorter, which could compensate the increased drying capacity of the steel chamber, and in turn, keep dried granules' LOD within specification limits from the start. To test this hypothesis, a follow-up experiment was performed, as described below.

To facilitate model-based adaption of DRS, an automated "DRS-ramp"[10] was introduced into the process-control system DeltaV. The DRS-ramp automatically initiates a pre-defined ramping procedure of DRS, as soon as wet granules enter the first drying chamber at manufacturing start. The ramp-height (+ 8 rph) and slope (0.80 rph/min) were defined based on the experiment from Figure 19 and similar pre-trials. Figure 20 A illustrates the ramping-procedure; Figure 20 B illustrates the response in dried granule's LOD, where it is confirmed that LOD remained within its specification limits from the start.

Generally, the height of the ramp and the slope still leave room for improvement in the future and have to be re-evaluated for any other product or drying settings. Moreover, other options to improve manufacturing start-up could be explored, like model-based adaption of drying air flow (DAV) instead, or in addition to DRS. Also, the pre-heating protocol itself could be changed, to avoid excessive pre-heating of the stainless steel chamber in the first place (i.e., by decreasing the pre-heating time to 1 hour, or by pre-heating until the expected outlet temperature during drying is reached).

[10] Programming and implementation of the designed DRS-ramp into DeltaV was executed by CM-Unit internal automation engineers.

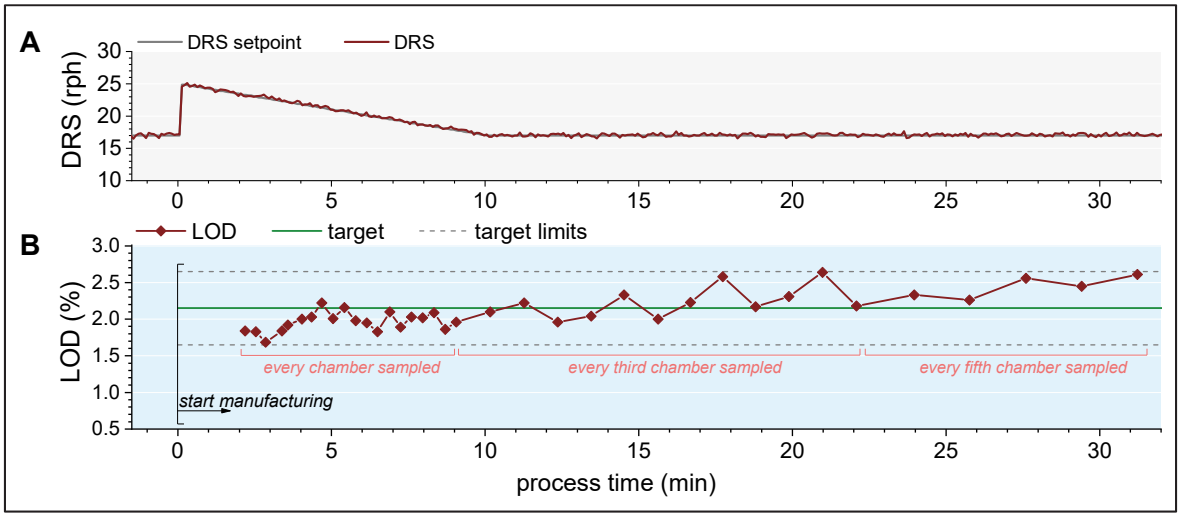

Figure 20: Predictive, model-based adaption of DRS (see A) during process start-up allows to control LOD within its specification limits (target limits) from the start (see B). For the first two rotations, every chamber was sampled and analyzed; later on only every third and then fifth chamber was sampled and analyzed.

While the trial was stopped after 32 minutes, since proof-of-concept for predictive start-up control was achieved, and LOD was found within its specification limits (see Figure 20 B), LOD still showed an ongoing upwards trend at this point. This is in line with the results from Figure 19, where thermal equilibration was only achieved after approximately 2 hours.

Therefore, it would be recommended as a next step, to combine model-based start-up control with PAT-based feedback control. This could enable the adaption of process parameters based on real-time LOD results, once the start-up phase is completed. PAT-based feed-back control from the very beginning of the process is not possible, if the location of the PAT-instruments causes time-delays between the physical drying process and the PAT-reading, as it was the case with the current setup (the NIRS was mounted at the dryer outlet, leaving it "blind" during the first rotation after manufacturing start). Therefore, the DRS-ramp during start-up has to be defined based on historical data; real-time PAT-based feed-back control could then take over once granules exit the dryer. Another option for the implementation of PAT-based feedback control is given in the next example.

Demonstration of PAT-based predictive feedback-control in real-time

In the previous two examples of model-based process control, process parameters were adapted based on offline IPC-measurements, or based on historical data that gave insights into the dynamic process behavior. In the next example, the developed descriptive process models were combined with real-time PAT-analyzers to facilitate PAT-based predictive feed-back control of LOD in real-time.

Therefore, a "PAT-Controller"[11] was designed and implemented into the process automation system DeltaV. It enables LOD control through the adaption of process parameters DRS and/or DAV, based on two different PAT-methods. In detail, either NIRS or MEB calculations were

[11] Programming and implementation of the designed PAT-Controller into DeltaV was executed by CM-Unit internal automation engineers

applied as PAT (see section 3.3.2, page 50 ff. for details on the PAT methods). The Controller compares the current PAT-based LOD with a pre-defined target-LOD, and adapts DRS and/or DAV accordingly, based on the previously established statistical process models. The aim of the Controller is to keep LOD as close as possible to the target value. Applied model terms for DAV and DRS are listed in Figure 18; the adaptable CPP-range was limited to 5 – 29 rph and 80 – 160 m^3/h, respectively.

In the first trial on the Controller, LOD control through the adaption of DRS, based on NIRS was investigated. Initially, the Controller was turned on at constant process conditions (see 6.4.6, page 121, for standard process parameters), to test if it remains stable when LOD remains constant. Later on, it was enabled while the granulation liquid feed rate was actively increased from 1.2 kg/h to 1.3 kg/h, to test if it is able to adequately compensate the induced process variation. Results are summarized in Figure 21.

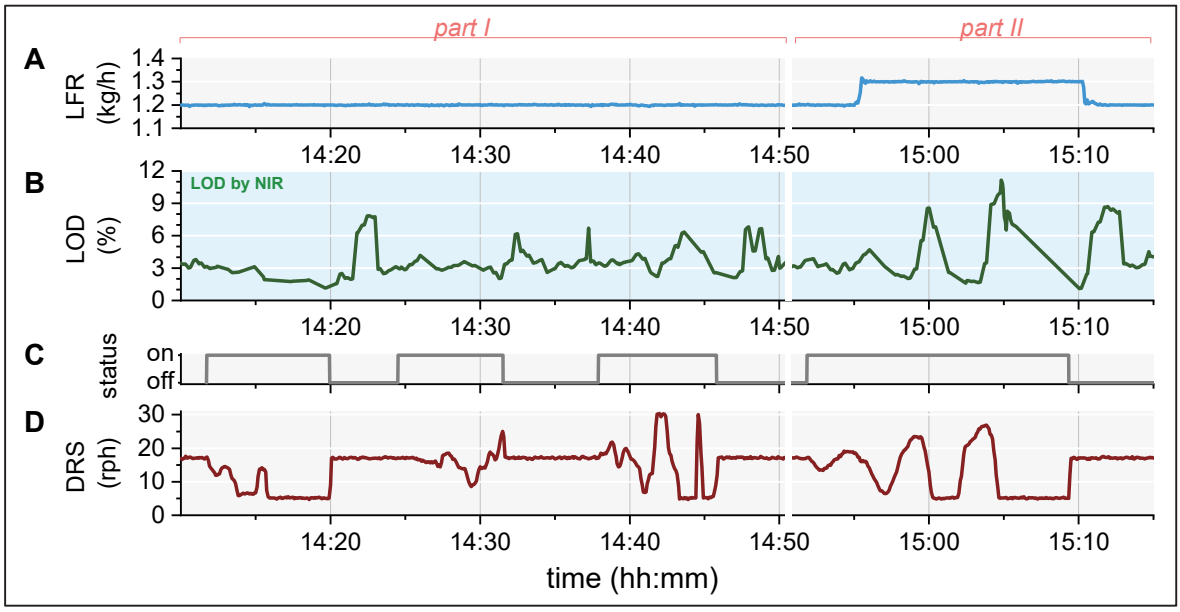

Figure 21: LOD control via NIRS by DRS. A: liquid feed rate; B: LOD of dried granules measured by NIRS; C: Controller status on/off; D: dryer-rotation speed (when Controller was off: DRS=17 rph; when Controller was on: DRS was adapted based on the current NIRS-LOD reading). In part I of the trial, the Controller behavior at constant process conditions was investigated. In part II, LFR was increased from 1.2 to 1.3 kg/h, to investigate if the Controller can adapt DRS accordingly.

In this trial, it became obvious that process control via NIRS and DRS was not successful with the current setup. Even in stable process conditions (Figure 21, part I), the Controller adapted DRS constantly and very aggressively. Generally, harsh variations in DRS cause huge variations in granule drying times (5 – 29 rph ≙ 9.6 – 1.7 minutes drying time), which in turn created massive fluctuations in dried granules' LOD. As a result, the Controller started to resonate between extreme DRS-settings and was unable to stabilize LOD (see Figure 21 B and D).

The same phenomenon was observed in the second part of the trial, where the liquid feed rate was increased (Figure 21, part II). It was hence concluded, that the combination of NIRS based DRS control is not feasible with the current Controller design. Especially the lag-time between the actual drying process (primary drying is done in the first 1-2 chambers of the rotation [22]), and the huge fluctuation in LOD caused by fluctuating drying times, caused enormous issues.

Improvements in the future could be made by decreasing the Controller aggressiveness (i.e. decrease the model term, better filtering of NIRS LOD data) or the implementation of lag-times and ramping-procedures during DRS adaption.

In the second trial on the Controller, LOD control through the adaption of DAV based on MEB was investigated. Initially, liquid feed rate was increased from 1.1 to 1.2 kg/h, while the Controller was enabled (all other process parameters were kept at standard settings, as listed in section 6.4.6, page 121), in order to test if it is able to compensate the induced variation in liquid feed rate. Then, the Controller was disabled and LFR was increased again, to investigate the impact on LOD without adaptive feed-back control. Results are summarized in Figure 22.

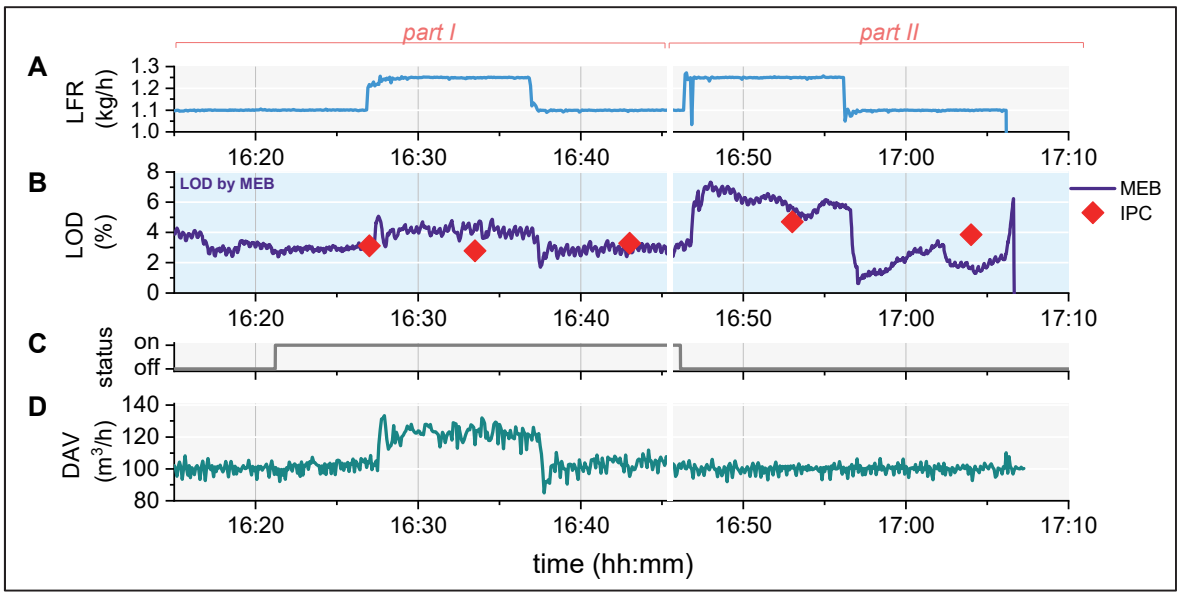

Figure 22: LOD control via MEB by DAV. A: liquid feed rate; B: LOD of dried granules measured by MEB and reference IPC; C: Controller status on/off; D: drying air flow. When Controller was off: DAV=100 m^3/h; when Controller was turned on: DAV was adapted based on the current LOD reading.

In this trial it was demonstrated, that LOD control through DAV and MEB is feasible. The increased LFR had a direct influence on MEB calculations. However, in part I the active Controller adapted DAV immediately, which resulted in stable LOD, as confirmed by offline IPC measurements (see Figure 22, part I: B and D). In part II, the Controller was disabled. Hence, DAV remained constant at 100 m^3/h, upon increasing LFR. As a consequence, LOD of dried granules increased from approximately 3 % to ~ 5 %, as indicated by MEB and confirmed by IPC (see Figure 22, part II: B and D).

In summary, the implementation of the PAT-based feed-back Controller for LOD via MEB and DAV demonstrated beneficial to process control. The results build a solid foundation for further trials and improvements in the future. Especially the Controller aggressiveness and data-filter times leave room for a more detailed evaluation. Generally, the Controller can be applied either to stabilize routine production runs or during development. During production, it can cope for uncontrolled, common variations (e.g. day-to-day variability can influence drying performance [22]). During development, it can be beneficial, when for example different L/S ratios in granulation are tested by an auto-DoE, but dried granules' LOD is supposed to stay within

specification limits, to allow tableting of the material in connected mode. Overall, the vast advantage of MEB-based control over NIR-based control is the absence of a lag-time between drying and measurement, making it a fast and effective control tool.

3.3. Defining the analytical basis of the control strategy: how to control?

3.3.1. Concept

In the previous section, dried granules' LOD, PSD, and API content were identified as CQAs in the investigated downstream CM process that need to be monitored in order to ensure the final drug product has acceptable quality at all times (see section 3.2.2, page 31). Continuous analysis of CQAs in real-time is feasible through suitable PAT-analyzers. The implementation of several orthogonal PAT analyzers for one CQA can increase the level of reliability and avoid process-downtime from PAT-failure. Therefore, at least two PATs for one CQA were selected, as outlined below.

For LOD, near infrared spectroscopy (NIRS) and mass- and energy balance calculations (MEB) were selected as suitable orthogonal methods. For PSD, NIRS and laser diffraction (LD) were selected. For API blend- and content uniformity (i.e. Diclofenac Sodium), two independent NIRS systems together with dynamic feed rate analysis were selected. The development, implementation, and validation (if applicable) of each method will be described in detail in the following sections.

While orthogonal methods can offer an increased level of reliability regarding process control, they can also raise questions in regard to data plausibility: what happens if the orthogonal methods show different quality results? How should the quality control strategy take action? To answer these questions, methods for data reconciliation between orthogonal PAT methods, based on multivariate statistical process control (MSPC) will be evaluated.

The combination of the selected orthogonal PAT analyzers and a suitable method for data reconciliation forms the analytical basis of the control strategy, as it defines *how* the product quality is controlled. This concept is illustrated in Figure 23, and will be discussed in detail in the following sections.

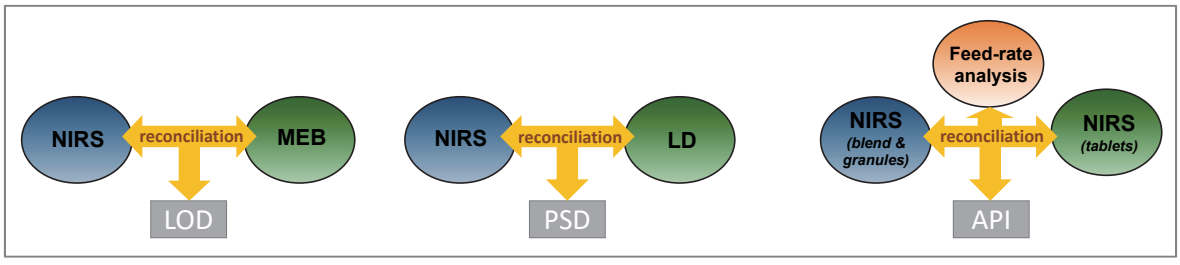

Figure 23: Overview of the analytical basis of the developed control strategy that aims to monitor CQAs dried granules' LOD, PSD, and API content (NIRS = near infrared spectroscopy, MEB = mass- and energy balance calculations, LD = laser diffraction).

3.3.2. Orthogonal PAT for LOD

3.3.2.1. Mass- and energy balance calculations[12]

The underlying principle of mass- and energy balance (MEB) calculations is the conservation of mass and the conservation of energy within a closed system. By analyzing directly measurable mass and energy flow rates and related parameters in the granulation and drying unit (e.g. feed rates, air flow rates, air humidity, temperatures), flow rates that cannot be measured directly can be calculated (e.g. moisture content of granules exiting the dryer). The design and application of MEB calculations is highly equipment specific, but product independent.

A thorough, step-by-step derivation of such calculations for the Glatt GPCG2 CM FBD, which was used in all performed trials in the presented project, was previously published in publication 4 (see page v). In this section the main findings from the manuscript are summarized, for details refer to the original publication [95].

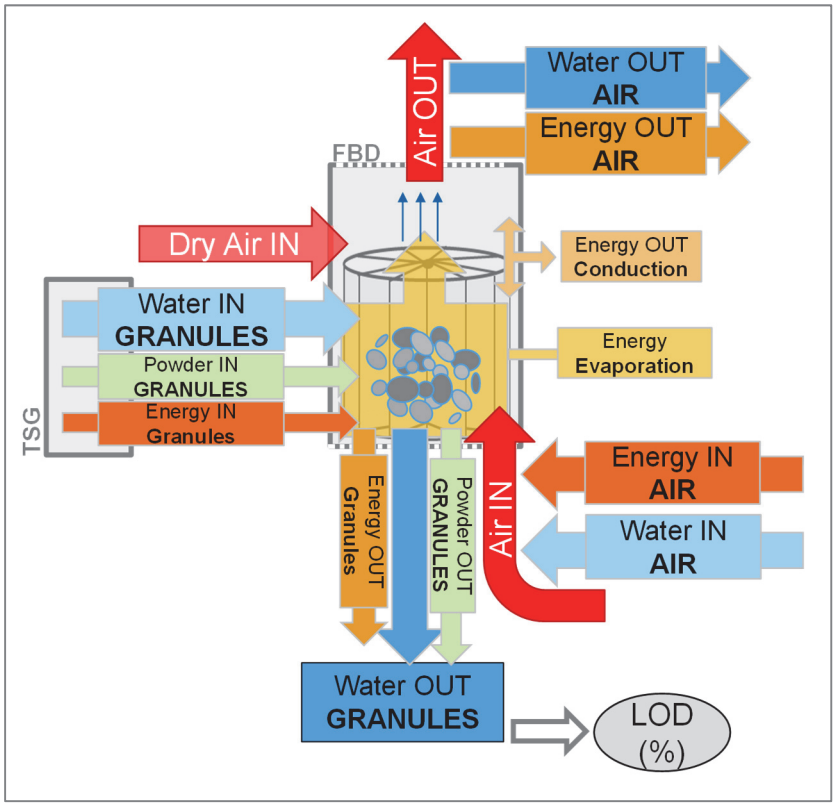

Figure 24: Conceptual overview of all factors included in the derived mass- and energy balance. Figure adapted from [95].

A conceptual overview of the designed mass- and energy balance is illustrated in Figure 24. In summary, water enters the dryer through wet granules and the inlet air, and exits through the outlet air and the dried granules. Powder blend enters through the wet granules and exits through

[12] Parts of this section have been previously published in Publication 4 (see page v)

the dried granules. Air enters with the inlet air stream and with compressed dry air (applied to clean the filters and to transfer granules); air exits with the outlet air stream. Energy enters the dryer via the heated air and wet granules heated during granulation, and leaves the system through the outlet air, with the dried granules, via conduction through the dryer walls, and is transformed into evaporation energy.

Drying behavior in individual process chambers

The Glatt GPCG2 CM FBD consists of a star-shaped rotor, divided into ten rotating process compartments that is inserted into a static drying chamber. Sensors for air flow rate, temperature, and humidity are located outside of the rotor & drying chambers (in detail: before and after the rotor, to measure inlet and exhaust parameters; see Figure 6 on page 14 for details of the dryer's internal sensors and their locations). Consequently, only average values of all ten process compartments are available for MEB calculations. For accurate LOD predictions, it needs to be ensured that the material dries comparably and reproducibly in all ten chambers.

To measure and compare granule temperature and corresponding air humidity and air temperature in the drying chambers at varying process conditions (e.g. variations in total material mass flow, temperature, air flow, sensor location), wireless sensors were temporarily installed inside the rotor. In detail, three sensors for granule temperature and three sensors for air humidity/air temperature where installed in separate drying chambers. Dimensions of the sensors and their setup in the drying chambers are illustrated in Figure 25; details on the experimental design can be found in [95].

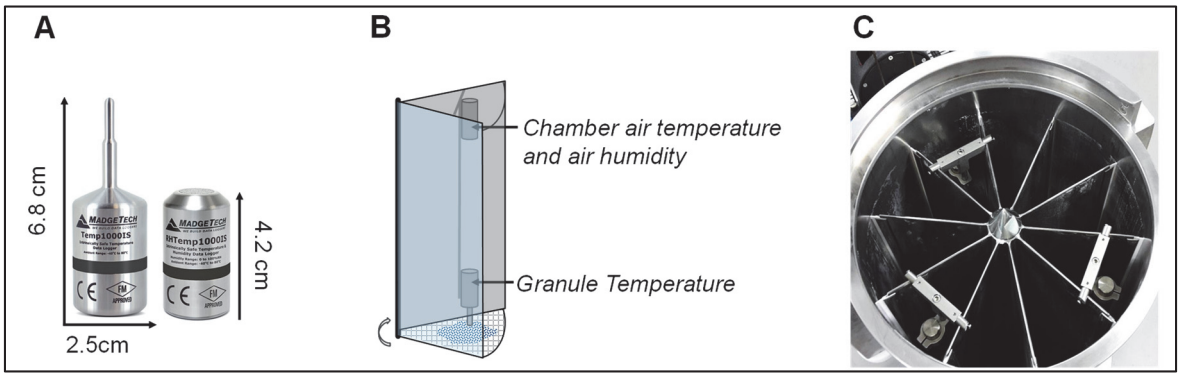

Figure 25: A: Dimensions of installed wireless sensors. B: Schematic view of sensor position in the individual drying chamber. C: top view of sensors installed in rotor (Figure A was adapted from [181, 182], B & C were adapted from [95]).

A selection of the results is displayed in Figure 26. In Figure 26 A, temperature- and humidity curves of a 30 minutes observation period were superimposed on each other. The obtained data demonstrated comparability between the three observed chambers, as well as repeatability between consecutive rotations, as the curve dynamics show similar, stable, and consistent progress. For a closer examination of the drying behavior, one single rotation cycle is plotted over the rotation time in Figure 26 B. The successive rotation phases filling and primary drying, secondary drying, and emptying are clearly distinguishable by the temperature and humidity progress along the timeline. Primary drying occurred within the first third of the rotation, which signifies the efficiency of the drying process. Generally, the observed curve dynamics are similar

to the ones known from common batch fluid-bed dryers [75]. In summary, all conducted trials confirmed comparable and reproducible drying behavior between the ten drying chambers, independent of the applied process conditions.

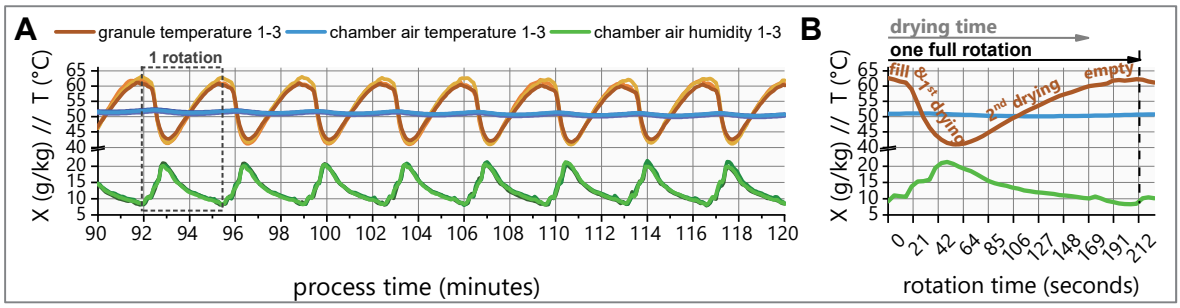

Figure 26: A: demonstration of comparability and reproducibility in three observed drying chambers. B: Dynamics of granule temperature and air humidity during one dryer rotation. The observed slow incline in air humidity after the wet granules entered the chamber is caused by the sensors relatively slow response time (> 30 seconds in still air conditions [183]) that cannot describe the actual step response adequately enough (Figure adapted from [95]).

Humidity bias and conductive energy dissipation

A temperature- and air flow dependent delta between the inlet and exhaust air humidity measurement was discovered during previous trials on the empty drying unit. This delta misleadingly implies that more water vapor exits the dryer than initially entered it. Despite a detailed investigation on the sensors, this obvious measurement error could not be fixed and hence had to be quantified. Also, the uninsulated stainless-steel container that encloses the drying rotor is susceptible to significant heat conduction, resulting in the dissipation of thermal energy not related to evaporation. In detail, relevant thermal energy dissipates between the location of the FBD-internal inlet air temperature sensor and the sieve bottom of the drying chamber (where granules are dried), as well as between the sieve bottom and the location of the exhaust air temperature sensor. To include the conductive energy dissipation in the MEB calculations, it had to be quantified.

Accordingly, a DoE-investigation of the empty drying unit was performed, to quantify the humidity delta and the conductive energy dissipation for the MEB calculations. Inlet temperature- and airflow-settings were systematically varied and their effects on exhaust temperature and -humidity, as well as their effect on the sieve bottom temperature were observed and quantified via regression analysis. To measure the temperature at the sieve bottom, wireless temperature sensors were installed in analogy to Figure 25; more details on the experimental design and results are described in [95].

Altogether, regression analysis of the observed factor-response relationships lead to three linear fit functions that permit to predict the humidity bias and conductive energy dissipation. First, the correlation of humidity delta ΔX_{OUT}, inlet humidity (X_{IN}), drying airflow (DAV), exhaust air temperature (T_{EX}), and measured exhaust air humidity (X_{OUT}), is described by the combination of the linear fit function in eq. 5 ($R^2 = 0.97$, $Q^2 = 0.93$) and eq. 6:

eq. 5 $$X_{OUT}\left[\frac{g}{kg}\right] = -11.7744 - 0.00317 * DAV + 0.03593 * T_{ex} + 1.21061 * X_{IN}$$

eq. 6 $$\Delta X_{OUT} = X_{OUT} - X_{IN}$$

Second, the measured temperature at the sieve bottom T_{sieve} [K] specifies the actual drying temperature DT_{real} [K], which is correlated to DAV and DT [K] according to eq. 7 (R^2 = 1.00, Q^2 = 0.99).

eq. 7 $$T_{sieve} = DT_{real}\,[K] = 45.85570 + 0.03222 * DAV + 0.83618 * DT$$

When the dryer is empty (i.e., no evaporation), DT_{real} is also equal to the temperature of the air that leaves the sieve bottom towards the dryer outlet. However, if wet granules are dried, a part of the thermal energy stored in the hot air stream reaching the sieve bottom is transformed into evaporation energy. In this case, the temperature of the air that leaves the sieve towards the outlet, equals the granule temperature $T_{granules}$ [K]. $T_{granules}$ is correlated to DAV and T_{EX} according to eq. 8 (R^2 = 0.98, Q^2 = 0.96).

eq. 8 $$T_{sieve} = T_{granules}\,[K] = (T_{ex} - 99.90810 - 0.04363 * DAV)/0.65070$$

Accordingly, in the empty dryer: $T_{sieve} = DT_{real} = T_{granules}$, and when wet granules are dried: $T_{granules} < DT_{real}$. The difference $\Delta T(DT_{real} - T_{granules})$ is directly correlated to the amount of water being evaporated. Refer to Figure 27 for a better understanding of the relationships between T_{sieve}, $T_{granules}$, and DT_{real}.

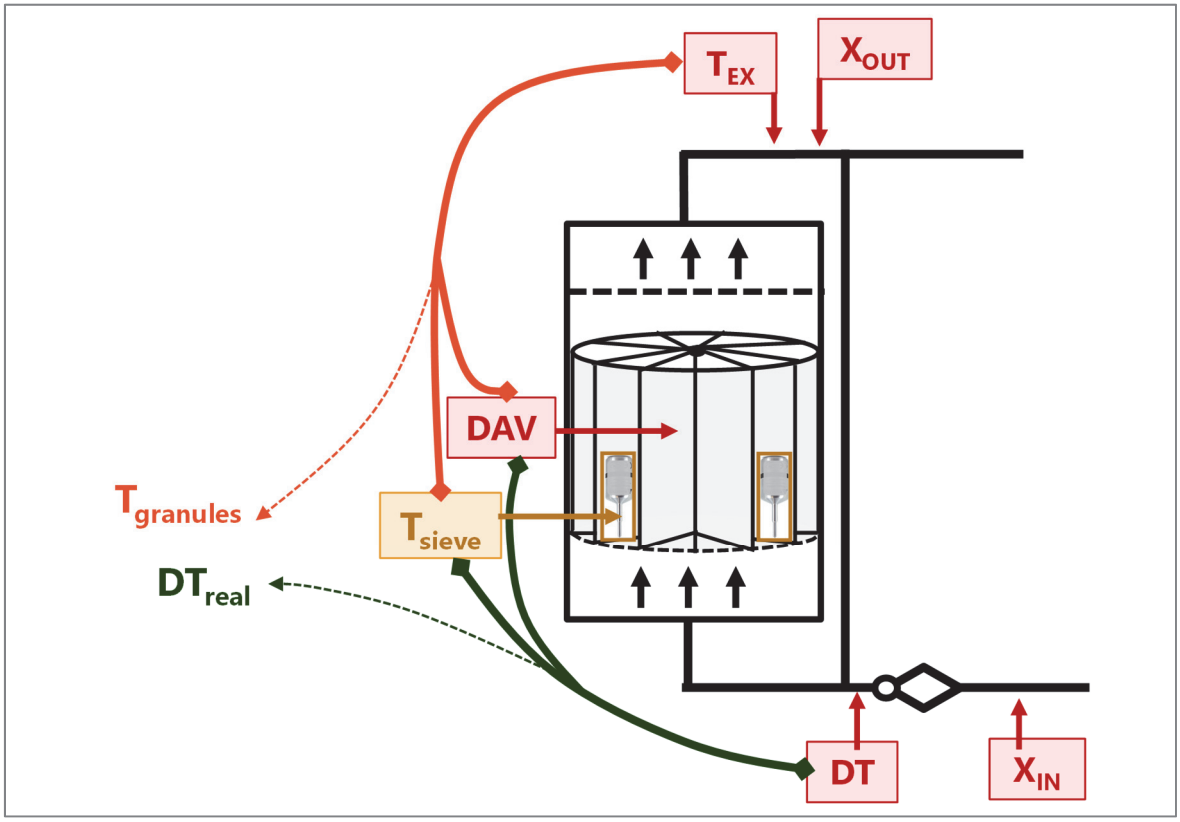

Figure 27: Overview of the relationships between T_{sieve}, $T_{granules}$, and DT_{real}. FBD-internal humidity and temperature sensors (in red) and wireless temperature sensors (in yellow), were used to quantify the humidity bias and conductive energy dissipation (Figure adapted from [95]).

Derivation of mass balance

The following formulas for mixtures of gases need to be considered, for the mass balance:

eq. 9 $p_{w-IN} * \dot{V}_0 = \dot{m}_{w-IN} * R_w * T_{room}$

eq. 10 $\dot{m}_{w-IN} = x_{IN} * \dot{m}_{a-IN}$

eq. 11 $p_{a-IN} * \dot{V}_0 = \dot{m}_{a-IN} * R_a * T_{room}$

eq. 12 $p_0 = p_{a-IN} + p_{w-IN}$

Where p_{w-IN} [Pa] is the partial pressure of water in the inlet air, $\dot{m}_{w-IN}$ $[\frac{kg}{h}]$ is the mass flow rate of water in inlet air, and R_w $[\frac{J}{kg*K}]$ is the specific gas constant of water vapor (R_w = 461.53 $\frac{J}{kg*K}$). $\dot{V}_0$ $[\frac{m^3}{h}]$ is the total inlet airflow rate at room temperature (T_{room} $[K]$). It can be calculated from the measured total air flow rate $D\dot{A}V_{total}$ $[\frac{m^3}{h}]$ and the measured drying temperature DT $[K]$, according to the universal gas equation [184]. x_{IN} $[\frac{g}{kg}]$ is the measured inlet humidity, p_{a-IN} [Pa] is the partial pressure of dry air in the inlet air, and $\dot{m}_{a-IN}$ $[\frac{kg}{h}]$ is the inlet mass flow rate of air. R_a $[\frac{J}{kg*K}]$ is the specific gas constant of dry air (R_a = 287.12 $\frac{J}{kg*K}$), p_0 [Pa] is the ambient air pressure (p_0 = 101300 Pa) [184, 185].

Combination of eq. 9 - eq. 12 gives the partial pressure of water in the inlet air p_{w-IN} $[Pa]$ (see eq. 13), which then allows to calculate p_{a-IN}, $\dot{m}_{a-IN}$ and $\dot{m}_{w-IN}$ from eq. 12, eq. 9, and eq. 10.

eq. 13 $$p_{w-IN} = \frac{p_0 * \dot{V}_0}{\dot{V}_0 + \frac{\dot{V}_0 * R_a}{x_{IN} * R_w}}$$

The mass flow rate of water or air in the fluidizing chambers ($\dot{m}_{w-IN-chamber}$ or $\dot{m}_{a-IN-chamber}$ $\left[\frac{\text{kg}}{h}\right]$, respectively) is given by the ratio between total inlet air flow $D\dot{A}V_{total}$ and chamber airflow $D\dot{A}V$, and $\dot{m}_{a-IN}$ or $\dot{m}_{w-IN}$, respectively [95]. Furthermore, the theoretical total liquid inlet flow rate $\dot{m}_{liquid-IN}$ $\left[\frac{\text{kg}}{h}\right]$ is defined by the granulation liquid feed rate $L\dot{F}R$ $\left[\frac{kg}{h}\right]$ and the initial moisture content LOD_0 [%] of the powder blend being fed at solid feed rate $S\dot{F}R$ $\left[\frac{\text{kg}}{h}\right]$ [95].

To include the material's residence time in the FBD into the calculations, all flow rates in unit/h (e.g. mass flow rate, volume flow rate), are divided by the current dryer rotation speed (rph), to be converted into flow rates in unit/rotation. Then, the total mass flow rate of water entering the dryer per rotation $\dot{m}_{H2O-IN}$ $[\frac{g}{rotation}]$ is defined by eq. 14:

eq. 14 $$\dot{m}_{H2O-IN} = \dot{m}_{liquid-IN} + \dot{m}_{w-IN-chamber}$$

Measured exhaust humidity X_{OUT} $[\frac{g}{kg}]$ needs to be corrected by the humidity correction term ΔX_{OUT}, as defined by eq. 5 and eq. 6 (page 52).

Chamber exhaust air mass flow rate $\dot{m}_{a-OUT-chamber}$ is calculated in analogy to $\dot{m}_{a-IN-chamber}$ from the ratio of measured bypass air flow rate $D\dot{A}V_{bypass}$ $\left[\frac{m^3}{h}\right]$ and measured total exhaust air flow rate $D\dot{A}V_{OUT}$ $\left[\frac{m^3}{h}\right]$. Accordingly, the mass flow rate of water exiting the chamber through the air $\dot{m}_{w-OUT-chamber}$ $\left[\frac{g}{rotation}\right]$ is calculated in analogy to $\dot{m}_{w-IN-chamber}$.

Then, the difference between $\dot{m}_{H2O-IN}$ and $\dot{m}_{w-OUT-chamber}$ defines the mass flow rate of water exiting the dryer with granules $\dot{m}_{H2O-OUTgran.}$ $\left[\frac{g}{rotation}\right]$. The theoretical total dry powder inlet flow rate $\dot{m}_{solid-IN}$ $\left[\frac{\text{kg}}{h}\right]$ is defined by the solid feed rate $\dot{SFR}$ $\left[\frac{\text{kg}}{h}\right]$ and LOD_0 [%] and equals the outlet mass flow rate of dry powder blend $\dot{m}_{solid-OUT}$ $\left[\frac{\text{kg}}{h}\right]$.

Finally, the moisture content LOD [%] of granules is calculated according to eq. 15. The reported value represents the average LOD per rotation.

eq. 15 $$LOD = \frac{\dot{m}_{H2O-OUTgran.}}{(\dot{m}_{H2O-OUTgran.} + \dot{m}_{solid-OUT})} * 100$$

The accuracy of the described LOD calculation is dependent on numerous factors, for example the accuracy of the calibration of the humidity delta, the accuracy of all involved sensors and measurements, and their respective response times. Especially humidity sensors are known to have rather slow response times in the range of 15 seconds and more [183]. Since every one of these uncorrelated and random uncertainties adds in quadrature to the accuracy of the whole LOD calculation, according to common rules of error propagation [186], minor deviations from reference analytics are expected.

Small fluctuations in process parameters between two data points like material mass flow, or drying air flow rate, have a huge influence on the calculated LOD at that time point, while the actual influence on granule LOD might be neglectable. Consequently, to avoid huge errors caused by small, short fluctuations in process parameters, it is recommended to observe trends or filtered data instead of individual raw values. Also, dead times between the different process units and sensor locations need to be considered, to reflect the residence time of mass and energy in the line.

Derivation of energy balance

Asides from predicting dried granules' LOD via mass balance calculation, the dryer's energy balance can be analyzed. It can aid in judging the dryer's thermodynamic equilibration status and therefore the validity of predicted LOD results.

The observed decrease in thermal energy between DT_{real} and $T_{granules}$ (see eq. 7 and eq. 8, page 53) can be characterized as evaporative heat flow loss $\Delta\dot{Q}_{obs}$ $\left[\frac{J}{rotation}\right]$, by means of the mass flow rate of air in the drying chamber ($\dot{m}_{a-IN-chamber}$), $\Delta T\left(DT_{real} - T_{granules}\right)$, and the isobaric specific heat of air c_a $[\frac{J}{kg*K}]$, according to eq. 16 ($c_a = 1006$ $\frac{J}{kg*K}$ [95, 185]).

eq. 16 $$\Delta\dot{Q}_{obs} = c_a * \dot{m}_{a-IN-chamber} * \Delta T\left(DT_{real} - T_{granules}\right)$$

$\Delta\dot{Q}_{obs}$ is compared to a theoretically expected decrease in heat flow $\Delta\dot{Q}_{calc}$ $\left[\frac{J}{rotation}\right]$, based on the sum of the heat flow required to heat up the wet granules ($\Delta\dot{Q}_{solid}$ and $\Delta\dot{Q}_{water}$) and the heat flow required to evaporate the amount of water determined above during LOD calculation ($\Delta\dot{Q}_{evap}$), see eq. 17 [95]:

eq. 17 $$\Delta\dot{Q}_{calc.} = \Delta\dot{Q}_{solid} + \Delta\dot{Q}_{water} + \Delta\dot{Q}_{evap}$$

Overall, $\Delta\dot{Q}_{calc.}$ should be equal to $\Delta\dot{Q}_{obs}$ in a thermally equilibrated system (within the feasible accuracy range, based on the prediction precision of DT_{real} and $T_{granules}$ and the overall sensor accuracy). Larger deviations could indicate an un-equilibrated drying chamber (e.g. after heat-up, as described in the controlled ramp-up example in section 3.2.6 (page 42 ff.), or that an issue with the LOD calculation has occurred (e.g. due to sensor failure, blocked transfer pipes, etc.)). Consequently, evaluating the energy balance adds a second layer of reliability to the above described LOD calculation [95]. An example for the application of mass- and energy balance calculations for real-time process analysis is provided in section 3.3.2.3 (page 60 ff.).

Transient phases

The presented MEB calculations are valid for stationary processes at constant process parameter settings. When parameters are intentionally changed from one setting to the other during granulation and drying, the calculations have to be extended to reflect those transient phases. This is especially important for big changes in fast adapting process parameters like DRS, DAV, and $\dot{m}_{tot}$, since their transient phase is usually shorter than the material's residence time in the granulator and dryer. In contrast, changes in DT or barrel temperature are executed rather slowly, and the transient phase is reflected by the gradually changing process values that are used for the calculations. Details on transient times and their implementation in the balance calculations can be found in [95].

Validation of Mass- and energy balance calculations

The derived mass- and energy balance calculations were validated with several external validation trials. To avoid duplication, the results from the validation trials are shown as part of the orthogonality demonstration between MEB and NIRS in section 3.3.2.3 (page 60 ff.). Details can also be found in [95].

Implementation in DeltaV

To facilitate real-time monitoring of LOD, the derived mass balance calculations were included into the CM process control system *DeltaV*. A screenshot of the resulting "LOD Soft Sensor"[13] is shown in Figure 28. The application allows to include up to five different solid feeders and two different liquid feeders. Dead times and filter times can be adapted manually: dead times consider time delays between the different process units and sensor locations; filter times define

[13] Programming and implementation of the LOD-estimator into DeltaV was executed by CM-Unit internal automation engineers

the averaging range of process values used for the calculation. Real-time LOD predictions made by the LOD Soft Sensor are presented in section 3.3.2.3 (page 60 ff.).

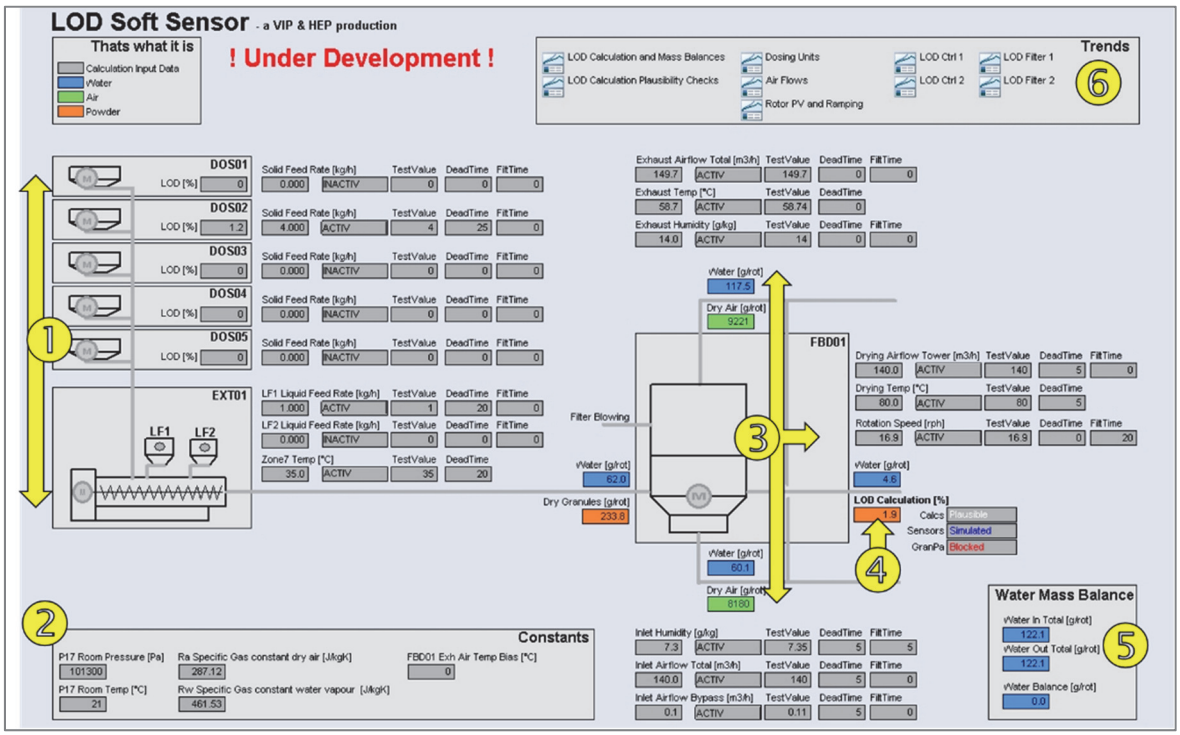

Figure 28: integration of the mass balance calculations in the process control system DeltaV. Current process values from the twin-screw granulator (1) and the continuous fluid-bed dryer (3), together with necessary constants and room conditions (2), are used to calculate the dried granules' LOD (4) in real-time. An overview of the water-mass balance (5) and various process trends (6) allow to judge the validity of the predicted LOD.

3.3.2.2. Near infrared spectroscopy for LOD analysis

Table 5: Variation of granule characteristics in calibration and validation samples.

Characteristic	Calibration range
LOD	1 – 11 %
API content	17.5 – 32.5 % (70 – 130 % of LC*)
PSD X10	20 – 230 µm
PSD X50	100 – 1020 µm
PSD X90	750 – 2300 µm

NIRS was selected as the second PAT method to monitor dried granules' LOD at the outlet of the drier. Method development was performed with a calibration data set containing 3142 spectra (2110 online and 1032 offline) and a validation data set containing 748 spectra (267 online and 481 offline). Spectra were collected from numerous different trials, to ensure sample characteristics were representative of the processes' expected variability in LOD, PSD and API content. An overview of the calibration range (based on reference analytics) is presented in Table 5.

Calibration and validation

Collected spectra were pre-processed via SNV and 1st Derivative. PLSR calibration against reference LOD analyses resulted in 3 PCs, which account for 90.2 % of spectral variability. Result from internal and external validation are summarized in Figure 29; RMSECV was 0.85 %, RMSEP was 0.74 %.

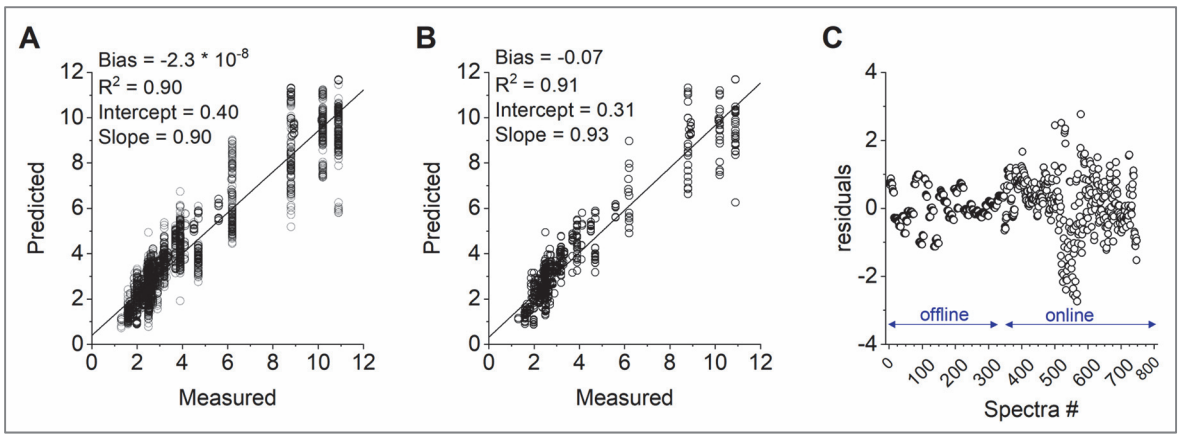

Figure 29: Summary of calibration and validation results for dried granules' LOD analysis by NIRS. Spectra were preprocessed by SNV and 1st Derivative. A: Measured vs. predicted plot of calibration data set (cross-validation). B: Measured vs. predicted plot of validation data set. C: Residuals plot of validation data set.

The wide range in predicted LOD values (compared to reference LOD, see Figure 29 A and B), is caused by the sample presentation in front of the NIRS probe. During reference analysis, approximately 5 g of sample are measured by loss-on-drying, giving a reasonable average description of the whole sample population. In contrast, the NIRS-light source scans a sample-area of approximately 4 mm^2 per acquired spectrum. Bigger granules can contain more water than smaller granules, due to different drying behavior. Therefore, the spectral variation and hence, the predicted LOD can fluctuate significantly, depending on the granule population that appears in front of the probe at the instant of spectral acquisition. This is further confirmed in Figure 29 C, as the residuals from online spectra are higher than from offline spectra. Since offline spectra were collected from granules that were stored in brown glass bottles over an extended period of time, LOD between the different granule populations had more time to equilibrate, compared to online measured granules. To reduce this effect, filtered NIRS predictions should be considered during process control.

Online validation and robustness testing

To test the methods accuracy of online LOD predictions and robustness towards PSD and API content variations, external validation with three independent online datasets was performed. The same experiments were used to demonstrate accuracy and robustness of NIRS methods for PSD and API blend uniformity in granules, as described in sections 3.3.3.1 and 3.3.4.2 (page 64 ff., and 72 ff., respectively).

For accuracy assessment, granules' LOD during a continuous granulation and drying experiment was intentionally varied between ~ 1 - 11 %, by adapting drying air flow (80 – 160 m^3/h),

rotation speed (30 – 5 rph), and temperature (80 – 90 °C), accordingly. Results are summarized in Figure 30. Good agreement was found between NIRS and IPC, demonstrating good online accuracy of the final NIRS method.

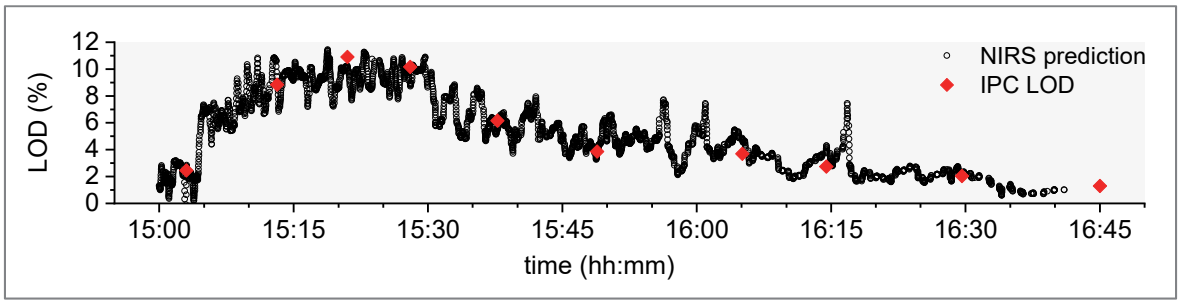

Figure 30: Online validation results for accuracy assessment. Predicted NIRS results are in good agreement with IPC results, demonstrating good accuracy of the calibrated method. (NIRS predictions were filtered with a moving average filter of 10 individual spectra).

For robustness testing towards variations in API content, powder blends containing 70, 95, 105, and 130 % of label claim API content were processed. This is important, as API and excipients will be fed by separate feeders into the production line in the future. Hence, variations in API content (here: Diclofenac Sodium) can occur in case of feeder disturbances and it needs to be ensured that the methods accuracy towards LOD prediction is not impacted. For robustness testing towards PSD variations, powder blend containing 100 % label claim API content was granulated with different L/S ratios (0.20 – 0.35 L/S; dried at constant conditions), which generated varying particle size distributions between ~ 200 – 1000 µm PSD X50. Variations in PSD can occur for example through unstable feeding behavior (in liquid and/or solid feeders). Nevertheless, LOD prediction through NIRS should not be impacted by such variations, to ensure robust process monitoring at all times.

Results from the two performed robustness testing trials are summarized in Figure 31, where NIRS-predicted LOD values were compared to reference IPC analysis and related to the induced variations in API content and PSD.

Overall, robustness towards variations in API content was demonstrated, as predicted LOD results are in good agreement with IPC, independent of the granule's API content (see Figure 31 A). Concerning PSD, good agreement between NIRS predicted LOD and IPC LOD was found. Since PSD was varied by adapting the L/S ratio during granulation (at constant drying conditions), PSD and LOD are highly correlated with each other. This makes it challenging to claim robustness towards PSD variations. Nevertheless, results demonstrate good accuracy at varying PSD (see Figure 31 B).

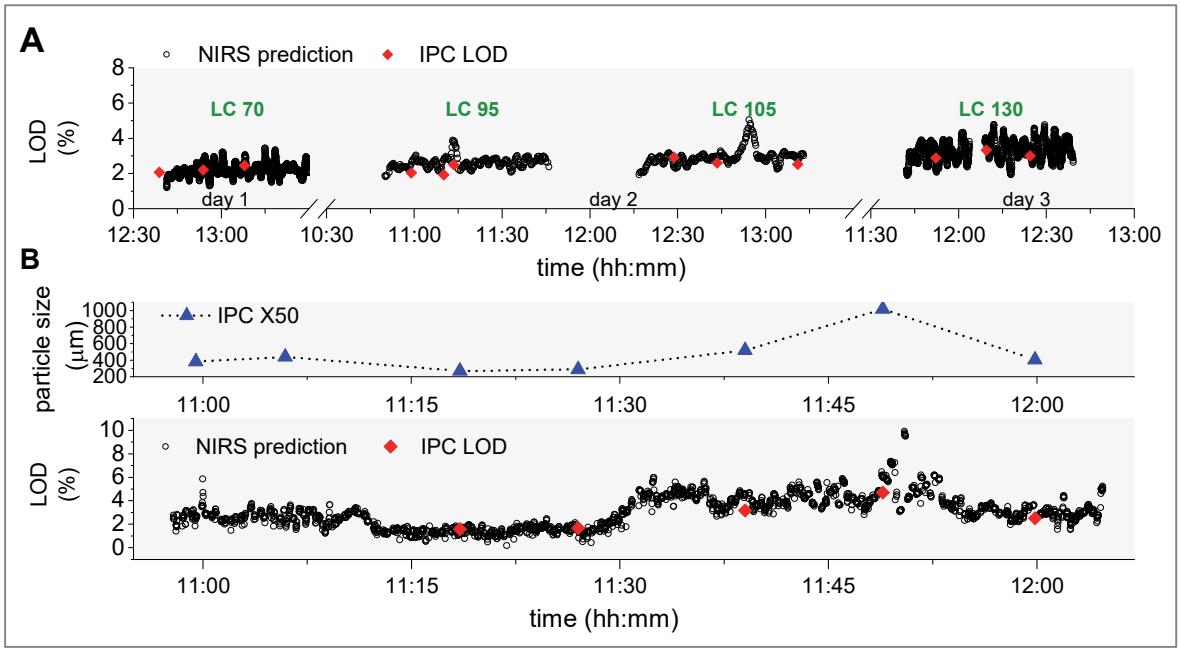

Figure 31: Robustness testing of the calibrated LOD method. LOD predictions demonstrated to be robust towards varying API content (A) and varying particle size distribution (B). (NIRS predictions were filtered with a moving average filter of 10 individual spectra).

Bias correction

After calibration and validation of the NIRS method, the spectrometer's reference standards were cleaned (= sanded) and re-calibrated. This re-calibration seemed to induce a bias in NIRS prediction of + 0.45 % LOD. The bias was determined by comparing IPC results with NIRS predictions from several comparable trials before and after the re-calibration. Due to limited available process data, extending the method with current data (collected with the cleaned reference standard) was not feasible. Instead, the determined bias of 0.45 % was subtracted from all NIRS LOD predictions that were done after the reference re-calibration. In the future, more 'new' data will be included into the method, to cope for the recalibrated standard. An example illustrating the observed bias is included in the supplementary data (see section 10.3, Figure S 2, page V).

3.3.2.3. Demonstration of orthogonality in LOD analysis

NIRS and MEB calculations are two independent, orthogonal PAT methods for LOD control. To demonstrate their comparability, a set of experiments was performed.

First, MEB (calculated via DeltaV by the LOD Soft Sensor, see Figure 28, page 57) and NIRS results, recorded in real-time from the controlled ramp-up trial described in section 3.2.6 (page 42 ff.) were compared to IPC measurements. A summary is illustrated in Figure 32. MEB is mostly influenced by primary drying, which occurs approximately in the first 2/10th of the dryer rotation [95]. In contrast, NIRS and IPC is measured after granules exit the dryer. Therefore, a time-delta of approximately 0.8*t_d (see eq. 2, page 15 for calculation of drying time t_d from dryer rotation speed DRS) is observed between MEB and NIRS/IPC, making a direct visual

comparison challenging (see Figure 32 A). Therefore, the curves were superimposed on each other in Figure 32 B, by shifting the MEB curve by + 0.8*t_d.

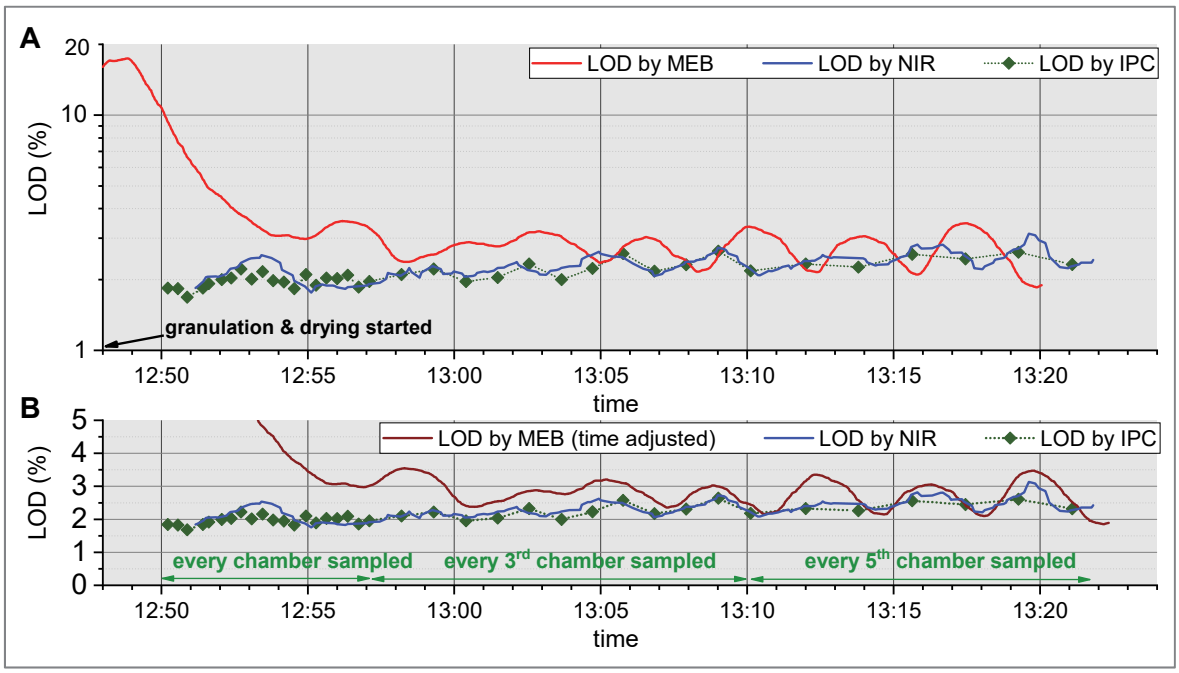

Figure 32: Demonstration of orthogonality between MEB and NIR. A: comparison between MEB, NIR, and IPC results with the original time line. B: MEB results were shifted by + 0.8*t_d, to allow a direct comparison of the three methods (MEB is mainly based on primary drying, which occurs at the beginning of the drying rotations while NIRS analyzes granules after they exited the dryer).

When considering Figure 32 B, NIRS showed very good agreement with IPC. MEB lacked sensitivity in the first ten minutes of the trial, but once the system was equilibrated, good comparability between MEB, NIRS, and IPC was found.

For a more comprehensive demonstration of orthogonality, two experiments were performed, during which the mass- and energy balance in the dryer was actively altered through 'on-the-fly' variation of different process parameters (PPs) that induced variations in LOD. In the first trial large LOD variations were induced (~1-11 % LOD), in the second trial, very small variations (~ 2-3 % LOD) were induced. Parts of the first trial were previously used to demonstrate accuracy of the developed NIRS method, as described in section 3.3.2.2, page 57 ff.

Details on the applied PPs are described in [95]. Results of NIRS, MEB, and IPC are summarized and compared in Figure 33. For a better overview, NIRS, MEB, and IPC were superimposed on each other, in analogy to Figure 32.

Overall, all three analytical methods show good agreement with each other. The NIRS method was developed for LOD < 11 %, which might cause the plateau at high LOD values observed in Figure 33 A. Extreme, short-term fluctuations in MEB (as seen frequently after a PP was changed), are caused by extreme but short fluctuations in the air flow rate or drying temperature. Those fluctuations have a significant influence on MEB calculations, while in reality they have no significant influence on granules' LOD.

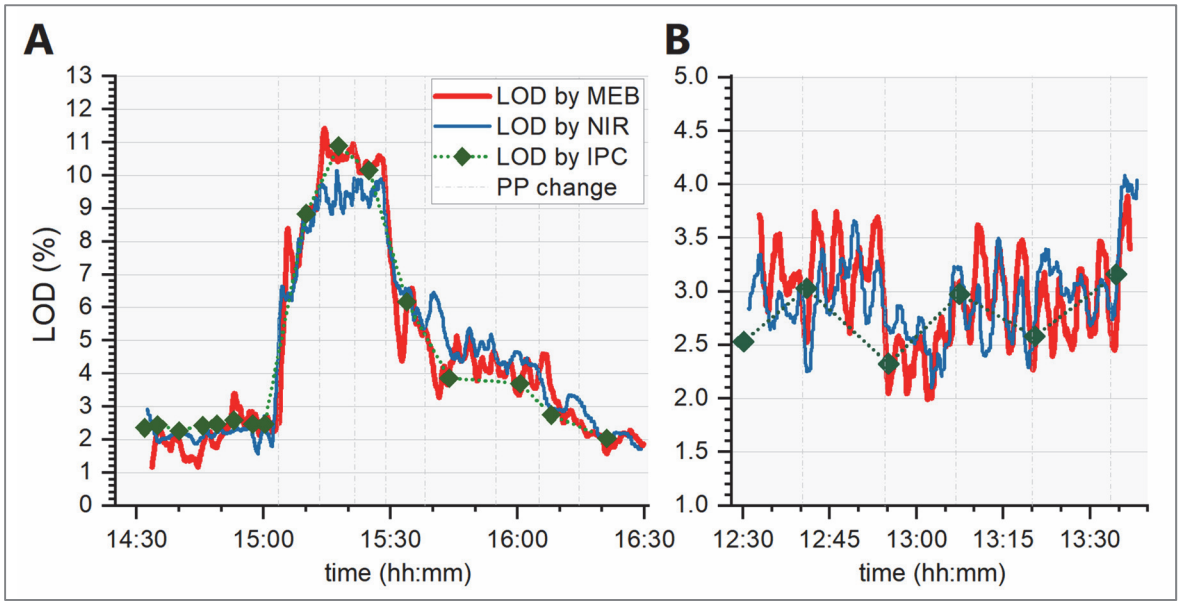

Figure 33: Comparison of NIRS predictions, MEB calculations, and reference IPC for the two experiments A and B. In experiment A, large variations in LOD were induced, in experiment B, small variations in LOD were induced. (MEB and NIR-predictions were filtered over the granules' respective drying time; Changes in process parameter (PP) setting steps are indicated by vertical lines). Figure adapted from [95].

The average absolute deviation between MEB and NIRS was 0.61 and 0.31 % LOD, for experiment A and B, respectively (i.e. overall average < 0.5 %). Especially experiment B demonstrated that even small variations in LOD are reflected by both PAT methods. Periodic fluctuations in LOD that seem to be caused by the process itself, were seen by both PAT methods, demonstrating again the sensitivity and redundancy of the two methods.

Asides from confirming orthogonality and suitability of the redundant signals, the performed experiments also demonstrated validity of MEB calculations, as predicted LOD was in good agreement with IPC results in all trials. The energy balance of the investigated trials can add another layer of certainty for LOD control, as shown in Figure 34. ΔQ_{obs} is the observed decrease in heat flow during drying (based on temperature measurements in the FBD), ΔQ_{calc} is the theoretically expected evaporative heat flow loss (based on MEB-predicted LOD results; see section 3.3.2.1, page 50 ff. for details).

During the start-up phase of experiment A (~ first hour of experiment), ΔQ_{calc} deviated from ΔQ_{obs}, due to the applied preheating protocol (see section 3.2.6, page 42 ff. for details on thermodynamic equilibration after heat-up). The deviation slowly decreased, as the extensive pre-heating was compensated by evaporative cooling. After approximately one hour the dryer was thermodynamically equilibrated, ΔQ_{calc} was in good agreement with ΔQ_{obs}.

Experiment B was conducted succeeding a different (unrelated) trial, hence the dryer was already equilibrated and no deviation was observed. While the results of the energy balance are not specific enough for direct control-actions, they are suitable to reconciliate mass balance predictions for plausibility if unexpected deviations are observed.

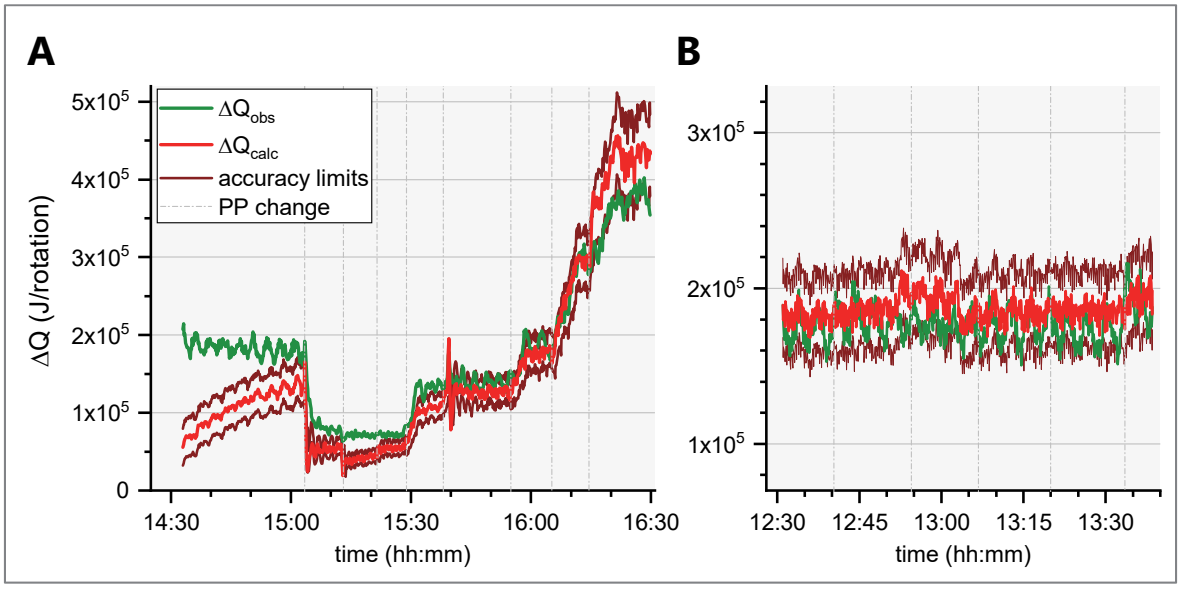

Figure 34: Energy balance calculations for experiment A and B (see Figure 33). Accuracy limits of ΔQ_{obs} are calculated based on the prediction accuracy of conductive heat dissipation (see [95] for details). Figure adapted from [95].

Generally, both analytical methods exhibited advantages and disadvantages, which verify the necessity for orthogonal, redundant PAT strategies. MEB is not sensitive enough in the first few minutes of the process, whereas NIRS shows accurate results as soon as granules exits the dryer (see Figure 32 B). Nevertheless, once the process is equilibrated, MEB has the advantage of no time delay between the actual drying process and the sample analysis (compared to NIRS). Consequently, MEB can indicate deviations in the process faster, allowing earlier intervention in case of a quality event. This was also demonstrated in section 3.2.6 (page 42 ff.), where automated feed-back loops based on NIRS and MEB were tested and compared. Overall, MEB is equipment specific but product-independent. Hence, MEB calculations can be used for process monitoring from the start of development, while NIRS requires method development before it can be applied.

In summary, validity of the MEB calculations as well as orthogonality between NIRS and MEB was demonstrated. The application of redundant, orthogonal PAT methods allowed reliable and accurate process monitoring of dried granules' LOD in real-time. The process control strategy should consider inherent system dynamics and apparent signal fluctuations in order to achieve a stable and robust process control.

3.3.3. Orthogonal PAT for PSD

3.3.3.1. Near infrared spectroscopy for PSD analysis[14]

Multivariate analysis of raw NIRS spectra enables the correlation of variances in NIRS absorption patterns to physical sample properties like particle size related information. Details on the method development and validation of a NIRS method for PSD monitoring has been previously published as Publication 2 (see page v). In this chapter the main outcomes of the calibration, validation, and robustness testing are summarized; for details refer to the original publication [187].

Calibration and validation

To ensure robust method development, samples selected for calibration and validation were representative of the anticipated variability in LOD, PSD, and API content. An overview of the calibration range was previously presented in Table 5 (see page 57; the same samples were used during LOD method development).

PLSR of the calibration data set against reference PSD results X10, X50, and X90 was performed, to generate three separate methods. For PSD X10, 9 principal components (PCs) were selected, that represent close to 85 % of the total variance. For PSD X50 and X90, 15 PCs were selected which represent close to 75 % of the total spectral variance. Loading plots and resampling statistics ensured that the model was optimized to its purpose, without the risk of over- or under fitting [187]. Usually, only PCs that can be explained by identified sample variations should be included into a PLSR calibration, in order to avoid prediction errors from black-box methods that are not fully understood [147]. Here, the inclusion of numerous PCs that could not be clearly attributed to known sample variations was justified by the diversity of the sample population. Samples originated from numerous different granulation trials at various process settings, causing many small differences in granules' physical properties. These can influence the spectral variance and hence PLSR results, as previously published by Nieuwmeyer et al. [147].

To validate the developed methods, linearity and accuracy was assessed via cross-validation of the calibration data sets and via prediction analysis of the internal validation datasets. Table 6 lists RMSECV/RMSEP, R^2, slope, bias, and intercept of calibration and validation results. Figure 35 plots reference values against NIRS-predicted values of the validation data sets, and Figure 36 plots the corresponding residuals (in % of the reference value). While R^2 from calibration and validation data are comparably low, values are within the suggested range for adequate NIRS calibrations of $0.95 > R^2 > 0.7$ [148]. The sample appearance in front of the small NIRS probe in contrast to the comparably large sample size measured by reference dynamic image analysis, is the main reason for low R^2 and large residuals [187]. Nevertheless, the range of sample population variation to the models prediction error (RPD) is within the accepted range for adequate NIRS methods ($3 < RPD < 1.75$) for all models. Furthermore, prediction errors are all within the suggested range of two times the standard laboratory error (PRL) and the ratios of

[14] Parts of this section have been previously published in Publication 2 (see page v)

calibration sample range (based on reference analytics) to prediction errors reach the accepted limit RER ≥ 10, which indicates high model utility (see Table 6).

Table 6: Summary of calibration and internal validation.

	PSD X10	**PSD X50**	**PSD X90**
Calibration dataset			
RMSECV (µm)	16	96	162
R^2	0.85	0.75	0.76
Slope	1	1	1
Bias (µm)	$-1*10^{-6}$	$1*10^{-4}$	$2*10^{-4}$
Intercept (µm)	$5*10^{-7}$	$1*10^{-4}$	$2*10^{-3}$
RPD	3	2	2
PRL	2	2	1
RER	13	10	10
Validation dataset			
RMSEP (µm)	17	97	174
R^2	0.86	0.73	0.74
Slope	0.99	0.98	0.99
Bias (µm)	-0.05	2.45	5.12
Intercept (µm)	1.01	8.78	18.99
RPD	3	2	2
PRL	2	2	1
RER	13	10	10

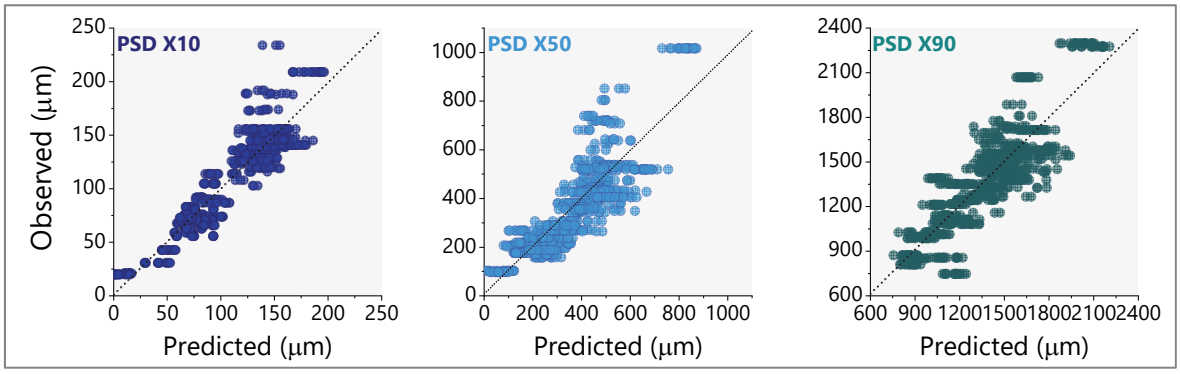

Figure 35: Observed (IPC) vs. predicted (NIRS) plot of the validation datasets gives a visual overview of slope, bias and intercept of the three models (Figure adapted from [187]).

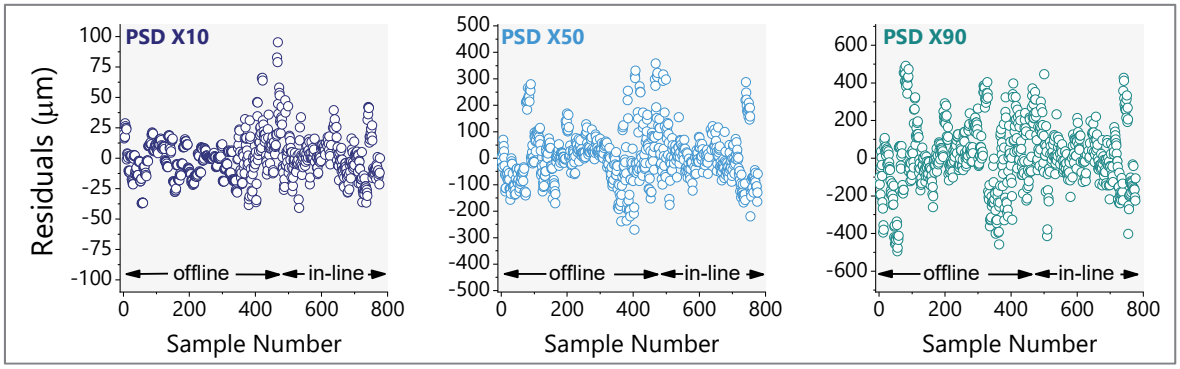

Figure 36: Residuals in the validation datasets are comparable between offline and in-line spectra (Figure adapted from [187]).

In summary, internal validation demonstrated acceptable model accuracy and precision for the intended purpose to observe sudden variations and trends in granule's particle size distribution after continuous granulation and fluid-bed drying.

Online validation and robustness testing

To provide further evidence that the selected models are accurate and robust and hence can be applied for routine in-line PSD monitoring of the described granulation and drying process, three external validation trials were performed (the same trials were used to demonstrate validity and robustness of NIRS method for LOD and API blend uniformity in dried granules, as described in sections 3.3.2.2 and 3.3.4.2, pages 60 ff. and 72 ff., respectively).

In the first trial, dried granules' PSD was altered over time by adjusting the liquid-to-solid ratio (L/S) during wet-granulation (L/S 0.2 – 0.35; at constant drying parameters). In the second trial, the methods robustness against water content (LOD) was demonstrated by varying LOD (1 – 11 % LOD absolute) at constant PSD, through the adaption of drying temperature, air-flow and residence time (DAV 80 – 160 m^3/h; DRS 5 – 30 rph; DT 80 – 90 °C; at constant L/S ratios). In the third validation trial, the methods robustness against varying API content was demonstrated by granulating powder blends containing 20 %, 25 %, and 30 % of API (absolute) at constant LOD and PSD (the formulation's target content is 25 % API content). Demonstration of robustness towards LOD and API content is important, as fluctuations in those characteristics can occur during routine manufacturing. Hence, the NIRS methods accuracy should not be impacted by such variations, to ensure accurate process monitoring at all times.

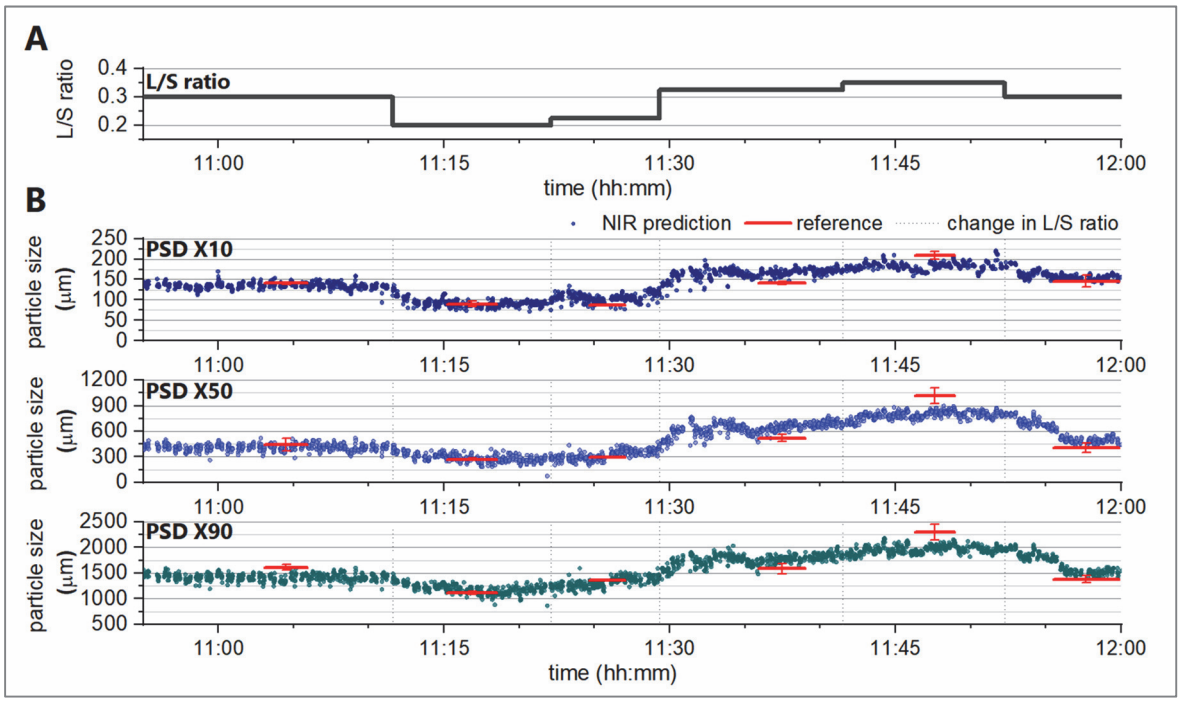

Figure 37: External in-line validation of the accuracy of selected models. A: L/S ratio during wet-granulation. B: NIRS-predicted PSD X10, X50, and X90 compared to IPC measured PSD. The length of the red bar indicates the sampling time for IPC measurement (Figure adapted from [187]).

Figure 37 summarizes the results of the first validation trial, testing the methods accuracy. Wet granules L/S ratio is plotted in relation to in-line NIRS-predicted values and reference IPC results. The plots demonstrate that the developed NIRS-methods can accurately monitor occurring trends and sudden changes in dried granules' PSD-fractions X10, X50 and X90 over time, as each performed step-change in L/S ratio is indicated by NIRS. The observed small deviations between reference and NIRS prediction are perceived as acceptable, as the methods intention is trend monitoring not precise prediction of granules particle size.

Granule PSD is highly correlated to wet granules L/S ratio and dried granule's LOD. To avoid prediction errors based on LOD, the methods robustness towards granule's water content was confirmed in the second external validation trial. Figure 38 plots dried granule's LOD (based on reference analytics, see Figure 38 A) in relation to in-line NIRS- and reference results for PSD (see Figure 38 B-D). Dried granules' LOD varied between approximately 2 % and 11 %. However, NIRS predictions of PSD X10, X50, and X90 were in close agreement with the reference results throughout the trial, demonstrating the methods robustness towards LOD.

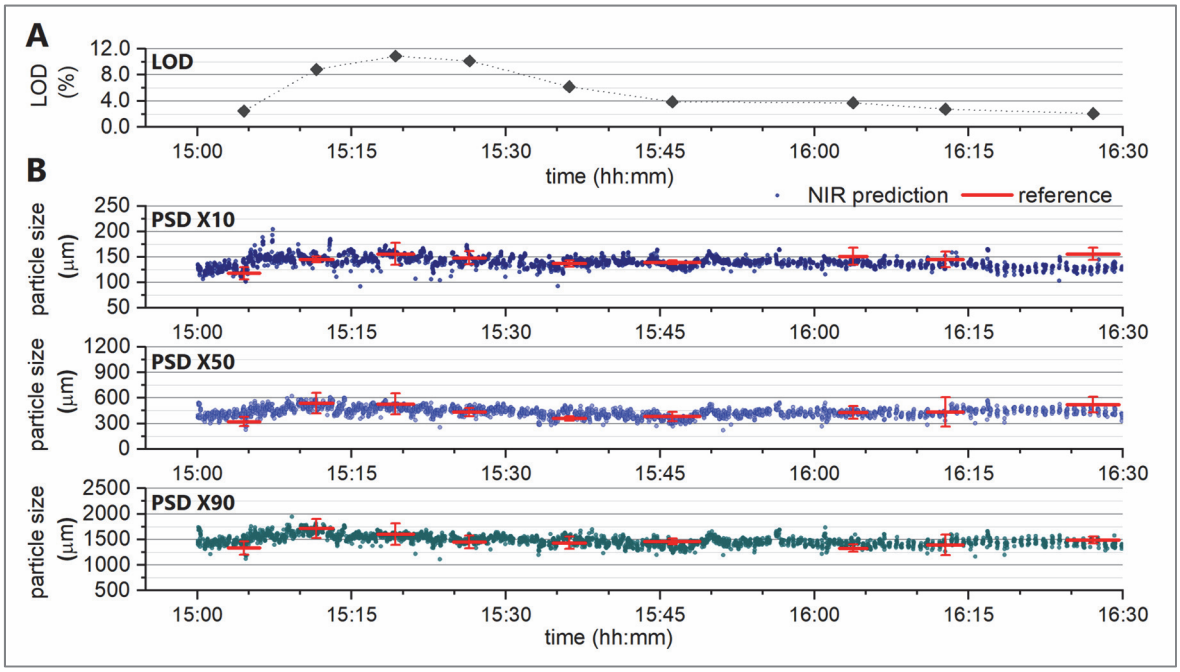

Figure 38: The methods robustness against variations in dried granules water content (LOD) was demonstrated. A: dried granules' LOD measured by reference analytics. B: NIRS-predicted PSD compared to IPC measured PSD (X10, X50, and X90, respectively) (Figure adapted from [187]).

The methods robustness towards varying API content (i.e. Diclofenac Sodium) was demonstrated in a third validation trial. Since the continuous manufacturing process will include a continuous feeder and blender upstream of TSG, variations in API content over time could occur, in case of feeder disturbances. Figure 39 plots in-line NIRS-predicted PSD of granules containing 20 %, 25 % and 30 % of API and offline reference PSD results. The granules' API content does not bias the NIRS predictions, as close agreement with the reference PSD analysis was demonstrated.

In summary, thorough external method validation with three independent in-line datasets demonstrated the methods ability to accurately monitor granules PSD during routine granulation and drying processes. Accurate PSD X10, X50 and X90 results were predicted in real-time and robustness against variations in LOD and API content was demonstrated. The large spread of NIRS-predicted PSD during internal and external validation can be explained by the sample size analyzed by NIRS compared to the sample size analyzed during reference analytics: The NIRS-light source scans a sample-area of approximately 4 mm^2 per spectrum, which represents a few milligrams of granules. Thus, the detected particle size depends significantly on the granule population in front of the probe at the time of spectral acquisition. In contrast, reference CamSizer measurement examines 5 g of sample, which provides a good average value of granules PSD. This was also previously discussed for NIRS-LOD method development, where similar effects were observed (see section 3.3.2.2, page 57 ff.).

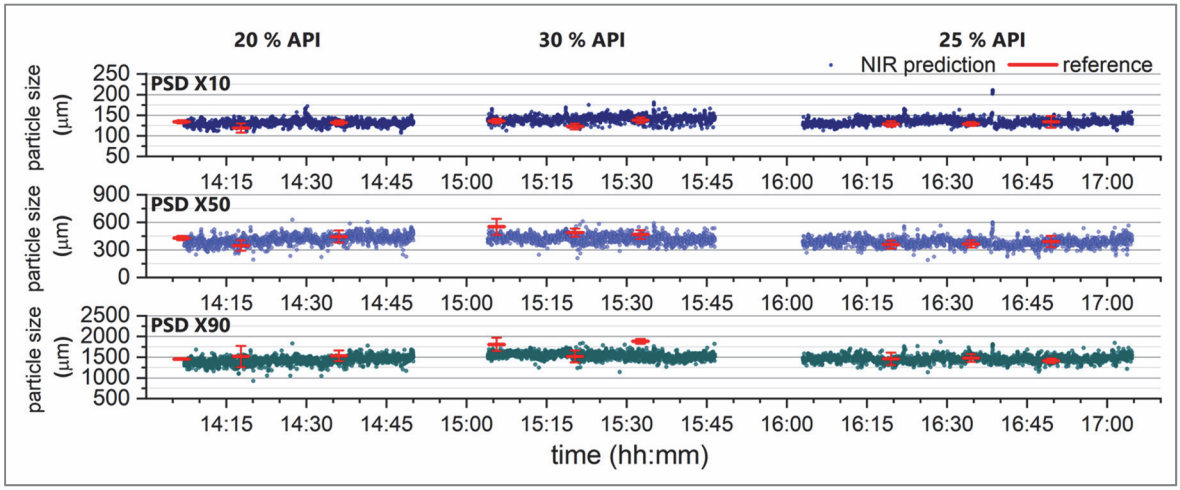

Figure 39: The methods robustness against variations in API-content was demonstrated. A-C: NIRS-predicted PSD compared to IPC measured PSD (X10, X50, and X90, respectively) at varying API content between 20 % and 30 % (Figure adapted from [187]).

3.3.3.2. Laser diffraction

Laser diffraction (LD) for particle size analysis is an absolute analysis method that does not require product-specific method development, since the instrument calculates particle sizes based on physical scattering principles. System verification checks with polydisperse reference materials can confirm the validity of the instrument. LD reports the particle size of the sample as the equivalent diameter of a sphere sharing the same diffraction pattern.

Theoretically, at-line sampling devices are available that can automatically withdraw samples from the production line and analyze them accordingly. Here, due to the GMP-status of the production site and the non-GMP status of the instrument, samples were collected manually and measured offline. Examples of PSD analysis via LD will be given in the next section.

3.3.3.3. Demonstration of orthogonality in PSD analysis

Due to technical issues and GMP-constraints, orthogonal PSD data from NIRS and LD for direct comparison with each other is only available from few experiments. However, by comparing both PAT-methods to reference dynamic image analysis (DIA), indirect demonstration of the two method's suitability to deliver redundant process information is possible.

The comparability between NIRS-based PSD analysis and reference DIA has been formerly presented in section 3.2.5 (page 34 ff.) and also during NIRS method validation and robustness testing in 3.3.3.1 (page 64 ff.). In both sections it was confirmed that the NIRS-based method allows accurate and robust monitoring of trends and sudden changes in PSD during routine granulation and drying processes. Refer to Figure 15 on page 39 and Figure 37 on page 66 for examples demonstrating orthogonality between NIRS and reference analytics by DIA.

To compare laser diffraction with DIA (and NIRS, when data was available), numerous granule samples from different trials were analyzed offline. For once, samples from the initial screening-DoE presented in section 3.2.4 (page 34) were analyzed. Additionally, samples from the auto-DoE presented in section 3.2.5 (page 34 ff.) were measured. NIRS data was only available from auto-DoE samples. Due to the instrument's technical restrictions, only samples with particle sizes < 1700 µm could be analyzed by LD.

A summary of the results from measured screening-DoE samples is shown in Figure 40; results from measured auto-DoE samples are shown in Figure 41.

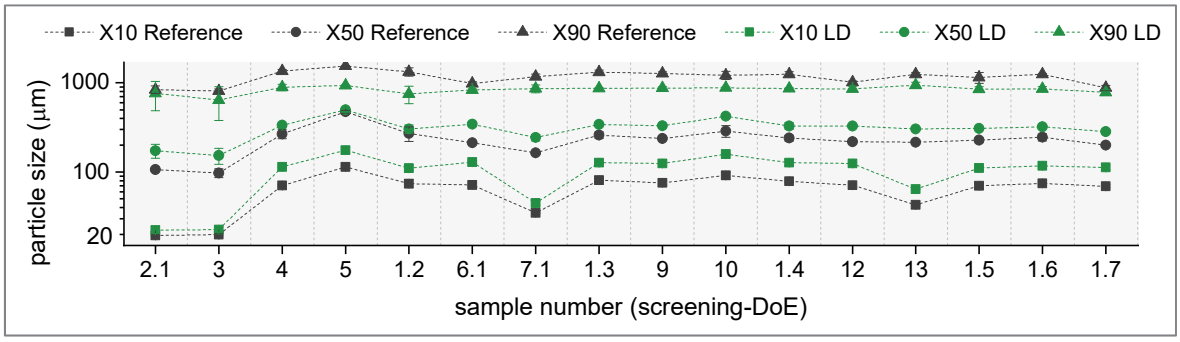

Figure 40: Comparison of laser diffraction and dynamic image analysis from screening-DoE samples. Due to restrictions in LD, only samples with particle sizes < 1700 µm could be analyzed by LD. Correlation coefficients (R) between reference and LD measurement were 0.99, 0.94, and 0.70 for PSD X10, X50, and X90, respectively.

Since the three analytical methods LD, NIRS, and DIA are based on fundamentally different physical principles, differences in the absolute values were to be expected. However, when considering the general trend of the results, good agreement was found. LD's applicability to particle sizes < 1700 µm inflicts constraints on the process control system that need to be considered: Implementation directly after the dryer (orthogonal to NIRS) is not feasible as granule sizes can be > 1700 µm and hence could cause blockage of the optical system. Consequently, statistical DoE-analysis based on LD measurement is also not possible; therefore, automatic process development by means of the Sequencer as described in section 3.2.5 (page 34 ff.) is not feasible with LD. However, LD could be implemented after milling and before compression, to analyze PSD of granules entering the tablet press.

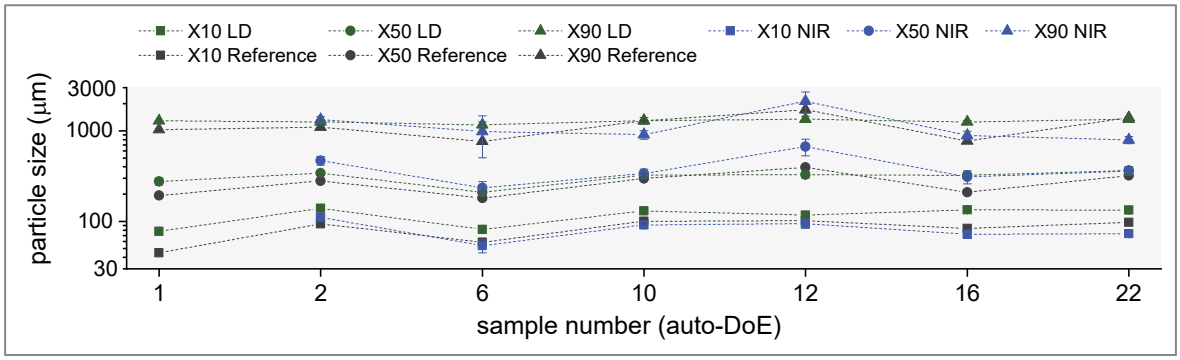

Figure 41: Comparison of laser diffraction, DIA and NIRS from auto-DoE samples. Due to restrictions in LD, only samples with particle sizes < 1700 µm could be analyzed by LD. No NIRS data was available for sample #1, due to technical issues. Correlation coefficients (R) between reference and LD were 0.88, 0.68, 0.85; and between reference and NIRS R=0.74, 0.85, 0.61, for PSD X10, X50, X90, respectively.

Other alternatives for orthogonal PAT for PSD monitoring include spatial filter velocimetry, online DIA, or focused beam reflectance measurement, as discussed in more detail in section 1.11.2 (page 19 ff.).

3.3.4. Orthogonal PAT for API content uniformity and blend uniformity[15]

3.3.4.1. NIRS to monitor API blend uniformity after continuous blending

NIRS method development for API blend uniformity after continuous blending was done with a calibration data set containing 425 spectra and a validation dataset containing 255 spectra (only online spectra). In detail, three powder blends containing 70, 100, and 130 % of the label claim Diclofenac Sodium content were prepared (Formulation B, see 6.2, page 117 ff.). The blends were poured manually through the blender PAT-chute, while spectra were recorded continuously. Each blend was poured twice, once for calibration and once for validation. The raw spectra dataset was cleaned by removing spectra with absorption > 0.35 at 1150 nm (high absorption was observed when the NIRS probe was not fully covered by blend).

Calibration and validation

For the calibration, spectra were pre-processed via SNV and 1st Derivative and calibrated against the weighted label claim (w/w %) of the prepared blends. Two PCs were selected, accounting for 97.8 % of spectral variation. RMSECV was 3.36 %, RMSEP was 3.23 %. Calibration results are summarized in Figure 42.

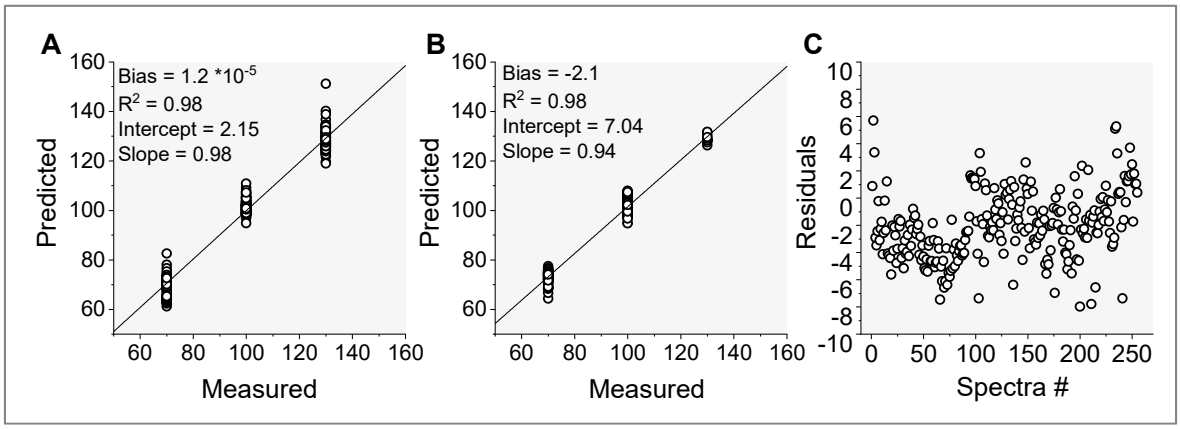

Figure 42: Summary of calibration and validation results for API blend uniformity after continuous blending. Spectra were preprocessed by SNV and 1st Derivative. A: Measured vs. predicted plot of calibration data set (cross-validation). B: Measured vs. predicted plot of validation data set. C: Residuals plot of validation data set.

No robustness testing was performed. For the intention of the developed method, such short development and validation procedure was acceptable. The wide spread in predicted API content per label claim might be due to non-homogeneous blends, as they were prepared in a glass bottle and blended by hand. In the future, the method will be improved with more data and validation runs, to include day-to-day variability and hence improve accuracy and robustness.

[15] Parts of this section have been previously published in Publication 3 (see page v)

3.3.4.2. NIRS to monitor API blend uniformity of dried granules

NIRS method development for API blend uniformity in dried granules (measured at the outlet of the drier) was performed with a calibration data set containing 3142 spectra (2110 online and 1032 offline) and a validation data set containing 748 spectra (267 online and 481 offline). Spectra were collected from numerous samples originating from various different trials and days, to ensure sample heterogeneity. In detail, calibration and validation samples varied in Diclofenac Sodium content (70, 80, 90, 95, 100, 105, 110, 120, and 130 % of label claim; i.e. 17.5 – 32.5 % Diclofenac Sodium content absolute), LOD (1-11 %), and PSD (~ 100 – 1000 µm PSD X_{50}); see Table 5 on page 57 for details. Parts of the applied spectral library were previously used to calibrate NIRS methods for LOD and PSD analysis (see sections 3.3.2.2 and 3.3.3.1, page 57 ff. and 64 ff., respectively).

For the calibration, spectra were pre-processed via SNV and 1st Derivative and then calibrated against reference HPLC analysis results via PLSR. 5 PCs were selected, which account for 94 % of spectral variability. The resulting model was tested by cross validation and an external validation data set; RMSECV was found to be 2.12 %, RMSEP was 2.22 %. Result from the internal and external validation are summarized in Figure 43.

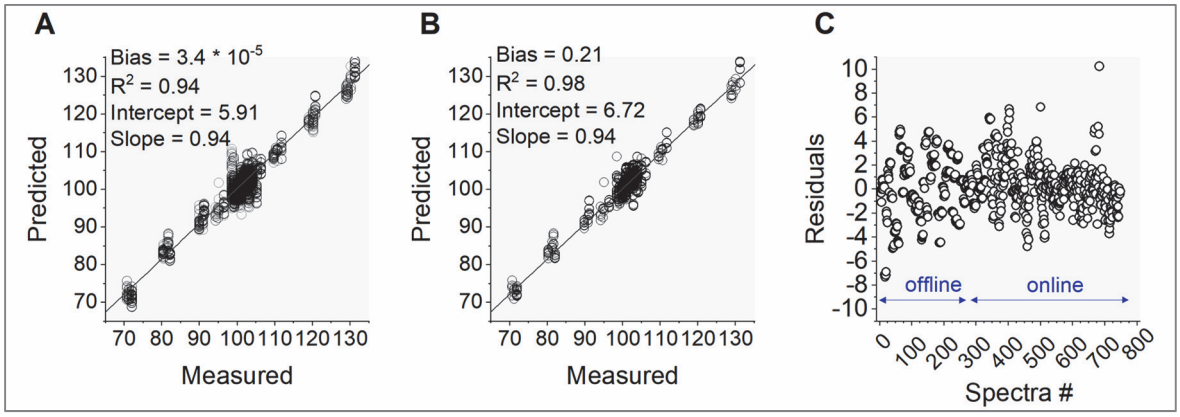

Figure 43: Summary of calibration and validation results for dried granules' API blend uniformity (measured after the drier). A: Measured vs. predicted plot of calibration data set (cross-validation). B: Measured vs. predicted plot of validation data set. C: Residuals plot of validation data set, no bias between offline and online data was observed.

Online validation and robustness testing

To demonstrate accuracy in API blend uniformity prediction and robustness towards PSD and LOD variations, further validation with three independent online validation datasets was performed. The same experiments were used to demonstrate validity and robustness of NIRS methods for LOD and PSD, as described in sections 3.3.2.2 and 3.3.3.1, page 57 ff., and 64 ff., respectively.

First, 8 different powder blends containing 70 – 130 % Diclofenac Sodium content (in % of label claim), were subsequently granulated and dried while online NIRS spectra were recorded and analyzed. Trials were performed on 3 consecutive days, offline HPLC analysis of collected samples was compared to the NIRS predicted API content; results are summarized in Figure 44. The method demonstrated excellent accuracy. Small deviations in individual spectra are caused

by poor sample presentation in the PAT-chute or dust sticking to the probe. Consequently, raw NIRS predictions should be filtered adequately during routine process monitoring.

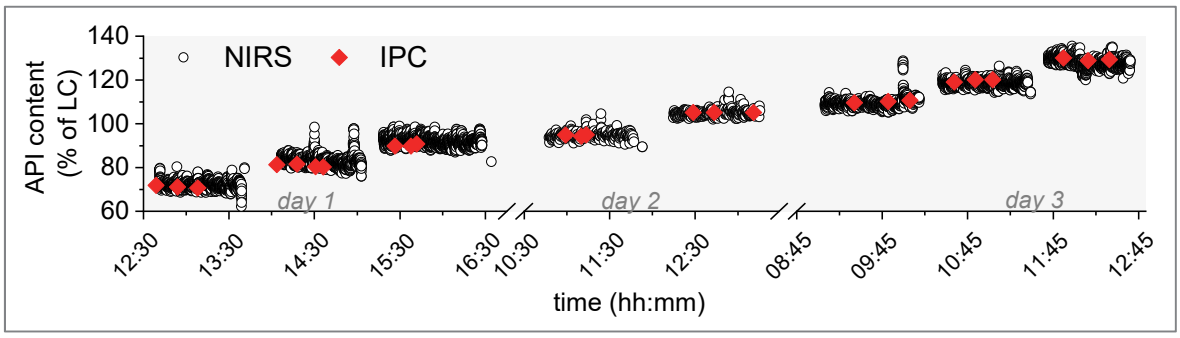

Figure 44: Demonstration of accuracy of real-time prediction of API blend uniformity in dried granules. (IPC = offline reference analysis of samples by HPLC). Trials were spread between 3 consecutive days.

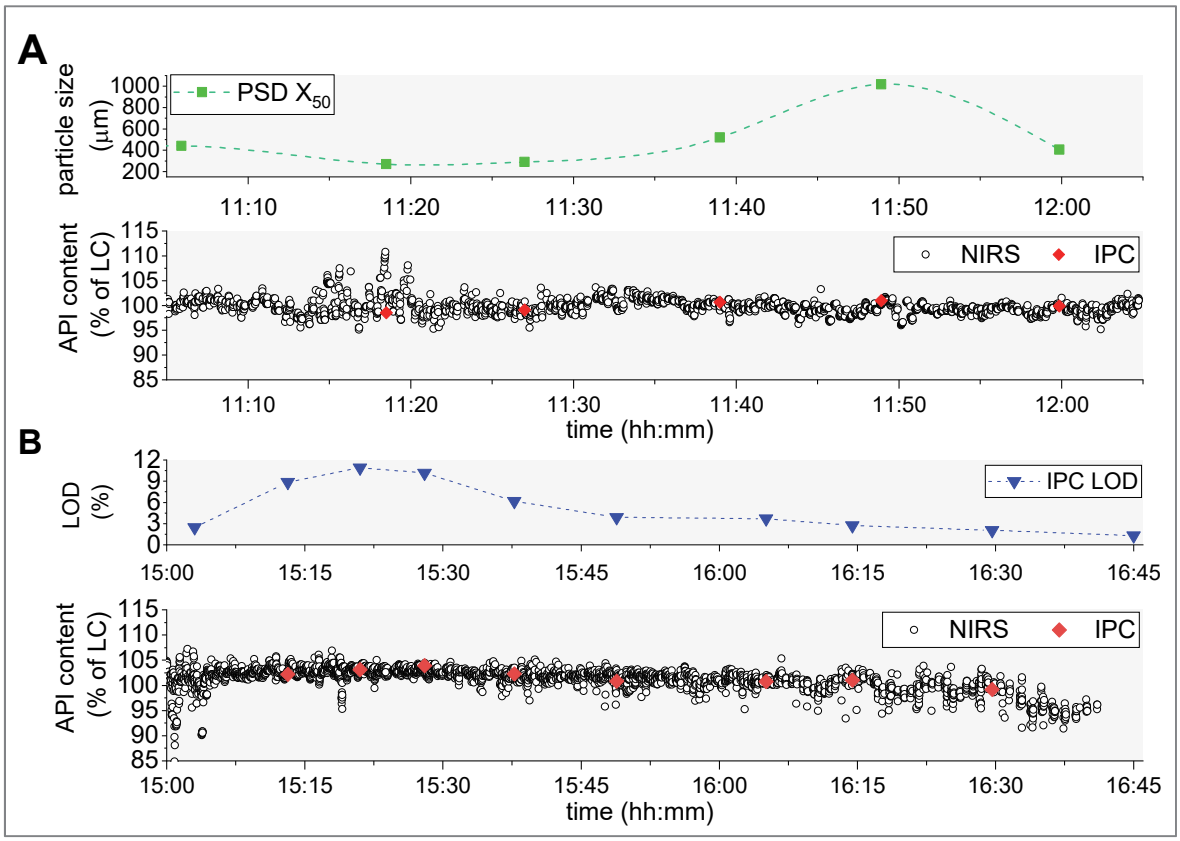

Figure 45: Robustness testing of the developed NIRS method for API blend uniformity in dried granules. The predictions are neither influenced by varying PSD (A) nor varying LOD (B). NIRS-predicted API contents are in good agreement with IPC results.

Second, for robustness testing, powder blend containing 100 % label claim API content was granulated and dried. In the first trial, the granules' particle size distribution was varied (~ 200 – 1000 µm PSD X_{50}) by adapting the L/S ratio during twin-screw wet-granulation (L/S 0.2 - 0.35). In the other trial, the granules' LOD was varied (~ 1 - 11 %), by adapting the drying conditions (DAV 80 – 160 m^3/h; DRS 5 – 30 rph; DT 80 – 90 °C).

Results are summarized in Figure 45. Granules' PSD X_{50} is plotted in comparison to API content in Figure 45 A, and granules' LOD is plotted in comparison to API content in Figure 45 B. In both trials it was demonstrated, that the developed method shows good robustness towards variations in PSD and LOD, since all NIRS-predicted API contents were in good agreement with IPC results.

3.3.4.3. NIRS for redundant control of API content in granules and tablets

To monitor API blend uniformity of granules in the tablet press feed frame and API content uniformity of tablets being ejected from the press, two NIRS methods were developed for two individual NIRS systems. Details on the development and validation have been published in Publication 3 (see page v). The following chapter summarizes the main outcomes of the study, for details refer to the original publication [179].

Comparison of NIR spectra from granules and tablets

Figure 46 displays an overview of available calibration spectra for granules (Figure 46 A) and tablets (Figure 46 B) after SNV normalization. Granule samples varied in LOD, PSD, and API content (Diclofenac Sodium); tablet samples varied only in API content (refer to [179] for details on the sample populations). In both plots, the main absorption of Diclofenac Sodium is observed at 1670 nm, caused by the first overtone of –CH. Absorption increases as the samples API content increases from 70 % to 130 % label claim. Additionally, the API's -OH peak at 1930 nm is detected. However, since the region between 1900 – 2000 nm is also highly correlated to water absorption, this peak is not suitable for API content quantification [147].

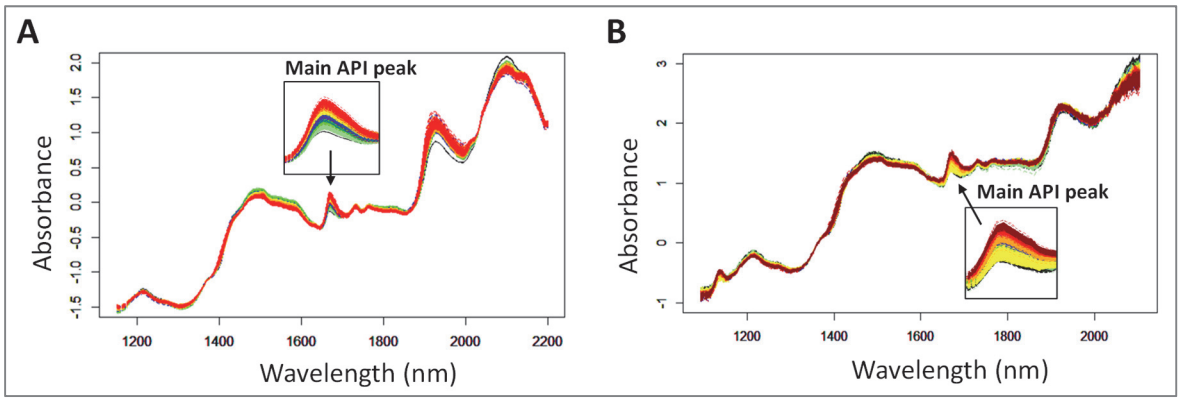

Figure 46: Near Infrared spectra after Standard Normal Variate (SNV) normalization, colored by API content (70 – 130 % LC). A: Granules in the tablet feed frame. B: Tablets (Figure adapted from [179]).

Generally, spectra from granules and tablets are comparable and both suitable for API content analysis. PCA analysis of tablet spectra indicated that the tableting speed has a significant influence on spectral acquisition (see Figure 47). While low to moderate tableting speeds of 17.000 and 30.000 tablets/h show no difference in the spectral PCA plot, spectra collected at high speeds of 70.000 tablets/h form a new cluster in the PC1 to PC2 score plot. Therefore, special care needs to be taken to design the calibration methods in a robust way that is not biased by the tableting speed.

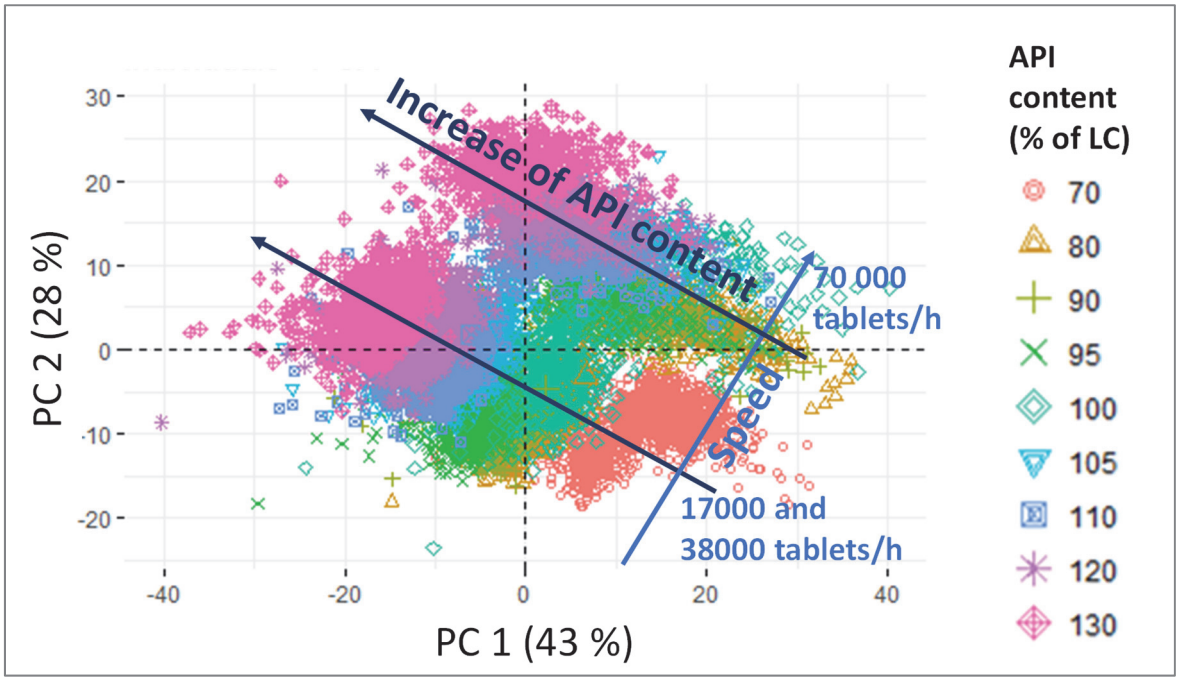

Figure 47: PCA plot of SNV-pretreated spectra at three different tableting speeds demonstrates the impact of the acquisition speed on tablets NIR spectra: Score plot PC1 vs PC2, colored by label claim 70-130 % (Figure adapted from [179]).

Qualitative monitoring of API content uniformity in tablets

Before quantitative calibration of NIRS spectra to the samples respective Diclofenac Sodium content was performed, different qualitative solutions for API content monitoring of tablets were assessed and compared. Qualitative analysis of NIRS spectra allows process monitoring without vast prior knowledge of the process and materials and especially, without performing a time-consuming calibration (e.g. during early stages of development). Examples for qualitative spectra analysis are single wavelength monitoring (SWM), Principal Component Analysis (PCA), and Independent Component Analysis (ICA). The three methods ability for qualitative process control was tested and compared experimentally.

In detail, pre-prepared granules varying in Diclofenac Sodium content were added sequentially to the tablet press hopper to induce steps in API content from 100 % to 130 % label claim, and then down to 70 % LC. Online spectra were collected from each tablet being ejected during the experiment; collected spectra were analyzed with the three qualitative analysis methods for comparison. The absorption of the main Diclofenac Sodium peak at 1670 nm was monitored for SWM analysis, where the use of SNV and 1st derivative preprocessing reduced the effect of the tableting speed enough to allow accurate monitoring of API-content trending. For PCA analysis, the scores of SNV and 1st Derivative preprocessed spectra were observed. Results were comparable to SWM, but a higher impact of tableting speed was detected. In contrast, ICA enables the separation of sources of variation, and thus allowed to separate the effect of the API content from the effect of tableting speed. Hence, ICA proved to be the more robust method for qualitative process control and provided an adequate solution for qualitative API content monitoring. An overview of the three assessed qualitative data analysis methods is provided in Figure 48 [179].

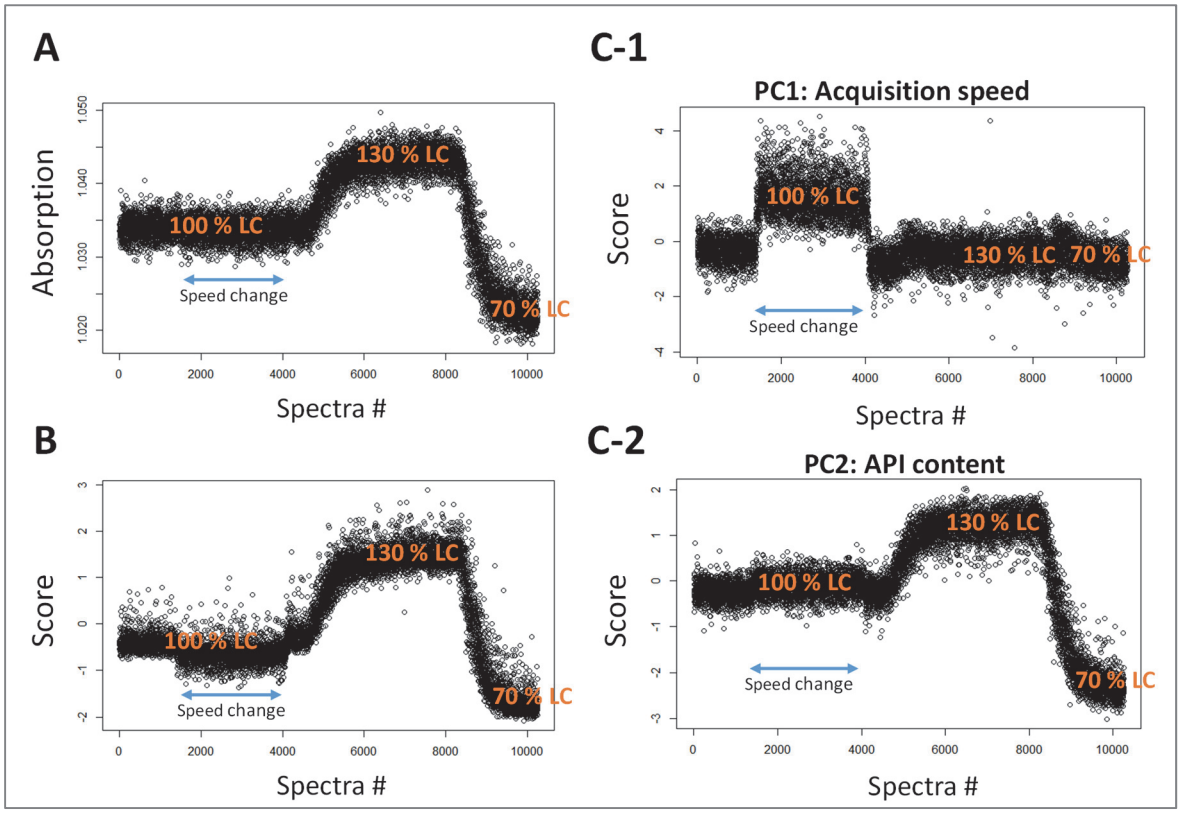

Figure 48: Comparison of qualitative approaches to monitor tablet content uniformity. A: Single wavelength monitoring with SNV and 1st Derivative preprocessed spectra. B: PCA scores of SNV and 1st Derivative preprocessed spectra. PCA scores are influenced by API content and speed, despite 1st derivative preprocessing (C) Independent Component Analysis (ICA) allows the separation of sources of variations tableting speed (C-1) and API content (C-2) (Figure adapted from [179]).

Quantitative monitoring of API content in granules and tablets

While qualitative spectral analysis can be useful for early stages of development, a quantitative method is required for accurate process control and real-time release dedications. During quantitative method development, different options for spectral sampling, calibration, and data preprocessing were assessed to develop the most suitable method; details were published in Publication 3 (see page v). In summary, SNV and 1st derivative were required to reduce the impact of process speed on spectral acquisition, and in-line and offline spectra had to be included into the calibration and validation data set for the best accuracy and robustness. Reduction of spectral range had a positive effect on spectral noise. No significant difference was observed when calibrating against HPLC reference values or the theoretical label claim (LC) of the used samples (based on mixing ratio between API and excipients during blend preparation), hence final calibration was done against LC. For tablets, spectra acquired at different tableting speeds had to be included for acceptable robustness.

Overall, for granules' content uniformity the final calibration resulted in SEC = 2.3 % and SEP = 2.2 % (with online data). For tablet content uniformity the final calibration resulted in a SEC = 1.9 % and SEP = 1.6 % with online data (see Figure 49 for details on the two calibrations).

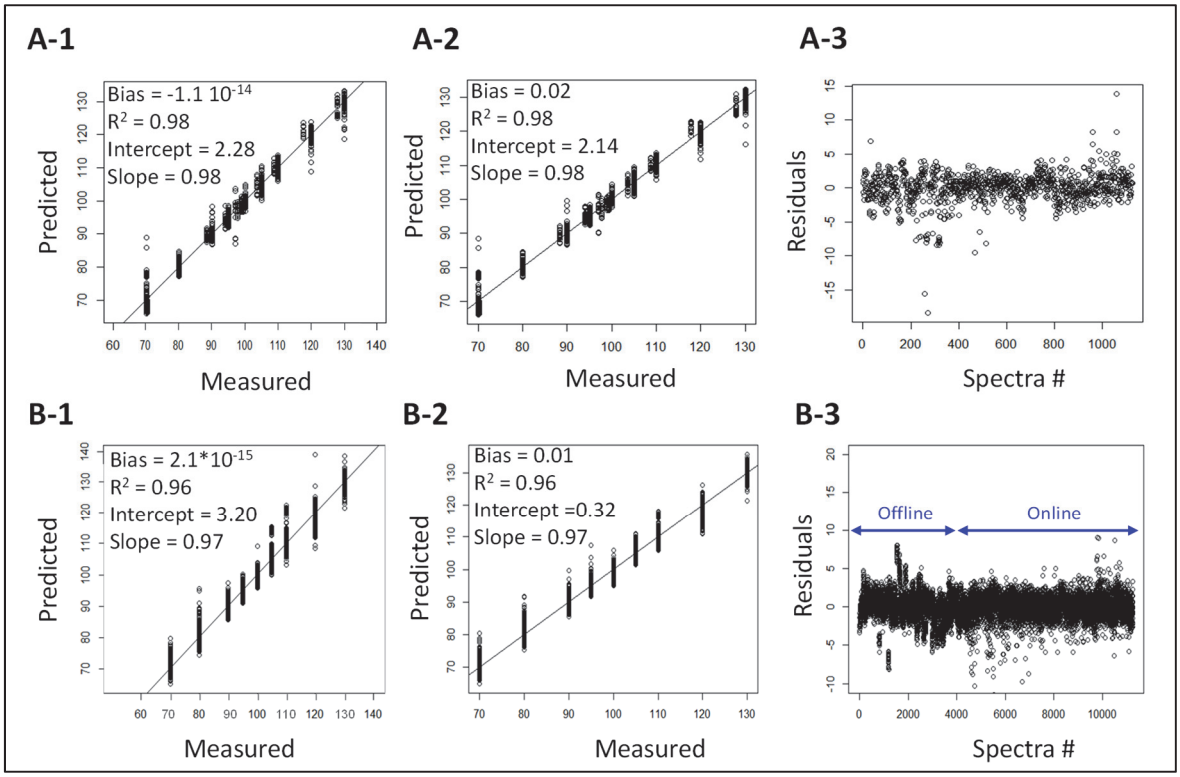

Figure 49: Summary of the prepared calibrations for API content of granules (A) in the tablet press feed frame and tablets (B) (spectra preprocessed by SNV and 1st Derivative). A-1 calibration data set, A-2 validation data set. A-3 Residuals from offline and online data, no bias was observed. B-1: calibration data set, B-2: validation data set, A-3: residuals from offline and online data, no bias was observed (Figure adapted from [179]).

Further details on performed online validation that demonstrated redundant monitoring of API content in granules and tablets can be found in the original publication [179], another example for redundancy in API content analysis will be given in the next section.

3.3.4.4. Demonstration of orthogonality in API content uniformity analysis

Commonly, orthogonal analytical methods refer to two individual procedures that use different physical principles to analyze the same sample characteristic [174]. Consequently, applying two separate NIRS-systems to redundantly monitor API content uniformity, does not fit the traditional definition of orthogonality. On the other hand, two separate instruments, from different suppliers, with different software, and different optical systems were used, and two separate methods were developed and validated. Therefore, the risk of both systems failing at the same time, or both methods being susceptible to the same robustness or validity errors, is low. For that reason, the two NIRS systems bring most of the benefits of true orthogonal PAT-strategies, even though they cannot be considered orthogonal in the classical sense [110, 111].

Another orthogonal alternative to API blend and content uniformity analysis, is provided through the monitoring of powder feed rates. When API and Excipients are fed with separate feeders, continuous analysis of the relative feed rates, combined with thorough, empirical knowledge of the materials residence distribution (RTD) in the line, allows to predict the API content in blends, granules, and final tablets.

To demonstrate orthogonal API content monitoring in tablets by redundant NIRS and feed rate analysis, a proof-of-concept experiment was performed. Two feeders were installed to feed API and an excipient pre-blend separately (Formulation B, see 6.2, page 117 ff.). The API content of tablets was then varied, by adjusting the relative feed rates between the two feeders accordingly. The API concentration of the material at the end of the production line was monitored by two independent NIRS systems: one installed in the tablet press feed-frame (analyzing granules before compression), and one at the ejection position of the press (analyzing every tablet). Moreover, the actual feed rates of both feeders were analyzed.

Figure 50 depicts an overview of the used experimental setup with the location of the feeders and the two NIRS probes in the continuous manufacturing line. The relative feed rates between feeder 1 and feeder 2 (containing API and Excipient pre-blend, respectively) were adjusted in 30 minute intervals from 100 %, to 130, to 70 %, and back to 100 % of the target API label claim (see eq. 20, page 120, for calculation of label claim).

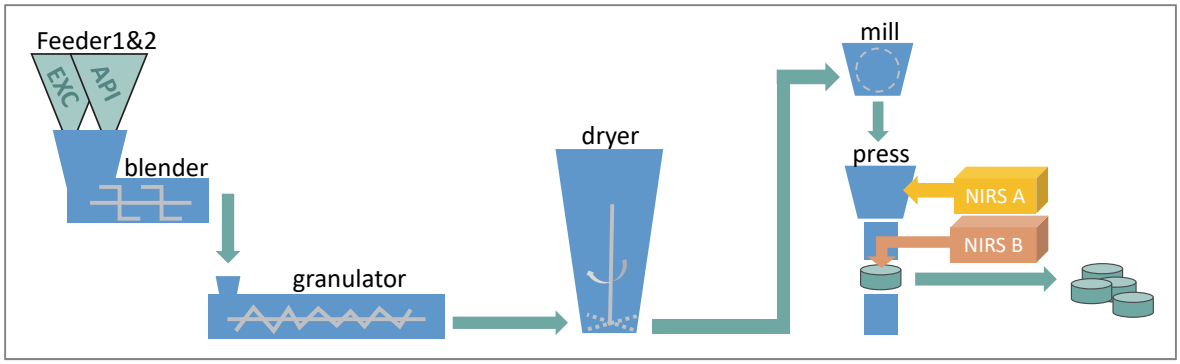

Figure 50: Description of experimental setup. NIRS A is installed in the tablet press feed-frame to analyze granules, NIRS B analyzes every tablet exiting the press. (DOS = feeders, BLE = blender, TSG = twin-screw wet granulator, FBD = fluid-bed dryer, MIM = mill, TAB = tablet press, NIRS = near infrared spectrometer).

The blend API content entering the process line (calculated from relative feed rates of feeder 1 and feeder 2), in comparison to the observed NIRS predictions in the tablet press feed frame and final tablets, is plotted in Figure 51. The step-responses were normalized to the overall effect, to plot Effect F over time t. The first step in API content is defined as the start of the experiment (t = 0). For once, Figure 51 demonstrates redundancy and orthogonality between the two NIRS probes, since the two plots show good comparability. NIRS B (see Figure 50) enables accurate and robust monitoring of tablet content uniformity in real-time, by scanning individual tablets. However, as the probe solely scans a tablets' surface for content uniformity prediction, the second NIRS installed in the feed-frame (NIRS A) adds a second layer of certainty. It demonstrates the granules blend uniformity shortly before tablet compression. Both signal dynamics are similar, which indicates that the material is compressed almost immediately after it enters the feed frame. In the future, the combination of the two NIRS probes with chemometric monitoring of compression parameters (e.g. compression force and fill depth) could facilitate 100 % real-time control of both, content uniformity and tablet weight variation, giving a clear picture of every single tablet that is produced [176-178].

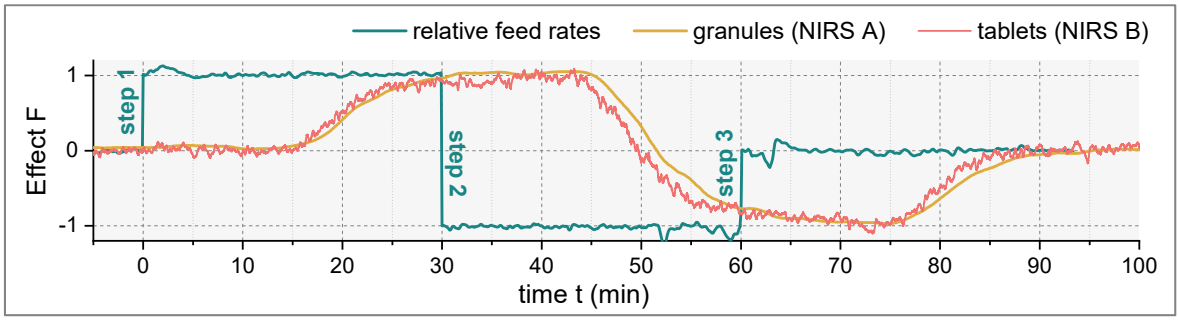

Figure 51: Proof-of-concept trial for orthogonal, redundant monitoring of API content by feeder analysis and two NIRS probes. Step changes were normalized to step height, to allow better comparison of effect F.

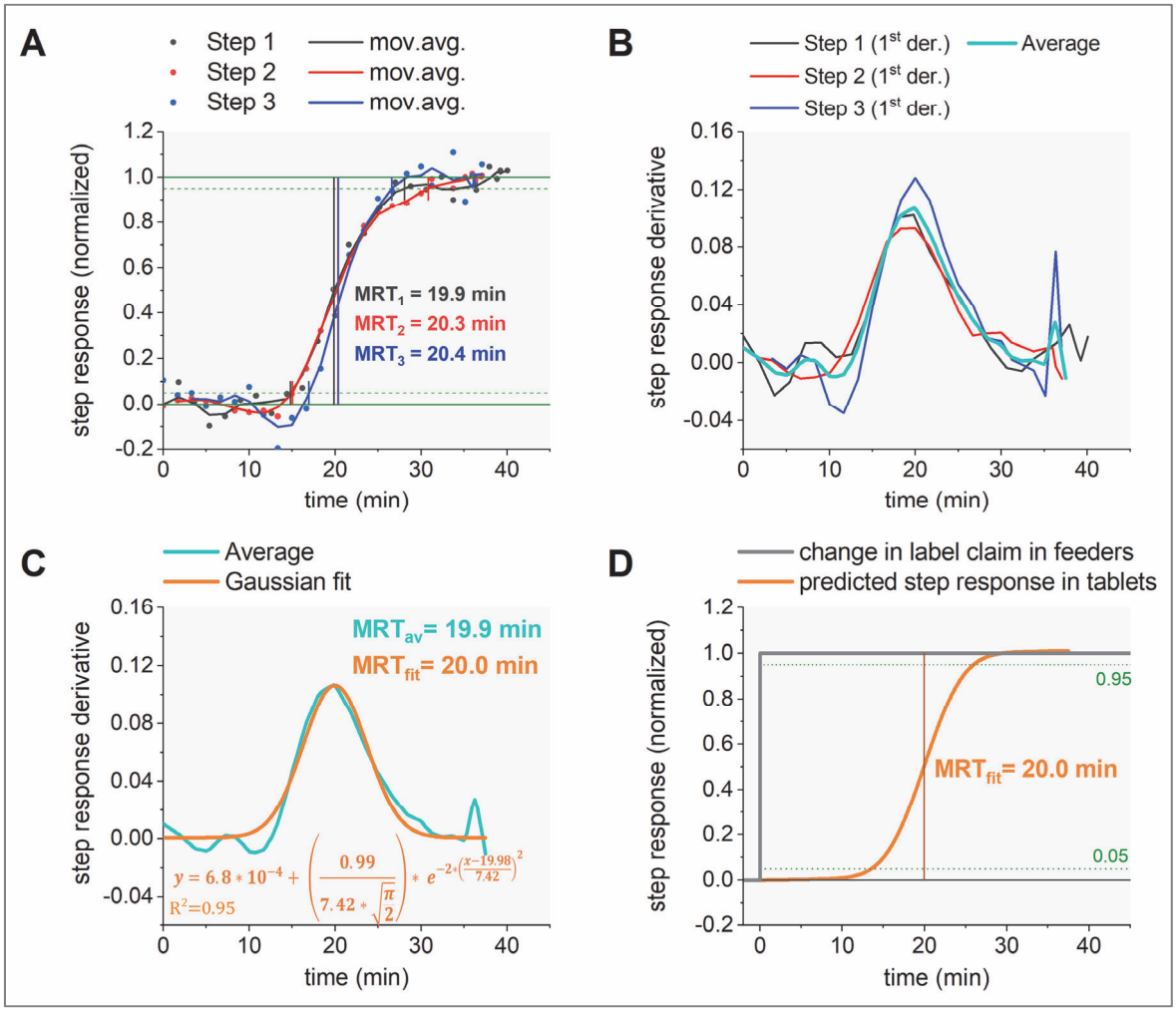

Figure 52 demonstration of API content monitoring through feed rate analysis in combination with RTD. The three steps in API content from Figure 51 were normalized to step their respective altitude (A) and differentiated by the 1st derivative (B). The average step response can be described by a Gaussian fit function (R^2=0.95) (C). Consequently, model-based prediction of step responses after changes in API content label claim (based on feed rate) becomes feasible (D).

Likewise, orthogonality can be achieved by monitoring the API and excipient feed rates in real-time, in combination with knowledge on the material's residence time distribution (RTD). Briefly, the three step changes induced in the experiment shown in Figure 51 (namely step 1: 100 % LC to 130 %; step 2: 130 % to 70 %, and step 3: 70 % to 100 % LC) allow to determine

the processes' mean residence time (MRT), as illustrated in Figure 52. Here, the induced step changes were investigated by analyzing each tablet exiting the tablet press by NIRS; similarly the RTD could be determined with reference HPLC analysis of timely samples. Plotting the normalized step-responses over time demonstrates that the step dynamics are comparable between all three performed steps, independent of step height or direction (see Figure 52 A; step-responses were normalized to the respective step-height). The first derivative of the three step responses resembles a Gaussian function (see Figure 52 B); therefore, the average derivative of the three step responses, can be fitted by a Gaussian function plot (see Figure 52 C). Finally, the integral of this Gaussian function facilitates the prediction of any other step response MRT in the future (see Figure 52 D). More details on determining the process' RTD, and the influence of different process parameters are presented in section 3.4 (page 99 ff.).

The unintentional occurrence of such huge steps in API content, as discussed above, is a rather unlikely scenario during commercial manufacturing. However, once a processes RTD is defined, the same principle can be applied to follow any other variation in the process line for quality control (e.g. a rapid, short-term increase in API feed rate after refill of the feeder hopper or a brief failure in the granulation liquid pump). In general, the method requires in-depth analysis of feeding and blending behavior and the materials RTD in relation to varying process parameters (i.e. back- and forward mixing behavior and hold-up). In summary, it was demonstrated that monitoring of API content uniformity by two NIRS probes and feed rate analysis, complies with orthogonal principles and allows accurate and redundant monitoring of API content during routine continuous manufacturing. With this knowledge, ejection of OOS-tablets and real-time release of the remaining product becomes feasible. The presented data will be analyzed again in more detail in section 3.4 (page 99 ff.), under the aspect of material residence time distribution at varying process conditions.

3.3.5. Managing redundant data from orthogonal PATs

3.3.5.1. Concept

When orthogonal PAT analyzers indicate similar quality characteristics, control actions can be clearly defined at a high level of control assurance. Conversely, if one PAT suddenly indicates a quality event while the other orthogonal analyzer remains constant, the control systems needs a systematic algorithm on how to proceed.

One feasible option for PAT data reconciliation is the evaluation of process data, with the general idea that product quality can be assumed to be in control, as long as all related process parameters prove to be in statistical control. Therefore, a deviation from quality as indicated by a drifting or shifting PAT, should also be detectable as a statistical deviation in the process data. If no deviation is observed in the process, it is more likely that the shifting PAT system has an issue not related to product quality and hence should be checked or replaced (e.g. lamp failure in NIRS). However, if a statistical deviation is detected in the process data, the control strategy has a strong indication that the process is drifting or shifting away from its target quality limits. In such a case, the control system is empowered with a high level of certainty to adapt the process conditions, in order to bring the product quality back under control.

Multivariate statistical process control (MSPC) is the most common methodology to monitor complex processes, where numerous parameters are to be considered and evaluated. One common approach to MSPC is the evaluation of multifactorial process data via principal component analysis (PCA), a method that summarizes the largest variabilities within the data matrix into principal components (PCs), with the aim to identify systematic information and variable relationships and to reduce the number of variables to monitor. By comparing PC statistics (≙ variation statistics) of the current process to a former state-of-control process, unusual process deviations can be detected. MSPC is an unspecific method that benchmarks process performance, without giving a clear indication of the deviation cause [167, 169, 170]. The following sections will first explore different options of MSPC in continuous manufacturing. Later, their applicability for PAT data reconciliation will be discussed.

3.3.5.2. Analysis of common variation

Generally, any process is susceptible to a certain level of common variation; the process is assumed to be in statistical control, as long as this level of variation is not exceeded. Such common variation is related to normal fluctuations in process parameters and process conditions that occur frequently but are not quality critical (e.g. small variations in feed rate or temperature settings, applied air flow, varying room relative humidity, etc.). The level of common variation can be evaluated from historical data of production batches, where product quality demonstrated acceptable (as confirmed by offline quality analysis, for example). Statistics on such process data then can serve as a reference standard to monitor subsequent production batches in real-time [169].

To generate a reference calibration dataset for MSPC, a set of experiments was performed. Since the main focus of the project was put on the redundant control of dried granules' LOD and PSD, only process units twin-screw wet-granulation and fluid-bed drying were considered. In detail,

granulation and drying was performed for three hours at constant process parameter settings (i.e., standard settings, see 6.4.6, page 121); the quality of the dried granules was monitored through offline reference analysis (IPC) of CQAs LOD and PSD every 15 minutes. 13 process parameters were selected for analysis by MSPC. Selection was for once based on the criticality matrix rating presented in section 3.2.3 and 3.2.4 (page 31 ff.). Additionally, secondary process parameters exhaust air temperature, exhaust humidity, filter pressure, sieve pressure, and granulator torque were included. Exhaust air temperature and exhaust humidity are defined by the inlet parameters and the characteristics and drying behavior of the input materials. Filter pressure describes the pressure difference at the outlet airflow filters of the dryer, and is largely related to the amount of fines in the granules and the overall runtime of the line. Sieve pressure is the pressure difference at the sieve bottom of the drying chambers and can indicate sticky and wet granules, in the case of a pressure increase and is also related to runtime. The granulator torque gives an indication of material hold up (degree of fill level) in the open volume of the screws and the stickiness and flow of the material.

A summary of the selected parameters and their observed common variation in the calibration experiment is presented in Figure 53 B; corresponding IPC results of granule samples are presented in Figure 53 A.

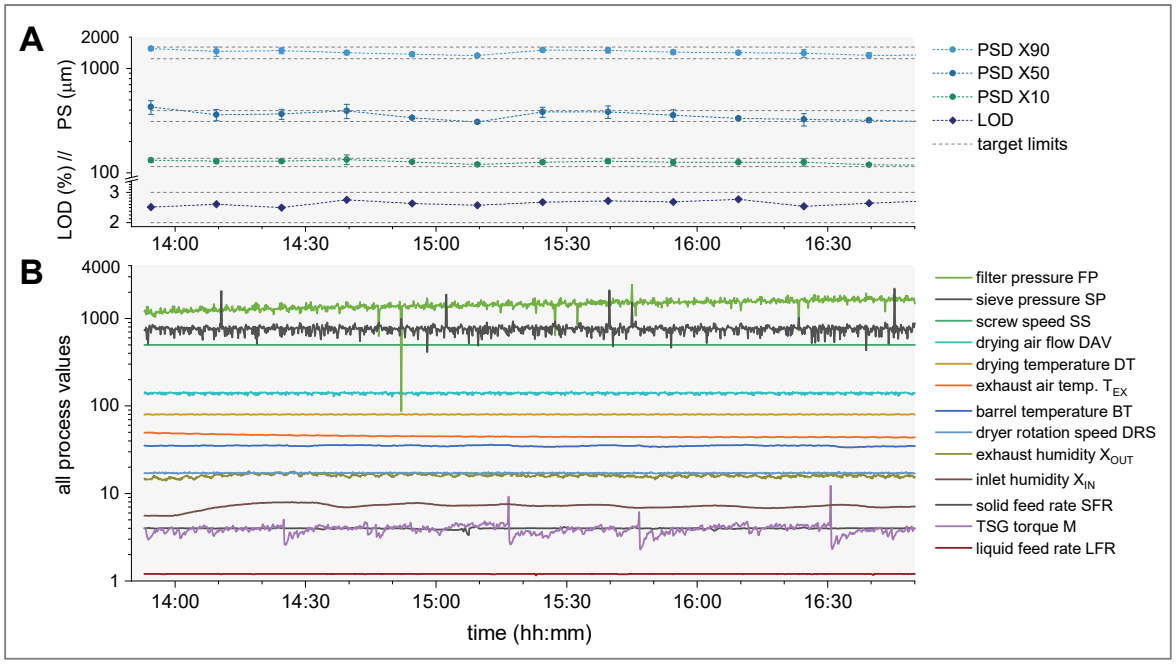

Figure 53: Calibration dataset for MSPC. A: reference analysis of granules samples demonstrated that the process was in control throughout the three hours of process time. B: Overview of analyzed process parameters during 3 hours of continuous granulation and drying.

Figure 53 A demonstrates that the process was in a state of control throughout the calibration experiment, as CQAs remained constant within their predefined limits at all times (target limits for LOD are defined based on powder blend $LOD_0 \pm 0.5$ % ($LOD_0 = 2.5$ %); limits for PSD X10, X50, and X90 are defined based on their common variation as quantified in [22] (namely ± 9, ± 12, ± 14 %, respectively). A numerical overview of observed process variations is listed in

Table 7. By comparing each parameters setpoint to the experimental average, minimum/maximum variations, and relative standard deviations (RSD), the overall amount of common variation can be judged. Largely, the observed common variation in process parameters ranged from 0.0 % RSD (in screw speed) up to 14.3 % RSD (in sieve pressure; see Table 7 for details), showing that the individual level of common parameter variation gives no indication on the product or process quality, as long as it stays constant throughout the process.

Table 7: Numerical analysis of the common variation observed in the calibration data set.

	SFR	LFR	BT	SS	M	DT	T_{EX}	DAV	X_{IN}	X_{OUT}	FP	SP	DRS
setpoint (SP)	4.0 kg/h	1.2 kg/h	35 °C	500 rpm	-- *	80 °C	-- *	140 m^3/h	-- *	-- *	-- *	-- *	17 rpm
average	4.0	1.2	35.1	500	3.9	80.0	45.1	139.9	7.2	16.0	1452	759	17.1
min (% of SP)	84	96	96	100	59	99	96	91	77	87	6	53	96
max (% of SP)	106	101	103	100	315	101	110	105	111	113	167	290	104
Span (% of SP)	22	5	7	0	256	2	14	14	34	26	161	237	8
RSD (%)	1.4	0.2	1.4	0.0	13.3	0.6	3.2	2.3	6.8	4.1	12.2	14.3	1.1

** min/max variation and relative standard deviation (RSD) was calculated from average value instead of SP if no SP is available. Refer to Figure 53 for abbreviations of process parameters.*

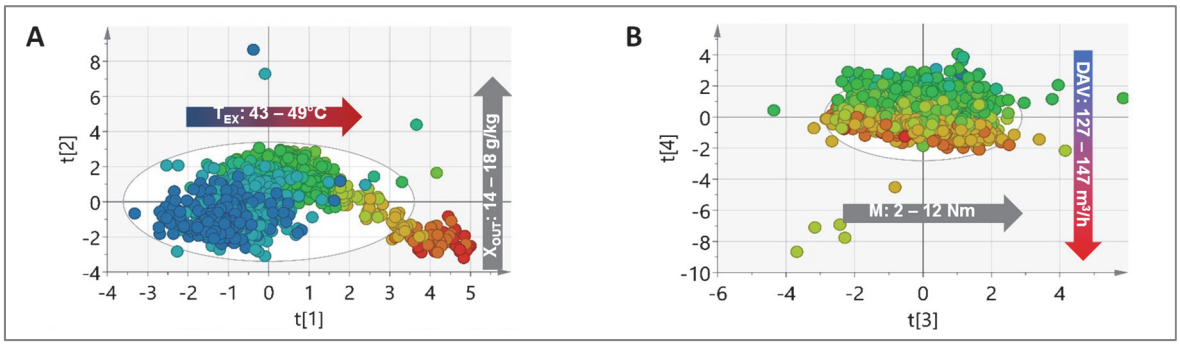

Figure 54: PCA score plot (calibration I). A: PC 1 vs. PC2, mainly attributed to the variation in outlet temperature T_{EX} and the outlet humidity X_{OUT} (colored according to T_{EX}). B: PC 3 vs. PC4, mainly attributed to the variation in granulator torque M and drying airflow DAV (colored according to DAV).

From the recorded process data, PCA was performed. Four PCs were selected, which account for 52 % of the overall variability (R2X); corresponding score plots for PC 1-4 are illustrated in Figure 54 A and B. Generally, principal components should be added during PCA, as long as 85 % R2X has not been reached and if added component deliver more than 5 % of R2X [166]. Hence, R2X of 52 % indicates that more components are required to describe the observed variability in the dataset properly. However, in the presented example, four PCs were sufficient to demonstrate the intended purpose of the control charts. Corresponding loading plots suggest that the 1st PC is mainly attributed to outlet temperature and filter pressure and partially to humidity, the 2nd PC is mainly attributed to humidity and partially to granulation parameters, the 3rd PC is attributed mainly to granulation parameters and partially to humidity, and the 4th PC to dryer airflow and sieve pressure (see Figure 54 A and B for details; for loading plots see supplementary data 10.4, Figure S 3, page V).

From the selected PCs, four calibration Shewhart control charts were created (further referred to as calibration I, see Figure 55). Shewhart charts plot the PCs over time, in relation to the target and the respective alert and action limits. The target in the control chart is defined from the average of the data set, alert and action limits are commonly set at two- and three-times of the observed standard deviation [166, 167]. The observed variations are classified as common process variations. Hence, the observed spikes in the charts are also classified as common variations, even though they are found outside of the alert and action limits. Action limits are defined at ± 3 * standard deviation, which represents approximately 99.73 % of the observed data in a normal distribution [188]. Consequently, the observed spikes outside of the action limits account for < 0.3 % of observed variation. They are most likely caused by fluctuations in the air flow triggered by the product filter blow-out, and by fluctuations in the granulator torque (see Figure 53 for comparison), that have no significant influence on product quality.

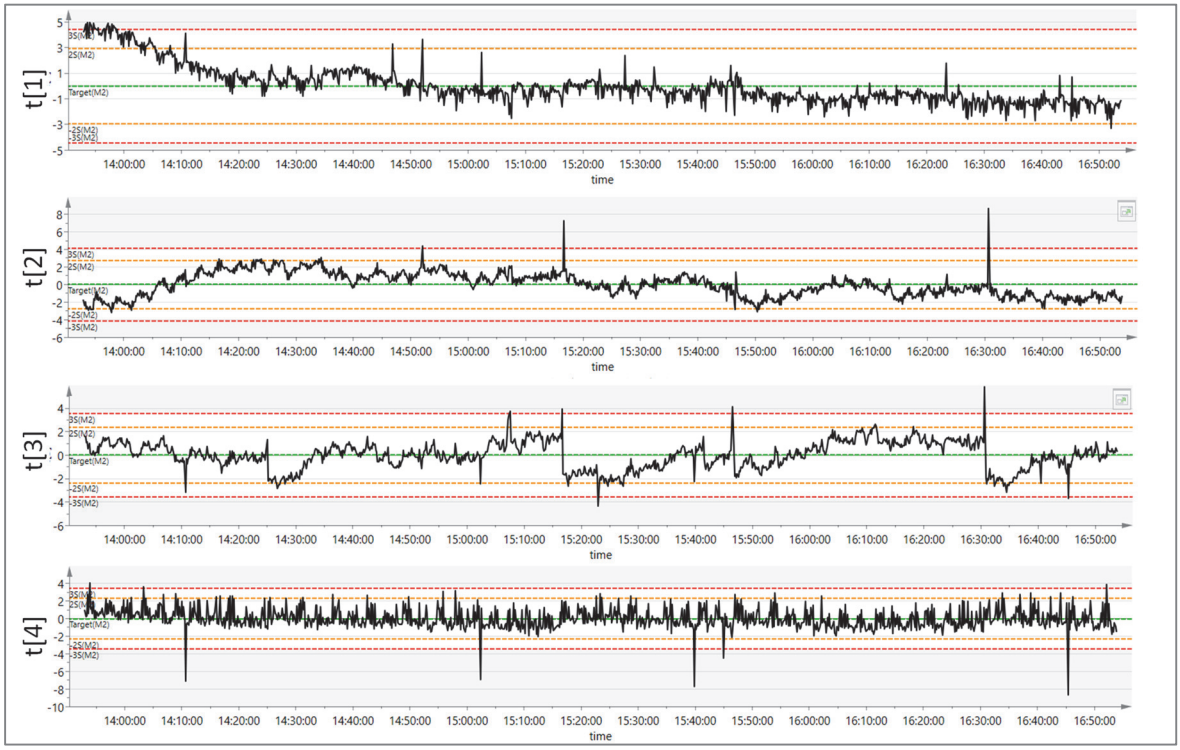

Figure 55: Shewhart control charts of calibration I, PC 1 – 4 (the action limit is set at two times the standard deviation s; the control limit is set at 3*s).

3.3.5.3. Detection of uncommon variation

To evaluate calibration I for its ability to detect uncommon process deviations, a validation experiment was performed, where process parameters liquid feed rate (LFR), drying air flow rate (DAV), and barrel temperature (BT) were sequentially varied at different magnitudes between 0.5 % - 10 % from their initial setpoint. The selection was based on PP criticality: LFR and DAV are CPPs for LOD and PSD, while BT is a nCPP [22]. A detailed list of the applied setpoint variations is provided in Table 8. Between each of the variations, process settings were

returned to the standard process conditions to allow re-equilibration of the system. A summary of the recorded process values and results from reference analytics is shown in Figure 56.

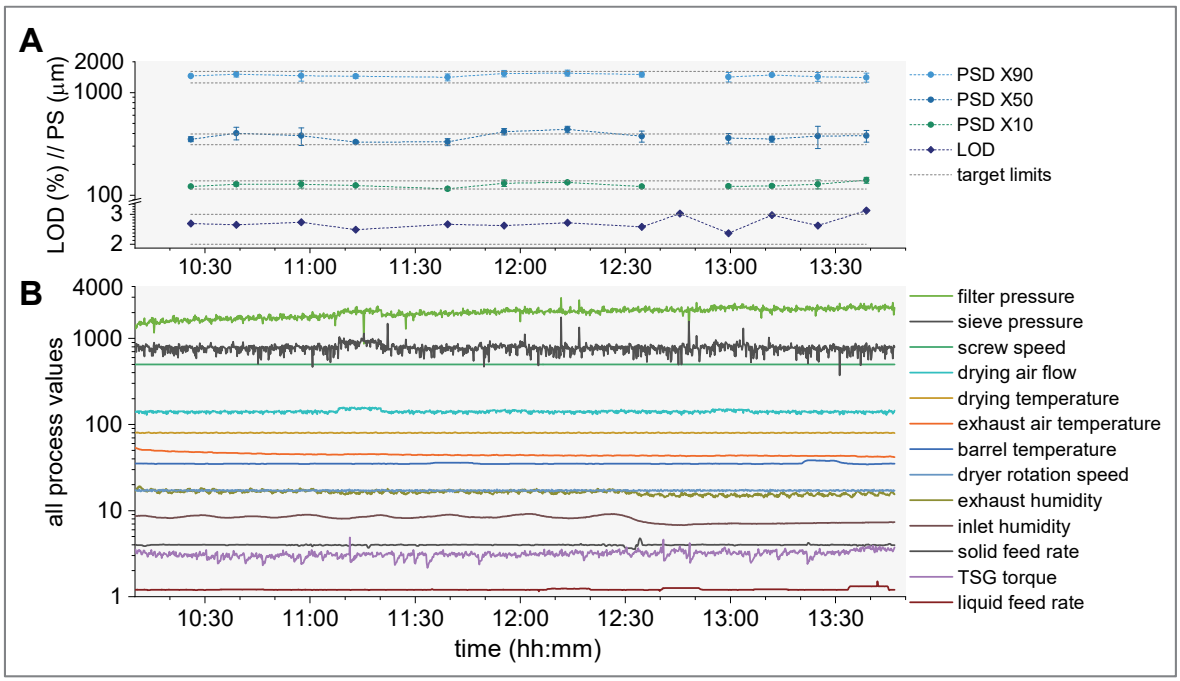

Figure 56: Validation data set for MSPC. B: Overview of related process parameters during the experiment. Variations in liquid feed rate, drying air flow, and barrel temperature were induced intentionally to test the calibration data set. A: Reference analysis results, target limits are based on the validation data set (No sample for PSD analysis was available for sampling point 12:45).

Table 8: Validation experiment: applied setpoint variations in process parameters LFR, DAV, and BT.

step	**a**	**b**	**c**	**d**	**e**	**f**	**g**	**h**	**i**	**j**	**k**	**l**
PP	LFR	DAV	DAV	BT	DAV	LFR	DAV	LFR	DAV	LFR	BT	LFR
magnitude [%]	0.5	0.5	10	3	3	3	1.5	5	5	1.5	10	10

Reference analyses demonstrated that almost none of the applied variations was highly critical for product quality. Solely, the very last sample of LOD and sample PSD X50 at 12:15 was found outside the upper target limits. However, due to the small margin of the deviation the impact on product quality is assumed to be rather low (see Figure 56 A).

By applying the validation data set to the calibration I-statistics, the detectability of the induced process variations was investigated. In detail, Shewhart control charts were generated from the validation data set, while applying target, alert-, and action limit statistics from calibration I. This allows statistical comparison of the two processes and hence, uncommon variation would be detected. Results are summarized in Figure 57 B. For better overview, variations in DAV, BT, and LFR over time are plotted in Figure 57 A (normalized to percent of the induced PP-variation; 0 % being the initial standard setpoint). Further, the time point of each PP-change is indicated with grey vertical lines and marked with the corresponding letters a-l (see Table 8 for reference).

When validation Shewhart-plots cross the calibration-based alert and action limits, uncommon process deviations are indicated. Insights into the nature of the out-of-control condition can be drawn from corresponding loading plots of the calibration [170]. Hence, when linking the validation Shewhart charts (Figure 57 B) to the actual process parameter variations (Figure 57 A), it became obvious that most of the induced variations were classified as uncritical (i.e. common variation).

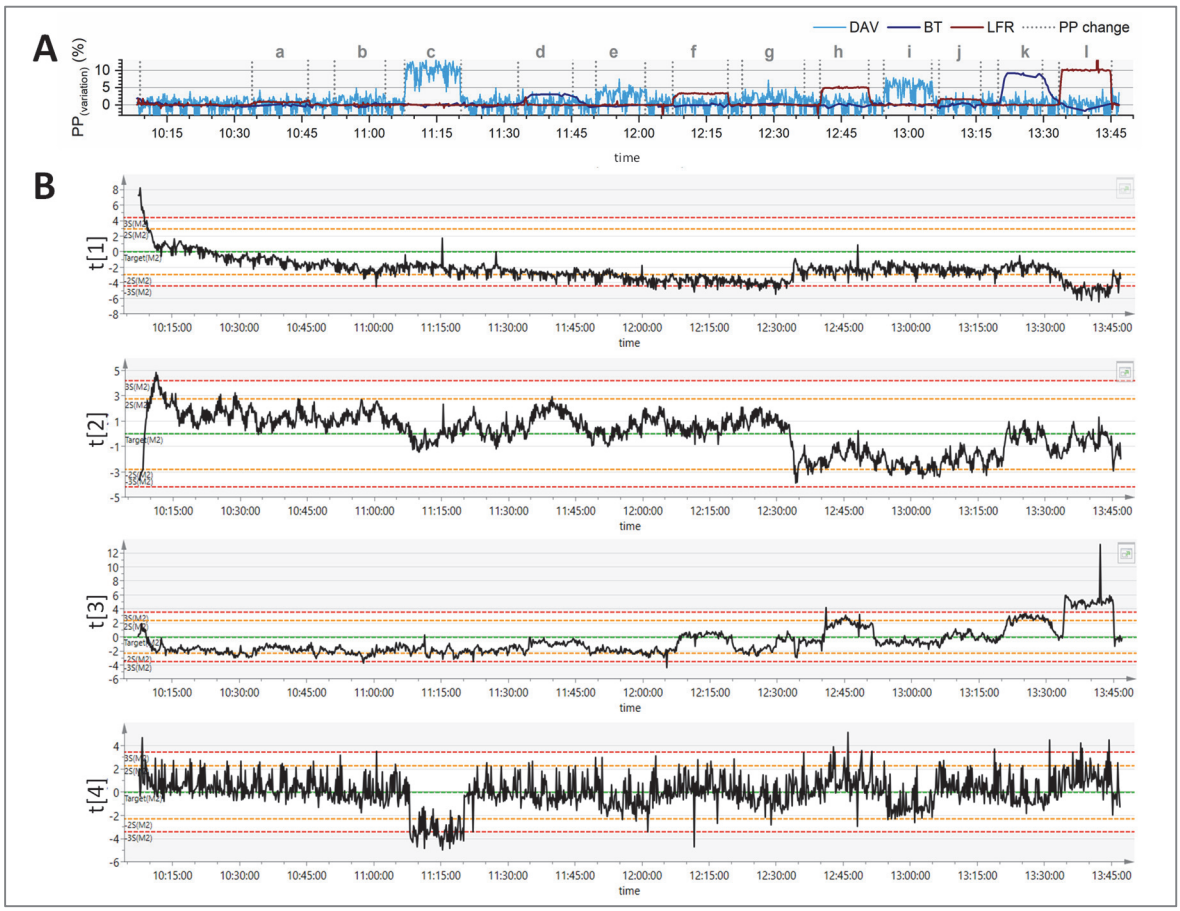

Figure 57: Validation data set Shewhart control charts for PC 1 to 4 (top to bottom action and control limits are based on the calibration dataset statistics for comparison).

In depth, increasing LFR, DAV, and BT by 0.5, 1.5, and 3.0 % (steps a, b, d-g, j), caused the respective charts to move towards the alert limits, without crossing the line. Therefore, deviations in this margin were classified as common variations by the charts. This agrees with reference analyses and Table 7, where the processes' common variation was quantified. Increasing LFR by 5 %, caused the control chart to touch the alert limit. This observation was supported by reference analysis, as LOD touched the upper target limit (see step h in Figure 57 A and PC 3 in Figure 57 B).

In contrast, increasing LFR by 10 % (step l; PC 3), caused the action limits being crossed, signifying a critical (= uncommon) variation. This quality incident was confirmed by IPC, since LOD crossed the upper target limit. In turn, increasing BT and DAV by 10 % resulted in an alert and action limit being crossed, even though no critical influence on CQAs was observed (step c

& k; PC 3 & 4). Lastly, in addition to the induced variations, an unintended uncommon process variation triggered a drift in PC 1 that caused the action limit being crossed, even though no quality critical effect was observed by reference analysis (according to the calibration loading plots, the drift is most likely related to outlet temperature or filter pressure).

In conclusion, calibration I control charts demonstrated general proof-of-concept, since only PP-deviations outside of the calibration range were indicated as quality events. However, not all of the induced uncommon variations were actually quality critical (e.g. BT and DAV of 10 %). The control chart response to the 10 % LFR increase seemed too drastic, compared to the rather low magnitude of CQA deviation. Therefore, it was concluded that more data is required for calibration. Instead of calibrating merely at the standard process conditions, calibration should occur at a wider range of uncritical proven process variations, to improve accuracy and specificity of the charts.

3.3.5.4. DoE-based MSPC calibration

To test this hypothesis, a DoE-based MSPC calibration was conducted, with the aim to include a wider range of common variation (further referred to as calibration II). To simplify this preliminary proof-of-concept trial, the focus was put on LOD control. Since SFR, LFR, and DAV have the most critical impact on LOD [22], the DoE was designed around these three PPs, while all others were set at standard process conditions.

In brief, the three factors were investigated on two levels in a full factorial design (2^3 = 8 trials + 3 trials at center point conditions). Center point settings were selected from the standard process conditions; the upper and lower levels were defined as ± ½**span* of the previously quantified common variation (see Table 7). An overview of the applied settings is listed in Table 9, a summary of the DoE-design and obtained LOD-responses is provided in the supplementary data (see section 10.4, Table S 3, page VI). Each of the 11 PP-combinations was applied for 30 minutes, resulting in 5.5 hours trial time.

Table 9: Overview of parameter range applied to calibrate the common variation in the process parameters.

Process parameter	SFR (kg/h)	LFR (kg/h)	DAV (m^3/h)
Center point (=standard setpoint)	4.0	1.20	140
DoE lower level (- ½ * span)	3.6	1.17	130
DoE upper level (+ ½ * span)	4.4	1.23	150

Recorded process data and corresponding reference LOD analysis results are illustrated in Figure 58. The induced variations in LFR, SFR, and DAV resulted in small variations in dried granules' LOD. Granules from DoE# 2 and 4 are theoretically considered OOS (3.07 and 3.13 % LOD, respectively). However, due to this very small deviation, they were considered acceptable for the MSPC calibration of common variation.

A new set of calibration Shewhart control charts was generated by adding the dataset of the DoE-based calibration to the initial calibration I dataset; the resulting charts of Calibration II are shown in see Figure 59. The combination of these two datasets, allowed to include a wider range in uncritical process conditions and a wider range in uncontrolled process parameters (i.e. filter pressure, sieve pressure, and inlet- & outlet humidity). Due to the new data being added,

the contribution of the PP-variations to the PCs have shifted slightly, compared to calibration I. Now, the 1st PC is mainly attributed to variations in humidity and granulation parameters, the 2nd mainly to airflow and humidity variations and partially to granulation parameters, the 3rd mainly to feed rates and exhaust temperature, and the 4th mainly to humidity and exhaust temperature. Loading plots are attached in the supplementary data (see section 10.4, Figure S 4, page VI).

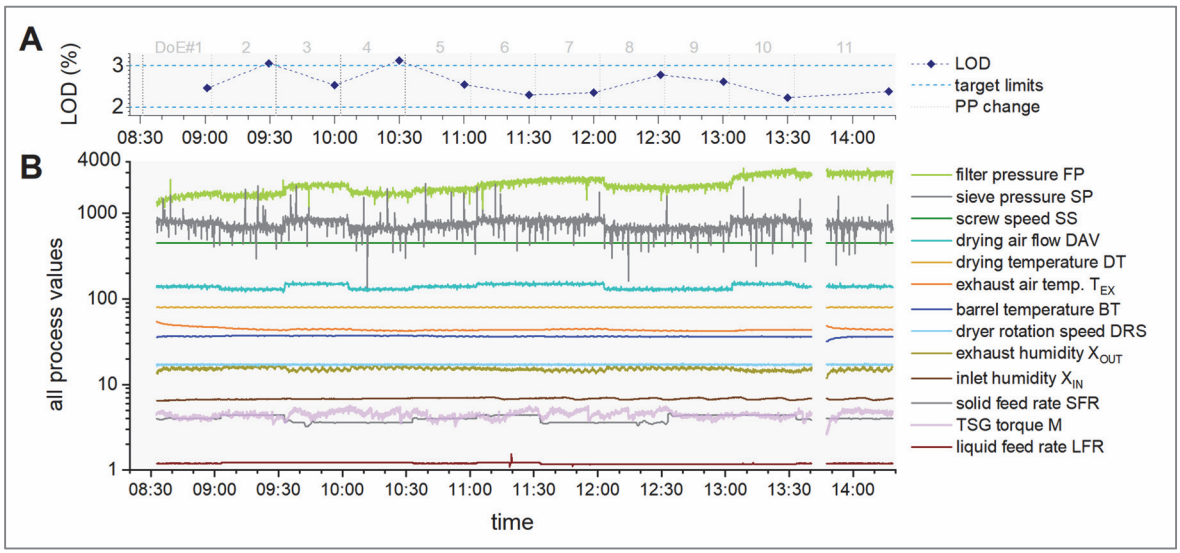

Figure 58: Overview of process parameters (B) and reference LOD analysis (A) recorded from DoE-based MSPC calibration (The experiment was briefly stopped at 13:10 and restarted at ~13:20, due to technical issues).

By applying the validation dataset from Figure 57 to calibration II, a corresponding set of validation Shewhart charts was created (see Figure 60). Variations in DAV are mainly represented in PC 2, while variations in LFR and BT are mainly represented in PC 3 (see loading plots in section 10.4, Figure S 4, page VI, for details). When linking the induced PP-variations to the Shewhart charts of PC 2 and PC3 (see Figure 60 A and B), it becomes obvious that all of the induced variations were represented in the calibration range and hence were classified as common (i.e. not quality critical). However, reference analytics indicated quality events around 12:15 (PSD X50) and 13:45 (see Figure 56). This suggests, that the new calibration is not sensitive enough in certain aspects. At the same time, PC 1 and PC 4 indicated critical (uncommon) process conditions in the first two-thirds of the experiment that seemed to have no critical impact on product quality; suggesting that the charts are still too sensitive in other aspects. In more detail: the increase in 10 % LFR was now detected as an incident close to the alert limit, rather than a highly critical one, even though the induced variation of 10% is four times higher than the DoE-calibrated LFR-range (± 2.5 %). Consequently, the DoE-based calibration created too wide control limits that are not sensitive to critical process conditions.

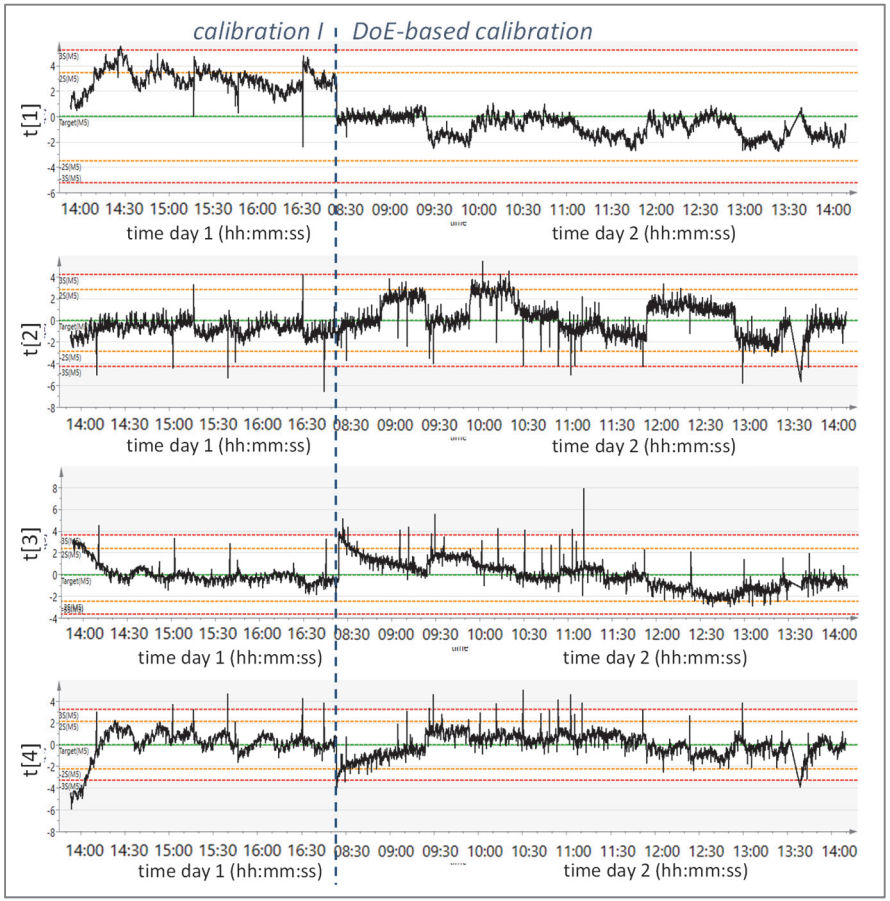

Figure 59: Calibration II (combined calibration from calibration I at constant process conditions (see data in Figure 53 B) and from DoE-based MSPC calibration (see data in Figure 58 B)).

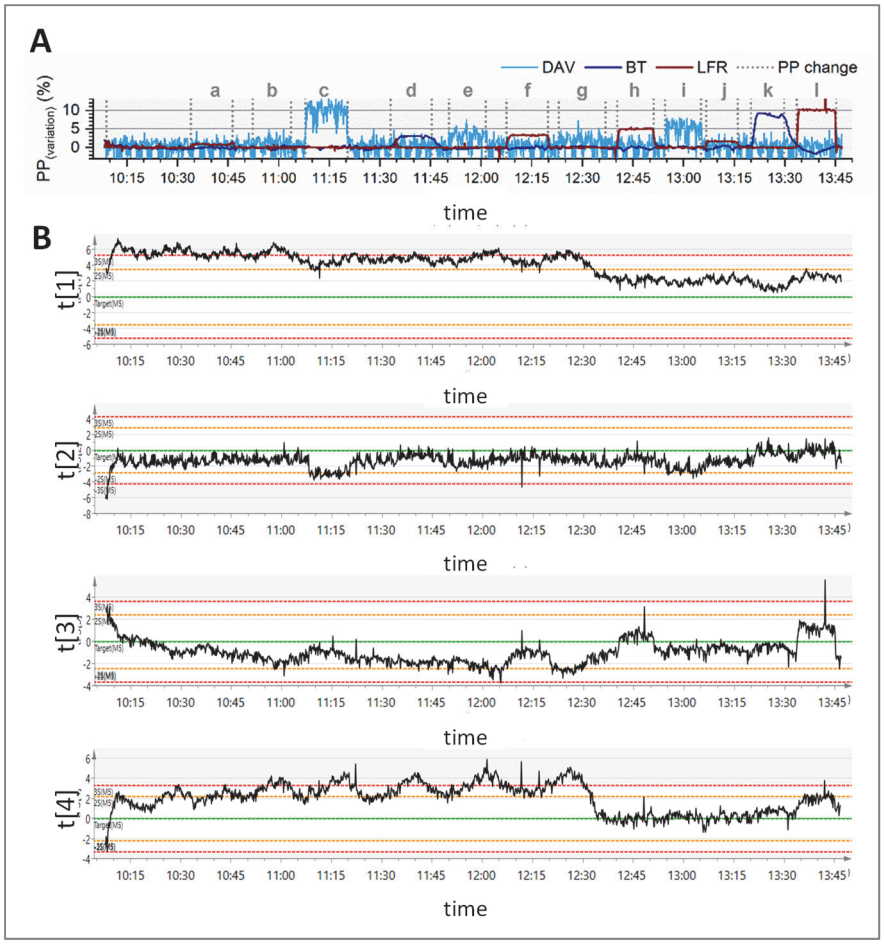

Figure 60: Validation II, based on calibration II. Now the induced variations in LFR, DAV, and BT are not indicated as critical quality events anymore (DAV is represented in PC 2, LFR and BT in PC 3). However, an uncommon variation in inlet humidity (as seen in PC 1 and PC 4) causes the charts action limits to be crossed.

In the meantime, PC 1 and PC 4 indicated critical process conditions that were not observed to be critical for product quality by IPC reference analysis (as shown in Figure 56 A). The uncommon variation is most likely related to inlet- and exhaust humidity, since much lower humidities were present during the calibration experiments than during the validation experiment. Consequently, such increased humidities were not observed as common variation during the calibration runs and hence classified as quality critical in the Shewhart charts. A direct comparison of inlet and exhaust humidities in the calibration- and validation runs is shown in the supplementary data, section 10.4, Figure S 5 (page VI).

In conclusion, DoE-based MSPC-calibration results in less sensitive charts on the one hand, that cannot indicate critical process conditions accurately. On the other hand, robustness to uncritical process conditions is still limited, since the inclusion of uncontrolled process variations (like inlet humidity) proves difficult, as they cannot be set to a certain value during calibration (e.g. inlet humidity is defined by the room humidity, which is controlled with a room monitoring system in the range of 30 – 70 % rH, equaling 4.6 – 10.9 g/kg at 21°C. It can vary within the controlled range depending on the weather and the season and other room conditions).

Consequently, instead of DoE-based calibration, more datasets from standard process conditions would be required for an accurate and robust calibration that covers all common, uncontrolled variations. Since such vast amounts of process data were not available, this approach could not be explored further.

Calibration of MSPC control charts based on extensive historical data is further referred to as the classical MSPC approach. In the next section an alternative methodology to classical MSPC calibration will be proposed and demonstrated and its applicability to PAT data reconciliation will be investigated.

3.3.5.5. Moving average calibration for MSPC and PAT data reconciliation

The previously discussed method of MSPC calibration via historical batch data is only applicable for processes running at fixed process parameter setpoints. When process parameters are to be adapted, for example to vary the total material mass flow, as it was described previously in section 3.2.6 (page 42 ff.), this approach is not practicable anymore, as a change in process parameter setpoints will change the chart's targets, making them unsuitable. A solution to this problem is proposed through a 'moving average' MSPC calibration.

In detail, the approach suggests to calibrate MSPC control charts from a moving average of the most recent process data, while orthogonal PAT analyzers demonstrate that the product quality is under control. If a deviation between the orthogonal PAT is observed, the moving average chart is "frozen" at the last time point when orthogonal PAT consistently confirmed good product quality. The deviating PAT data is then reconciled, by comparing current MSPC process data (from after the deviation) to the previous "frozen" MSPC charts. If no process deviation between the frozen and the current MSPC data can be detected, the varying PAT-analyzer should be investigated. If a deviation is detected between the two MSPC charts, it is likely that the process shifted and hence a sudden quality event occurred. Likewise, if both orthogonal PATs shift or drift out of their respective target limits at the same time and the same direction, process parameters can be adapted without consulting MSPC charts first.

Since the classical calibration approach has to be based on historical data from numerous days, the new proposed MSPC methodology would save time and resources. Furthermore, since it would only be applied as a process monitoring tool in cases where solely one of the specific orthogonal PAT analyzers indicates a deviation, faulty process control actions, based on unspecific erroneous MSPC-alerts could be avoided. Due to the dynamic calibration, variations in PP setpoints can be included in the charts. An illustration of the two basic principles 'classical' and 'moving average' for MSPC-based process monitoring and PAT data reconciliation is presented in Figure 61 A and B, respectively.

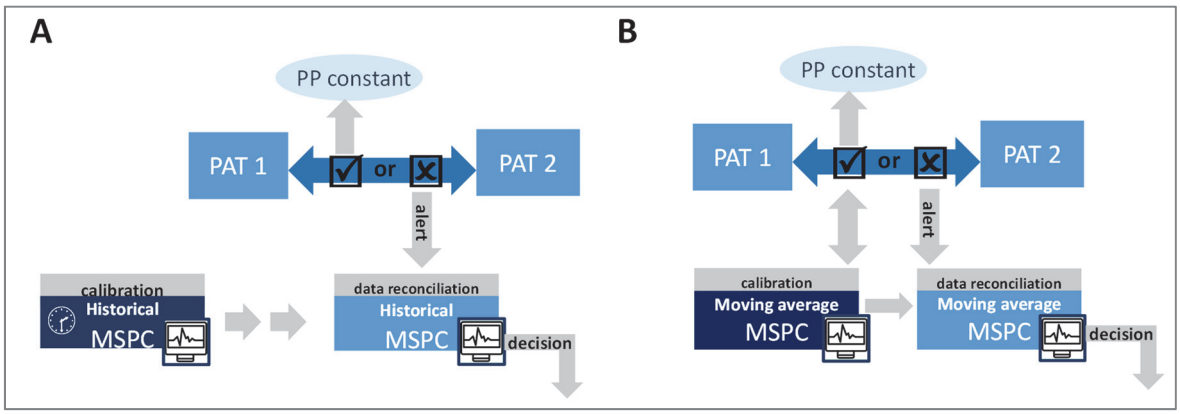

Figure 61: A: classical MSPC approach, where the calibration is based on historical batch data that demonstrated to result in acceptable product quality based on offline, reference IPC analysis. B: moving average MSPC approach, where the calibration is based on a moving average filter of recent process data, while orthogonal PAT demonstrated that the process and product quality is under control.

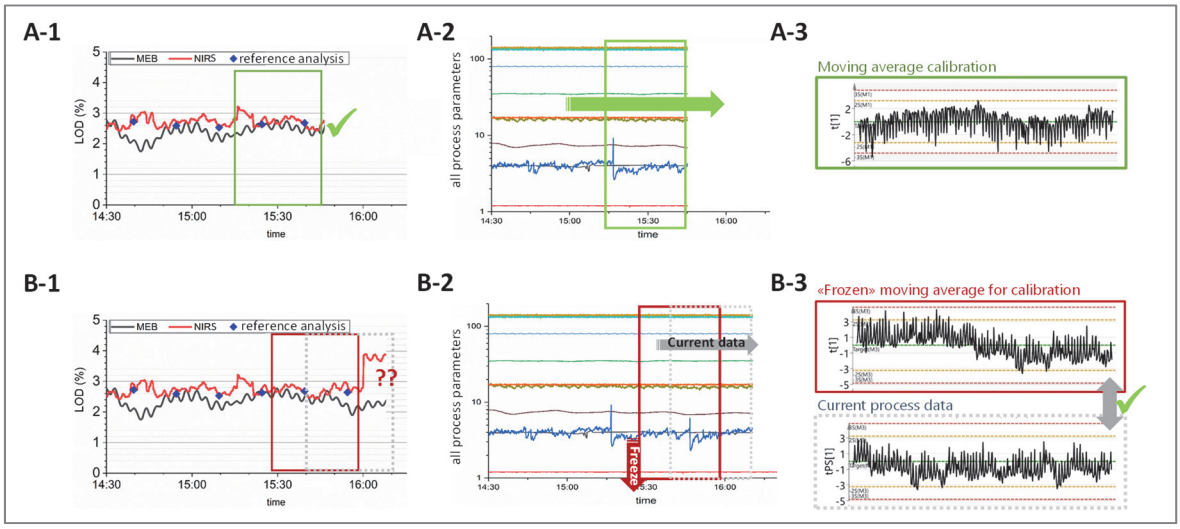

Figure 62: illustration of moving average MSPC calibration approach. A: orthogonal PAT NIRS and MEB are in good agreement with each other. Hence, moving average calibrations of MSPC are recorded from process parameters (A-2 and A-3; only one PC is shown as an example for the calibration control chart). B: orthogonal PAT analyzers differ from each other (B-1). The moving average calibration is "frozen" to compare the current process parameters to the frozen calibration chart (B-2 and B-3). Since no deviation is observed, the process can continue and the deviating PAT should be checked.

The principle of the moving average calibration is further demonstrated in Figure 62 through an example, where NIRS and MEB is used as orthogonal PAT for LOD analysis. In Figure 62 A,

NIRS and MEB are in good agreement with each other. Hence, moving average calibrations of MSPC are recorded from process parameters but not applied for process control. In Figure 62 B, the orthogonal PAT analyzers suddenly start to differ from each other (simulated incident). Therefore, the moving average calibration is "frozen" at the last time point, when quality was indicated acceptable by both PAT. Then, the current process parameters are compared to the frozen calibration chart. As no deviation is observed between the frozen MSPC chart and the current chart, the process can continue as it is and the deviating PAT has to be checked (e.g. fouling of the NIRS probe could cause such a sudden deviation).

The proposed moving average MSPC approach was further tested on real process data, collected during the automatic feed-back process control experiment (as described in section 3.2.6, page 42 ff.). In this trial, SFR and LFR were varied intentionally, in order to change the mass- and energy balance in the dryer. An automated feed-back Controller was applied to adapt DAV according to the MEB-based LOD predictions, with the aim to compensate the induced variations in SFR and LFR and to keep LOD stable.

An overview of the three process parameters SFR, LFR, and DAV during the experiment, as well as NIRS and MEB results in comparison to reference sample analysis results for LOD is provided in Figure 63. The squares "a-f" in Figure 63 mark different time-frames in the dataset that were analyzed by MSPC, to demonstrate the moving average MSPC calibration approach.

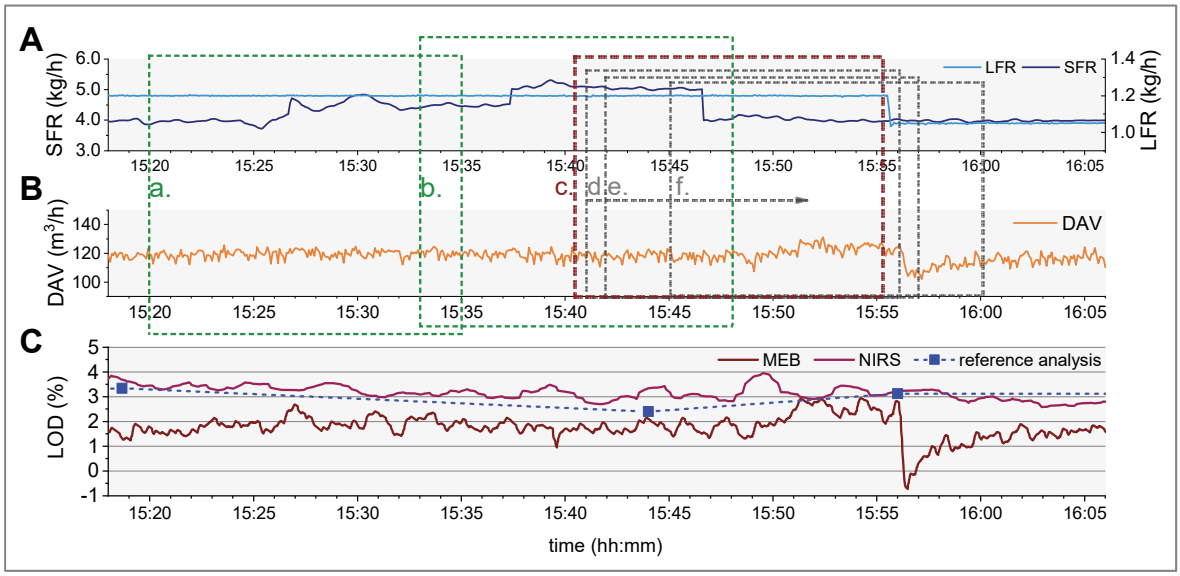

Figure 63: overview of SFR, LFR, and DAV, as well as NIRS, MEB, and reference analysis results. The indicated squares a-f mark different time-frames in the dataset that were analyzed by MSPC, to demonstrate the moving average MSPC calibration approach.

An overview of the time-frames is provided in Table 10. Process parameters for MSPC calibration were selected in analogy to the previous examples. A detailed overview of the recorded process values is supplied in the supplementary data (see section 10.4, Figure S 6, page VII).

Table 10: overview of marked time-frames a-f as indicated in Figure 63. Each time-frames was 15 minutes long. Time-frames a-c were used as calibration datasets, d-f were used as validation datasets.

time-frame	moving averaging time frame	purpose/type
a	15:20:00 – 15:35:00	calibration
b	15:33:00 – 15:48:00	calibration
c	14:40:30 – 15:55:30	calibration freeze
d	15:41:00 – 15:56:00	validation
e	15:42:00 – 15:57:00	validation
f	15:45:00 – 16:00:00	validation

In detail, time-frames 'a' and 'b', show two examples in the experiment, were both orthogonal PAT NIRS and MEB remained constant and in agreement with each other, even though the solid feed rate was varied (see Figure 63). Since both PAT methods are based on different physical principles, small differences in the absolute values are expected; NIRS indicated LOD at the upper target limit, and MEB indicated LOD at the lower target limit. However, in the context of MSPC for data reconciliation, the overall trend is important, not the absolute values of NIRS and MEB (refer to section 3.3.2.3, page 60 ff., for a detailed discussion on NIRS - MEB deviations). From the two time-frames a and b, calibration Shewhart charts were generated, as shown in Figure 64

Figure 64. As the two charts were calibrated from different data, the respective chart limits differ (see for example PC 1 in Figure 64: in "a" the action limits are located at ± 5.5, whereas in "b" they are located at ± 4.8); however both charts represent common variation, since both PATs indicated stable LOD (i.e. suggesting that the enforced variations in SFR had no critical impact on LOD). In contrast, time-frames 'c-f' serve as an example were the two PATs differed and MSPC was required for data reconciliation. In detail, LFR was decreased from 1.20 to 1.05 kg/h around 15:55:30 (hh:mm:ss). This decrease had an instant effect on MEB, but no visible effect on NIRS, causing the two orthogonal PAT to deviate (see Figure 63 A and C, respectively). The moving average calibration was hence "frozen" at this time-point (time-frame c, Figure 63); the "frozen" calibration Shewhart chart is shown in Figure 65 c. The following three time-frames 'd-f' represent the progressing process; they were applied to the calibration statistics of Shewhart chart c, in order to investigate any potential process deviations between the current process data and the previous 'frozen' data (when both orthogonal PAT results were still in agreement with each other); see Figure 65 d and Figure 66 e and f. Here, a vast deviation was detected instantly in PC 2, once LFR was decreased. According to the loading plots of calibration "c", PC 1 is mainly attributed to variations in LFR, T_{EX}, and torque M (see supplementary data for loading plots, section 10.4, Figure S 7, page VII).

Therefore, the sudden decrease in LOD as indicated by MEB, was confirmed as an uncommon process deviation by the Shewhart control charts. In such a case, the process control system is empowered to adapt related process parameters accordingly, even though the quality event was (not yet) observed by NIRS (due to the time delay between MEB and NIRS analysis). In the presented example, DAV was decreased based on the MEB results, to compensate the decrease in LFR. LOD therefore remained constant and hence no deviation was observed by NIRS, once the granules exited the dryer.

If no process deviation had been observed by MSPC, it would have been more likely, that the MEB faced an issue not related to product quality. In such a case, the plausibility of the

calculated results should be assessed manually. However, since many of the process parameters included into the MEB calculation are also represented in the MSPC control charts, a sensor failure (e.g. in humidity measurement) would be picked up by the control charts and the MEB calculation, simultaneously. Generally, a scenario like this is difficult to simulate and has to be investigated in more detail in the future. Conversely, a deviation indicated by NIRS that is not observed by MEB and MSPC, suggests an issue with the NIRS probe; hence the probe should be checked for potential issues.

In summary, MSPC together with the proposed dynamic moving average calibration/validation mechanism demonstrated to be a valuable tool for data reconciliation of orthogonal PAT analyzers in CM. When applying the classical approach of MSPC calibration, numerous batches that reflect all potential uncommon variations have to be included into the calibration. Once a suitable calibration is created, the same methodology for data reconciliation can be applied; however it is only suitable for processes with constant material throughput. In contrast, the moving average approach requires no historical data, but data reconciliation is not possible within the first few minutes, since a certain amount of data is required for the initial calibration. The approach is less prone to indicate non-critical process variations as critical ones, since the charts are only applied, once a deviation in orthogonal PAT is observed. Therefore, variations in inlet humidity for example will be disregarded, unless they have an impact on product quality that is seen by PAT.

However, a lot more data has to be collected in the future, before the method can be implemented into routine CM-production. For once, the length of the moving average time frame has to be investigated. It will impact the sensitivity and reactivity of the chart. Also, the practical implementation of such a moving averaging Shewhart chart analysis in the process control system needs to be assessed. If more process units are to be included into the control system, the PCA analysis will become more complex and more PCs will be required to describe the monitored variation adequately.

Also, the charts itself have to be better understood: In the described example from Figure 63, the deviation in the Shewhart control charts is highly obvious (see Figure 65 ‘d’, PC 2). Since this might not always be the case, decision trees need to be implemented in the future, that define what kind of deviations in the quality control charts call for adaptive control actions. For example, the so-called Nelson rules [189] suggest eight standard tests to be performed, in order to detect uncommon variations in process control charts; based on the idea that certain patterns are very unlikely to occur in stable processes. Such patterns are for example the occurrence of one point being more than 3 standard deviations away from the target, nine points in a row on the same side of the target line, or two out of three points in a row more than 2 standard deviations from the center line on the same side. However, those rules should always be verified during process development and calibration of the charts, since they might not be true for all processes (e.g. as seen during calibration, single values found outside of the control limits are not critical in the described continuous manufacturing process; see spikes in Figure 55 and Figure 59 outside of the action limit) [188, 189].

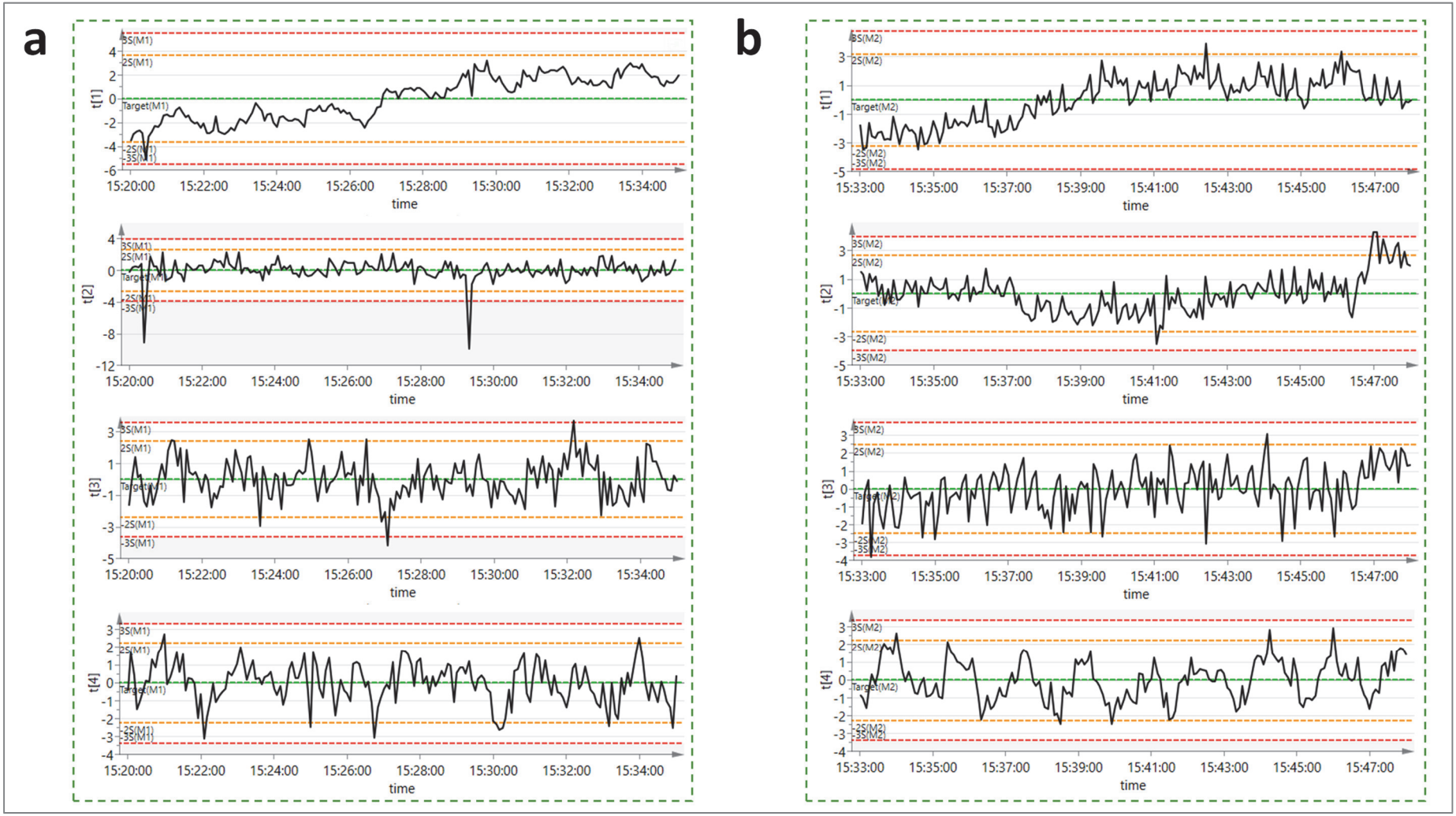

Figure 64: Moving average calibration Shewhart charts a and b. Orthogonal PAT NIRS and MEB are constant and in agreement, hence Shewhart charts are not considered for process control. Since the two charts are calibrated from different data, the chart limits change when moving from a to b (e.g. in PC 1 from ± 5.5 in a to ± 4.8 in b).

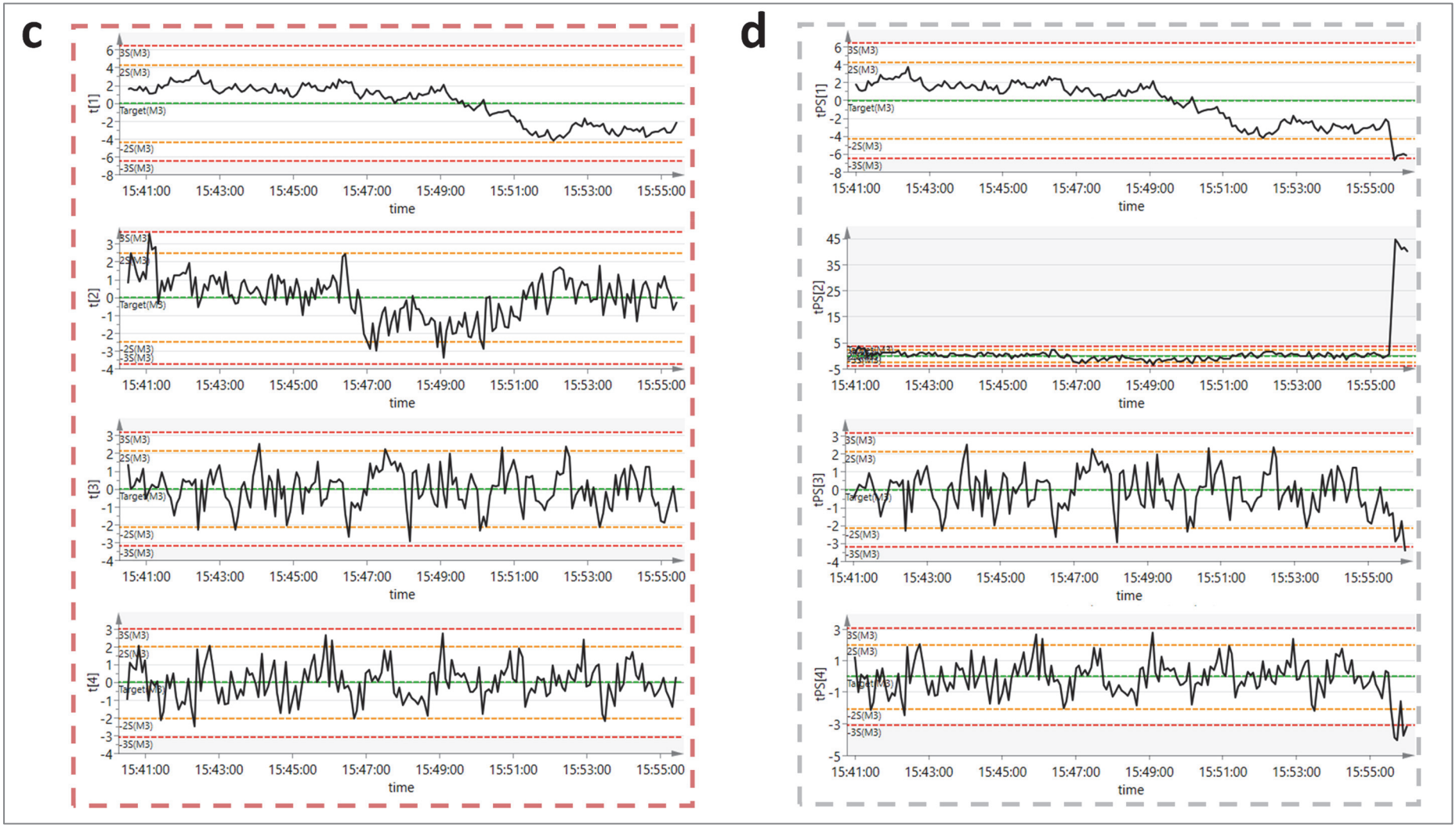

Figure 65. The moving average Shewhart chart "c" is frozen at 15:40:30 – 15:55:30, since a deviation between NIRS and MEB was observed. The new, current process data (d) is then compared to the calibration statistics of the frozen chart "c" (i.e., the limits in d are equal to the limits in c). It becomes obvious, that a large statistical deviation in PC 2 is detected.

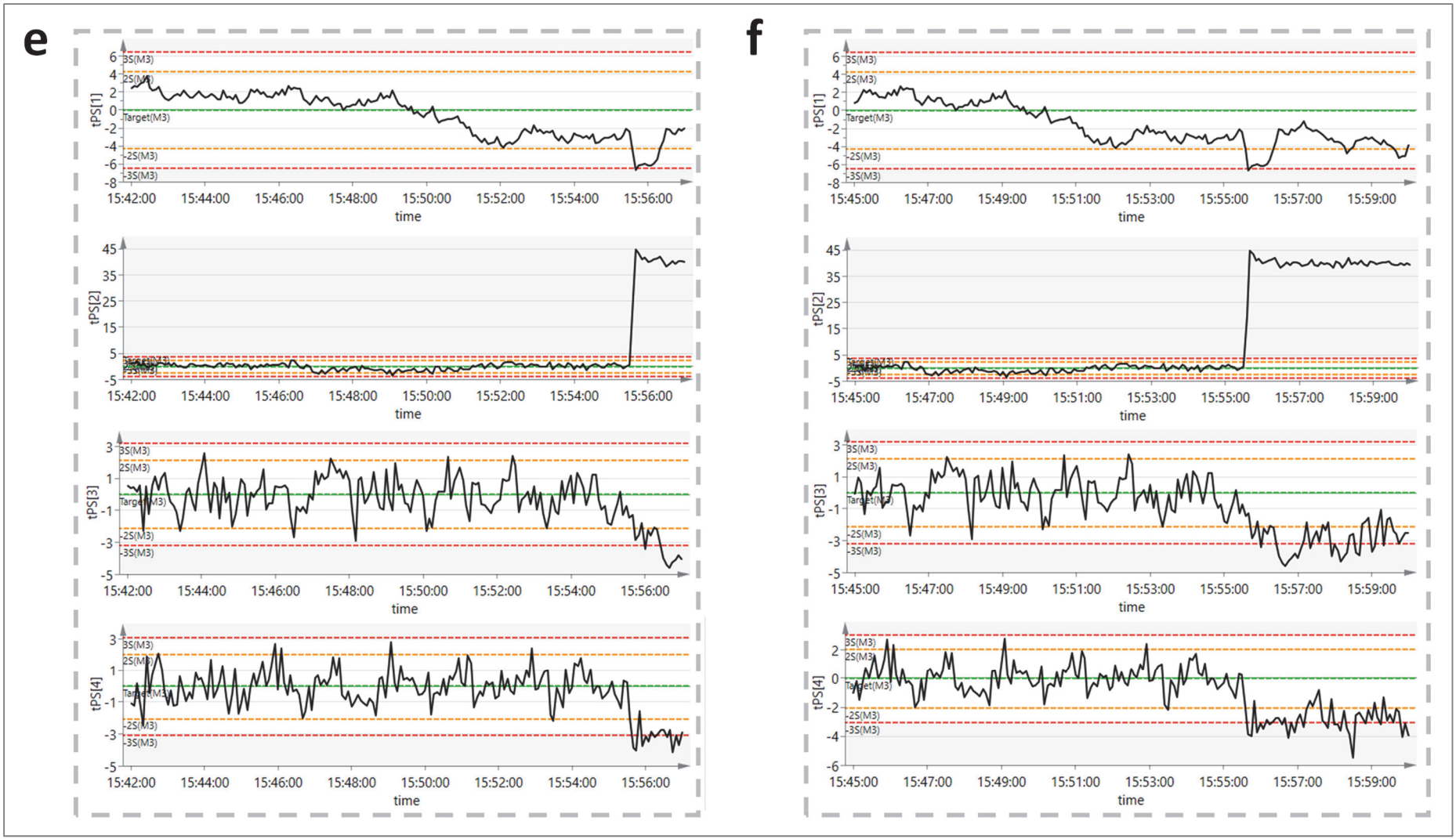

Figure 66: As more process data is recorded, it becomes even more obvious, that the process shifted. Consequently, the process control system is enabled to adapt process parameters (e.g. DAV) with a high level of certainty, even though NIRS did not show a deviation in LOD (the limits in e and f are defined by the frozen control chart from Figure 65 c).

Also, suitable target limits for each of the orthogonal PAT analyzers need to be evaluated carefully, based on their respective accuracy and reactivity. For example, MEB reacts instantly to changes in the drying behavior, but tends to overestimate those variations. In turn, NIRS can indicate changes in product quality only once the product exits the dryer but might be less sensitive to small changes, depending on the sample presentation and averaging filter applied (see section 3.3.2.3, page 60 ff.). Consequently, lag-times between the different PAT analyzers, their sensitivity, as well as the Controllers reaction speed needs to be evaluated in more detail in the future.

Finally, the described experiments and examples solely focused on orthogonal redundant control of LOD. In the future, the applicability of moving average MSPC control charts to PSD and API-content control needs to be investigated.

3.4. Understanding the dynamics of the process: when and where to control?

3.4.1. Concept

In the previous sections, the implementation and validation of real-time redundant PAT analyzers was described, as well as the development, implementation, and testing of predictive model-based control actions. Orthogonality of PAT analyzers was demonstrated and methods for data reconciliation were presented.

However, only by knowing *what* material is *when where*, the control system is able to precisely steer the manufacturing process in case of quality events. Consequently, knowledge of the system dynamics is required for a complete automatic redundant process control strategy. Hence, material residence times between the powder feeders and the exit of the tablet press under varying process conditions was analyzed in detail; the results are provided in the following section.

3.4.2. Analysis of the material's residence time distribution

To analyze the system dynamics, a set of experiments was performed: two powder feeders were installed into the continuous manufacturing line, separately feeding an excipient pre-blend and API into a continuous blender (i.e., Setup B with Formulations B-1 and B-2, as described in sections 6.1 and 6.3, page 117 ff.). By consecutively adapting the feed rate ratio between the two feeders, the API content in the final blend being processed into tablets was varied between 130 % and 70 % of the target label claim (LC) in three successive steps: from 100 % LC to 130 % LC, down to 70 % LC, and back up to 100 % LC.

The dynamics of the step responses were analyzed at different locations in the line via NIRS: a probe was installed at the blender outlet, the dryer outlet, in the tablet press feed frame, and at the tablet ejection point. Tablet samples for offline reference analysis by HPLC were collected every 15 minutes at the press outlet. A schematic overview of the line setup and the NIRS probe locations and HPLC sampling point is depicted in Figure 67. For details on NIRS method development and validation, see section 3.3.4 (page 71 ff.).

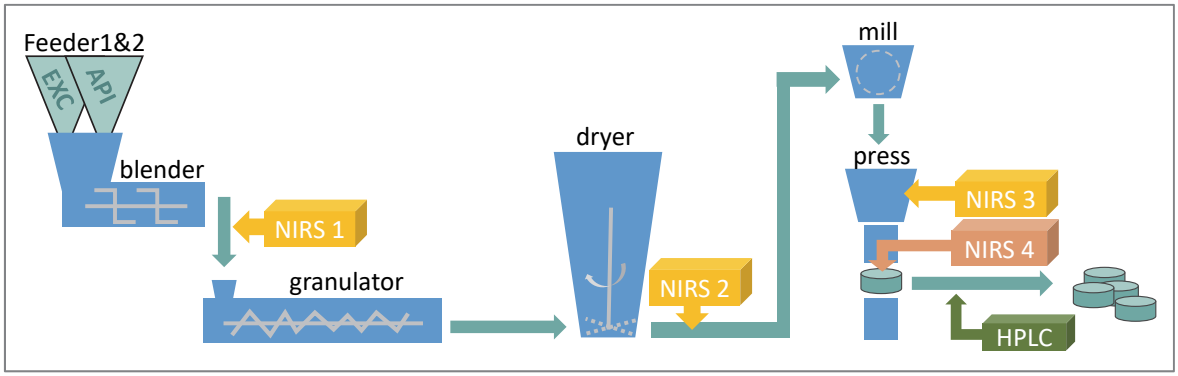

Figure 67: Overview of installed NIRS probes in the continuous manufacturing line and location of the sampling point for reference HPLC analysis during RTD trials.

Parts of the presented data have been previously analyzed in section 3.3.4.4 (page 77 ff.), where the application of feed rate analysis in combination with thorough knowledge on the materials' residence time distribution was demonstrated as an orthogonal PAT method for API content uniformity analysis in dried granules and tablets.

Details on the applied relative feed rates $\dot{FR}_{rel}$ (as % of the total solid feed rate $S\dot{F}R_{tot}$) that were used to vary the API content in the final blend, are listed in Table 13 (see page 119). The API target content is 25 % API absolute, which corresponds to 100 % LC. A representative overview of the executed steps in LC, together with an exemplary response dynamic in the line as it could be detected by NIRS, is shown in Figure 68 A. The dynamic of each step response (as observed by NIRS) was analyzed according to Figure 68 B. In detail, each step was normalized to its respective step-height (start = 0; end of step = 1); the time point of LC-change in the relative feed rates was defined as t_{step} = 0 min. Then, the event propagation time (between the feeders and the NIRS position) at the 5 % response level and 95 % response level (EPT5 and EPT95, respectively) was analyzed. Furthermore, the mean residence time (MRT) of the step was investigated.

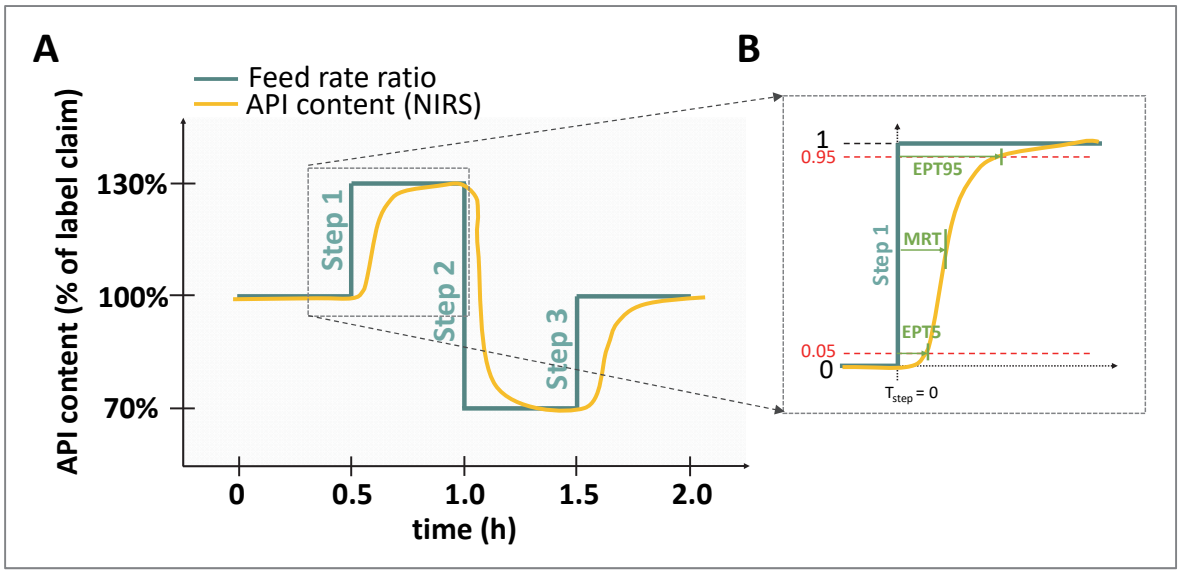

Figure 68: A: schematic overview of performed steps in API content through the systematic variation in feed rates of API and Excipients, and an exemplary step response in the material's API content (as it could be measured by NIRS). B: The curve dynamics were analyzed by calculating EPT5, EPT95, and MRT of each performed step.

To consider the influence of various process conditions on the response dynamics, the described LC-steps were investigated at different total solid feed rates ($S\dot{F}R_{tot}$; i.e. total solid mass flow rate), different L/S ratios of wet granules, and at different dryer rotation speeds (DRS). Furthermore, the repeatability of the RTD assessment was investigated.

Table 11 gives a detailed overview of the selected process conditions on $S\dot{F}R_{tot}$, L/S ratio, and DRS. Repeatability was investigated in combination with $S\dot{F}R_{tot}$, since the trial at standard condition was repeated four times (see trial #1, 3, 4, and 6 in Table 11). To keep the LOD of dried granules in a suitable range for compression, the effects of varying $S\dot{F}R_{tot}$ and L/S ratio on LOD were compensated, by adapting the drying conditions (DRS and DAV) accordingly

(model-based adaption via the results presented in section 3.2, page 31 ff.). To keep the hopper fill level constant during varying $S\dot{F}R_{tot}$, compression speed (CS) was adapted to the respective material throughput (see Table 11 for details).

Every LC condition was set for 30 minutes; hence, each trial lasted two hours (4 * 30 minutes). The execution of the different LC-steps every 30 minutes was completed automatically with the Sequencer (see section 3.2.5, page 34 ff. for details on the Sequencer). All trials were performed on four consecutive days.

Table 11: Overview of investigated process conditions. At each condition, the three LC steps as described in Figure 68 A, were executed, hence every trial lasted 2 hours.

trial #	type	$S\dot{F}R_{tot}$	L/S	DRS	DAV	CS
1	$S\dot{F}R_{tot}$ & repeatability	4.0	0.3	17	130	11.4
2		**2.0**	0.3	30	104	5.7
3		4.0	0.3	17	130	11.4
4		4.0	0.3	17	130	11.4
5		**6.0**	0.3	5	160	17.1
6		4.0	0.3	17	130	11.4
7	L/S	4.0	**0.2**	30	101	12.4
8		4.0	**0.4**	5	160	10.6
9	DRS	4.0	0.3	**10**	130	11.4
10		4.0	0.3	**24**	130	11.4

*CS = compression speed in 10^3 * tablets/h*

Figure 69 illustrates a summary of results. Step responses were normalized to the step height, to plot the response effect F over time t; where LC 100 % equals F = 0, the respective maximum and minimum altitude equals F = ±1 (representing LC 130 % and LC 70 %, respectively).

Due to technical issues, data from NIRS 4 (tablets) is only available for trials #9 and #10. The corresponding NIRS-method was developed with sample-LODs in the range of ~ 2.5 ± 0.5 %, as this is the usual specification range of granules to be compressed. In the conducted trials #9 and #10, compressed tablets exceeded this LOD range (LOD = ~ 3-5 %). Since the method was not robust towards LOD variations, API predictions were biased (see 3.3.4.3, page 74 ff. for details on method development). Therefore, the predicted API content from NIRS 4 was corrected by a LOD-dependent correction factor. This correction factor solely influences the absolute height of the step response, not the dynamics in respect to time. In Figure 69 the corrected results are depicted; uncorrected predictions and the calculation of the correction factor are demonstrated in the supplementary data (see section 10.6, Figure S 8, page XI). In the future, the method of NIRS 4 should be enhanced for robustness towards LOD variations.

Reference analytics of tablets by HPLC was used to confirm the NIRS predictions from NIRS 3 and NIRS 4 (corrected data). Due to the vast number of samples, only tablets from trial #1, #9, and #10 were analyzed.

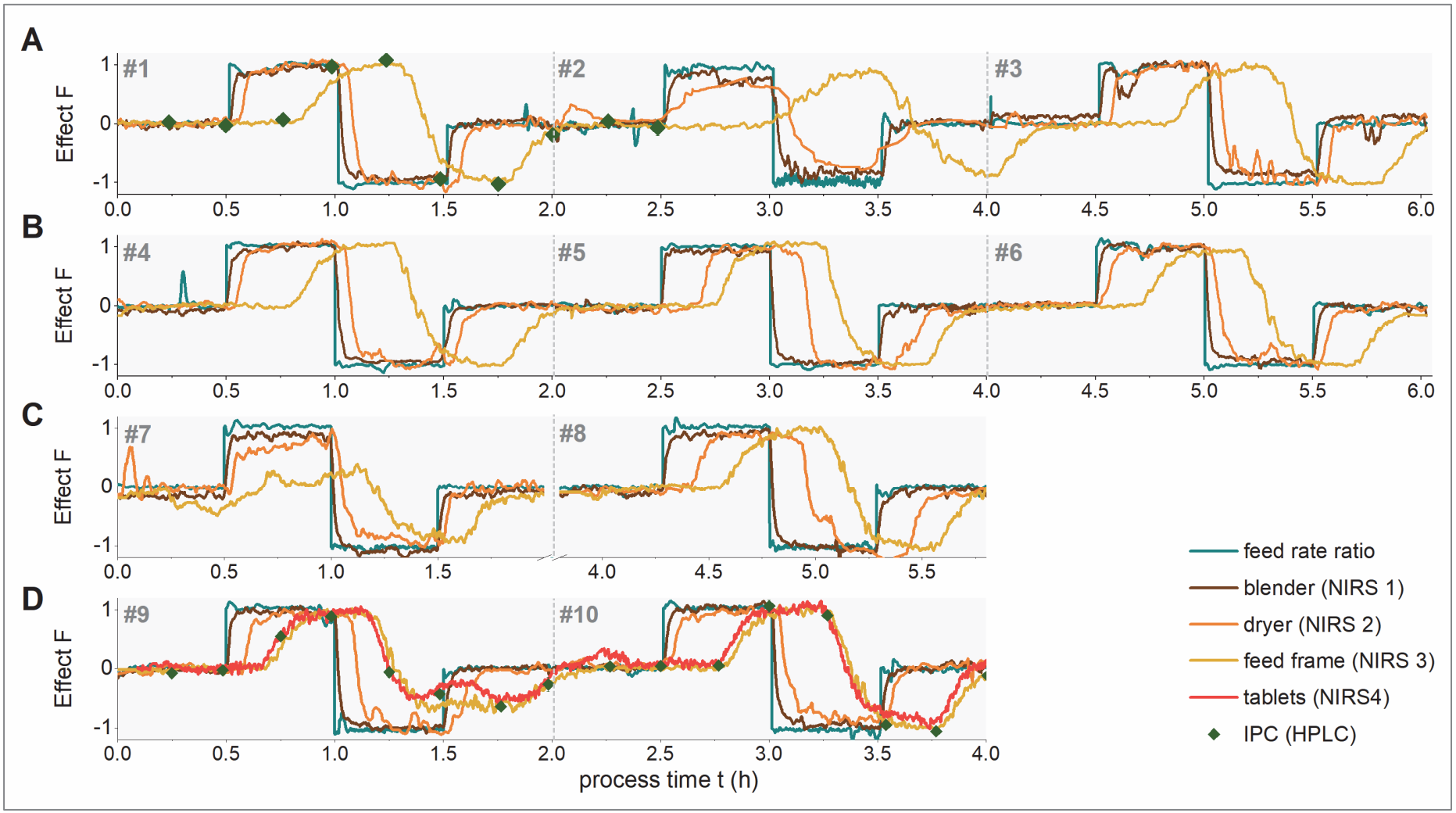

Figure 69: Overview of RTD results. Step responses were normalized to the step height, to show the response effect F over time t. A/B: $S\dot{F}R_{tot}$ & repeatability (trials #1-6); C: L/S ratio (trials #7-8), D: DRS (trials #9-10).

First, a few general observations can be made on the results shown in Figure 69: For once, the low $S\dot{F}R_{tot}$ in trial #2 caused issues with the spectral acquisition in NIRS 1 and NIRS 2, as the mass flow did not sufficiently cover the probes, which resulted in irregular curves that might not be fully representative of the actual process dynamics (see Figure 69 A, #2). Furthermore, sporadic blockage of the PAT-chute after the blender caused irregularities in NIRS 1-prediction (observed as sudden "dips" in predicted API content, mainly seen in trials #2 and #3 in Figure 69 A). Blockage was avoided in all following experiments, by manually applying compressed air pulses to the chute every 15 minutes. Furthermore, in trial # 7 NIRS 3 seemed to have a problem, as the curves show irregular and atypical dynamics (potentially caused by fouling of the probe due to dry and dusty material). Only the last step response was considered for analysis in this trial. In trial #9, irregular material hold-up in the PTS-hopper on top of the mill was observed. For once it was noticed during the trial, that the tablet press hopper fill-level increased abruptly and unexpectedly, even though the compression speed was not adapted. Furthermore, NIRS 3 and NIRS 4 both showed an uncommon increase in API content, suggesting that material from LC-step 130 exited the PTS hopper later than usual. Consequently, results were not considered during the analysis.

Overall, reference HPLC results are in good agreement with NIRS results from the tablet press feed frame and the tablets (NIRS 3 and NIRS4, respectively) confirming the validity of NIRS predictions and hence HPLC analysis of the remaining samples was not necessary (see trial #1, #9, and #10 in Figure 69 for reference HPLC results).

For a more detailed analysis of the conducted experiments, EPT5, EPT95, and MRT was calculated from each trial, each step, and each NIRS sampling point (see Figure 68 B for details on the calculation). A summary table of the results is included in the supplementary data (section 10.5, Table S 4, page VIII ff.). Generally, EPT5/95 and MRT refer to the times between the feeders ($t_{step} = 0$) and the respective sampling points; ΔEPT5/95 and ΔMRT refer to the time-deltas between two sampling points (e.g. from dryer outlet to feed frame).

By investigating the obtained EPT and MRT results in regard to the different process conditions applied, several main conclusions on RTD could be drawn:

- At standard process conditions, the average MRT to blender outlet was 1.1 minutes, average MRT to dryer outlet was 4.5 minutes, and average MRT to tablet press feed frame was 21.3 minutes. Repeatability of ΔMRT assessments at standard conditions was ~ ± 22 % (relative to the observed mean residence time), independent of the NIRS sampling position.
  Overall, the shortest observed EPT5 to the feed frame was 11 minutes; the longest EPT95 to the tablet press feed frame was 40 minutes (in the four standard setting trials). Accordingly, in case of a critical quality event in the feeders, ejection of OOS-material after the tablet press should start 11 minutes after the event, collection of good quality tablets can continue 40 minutes after the end of the event (when considering a worst-case scenario at standard process conditions). Time frames for other quality events (e.g. in the dryer) or other ejection points (e.g. after the dryer) can be calculated accordingly from ΔMRT results (see Figure 70 for details). Generally, the duration of such a quality event needs to be considered in such a scenario as well and the impact of time should be investigated in more detail in the future (as

short quality events in the feeders, might not necessarily cause critical quality deviations in the final product, due to back- and forward mixing tendencies in the line).

Generally, for all above stated conclusions it is assumed that MRT to feed frame is comparable to MRT to tablets, since no tablet NIRS data was available in these trials. Data that confirms the comparability between the two sampling points is provided further below.

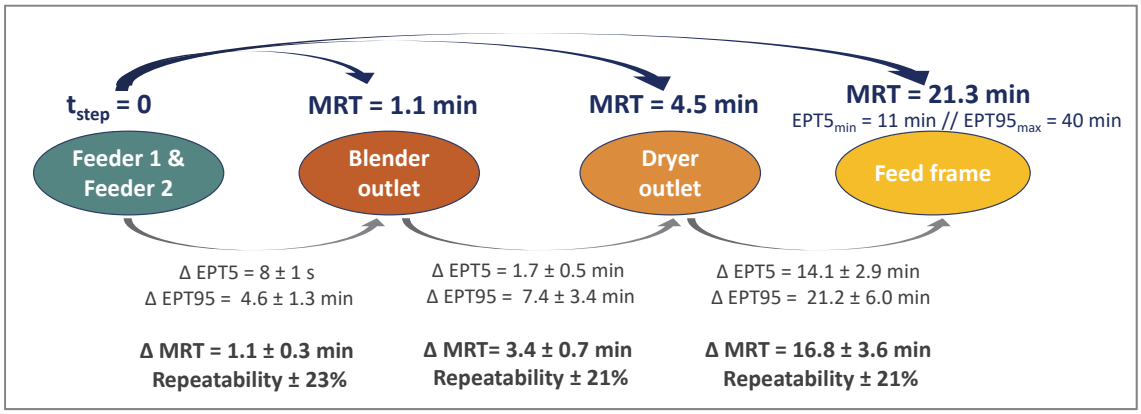

Figure 70: Summary of RTD results at standard process conditions. The average MRT of the whole production line (powder to tablets) is 21.3 minutes. Repeatability is ~ ± 22 %, independent of the sampling position (no data from NIRS 4 was available for these trials).

- Each trial included two 30 % steps (from 100 to 130, and from 70 to 100 % LC), and one 60 % step (from 130 to 70 %LC). Comparison of the four trials at standard process conditions, demonstrated that no significant difference in MRT between the 30 % and the 60 % steps was seen. This indicated that the step-height does not influence the response dynamics in the line (see Figure 71 for details). As a consequence, the three steps were analyzed together in all subsequent evaluations (i.e. three steps per process condition were investigated (n=3), which permitted good statistical evaluation of the results).

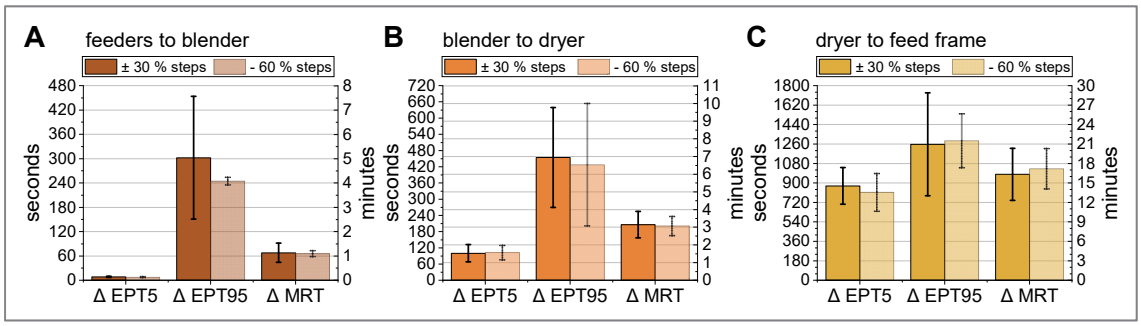

Figure 71: Comparison between 30 % and 60 % step amplitude: no significant difference was observed, indicating that the step height has no effect on the residence time distribution in the line.

- According to trials #1 – #6, $S\dot{F}R_{tot}$ had no significant influence on MRT to blender outlet (see Figure 72 A). Between blender and dryer, the observed influence on ΔMRT was directly correlated to drying time t_d and hence DRS (DRS was adapted in this experiment to keep LOD constant at varying $S\dot{F}R_{tot}$). By subtracting the respective drying time t_d from ΔMRT, the effect was eliminated. Consequently, $S\dot{F}R_{tot}$ had no effect on the blender ΔMRT at constant DRS (see Figure 72 B for details; see eq. 2, page 15 for calculation of t_d).

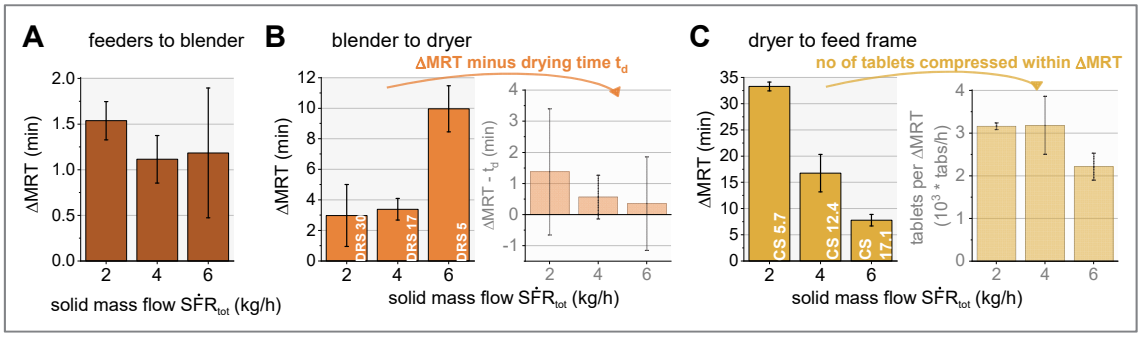

Figure 72: Influence of SṀR$_{tot}$ on ΔMRT between the feeders and the blender (A); the blender and the dryer (B); the dryer and the tablet press feed frame (DRS = dryer rotation speed in rph, CS = compression speed in 10^3 *tablets/h).

Likewise, compression speed was directly correlated to ΔMRT between dryer outlet and feed frame, as expected (variations of SṀR$_{tot}$ were compensated by adapting the compression speed in the press, to keep the level in the hopper constant; see Figure 72 C, left). However, when considering the number of tablets being compressed during ΔMRT (i.e. ΔMRT*CS), it became obvious that slow and moderate compression speeds (5.7 – 12.4 *10^3 tabs/h) showed comparable dynamics; whereas less tablets were compressed during ΔMRT at a high tableting speed (17.1*10^3 tabs/h; Figure 72 C, right). These findings imply that less tablets are compressed during the transient phase; hence less waste is produced in case of a quality event, when tableting at high speeds and high solid mass flow.

- When considering variations in DRS, ΔMRT between blender outlet and dryer outlet was comparable to the respective drying time t_d, allowing precise prediction of ΔMRT based on DRS (see Table 12 for details). Furthermore, these findings indicate that the residence time in the granulator and the transfer tube between granulator and dryer seems neglectably small. Also, no significant influence of DRS on ΔMRT between dryer and feed frame was observed, as expected. Likewise, no significant influence of L/S on ΔMRT between blender and dryer was observed, which agrees with above mentioned observation, that RTD in the granulator seems neglectably short.

Table 12: Influence of dryer rotation speed DRS. ΔMRT is directly correlated to DRS and hence t_d. As a consequence, ΔMRT between blender outlet and dryer outlet can be predicted based on DRS; the residence time in the granulator is neglectable.

DRS	t_d (min)	average ΔMRT (min)	± stdev ΔMRT (min)
5	9.6	9.5	2.2
10	4.8	5.5	1.0
24	2.0	2.6	0.4
30	1.6	2.0	1.0

- Negative residence times were observed between NIRS 3 (tablet press feed frame) and NIRS 4 (tablets), suggesting that a portion of the material takes a short-cut in the tablet press feed frame, without passing the location of NIRS 3. This might also be the reason for the observed small deviations in API content. While NIRS 4 scans every single tablet, NIRS 3 scans solely the fraction of material that passes by the probe. Since both spectrometers were connected to the process control system DeltaV, an error of the spectral time stamps was excluded.

On average, ΔMRT between feed shoe and tablets was -2.1 ± 0.2 minutes (trial #9, step 2 and step 3 excluded from the average, due to irregular curves caused by material hold up in PTS-hopper; see Figure 73 for details). Since the observed time difference is rather small, it can be neglected.

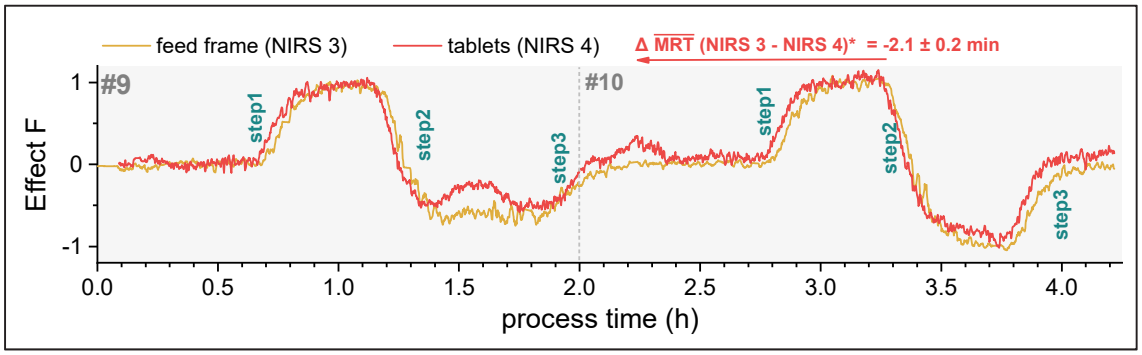

Figure 73: A negative residence time was observed between the tablet press feed frame and the individual tablets (NIRS 3 and NIRS 4) *(*trial #9, step 2 and 3 excluded from average calculation, due to the irregular curve, caused by holdup in the PTS hopper).*

Asides from the main observations summarized above, several related process- observations were made that should be investigated further in the future:

- The occurrence of material hold-up in the PTS-hopper (as observed in trial #9) should be inspected in future trials, as such hold up is unpredictable and can induce errors in the process control strategy. Re-design of the hopper or the implementation of a stronger vibration unit on the hopper might be a suitable solution.

- Low $S\dot{F}R_{tot}$ in combination with high DRS causes issues with the spectral acquisition of NIRS 2, since low amounts of granules are ejected from the dryer constantly. As a consequence, the NIRS probe is not fully covered with material, which results in high absorption spectra. In the future, the PAT-chute at the dryer should be re-designed. Syncing the exit cycle of the dryer with the exit cycle of the outlet valves (and hence the NIRS acquisition), could be an easy fix for this problem.

- The PAT chute installed at the blender outlet showed tendency to block over time, resulting in the analysis of static blend buildup in front of the probe, while the powder exiting the blender was flowing through the overflow chute. The installation of a compressed air tube that automatically supplies regular air pulses to the probe should be sufficient in avoiding such blockage.

- The observed negative residence times between the feed frame and the tablets imply a short-circuit flow in the hopper and feed frame that should be investigated in more detail in the future, as this might cause unnecessarily wide apparent RTDs at this point. Overall, the tablet press feed frame has the highest impact on overall RTD. While the rest of the line shows nearly perfect plug flow behavior, the feed frame causes extensive back- and forward mixing of material, and hence widens the RTD. Consequently, it should be investigated how to improve the flow and RTD in the feed frame in the future (e.g. by re-designing the feed frame

with smaller hopper volume, to avoid extensive back- and forward mixing). The reality is that NIRS 3 records powder that resides in the feed frame slightly longer than the majority of the powder stream due to its obviously off-centered location with regard to the powder flow pattern inside the feed frame.

In summary, thorough knowledge about the process dynamics at varying process conditions was generated. It was demonstrated, that the influence of the dryer rotation speed can be predicted from the corresponding drying time. However, it needs to be ensured that no product sticks to the dryer walls or filters and hence recirculates. Total solid material mass flow has a direct influence on the tableting step, since the compression speed needs to be adapted accordingly. At faster compression speeds (and hence higher solid mass flows), less tablets are compressed during a transient phase, which would reduce overall waste production in case of a quality event. The L/S ratio has no significant influence on RTD; the residence time in the granulator is neglectably short. An apparent negative residence time between the feed frame and the tablets suggests that the step dynamics reach the final product, before they are seen in the tablet press feed frame, but can be explained by a position of the NIRS 3, that looks at material that moves slower than the main stream.

Above suggested enhancements on the methodology and the production line will further improve (i.e. shorten) the residence time distribution in the line, allowing more precise analysis and hence more accurate prediction in case of quality events. In the future, for any new process conditions, process units, or new products, the RTD and repeatability at standard settings should be assessed according to the presented methodology. Additionally, the RTD at high and low DRS should be investigated (to exclude recirculation in the dryer), as well as the RTD at different tableting speeds and solid mass flows (to calibrate the observed non-linearity between CS and MRT). With such a comprehensive investigation, sufficient knowledge on the product RTDs of the entire line can be generated. This in turn allows to implement a thorough redundant process control strategy that can steer the process in case of quality events through the adaption of process parameters and the precise and accurate ejecting of OOS-material from the line, perfectly aligned with the system dynamics of the line. If further investigations on several other products would demonstrate that the RTD is product independent, then the extent of such investigations could also be reduced in the future.

4. Summary and Outlook

Continuous manufacturing promises low variability in final drug product quality, facilitates dynamic operation procedures, and has the potential for real-time release approaches. However, these promises can only be kept, if a suitable process control strategy is in place. In this work, a redundant process control strategy for continuous manufacturing by twin-screw wet-granulation and fluid-bed drying was developed that can ensure consistent drug product quality at all times. Three main steps were completed:

First, the intention of the control strategy was defined, in order to know what to control. Dried granules' particle size distribution (PSD), moisture content (LOD), and active pharmaceutical ingredient (API) content are intermediate critical quality attributes (CQAs) of the investigated production process that have to be controlled, as they all define final tablet quality. Methodological process risk assessment via fish-bone analysis and criticality matrix rating identified all potentially critical process parameters (pCPPs) and material attributes (pCMAs), that could have a critical impact on intermediate CQAs LOD and PSD (control of API content uniformity was not considered in this part). Potentially critical factors and the influence of runtime on CQAs were then investigated by means of a screening DoE and selected follow-up trials. An automatic "Sequencer" was developed and implemented, to allow the simultaneous adaption of numerous process parameters in the line at pre-defined time points 'on-the-fly', to enable fully automated DoE-based process development. The Sequencer in combination with real-time analysis of LOD by orthogonal PAT allowed the construction of a comprehensive process model, without the need for operator intervention. With less than 24 hours runtime and less than ten kilograms API consumption for a full DoE-development trial, this approach demonstrated two of the repeatedly claimed benefits of CM technology: reduced material consumption in development and reduced manual labor. Overall, the trials identified and quantified all critical process parameters and material attributes. The quantified factor-response relationships were then applied for predictive, model-based control actions, where it was demonstrated that the developed models allow precise adaption of related process parameters, in order to keep dried granules' LOD within its pre-defined target limits at varying material mass flow rates. Furthermore, it was possible to eliminate the usually required equilibration phase (after start-up) via model-based adaption of the dryer rotation speed. Also, automated PAT-based predictive feed-back control in real-time was implemented for LOD and proof-of-concept was provided.

In the second part of the project, the analytical basis of the control strategy was defined by selecting and implementing suitable orthogonal PAT-analyzers that allow real-time monitoring of intermediate CQAs LOD, PSD, and API content. For LOD, near infrared spectroscopy (NIRS) and mass and energy balance (MEB) calculations were selected. A thorough NIRS method calibration and validation was performed (RMSEP = 0.74 %) and robustness towards varying PSD and API content was demonstrated. For MEB, a detailed dryer investigation in combination with thermodynamic principles allowed at a step-by-step derivation of MEB calculations. Orthogonality of the two methods was demonstrated by numerous validation trials, where the average deviation between NIRS and MEB was found < 0.5 %. The necessity for orthogonal, redundant PAT strategies was demonstrated, since NIRS shows accurate results as soon as

granules exit the dryer, whereas MEB lacks sensitivity in the first few minutes; MEB however indicates process fluctuation earlier than NIRS once the process is equilibrated.
Regarding PSD, NIRS and laser diffraction (LD) were selected as suitable orthogonal PAT. Variances in NIRS absorption patterns were calibrated to particle size fractions X10, X50, and X90, with three independent methods (RMSEP = 17, 97, 174 µm for PSD X10, X50, and X90, respectively). Methods were validated via linearity and accuracy, and their robustness towards varying LOD and API content was demonstrated. LD is an absolute analysis method that does not require method development. Orthogonality of both methods was demonstrated directly and indirectly via reference dynamic image analysis. Since the methods are based on fundamentally different physical principles, absolute values cannot be compared. However, the overall trends demonstrated comparability and hence orthogonality. For API blend- and content uniformity, two independent NIRS systems and dynamic feed rate analysis were selected as orthogonal PAT. NIRS methods for API blend uniformity (after continuous blending), dried granules content uniformity (measured after drying and in the tablet press feed-frame), and API content uniformity (in final tablets) were developed and validated (RMSEP = 3.2, 2.2, and 1.6 %, respectively). Since two independent NIRS systems were applied, the two methods for feed-frame analysis of granules and final tablets were considered as orthogonal in the broader sense, their comparability was demonstrated. Furthermore, model-based prediction of dynamic step responses in combination with feed rate ratio analysis (between API and excipient feeders) demonstrated orthogonality to NIRS. For cases where orthogonal PAT analyzers disagree with each other, multivariate statistical process control charts were investigated as a method for data reconciliation. For once, the classical approach of calibrating statistical reference control charts from historical batch data was evaluated for its applicability to continuous manufacturing. The method demonstrated time- and recourse consuming, as numerous datasets are required to comprehensively characterize the overall level of common variation. An alternative approach was proposed by analyzing a moving average of the most recent process data for calibration. Meanwhile, the state-of-control of the process is verified by orthogonal PAT analyzers. It was confirmed that deviations in orthogonal PAT can be reconciled via this approach.

In the third and last section of the thesis, the dynamics of the manufacturing process at varying process conditions were investigated, in order to know when and where to control. Thus, different steps in API content of the processed material where induced and the dynamic of the step response through the whole production line (from powder to tablets) was analyzed with four NIRS probes, placed at strategic locations within the line. In summary, the standard mean residence time (MRT) from the feeders to the tablet press feed frame is 21 minutes (at the investigated standard process conditions); MRT between feed-frame and the final tablets demonstrated to be comparable. The step altitude does not impact the step dynamics, the same is true for the L/S ratio of the wet granules. The impact of the dryer rotation speed on MRT is directly correlated to the respective drying time. Furthermore, solid material mass flow defines compression speeds, at higher speeds the transient phase of a step response is decreased. The generated knowledge on the material's residence time distribution, allows the process control strategy to specifically adapt process parameters in case of quality events and to precisely and accurately divert OOS-material from the line.

In summary, risk analysis, DoE-based process analysis, and the investigation of the material's residence time distribution (RTD) forms the basis for predictive model-based control actions. Implementation of orthogonal PAT in combination with MSPC-based strategies for data-

reconciliation allow redundant monitoring of related critical quality attributes. In combination, a control strategy is constructed, that enables continuous process monitoring in real-time and the predictive adaption of process parameters and the precise diversion of OOS-material, in case of quality events. As a result, high quality product, eligible for real-time release is manufactured at all times. An overview of the developed control strategy is illustrated in Figure 74.

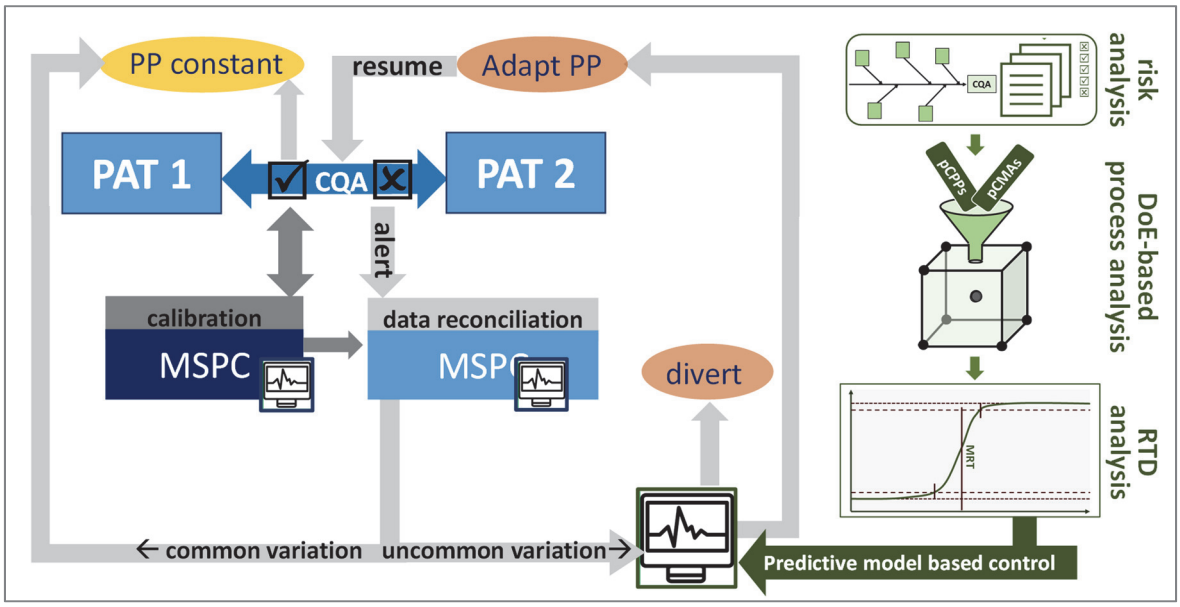

Figure 74: Summary of the redundant process control strategy for continuous manufacturing. Risk analysis, DoE-based process analysis and investigation of the material's residence time distribution (RTD) forms the basis for predictive model-based control actions. Orthogonal PAT combined with MSPC-based data-reconciliation allows redundant monitoring of related critical quality attributes (CQAs). In combination, a control strategy is constructed, that enables continuous process monitoring and control in real-time.

In the future, the developed methodology can be transferred to any new products processed on the continuous manufacturing plant, as it provides a universal tool for systematic control strategy development. Automatic process development by means of the Sequencer and PAT-based CQA analysis can be further improved with a more suitable real-time PAT for PSD analysis. Also, PAT-based predictive feed-back control in real-time will improve, once MSPC-based data reconciliation is implemented to increase the level of assurance for each control decision. The software-integration of the moving average MSPC-based data reconciliation is a challenge yet to be solved. Ultimately, the described control strategy will enable the full potential of pharmaceutical continuous manufacturing by improving its flexibility, efficiency, and safety. Like-wise it can aid in decreasing overall manufacturing costs and hence has the potential to decrease overall healthcare costs in the future.

5. Zusammenfassung und Ausblick

Die kontinuierliche Herstellung von Arzneimitteln verspricht eine geringere Variabilität in der Produktqualität, erlaubt dynamische Prozessanpassung und kann Produktfreigabe in Echtzeit ermöglichen (real-time release). Diese Versprechen können jedoch nur gehalten werden, wenn eine geeignete Prozesskontroll- und Regelungssstrategie vorhanden ist (fortlaufend als Kontrollstrategie bezeichnet). In der vorliegenden Arbeit wurde eine redundante Kontrollstrategie für die kontinuierliche Arzneimittelfertigung mittels Doppelschnecken-Nassgranulation und Wirbelschichttrocknung entwickelt, die eine jederzeit gleichbleibende Arzneimittelqualität gewährleisten kann. Dafür wurden drei Fragestellungen beantwortet:

Im ersten Teil der Arbeit wurde die Intention der Kontrollstrategie definiert, mit dem Ziel zu wissen was kontrolliert werden muss. Die Partikelgrößenverteilung (PSD), der Feuchtigkeitsgehalt (LOD) und der Gehalt an aktiven pharmazeutischen Inhaltsstoffen (API) des getrockneten Granulats sind intermediäre kritische Qualitätsmerkmale (CQAs) die kontrolliert werden müssen, da sie die finale Tablettenqualität beeinflussen. Methodische Prozessrisikobewertung mittels Ursachen-Wirkungs-Diagrammen und Kritizitätsmatrix-Analyse, identifizierten potenziell kritische Prozessparameter (pCPPs) und Materialattribute (pCMAs), die intermediäre CQAs LOD und PSD beeinflussen könnten (die Einheitlichkeit des Wirkstoffgehalts wurde in diesem Teil nicht berücksichtigt). Der Einfluss dieser potenziell kritischen Faktoren auf die CQAs, sowie der Einfluss der Prozesslaufzeit, wurde anschließend mittels eines Screening-DoEs und ausgewählten Folgeversuchen untersucht. Um die gleichzeitige Anpassung mehrerer Prozessparameter zu vordefinierten Zeitpunkten zu erleichtern, und somit eine vollautomatische DoE-basierte Prozessentwicklung zu ermöglichen, wurde ein "Sequenzer" entwickelt und implementiert. Der Sequenzer in Kombination mit der PAT-basierten Echtzeitanalyse von LOD ermöglichte es quantitative Prozessmodelle zu generieren, ohne dass ein Labormitarbeiter bei der Durchführung der Versuche eingreifen musste. Mit einer Laufzeit von weniger als 24 Stunden und einem Wirkstoffverbrauch von weniger als zehn Kilogramm für eine vollständige DoE-basierte Prozessuntersuchung, bestätigte dieser Ansatz zwei der wiederholt behaupteten Vorteile der CM-Technologie: geringerer Materialverbrauch in der Entwicklung und geringerer Bedarf an manueller Arbeitskraft.
In den Versuchen wurden alle kritischen Prozessparameter und Materialeigenschaften identifiziert und quantifiziert. Die quantifizierten Faktor-Effekt-Beziehungen wurden anschließend für modellbasierte Regelungsaktionen eingesetzt. Es wurde gezeigt, dass die entwickelten Modelle eine präzise Anpassung der zugehörigen Prozessparameter ermöglichen, um den LOD der getrockneten Granulate innerhalb der vordefinierten Sollgrenzen zu halten, selbst bei variierendem Massendurchsatz. Darüber hinaus war es möglich, die üblicherweise erforderliche Äquilibrierungsphase (nach der Inbetriebnahme) durch eine modellbasierte Anpassung der Trocknerdrehzahl zu eliminieren. Eine automatische, PAT-basierte Rückkopplungsregelung für LOD in Echtzeit wurde ebenfalls implementiert und erfolgreich getestet.

Im zweiten Teil des Projekts wurde die analytische Grundlage der Kontrollstrategie durch die Auswahl und Implementierung geeigneter orthogonaler PAT-Systeme definiert, um eine Echtzeit-Überwachung der intermediären CQAs LOD, PSD und API-Gehalt zu ermöglichen. Für LOD wurden Nahinfrarotspektroskopie (NIRS) und Massen- und Energiebilanzrechnungen

(MEB) ausgewählt. Dementsprechend wurde eine NIRS-Methode kalibriert und validiert (RMSEP = 0,74 %) und die Robustheit gegenüber unterschiedlichen PSD und API-Gehalten nachgewiesen. Anhand einer detaillierten Untersuchung des kontinuierlichen Wirbelschichttrockners in Kombination mit thermodynamischen Prinzipien wurde die MEB schrittweise hergeleitet. Die Orthogonalität der beiden Methoden wurde in mehreren Validierungsversuchen nachgewiesen, wobei die durchschnittliche absolute Abweichung zwischen NIRS und MEB < 0,5 % LOD war. Die Notwendigkeit orthogonaler, redundanter PAT-Strategien wurde durch die Unterschiede der beiden Methoden deutlich: NIRS zeigt genaue Ergebnisse, sobald Granulat den Trockner verlässt, während MEB in den ersten Prozessminuten Zeit zum Äquilibrieren braucht; dafür zeigt MEB Prozessschwankungen deutlich früher an als NIRS, sobald der Prozess im Gleichgewicht ist.
Für PSD wurden NIRS und Laserbeugung (LD) als orthogonale PAT ausgewählt. Drei separate NIRS-Methoden für die Partikelgrößenanteile X10, X50 und X90 wurden kalibriert (RMSEP = 17, 97, 174 µm für PSD X10, X50 und X90); Linearität und Genauigkeit der Methode, sowie Robustheit gegenüber unterschiedlichen LOD und API-Gehalten wurden validiert. LD ist eine absolute Analysemethode, die keine Methodenentwicklung erfordert. Die Orthogonalität beider Verfahren wurde direkt und indirekt mittels dynamischer Bildanalyse als Referenz gezeigt. Da die Verfahren auf grundsätzlich unterschiedlichen physikalischen Prinzipien basieren, wurden statt den Absolutwerten die Trends verglichen. Für die Gleichförmigkeit des API-Gehalts wurden zwei unabhängige NIRS-Systeme sowie die Dosierratenanalyse (in Abhängigkeit der Prozessdynamik) als orthogonale PAT ausgewählt. NIRS-Methoden für die API-Mischgüte (nach der kontinuierlichen Mischung), die API-Mischgüte im Granulat (gemessen nach der Trocknung und im Füllschuh der Tablettenpresse) und die Gleichförmigkeit des Gehalts in den finalen Tabletten wurden entwickelt und validiert (RMSEP = 3,2, 2,2 bzw. 1,6 % für Mischung, Granulat, und Tabletten). Da zwei unabhängige NIRS-Systeme eingesetzt wurden, gelten die beiden NIRS-Methoden für Granulat (im Füllschuh) und Tabletten im weiteren Sinne als orthogonal; ihre Vergleichbarkeit wurde gezeigt. Darüber hinaus wurde gezeigt, dass die modellbasierte Vorhersage dynamischer Sprungantworten in Kombination mit der Analyse der Dosierraten (zwischen API und Hilfsstoffzuführungen) sich als orthogonales PAT zu NIRS verwenden lässt.
Für Fälle, in denen sich orthogonale PATs widersprechen, wurden multivariate statistische Prozessregel-Diagramme (MSPC Diagramme) als Methode zum Datenabgleich untersucht und etabliert. Einerseits wurde die klassische Kalibrierung von MSPC Diagrammen anhand historischer Chargendaten untersucht. Das Verfahren benötigt viel Zeit und Ressourcen, da zahlreiche Datensätze erforderlich sind, um die gesamte normale Variation eines Prozesses zu erfassen. Ein alternativer Ansatz wurde vorgeschlagen und getestet, in dem ein gleitender Durchschnitt aktueller Prozessdaten für die Kalibrierung verwendet wurde, währenddessen die Produktqualität mittels orthogonaler PAT kontrolliert wird. Es wurde gezeigt, dass Abweichungen zwischen orthogonalen PATs über diesen Ansatz verifiziert werden können.

Im dritten und letzten Abschnitt der Arbeit wurde die Dynamik des kontinuierlichen Herstellungsprozesses bei variierenden Prozessbedingungen untersucht, mit dem Ziel zu wissen, wann und wo kontrolliert werden muss. Es wurden Sprünge im Wirkstoffgehalt des prozessierten Materials induziert und die Progression der Sprungantwort durch die gesamte Produktionslinie untersucht (vom Pulver bis zur Tablette). Mittels vier NIRS-Sonden, die an strategischen Stellen innerhalb der Linie platziert wurden, konnte die Verweilszeitverteilung der gesamten Linie

analysiert werden. Zusammenfassend zeigten die Ergebnisse, dass bei den untersuchten Standardprozessbedingungen die mittlere Verweilzeit (MRT) von der Pulverdosierung zum Füllschuh der Tablettenpresse 21 Minuten beträgt; die MRT zwischen Füllschuh und den fertigen Tabletten war vergleichbar. Des Weiteren zeigte die Höhe der induzierten Sprünge keinen Einfluss auf die Dynamik, ebenso wenig wie das L/S-Verhältnis (Wasser zu Feststoff Verhältnis) der nassen Granulate. Der Einfluss der Trocknerdrehzahl auf die MRT ist direkt mit der Trockenzeit korreliert. Darüber hinaus definiert der Massendurchsatz die Kompressionsgeschwindigkeit; bei höheren Geschwindigkeiten wird die transiente Phase einer Sprungantwort verringert. Das generierte Wissen über die Prozessdynamik ermöglicht es der Kontrollstrategie Prozessparameter bei Qualitätsereignissen gezielt anzupassen und OOS-Material präzise auszuschleusen.

Zusammenfassend bilden Risikoanalyse, DoE-basierte Prozessanalyse und die Untersuchung der Materialverweilzeitverteilung die Grundlage für modellbasierte Regelungsmaßnahmen. Die Implementierung orthogonaler PAT in Kombination mit MSPC-basierten Strategien für den Datenabgleich ermöglicht eine redundante Überwachung der kritischen Qualitätsmerkmale. In Kombination ergibt sich eine Kontrollstrategie, die eine kontinuierliche Prozessüberwachung in Echtzeit, die vorausschauende Anpassung von Prozessparametern, sowie die präzise Ausschleusung von OOS-Material nach Qualitätsereignissen ermöglicht. Dadurch wird jederzeit ein qualitativ hochwertiges und für die Echtzeitfreigabe geeignetes Produkt hergestellt. Ein Überblick über die entwickelte Regelstrategie ist in Figure 74 (siehe S. 111) dargestellt.

In Zukunft kann die entwickelte Methodik auf neue Produkte übertragen werden, die in der kontinuierlichen Produktionsanlage verarbeitet werden, da sie ein universelles Werkzeug für die systematische Entwicklung von Kontrollstrategien darstellt. Die automatische Prozessentwicklung mit Hilfe des Sequencers und die PAT-basierte CQA-Analyse kann mit einem geeigneteren PAT-system für PSD erweitert werden. Auch die PAT-basierte Rückkopplungsregelung in Echtzeit wird sich verbessern, sobald der MSPC-basierte Datenabgleich implementiert ist, da er die Sicherheit jeder Regelungsentscheidung erhöht. Die Software-Integration der MSPC-Kalibrierung mittels gleitenden Durchschnitts ist eine noch zu lösende Herausforderung. Letztendlich wird die beschriebene Kontrollstrategie helfen das volle Potenzial der pharmazeutischen kontinuierlichen Produktion auszuschöpfen, da sie Flexibilität, Effizienz und Sicherheit verbessert. Ebenso kann sie dazu beitragen, die Herstellungskosten zu senken, und somit potenziell auch die allgemeinen Kosten im Gesundheitssystem zu senken.

6. Materials and Methods[16]

6.1. Materials

Diclofenac Sodium (Acros Organics, Geel, Belgium and Novartis Pharma AG, Stein, Switzerland) was used as model drug substance in all trials.

The following excipients were used in all performed trials: Sodium Starch-Glycolate (Explotab SSG Type A (Ph.Eur.), JRS Pharma GmbH & Co KG, Rosenberg, Germany), Sodium Stearyl Fumarate (Lubripharm ® SSF NF/EP/JP, SPI Pharma, Inc., Wilmington, Delaware, USA), Hypromellose (Benecel TM E5 Pharm Hypromellose, Ashland, Rotterdam, Netherlands), Calcium Hydrogen-Phosphate Anhydrous (Anhydrous EMCOPRESS, JRS Pharma GmbH & Co KG, Rosenberg, Germany), Microcrystalline Cellulose (Vivapur 102, JRS Pharma GmbH & Co KG, Rosenberg, Germany), and Colloidal Silicon Dioxide (AEROSIL® 200 Pharma, Evonik Resource Efficiency GmbH, Hanau, Germany). Purified water was used as granulation liquid in all trials.

6.2. Formulations

Depending on the conducted trials and the equipment setup, different formulations were prepared from the above listed materials (6.1):

Formulation A:

25.0 % Diclofenac Sodium, 5.0 % Sodium Starch Glycolate, 5.0 % Sodium Stearyl Fumarate, 4.0 % Hypromellose, 12.2 % Calcium Hydrogen-Phosphate Anhydrous, and 48.8 % Microcrystalline Cellulose.

To prepare granules at varying API content for NIRS method calibration, 8 formulations containing 70, 80, 90, 95, 105, 110, 120, and 130 % of the original Diclofenac-Na content were prepared (i.e. 17.5 - 32.5 % Diclofenac Sodium absolute). In these cases, the amounts of Microcrystalline Cellulose and Calcium Hydrogen-Phosphate Anhydrous were adjusted accordingly, while keeping their ratio constant at 80:20. Sodium Starch-Glycolate, Sodium Stearyl Fumarate, and Hypromellose were kept at 5 %, 5 %, and 4 %, respectively.

Formulation B:

B-1: 98.0 % Diclofenac Sodium was blended with 2.0 % Colloidal Silicon Dioxide.

B-2: 6.7 % Sodium Starch-Glycolate, 6.7 % Sodium Stearyl Fumarate, 5.3 % Hypromellose, 17.1 % Calcium Hydrogen-Phosphate Anhydrous and 64.3 % Microcrystalline Cellulose.

B-1 and *B-2* were then blended together in a continuous blender at varying ratios, as described in more detail in 6.4.1 (page 119 f.).

[16] Parts of this section have been previously published in Publications 1-4 (see page v)

6.3. Equipment setup

Two different setups were used in the conducted trials: *Setup A* and *Setup B*. In *Setup A*, a pre-blend containing API and excipients (i.e. *Formulation A*, see 6.2) was fed into the granulation unit by one feeding system. In *Setup B*, an API pre-blend (*Formulation B-1)* and a separate excipient pre-blend (*Formulation B-2*) were fed individually by two dosing units into a continuous blender (see 6.2); the blender outlet was directly connected to the twin-screw wet-granulation unit (see 6.4.3).

With both setups, either granules were collected after the dryer (see 6.4.4) for analysis or tablets were collected after exiting the tablet press (see 6.4.5). In trials, where granules were collected, no tablets were compressed.

Setup A was used in the majority of trials (standard setup), Setup B was used to investigate the material's residence time distribution in the line section 3.4 (page 99 ff.). An overview of the two different setups and all involved process units is provided in Figure 75.

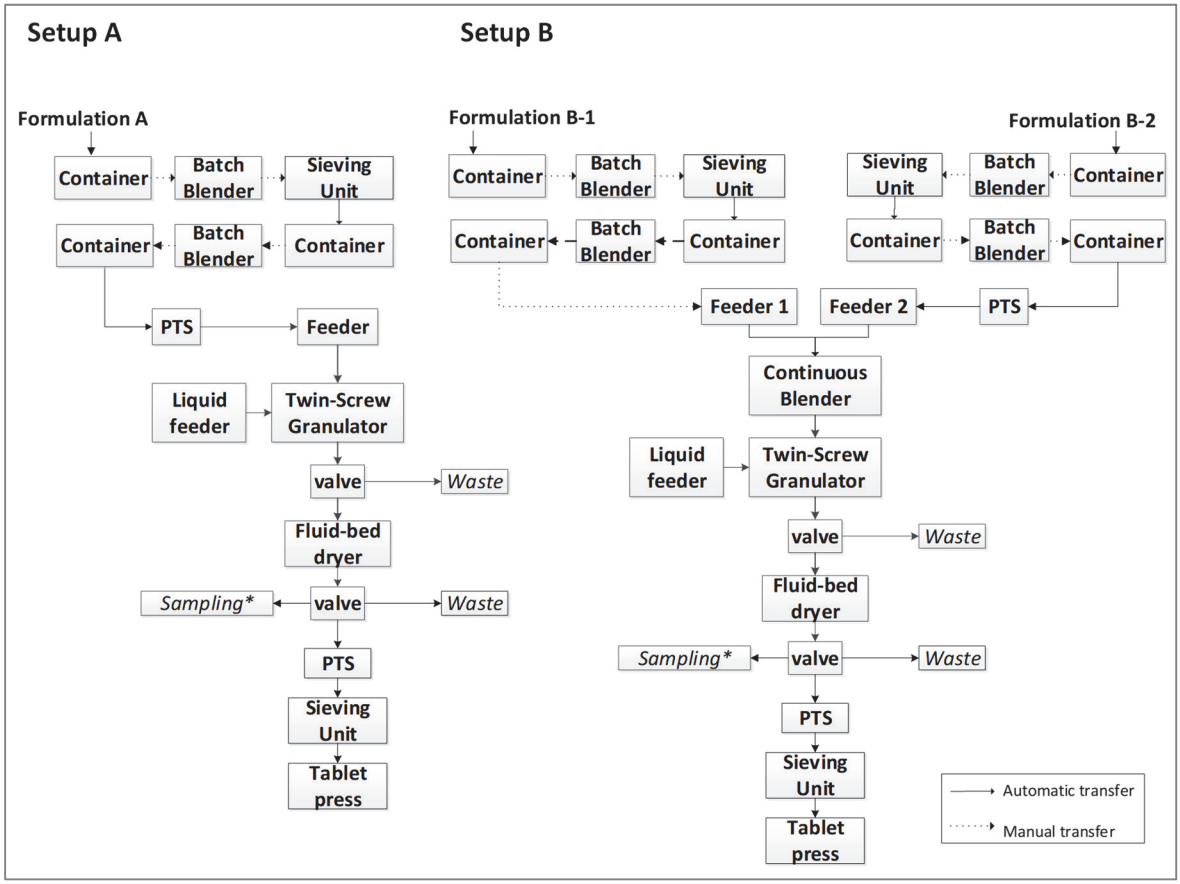

Figure 75: Overview of the two applied setups. (PTS=powder transfer system; *for some trials, granules were sampled after the dryer for analysis, and the tablet press was not used).

6.4. Production methods

6.4.1. Preparation of powder blends and powder feeding

Formulation A:

All ingredients for Formulation A (see 6.2) were weighted into a drum and blended two times for 5 minutes at 20 rpm with a Turbula Mixer for batch sizes of 5 kg (T10B, WAB AG Maschinenfabrik, Muttenz, Switzerland) or for 10 minutes at 11 rpm in a Pharma Telescope Blender PTM 300 (LB Bohle GmbH, Ennigerloh, Deutschland) for batch sizes > 5 kg. Batch size varied depending on the experiment between 5 and 100 kg. Between the two blending steps, the blend was sieved through a 1.25 mm-mesh sieve to break agglomerates (Oscillowitt-Lab type MF-lab, Frewitt, Granges-Paccot, Switzerland). The powder blend was then fed by a loss-in-weight powder feeder (K-Tron T20, Coperion K-Tron GmbH, Niederlenz, Switzerland) into the connected twin-screw wet granulation unit (6.4.3). Solid feed rate ($S\dot{F}R$) was varied between 2.0 – 8.0 kg/h, depending on the experiment (details will be stated in the respective sections; see 3.1 -3.4, page 29 ff.).

Formulation B:

Ingredients for Formulations B-1 and B-2 (see 6.2) were weighted into two separate containers and blended separately two times for 10 minutes at 11 rpm in a Pharma Telescope Blender PTM 300 (LB Bohle GmbH, Ennigerloh, Deutschland). Between the two blending steps, the blends were sieved through a 1.25 mm-mesh sieve to break agglomerates (Oscillowitt-Lab type MF-lab, Frewitt, Granges-Paccot, Switzerland). Batch size for B-1 was 38 kg and 113 kg for B-2.

The two formulations were then fed by two separate dosing units (K-Tron T20, Coperion K-Tron GmbH, Niederlenz, Switzerland) into a continuous blending unit (Hosokawa Modulomix, Hosokawa Micron B.V., Doetinchem, Netherlands), to prepare the final blend. Blender paddle speed was set to 750 rpm. Powder exiting the blender was directly fed into a connected twin-screw wet granulation unit (6.4.3).

Formulation B was used during trials on the material's residence time distribution (see section 3.4, page 99 ff.). The feed rate ratio between B-1 and B-2 was varied, in order to generate final blends with 17.5, 25.0, or 32.5 % Diclofenac-Na content. See Table 13 for details on the applied relative feed rates ($\dot{F}R_{rel}$) between feeder 1 (containing B-1) and feeder 2 (containing B-2).

Table 13: Relative feed rates (%) between Formulation B-1 and B-2, in order to generate final blends (Formulation B, see 6.2) at varying label claims.

Formulation	100 % LC	130 % LC	70 % LC
$\dot{F}R_{rel}$ B-1 (%)	25.51	33.16	17.86
$\dot{F}R_{rel}$ B-2 (%)	74.49	66.84	82.14

For B-1, solid feed rate $S\dot{F}R_1$ was varied between 0.4 – 2.0 kg/h; for B-2, $S\dot{F}R_2$ was varied between 1.3 – 4.9 kg/h. $S\dot{F}R_{tot}$ [kg/h] is defined by eq. 18, as the sum of feed rate of B-1 and of B-2 ($S\dot{F}R_1$ and $S\dot{F}R_2$, respectively).

eq. 18 $$S\dot{F}R_{tot} = S\dot{F}R_1 + S\dot{F}R_2$$

Standard feed-rates ($S\dot{F}R$ in case of Formulations A, where only one feeder was applied and $S\dot{F}R_{tot}$ in case of Formulation B, where two feeders were applied) are listed in section 6.4.6 (page 121).

To prepare blends at varying API content for NIRS method calibration after continuous blending, 100 g of Formulation B with 17.5, 25.0, or 32.5 % Diclofenac-Na content (i.e., 70, 100, and 130 % LC) were prepared, by blending together B-1 and B-2 in a brown glass bottle. The stoichiometric fractions of B-1 and B-2 were defined in analogy to the relative feed rates listed in Table 13 (see 6.2 for details on B-1 and B-2).

6.4.2. Label claim

The target API content of the prepared formulations was 25 % Diclofenac-Na. Variations in API content are reported as variations in label claim (LC). Accordingly, 25 % Diclofenac-Na (absolute) refers to 100 % LC.

LC of final blends was calculated according to eq. 19 for Formulation A (batch blending) and according to eq. 20 for Formulation B (continuous blending); see 6.2 and 6.4.1.

eq. 19 $$LC(\%) = \frac{m(API)}{m} * 100 * \frac{100}{25}$$

eq. 20 $$LC(\%) = \frac{98 * \dot{F}R_{rel}(B-1)}{target}$$

Where *m(API) [kg]* is the total mass of API in the blend, *m [kg]* is the total mass of the final blend. $\dot{F}R_{rel}$ *(B-1)[%]* is defined in Table 13, depending on the desired API content; t*arget [%]* refers to the target API content of 25 % Diclofenac-Na.

6.4.3. Twin-screw wet-granulation

Continuous wet-granulation was performed on a Thermo Fisher Pharma 16 Twin Screw Granulator (TSG) (Thermo Fisher Scientific, Karlsruhe, Germany) with screw diameter (D) of 16 mm and a total screw length of 53 ¼ x D Screw configuration was as follows (from inlet to outlet of the barrel): 2 D Feed Screw Elements (FSE), 2 D Long Helix Feed Screws, 22 D FSE, 2 ¼ D 30° Mixing Element, 22 D FSE, 3 D Distributive Feed Screw Elements.

The powder blend was fed through the first feeding port in the barrel. Granulation liquid at room temperature was fed through the second port of the TSG-barrel by a custom made dispensing pump system (based on Watson Marlow, Zollikon, Switzerland) through a nozzle of 2.5 mm inner diameter. Feeder-calibration was performed each day by the feeder's internal calibration modes. Refill of feeders was performed manually, before the hopper-fill level decreased by more than 50 %. The twin-screw wet-granulator was directly connected to a continuous fluid-bed dryer (6.4.4).

Wet granules' L/S-ratio was set to 0.3 in most trials; standard granulation settings are listed in section 6.4.6 (page 121). Barrel temperature was varied between 30 – 40 °C during screening DoE (3.2.4, page 34). To vary the granules' particle size distribution and moisture content during NIRS method calibration and validation, L/S was varied between 0.20 – 0.35 (see 3.3.2.2, page

57 ff.; 3.3.3.1, page 64 ff.; 3.3.4.2, page 72 ff.). During DoE-assessment, L/S was varied between 0.16 – 0.58 (screening DoE, section 3.2.4, page 34) and 0.20 – 0.40 (auto DoE, section 3.2.5, page 34 ff.). Screw speed and the liquid feed rate was varied between 100-800 rpm, and 0.65 – 2.4 kg/h, respectively; depending on the conducted experiments (details will be listed in the respective sections, see 3.1 -3.4, page 29 ff.).

6.4.4. Continuous fluid-bed drying

Continuous fluid-bed drying of wet granules was performed on a Glatt GPCG 2 CM fluid-bed dryer (Glatt GmbH, Binzen, Germany). The dryer's product container holds a 10-segmented rotor whose ten chambers are sequentially but continuously filled with wet granules supplied from the TSG-outlet (6.4.3). The wet granules then travel $8/10^{th}$ of a full rotation from the inlet port towards the dryer outlet, while being dried on a bottom plate with a pore-size of 25 µm at variable rotor speeds, drying temperatures and airflow rates. Dried granules are then discharged from the dryer outlet by compressed air (2 bar) followed by two alternating valves.

Standard drying settings are listed in section 6.4.6 (page 121). Overall, drying temperature was varied between 65 – 95 °C, drying airflow between 70 – 160 m^3/h, and dryer rotation speed between 5 – 30 rph, depending on the conducted trials; details will be stated in the respective chapters (see 3.1 -3.4, page 29 ff.).

Relevant equations to calculate the dryer's rotation time, granule's drying time, and respective chamber fill mass, in regard to the dryers rotation speed is described by eq. 1 - eq. 3 (see page 15).

6.4.5. Sieving and tableting

For trials on the whole CM-line, dried granules exiting the dryer were transferred from the dryer (6.4.4) to a sieving unit by a powder-transfer-system (PTS11, CT Systems, Tortona, Italy). The dried granules were then sieved through a 1.25 mm sieve (Oscillowitt-Lab type MF-lab, Frewitt, Granges-Paccot, Switzerland) directly before compaction in a rotary tablet press (Fette 1200i, FETTE Compacting, Schwarzenbek, Germany), with eight round, biconcave punches of 10 mm diameter at tableting speeds between 17.000 and 70.000 tablets/hour. No pre-compression was performed; main compression force was set to 10 kN, target tablet weight was 348 mg.

6.4.6. Trial execution and standard process parameters

Unless stated otherwise in the results (see 3.1 -3.4, page 29 ff.), all experiments were performed according to the following general procedure: Before the first trial of the day, the empty dryer was preheated at the designated drying temperature and airflow rate of 150 m^3/h for two hours. Heating of the TSG-barrel at the desired process temperature was started simultaneously. Once the temperature equilibration of the equipment was completed, granulation and drying was started. Dried granules were discarded during a ramp-up period of 20 minutes before sampling, in order to equilibrate the process and avoid transient effects affecting the results. When a temperature change was required between experiments, granulation was stopped and equilibration time of 60 minutes was given to the system at the new designated temperature settings.

Standard process parameters are listed in Table 14. If other settings were applied, it will be stated in the respective sections (see 3.1 -3.4, page 29 ff.).

Table 14: standard process parameters applied in all experiments, unless stated otherwise.

Process Unit	Process parameter	Abbreviation	Standard setpoint
Solid Feeder*	Solid feed rate/ total solid feed rate	SFR / SFR_{tot}	4.0 kg/h
Continuous Blender+	Speed	-	750 rpm
Liquid feeder	Liquid feed rate	LFR	1.2 kg/h
Twin-screw granulator	Barrel Temperature	BT	35 °C
	Screw Speed	SS	450 rpm
Continuous fluid-bed dryer	Drying air flow	DAV	140 m^3/h
	Drying temperature	DT	80 °C
	Dryer rotation speed	DRS	17 rph

**for setup A, one feeder was applied feeding blend at a defined solid feed rate (SFR); for setup B, two feeders were applied, feeding different ratios of blend B-1 and B-2, as listed in Table 13 (see 6.2, 6.3, and 6.4.1 for details on A and B); SFR_{tot} is the sum of both feed rates of B-1 and B-2 (see eq. 18, page 119).*
+only used in Setup B.

6.4.7. Process control system DeltaV

The equipment units described in 6.4.1 - 6.4.6, were controlled through the process control system DeltaV E100, Version 11.3.1 (Emerson Process Management, St. Louis, Missouri, USA).

6.4.8. Sampling of granules

If no tableting was performed, dried granules were collected from the dryer outlet (6.4.4) in a PE-bag. Either one full rotation of granules was collected in a bag, or individual chambers were collected (details will be given in the respective sections, see 3.1 -3.4, page 29 ff.). If a full rotation was sampled, the sample was carefully mixed, before reference analysis was performed.

6.5. Reference analysis of samples

6.5.1. Analysis of water content (LOD)

Sample LOD was measured with a loss-on-drying moisture analyzer (HS153, Mettler Toledo, Greifensee, Switzerland), by drying approximately 5 g of granules at 106°C, until the drying rate was lower than 1 mg/ 50 s. Granules were measured immediately after sampling and the average sample-LOD and standard deviation (in w/w %) was calculated from three consecutive measurements, unless stated otherwise.

6.5.2. Analysis of particle size distribution (PSD)

PSD of dried granules was analyzed by two different dynamic image analyzers: CamSizerXT (Retsch Technology, Haan, Germany) and Qicpic Gradis L (Sympatec GmbH, Clausthal-Zellerfeld, Germany). CamSizer XT is equipped with an X-Jet module operating at 30 kPa dispersion pressure and is suitable for fine and sticky granule samples in the range of

1 µm - 3 mm. Qicpic is equipped with a gravity dispersion unit and is suitable for a wider range of particle sizes (1µm - 10mm).

Qicpic was used for all screening-DoE samples, as few samples were too coarse for CamSizer analysis. All other samples were analyzed by CamSizer. With both analyzers, each sample was measured three times with approximately 5 g of granules per measurement, and the average PSD was calculated. Both techniques report volume-based particle size distributions, calculated based on the smallest of all maximum chord lengths of the particle projection (inner width); quantiles X_{10}, X_{50} and X_{90} were calculated for data analysis.

6.5.3. Analysis of API content by HPLC

Content of Diclofenac Sodium in the collected samples was quantified by HPLC with an Agilent 1260 analytical system (Agilent Technologies, Santa Clara, CA, USA), equipped with a 250 x 4.6 mm YMC Pack ODS-AM Column (YMC CO. LTD., Kyoto, Japan). A mixture of Methanol and 0.8 g $NaH_2PO_4*H_2O$ in water at pH = 2.5 (adjusted with H_3PO_4 85%) was used as mobile phase, with gradient mixing of 35/65 at 0-10 minutes, 65/35 at 11-30 minutes, and 35/65 at 31-35 minutes at a flowrate of 1.5 ml/min. Column temperature was 40 °C, detection wavelength was 254 nm. The sample solvent contained 320 ml tri-sodium citrate di-hydrate 1 % and 680 ml Ethanol 90 %. For sample preparation, 80 mg of dried granules or 80 mg of crushed & homogenized tablets were dissolved ad 100 ml solvent and filtered through a 1 µm glass filter before injection of 40 µl for analysis. Results were corrected for the samples measured water content. Diclofenac Sodium 99.9 % in solvent was used as reference standard.

6.6. Process Analytical Technologies

6.6.1. Laser diffraction

A Sympatec Mytos laser diffraction analyzer (Sympatec GmbH, Clausthal-Zellerfeld, Germany) was used for particle size analysis. Due to GMP-constraints, samples were measured offline. Each sample was measured three times with approximately 5 g of granules per measurement, and the average PSD was calculated. The systems measures scattering intensity as a function of the scattering angle, wavelength and polarization of light and reports the determined particle size as the equivalent diameter of a sphere sharing the same diffraction pattern. Laser diffraction is an absolute analysis method, that does not require method development. The systems measurement range is limited to particle sizes between 0.25 µm to 1,75 µm.

6.6.2. Mass- and energy balance calculations

Mass- and energy balance (MEB) calculations allow the estimation of not directly measurable process values, through the analysis of directly measurable mass- and energy flow rates and related parameters (e.g. temperature-, humidity-, air flow-, and mass flow measurements). Such calculations are highly equipment specific. In the presented thesis, a thorough MEB calculation was derived for the investigated drying unit Glatt GPCG 2 CM fluid-bed dryer.

Initial calculations were performed in Microsoft Excel 2016 (Microsoft Corporation, Washington, USA). In later stages of the project, calculations were implemented into the plant

internal process control system DeltaV as a so-called "LOD-Estimator", that allows the prediction of dried granules' LOD in real-time, based on corresponding real-time process data. Details on the calculations and the implemented LOD-Estimator are provided in the respective results section (see 3.3.2.1, page 50 ff.).

6.6.3. NIR spectroscopy

6.6.3.1. Spectral acquisition

NIR spectroscopy was used for the analysis of dried granules moisture content (LOD), for dried granules particle size distribution (PSD), for API blend uniformity in powder blend and dried granules, and for API content uniformity in final tablets. The instruments and the installation of the four NIR probes is presented in Figure 76.

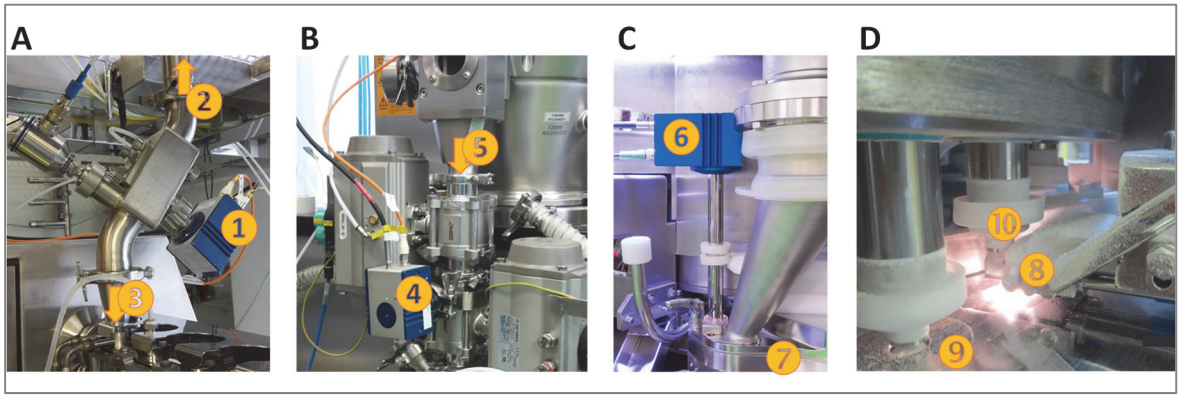

Figure 76: Setup of the four installed NIRS-probes. A: measuring flowing blend after continuous blending ((1) probe, (2) connection to continuous blender, (3) connection to twin-screw wet-granulator). B: measuring dried granules after continuous drying, probe (4) installed at the dryer outlet (5) between two alternating discharge valves. C: measuring dried granules after sieving ((6) probe installed in the tablet press feed-frame (7)). D: measuring individual tablets with a probe (8) inserted below the upper punch (10) right before the tablet exits the die (9).

NIR spectra of powder blend and granules were collected with a multichannel diode array NIR spectrometer in combination with the SentroProbe DR LS measurement probe (SentroPAT FO, Sentronic GmbH, Dresden, Germany). Spectra were collected in diffuse reflectance mode over the spectral range from 1150 – 2100 nm by averaging 60 scans of 0.011 s integration time at a resolution of 2 nm. External referencing was performed before each trial, using a certified 99 % reflectance Spectralon® standard. Internal referencing during processing was performed every 30 minutes with an internal PTFE-wavelength standard located in the measurement probe. Three probes were installed into the line: after continuous blending (if applicable; installed in PAT-chute measuring flowing powder), after continuous drying at the outlet of the dryer (installed between two alternating discharge valves, allowing static sample measurement), and in the tablet press feed frame (measuring granules while they are agitated with a feeding-paddle). For offline NIRS analysis, the probe was directly placed into the granule sample.

A VisioNIR LS instrument (VisioTec GmbH, Laupheim, Germany) was used to analyze tablet content uniformity. In-line spectra of tablets for calibration and validation were measured in reflection mode in the tablet press using 32 scans of 0.004s, an 8 cm^{-1} resolution, and a spectral

range of 4000-10000 cm^{-1}. Offline spectra for calibration were measured at the same settings in static mode outside of the tablet press. The distance between tablets and the probe head was fixed at 3 mm. In-line spectra were collected at three different tableting speeds (17000, 30000 and 70000 tablets per hours).

With both instruments, a background spectrum was acquired every hour for off-line samples and before the campaign for in-line acquisition.

6.6.3.2. Spectral pre-processing, calibration, and validation

Physical sample characteristics such as particle size, morphology, or sample presentation can have an impact on spectral slope and baseline offset. Since such variances are thought to be desired effects when correlating particle size related information to NIRS spectra, no data preprocessing of raw spectra was performed for PSD method development [110, 121].

For LOD and API content method development, those spectral variances are undesired as they can mask the specific spectral information related to chemical sample characteristics. Hence, spectra were pre-processed by standard normal variate (SNV) combined with first derivative (gap of 5) for spectral adjustment and reduction of noise [157].

Details on the datasets (e.g. number of online and offline spectra, calibration range, and sample characteristics) used to calibrate and validate the respective NIRS methods are provided in the corresponding results sections. For LOD and PSD methods, spectra were calibrated via PLS regression against reference analysis results (see section 6.5, page 122 ff. for details on reference analysis; see 6.6.3.3, page 126 f. for details on PLS regression). For API content methods, spectra were calibrated via PLSR either against reference analysis results or the calculated API content based on weight (w/w (%)); details will be provided in the respective sections on method development (see 3.3.4, page 71 ff.).

Calibrations were assessed via linearity, range, and robustness, according to current guidelines on validation of NIR methods. To test linearity and range, calibration and validation samples were plotted against values obtained from reference analytics, as recommended by EMA. Results were evaluated by considering the range, the coefficient of determination (R^2), the intercept, the slope, and the bias. Generally, R^2 greater or equal to 0.95 should be observed while the slope and intercept are expected to be as close as possible to 1, and 0, respectively [134]. A guideline scale that was specifically developed for NIRS predictive models by Malley et al. [148] considers $R^2 > 0.95$ as successful and $R^2 < 0.7$ as inadequate.

Accuracy was demonstrated by evaluating root mean square error of cross-validation (RMSECV) and of prediction (RMSEP). RMSECV is a common resampling statistic calculated from the calibration data set by the leave-one-out method. RMSEP is based on predictions made from the validation dataset. Furthermore, a graphical evaluation of residues from the validation samples allowed to determine their minimum and maximum [134]. To demonstrate robustness, common variations during routine analyses should not affect the ability of the method [134, 135, 190]. Details on the robustness evaluation for each method are provided in the respective results sections (see 3.3.2.2, page 57 ff.; 3.3.3.1, page 64 ff., and 3.3.4 page 71 ff.).

For PSD model assessment, the ratio of prediction to deviation (RPD), the ratio of prediction error to laboratory error (PRL), and the range error ratio (RER) were evaluated in addition to the above mentioned assessment methods. RPD represents the relationship between the variation in sample population and the model's prediction error, calculated as the ratio of reference standard deviation and RMSECV or RMSEP. Above cited guideline by Malley et al. [148] considers NIRS models with RPD > 3 successful and RPD < 1.75 inadequate, depending on the intended purpose. PRL represents the ratio of RMSEP or RMSECV to the standard error laboratory SEL (here: calculated from reference repeatability). PRL should be ≤ 2 for excellent models. RER is calculated as the ratio of calibration sample range (based on reference analytics) and RMSECV or RMSEP. RER ≥ 10 indicates high model utility, 3 < RER < 10 indicates that practical utility is limited [32, 33, 134, 135, 168].

6.6.3.3. Chemometric methods

Qualitative methods: Principal Component Analysis and Independent Component Analysis

Principal Component Analysis (PCA) is an unsupervised method used to highlight similarities and differences in a set of observations using linearly uncorrelated variables called Principal Components (PCs). This procedure permits a visualization of the repartition of the dataset and in this case the spectra that requires no previous knowledge about the available data. PCA was applied in order to have a first overview of the sample distribution and for qualitative process monitoring [159].

Independent Component Analysis (ICA) is a special case of blind source separation that performs a decomposition of a multivariate signal (i.e. spectra) into independent non-Gaussian components (also called latent variables or sources) with the assumption that the components are statistically independent. In contrast to PCA, where original signals cannot be recovered from a multivariate one, ICA can apply information on statistical independence to recover the original sources. There are numerous algorithms available that do ICA, all differing in the way independence is defined. In the presented work it was defined by maximizing non-Gaussianity according to Hyvarinnen et al [162]. Further details on the mathematics behind ICA can be found in literature [160, 161]. ICA was applied for qualitative process monitoring.

Quantitative method: Partial Least Squares regression

Partial least squares regression (PLSR) was carried out on the preprocessed NIRS spectra with a full cross-validation using a non-linear iterative PLS-algorithm. PLS is the most used chemometric algorithm for regression calibrations [163]. PLSR was applied for quantitative NIRS method calibration against LOD, API content, and PSD.

6.6.3.4. Software and statistical computation for NIRS method development

The "Sentro Suite" package (version 2) (Sentronic®, Dresden, Germany) was used for spectra acquisition of blend and dried granules. SIMCA software (version 13.3, Umetrics/Sartorius, Umea, Sweden) was used to compute the calibrations.

The "NovaPAC/NovaMath" package (Prozess Technologie Inc. ®, St. Louis, Missouri, USA) was used for spectra acquisition of tablets in the tablet press. Unscrambler® version 10.5

(CAMOs Software AS, Oslo, Norway) was used for the preprocessing, the PLS computation for in-line prediction.

Hierarchical Calibration development module (version 1.5 - CAMOs Software AS, Oslo, Norway) was used to create the in-line calibration.

R Software (version 3.3.3, The R Foundation for Statistical Computing) was used for computation with RStudio (Version 0.99.878 – RStudio, Inc.) as interface.

The following libraries were used: Library signal (version 0.7-6) for preprocessing, library PLS (version 2.6.0) for Partial Least Square regression, Library HyperSpec (version 0.99) for spectral importation, FactoMineR (version 1.36), Factoextra (version 1.0.5) and Factoshiny (version 1.0.5) for Principal Component Analysis and library ICA for Independent Component Analysis (version 1.0-1).

6.6.4. Wireless Temperature- and Humidity Sensors

To investigate the continuous fluid-bed dryer in detail, wireless temperature- and humidity sensors (MadgeTech Temp1000IS and RHTemp 1000IS, MadgeTech Inc., Warner, NH, USA) were installed inside of three process compartments of the rotating fluidizing chamber with a custom made holding system.

The sensors are suitable for temperatures between -40 °C to 80 °C with a resolution of 0.01 °C and a calibrated accuracy of ± 0.5 °C and humidity between 0 % rH to 100 % rH with a resolution of 0.1 % rH and a calibrated accuracy of ± 3 % rH. Sensors were programmed to log a data point every five seconds. Data was analyzed offline, once the respective trials were completed.

6.7. QbD-based Process Development

6.7.1. Risk Assessment

Risk assessment was conducted in two-steps. First, fishbone diagrams for TSG and FBD were created, that list all conceivable process parameters and material attributes (further summarized as *variables*) that could potentially vary over the course of production. For better overview, the diagrams are divided into the five sub-categories: environment, materials, process parameters, machine, and people. To ensure that all possible scenarios were reflected during risk assessment, formulators, process engineers and analytical experts were included into the discussion.

In the second step of the risk assessment, each variable was individually reflected in a criticality matrix rating. If a sound justification was presented that the probability for a certain variable to fluctuate during production is low, it was downgraded to not-critical. All remaining variables were defined as pCPPs or pCMAs (potentially critical process parameters or material attributes, summarized as *factors*) that need to be investigated in detail for their criticality on dried granules critical quality attributes (CQAs) LOD and PSD (summarized as *responses*).

6.7.2. DoE Design and trials execution

Screening DoE

A fractional factorial screening DoE on two levels with $2^{7-4} = 16$ different factor level combinations and 3 repetitions at the center point settings was designed from seven quantitative pCPPs, as identified during risk assessment. The design allows modeling of linear factor-response relationships at resolution IV: three-factor interactions are confounded with main effects, and two-factor interactions cannot be fully resolved as they are partially confounded among each other, quadratic effects cannot be identified distinctively, but can be suggested from statistical methodologies. Details on the selected factors and the design are provided in the respective results section (see 3.2.3 and 3.2.4, page 31 ff.).

Auto DoE

A fractional factorial screening-DoE on two levels with $2^{6-2} = 16$ different factor level combinations and 3 repetitions at the center point settings (resolution IV) was designed from six quantitative pCPPs. Details on the selected factors and the design are provided in the respective results section (see 3.2.5, page 34 ff.).

6.7.3. Software

Design of experiments and evaluation of results was performed with software package MODDE 11 (Sartorius-Stedim, Malmö, Sweden), Origin Pro 2016 (Origin Lab Corporation, Northampton, USA) and Microsoft Excel 2010 (Microsoft, Redmont, USA).

During the auto-DoE, process parameters were changed automatically by the "Sequencer", an in-house developed software tool implemented into the plant's process control system DeltaV. With the Sequencer, up to 8 process units, with up to 10 process parameters (PPs) per process unit and up to 30 individual PP-steps can be defined. The Sequencer then enables the simultaneous adaption of all selected PPs at pre-defined time points.

6.8. Application of statistical descriptive models for process control

To enable model-based process start-up, an automated "DRS-ramp" software tool was developed in-house and implemented into the plant's process control system DeltaV. The DRS-ramp initiates a pre-defined ramping procedure of the dryer rotation speed (DRS), once wet granules enter the dryer upon production start. By entering a respective ramp-height and –slope, the operator can define the ramp-characteristics. Details on the selection of ramp-height and –slope are presented in the respective results section (see 3.2.6, page 42 ff.).

To enable PAT-based predictive feedback-control in real-time a "PAT-Controller" was developed in-house and implemented into the plants process control system DeltaV. The software tool enables the adaption of process parameters DRS and drying air flow (DAV), based on PAT-results provided by either NIRS or mass- and energy balance calculations.

6.9. Multivariate statistical process control

6.9.1. Calibration and validation

Multivariate statistical process control charts were calculated from corresponding process data. Data was analyzed via PCA, corresponding PCs were plotted in Shewhart control charts against time (see 6.6.3.3, page 126 f., for details on PCA). The target is equal to the normalized process average, warning and control limits were set at the 95 % and 99 % limits (i.e. ± 2 and ± 3 standard deviations), according to common literature guidelines [158, 167, 171]. Calibration Shewhart charts were prepared from process data representing the common variation in the respective parameters, validation charts were prepared from test-trials by applying their respective PC statistics to the control limits of the calibration charts. Details on the selected process parameters to analyze and the selected data for calibration and validation charts are provided in the respective results section (see 3.3.5, page 81 ff.).

6.9.2. Software

Multivariate data analysis of process data and generation of Shewhart control charts was performed in SIMCA software (version 14.1, MKS Umetrics, Umea, Sweden).

6.10. Analysis of residence time distribution

The material's residence time distribution in the line at various process conditions was analyzed by four NIRS probes placed at the outlet of the blender, the outlet of the dryer, in the tablet press feed-frame, and at the ejection point of the final tablets in the press, respectively. Different steps in API-content were induced by varying the feed rate ratio of the two powder feeders (containing Blend B-1 (API) and B-2 (Excipients)) between 70 – 130 % of LC (see 6.4.1 and 6.4.2, page 120, for details on Blend B-1 and B-2 and calculation of LC). Details on the varied process conditions are provided in the respective results section (see 3.4, page 99 ff.).The progression of the step responses between the feeders and the four NIRS probes was analyzed as follows:

Each observed step response (as measured by NIRS) was normalized over the respective step-height (i.e. start of the step = 0, end of the step = 1) to plot effect *F* as a function of time *t*. The starting point of each step was defined as t_0 (i.e., the time point, when the feed rate ratio of the two feeders was adjusted); the end of each step was defined as the time when the observed step response *F* remained constant (t_{max}).

For once, the event propagation time (EPT[17]) of effect *F* crossing the lower and upper noise limit was analyzed. The lower noise limit was defined at the 5 % limit, and the upper at the 95 % limit (in respect to the normalized 0-1 range of the normalized effect *F*). The so called EPT5 and EPT95, mark the time points between which the observed response F can be classified as significant. 5 %-limits were selected as a compromise between ensuring that signal-noise is not registered as response, to improve reproducibility of results, while still covering 90 % of the observed interval as a significant response. To further improve the accuracy and repeatability, a

[17] EPT is Novartis internal nomenclature

moving average of *F* was used to calculate the intercept between F and the 0.05/0.95 line (n=3), rather than the raw data.

Additionally to EPT5 and EPT95, the mean residence time (MRT) was calculated as the integral of (1-F) over the response time t ($t_0 \rightarrow t_{max}$), as described in eq. 21. A graphical illustration of EPT5, EPT95, and MRT is provided in Figure 77.

eq. 21 $$MRT = \int_{t_0}^{t_{max}} \{(1 - F) * dt\}$$

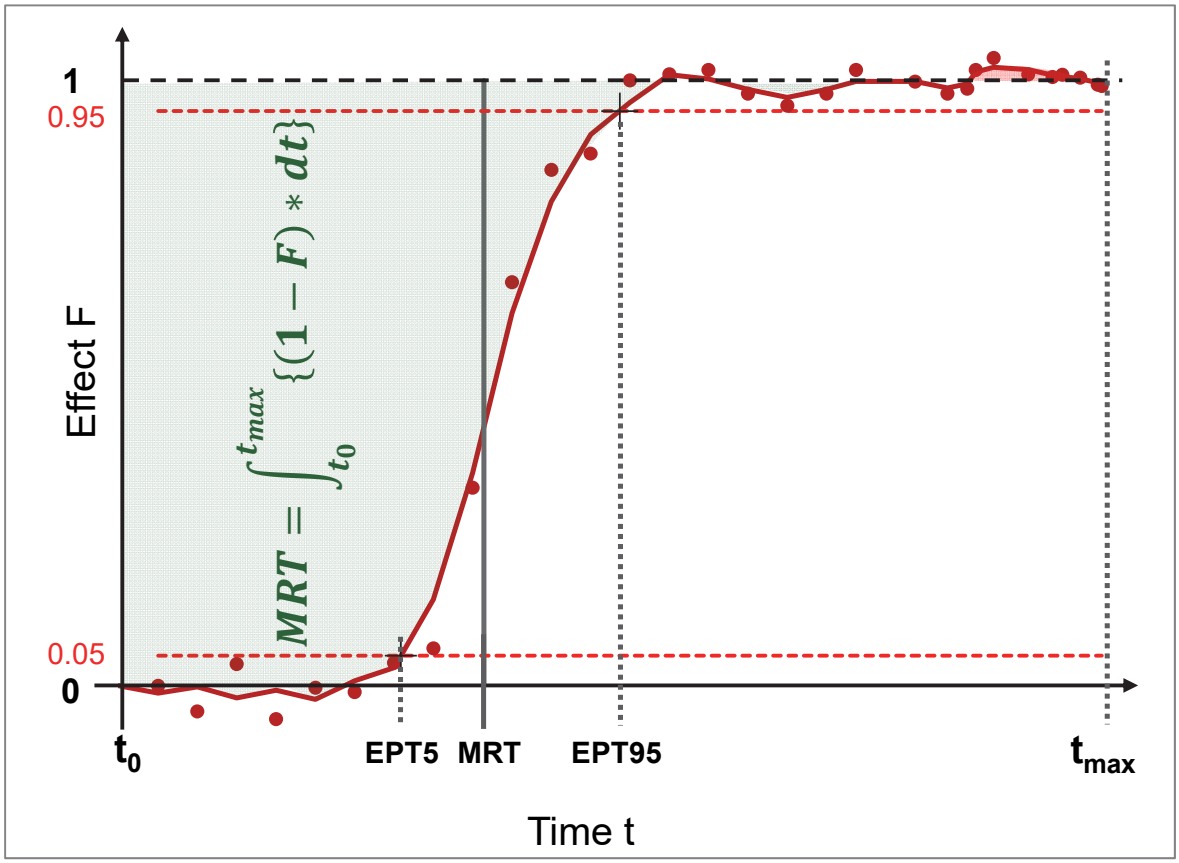

Figure 77: Graphical illustration of ETP5, EPT95, and MRT.

7. References

[1] Ierapetritou, M., Muzzio, F., and Reklaitis, G. 'Perspectives on the continuous manufacturing of powder-based pharmaceutical processes', *American Institute of Chemical Engineers Journal*, 2016. 62(6): pp. 1846-1862.

[2] Chatterjee, S. (2012). 'FDA perspective on Continuous Manufacturing' [PowerPoint presentation], IFPAC Annual Meeting in Baltimore, Maryland, USA. Available at: https://www.fda.gov/downloads/AboutFDA/CentersOffices/OfficeofMedicalProductsandTobacco/CDER/UCM341197.pdf (Accessed: 12th of June 2017).

[3] Manyika, J., Sinclair, J., Dobbs, R., et al. (2012). 'Manufacturing the future: The next era of global growth and innovation' [online], McKinsey Global Institute. Available at: https://www.mckinsey.com/business-functions/operations/our-insights/the-future-of-manufacturing (Accessed: 18th of July 2017).

[4] Malhotra, G. (2015). 'Continuous Process in Pharmaceutical Manufacturing: Considerations, Nuances and Challenges: A review of the business and process considerations for continuous processing in pharma manufacturing' [online], Contract Pharma. Available at: https://www.contractpharma.com/issues/2015-06-01/view_features/continuous-process-in-pharmaceutical-manufacturing-considerations-nuances-and-challenges (Accessed: 18th of July 2017).

[5] US Department for Health and Human Services. (2004). 'Guidance for Industry: PAT - A Framework for Innovative Pharmaceutical Development, Manufacturing and Quality Assurance', US Food and Drug Administration. Available at: https://www.fda.gov/downloads/drugs/guidances/ucm070305.pdf.

[6] Allison, G., Cain, Y.T., Cooney, C., et al. 'Regulatory and Quality Considerations for Continuous Manufacturing: May 20 – 21, 2014 Continuous Manufacturing Symposium', *Journal of Pharmaceutical Sciences*, 2015. 104(3): pp. 803-812.

[7] The Brookings Institution. (2015) 'Promoting Continuous Manufacturing in the Pharmaceutical Sector – Discussion Guide' [online], Center for Health Policy at Brookings. Available at: https://www.brookings.edu/wp-content/uploads/2015/10/Continuous-manufacturing-discussion-guide.pdf (Accessed: 18th of July 2017).

[8] Srai, J.S., Badman, C., Krumme, M., et al. 'Future Supply Chains Enabled by Continuous Processing – Opportunities and Challenges: May 20 – 21, 2014 Continuous Manufacturing Symposium', *Journal of Pharmaceutical Sciences*, 2015. 104(3): pp. 840-849.

[9] The European pharmaceutical manufacturer. (2017). 'Large volumes only! How continuous manufacturing can benefit pharma' [online], EPM Magazine. Available at: https://www.epmmagazine.com/opinion/large-volumes-only/ (Accessed: 31st of May 2018).

[10] Lee, S.L., O'Connor, T.F., Yang, X., et al. 'Modernizing Pharmaceutical Manufacturing: from Batch to Continuous Production', *Journal of Pharmaceutical Innovation*, 2015. 10(3): pp. 191-199.

[11] Moses, H. 3rd, Dorsey, E.R., Matheson, D.H., Thier, S.O. 'Financial anatomy of biomedical research', *Jama*, 2005. 294(11): pp. 1333-42.

[12] Munos, B. 'Lessons from 60 years of pharmaceutical innovation', *Nature Reviews Drug Discovery*, 2009. 8(12): pp. 959-68.

[13] Martin, J. (2017). 'No Easy Answers for Drug Pricing' [online], Pharmaceutical Manufacturing. Available at: http://www.pharmamanufacturing.com/articles/2017/no-easy-answers-for-drug-pricing/ (Accessed: 25th of July 2017).

[14] Price, E. (2014). 'Trends and Predictions for API Drug Manufacturing' [online], PCI Synthesis. Available at: http://www.pcisynthesis.com/2015-trends-and-predictions-for-api-drug-manufacturing/ (Accessed: 25th of July 2017).

[15] Jogalekar, A. (2014). '(Don't) Mind the Gap: Manufacturing Costs and Drug Prices' [online], Scientific American Blogs. Available at: https://blogs.scientificamerican.com/the-curious-wavefunction/dont-mind-the-gap-manufacutring-costs-and-drug-prices/ (Accessed: 25th of July 2017).

[16] Schuhmacher, A., Gassmann, O., Hinder, M. 'Changing R&D models in research-based pharmaceutical companies', *Journal of Translational Medicine*, 2016. 14: p. 105.

[17] Kupferschmidt, K. 'Germany moves to lower drug prices', *CMAJ : Canadian Medical Association Journal*, 2011. 183(2): pp. E77-E78.

[18] Michalopoulos, S. (2017). 'Lawmakers warn EU pharma industry about drug pricing' [online], Foundation Euractiv. Available at: https://www.euractiv.com/section/health-consumers/news/lawmakers-warn-eu-pharma-industry-about-drugs-pricing/ (Accessed: 26th of July 2017).

[19] Edney, A., Sink, J. (2017). 'Trump Administration Prepares a Drug Pricing Executive Order, Sources Say' [online], Bloomberg L.P. Available at: https://www.bloomberg.com/news/articles/2017-06-15/trump-administration-said-to-ready-drug-pricing-executive-order (Accessed: 26th of July 2017).

[20] Kuehn, S.E. (2015) 'Janssen Embraces Continuous Manufacturing for Prezista' [online], Pharmaceutical Manufacturing. Available at: http://www.pharmamanufacturing.com/articles/2015/janssen-embraces-continuous-manufacturing-for-prezista/ (Accessed: 26th of July 2017).

[21] ICH. (2009). 'ICH Harmonized Tripartite Guideline: Pharmaceutical Development Q8(R2)' Available at : https://www.ich.org/fileadmin/Public_Web_Site/ICH_Products/Guidelines/Quality/Q8_R1/Step4/Q8_R2_Guideline.pdf.

[22] Pauli, V., Elbaz, F., Kleinebudde, P., Krumme, M. 'Methodology for a Variable Rate Control Strategy Development in Continuous Manufacturing Applied to Twin-Screw Wet-Granulation and Continuous Fluid-Bed Drying', *Journal of Pharmaceutical Innovation*, 2018. 13(3): pp. 247-260.

[23] Meekings, K.N., Williams, C.S., Arrowsmith, J.E. 'Orphan drug development: an economically viable strategy for biopharma R&D', *Drug Discovery Today*, 2012. 17(13-14): pp. 660-664.

[24] Boughton, P. (2017) 'Continuous manufacturing advances - Richard Steiner reports on the changing face of drug development and production' [online], Scientist Live. Available at: https://www.scientistlive.com/content/continuous-manufacturing-advances (Accessed: 19th of January 2017).

[25] Song, C.H., Han, J.-W. 'Patent cliff and strategic switch: exploring strategic design possibilities in the pharmaceutical industry', *SpringerPlus*, 2016. 5(1): p. 692.

[26] EMA Committee for Proprietary Medicinal Products and EMA Committee for Veterinary Medicinal Products. (2001). 'Note for Guidance on Process Validation', European Medicines Agency. Available at: https://www.ema.europa.eu/documents/scientific-guideline/note-guidance-process-validation_en.pdf.

[27] Schaber, S.D., Gerogiorgis, D.I., Ramachandran, R., et al. 'Economic Analysis of Integrated Continuous and Batch Pharmaceutical Manufacturing: A Case Study', *Industrial & Engineering Chemistry Research*, 2011. 50(17): pp. 10083-10092.

[28] Dave, V.S., Saoji, S.D., Raut, N.A., Haware, R.V. 'Excipient variability and its impact on dosage form functionality', *Journal of Pharmaceutical Sciences*, 2015. 104(3): pp. 906-15.

[29] Vercruysse, J., Delaet, U., Van Assche, I., et al. 'Stability and repeatability of a continuous twin screw granulation and drying system', *European Journal of Pharmaceutics and Biopharmaceutics*, 2013. 85(3): pp. 1031-1038.

[30] US Food and Drug Administration. (2017). 'Code of Federal Regulations Title 21 - General Section 210.3: Current good manufacturing practice in manufacturing, processing, packing, or holding of drugs'. Available at: https://www.accessdata.fda.gov/scripts/cdrh/cfdocs/cfcfr/CFRSearch.cfm?fr=210.3 (Accessed: 17th of July 2018).

[31] Liu, R., Li, L. Yin, W., et al. 'Near-infrared spectroscopy monitoring and control of the fluidized bed granulation and coating processes – A review', *International Journal of Pharmaceutics*, 2017. 530(1-2): pp. 308-315.

[32] US Department of Health and Human Services. (2015). 'Guidance for Industry: Analytical procedures and methods validation for drugs and biologics', US Food and Drug Administration. Available at: https://www.fda.gov/downloads/drugs/guidances/ucm386366.pdf.

[33] Vervaet, C., Remon, J.P. 'Continuous granulation in the pharmaceutical industry', *Chemical Engineering Science*, 2005. 60(14): pp. 3949-3957.

[34] US Food and Drug Administration. (2017). 'Code of Federal Regulations Title 21 – part 11: Electronic Records, Electronic Signatures'. Available at: https://www.accessdata.fda.gov/scripts/cdrh/cfdocs/cfcfr/CFRSearch.cfm?CFRPart=11 (Accessed: 17th of July 2018).

[35] Committee for Medicinal Products for Human Use. (2012). 'Guideline on Real Time Release Testing', European Medicines Agency. Available at: https://www.ema.europa.eu/documents/scientific-guideline/guideline-real-time-release-testing-formerly-guideline-parametric-release_en.pdf.

[36] Shanley, A. 'Moving Toward Real-Time Release Testing', *Pharmaceutical Technology*, 2017. 41(7): p. 54.

[37] Kazemi, P., Khalid, M.H., Pérez Gago, A., et al. 'Effect of roll compaction on granule size distribution of microcrystalline cellulose-mannitol mixtures: computational intelligence modeling and parametric analysis', *Drug Design, Development and Therapy*, 2017. 11: pp. 241-251.

[38] Idakiev, V., Mörl, L. 'Study of residence time of disperse materials in continuously operating fluidized bed apparatus', *Journal of Chemical Technology and Metallurgy*, 2013. 48(5): pp. 451-456.

[39] Gao, Y., Muzzio, F., Ierapetritou, M. 'A review of the Residence Time Distribution (RTD) applications in solid unit operations', *Powder Technology*, 2012. 228: pp. 416–423.

[40] Matsuda, Y. (2016). 'PMDA Perspective on Continuous Manufacturing' [PowerPoint presentation], Japanese Pharmaceutical and Medical Devices Agency. Available at: https://www.pmda.go.jp/files/000218273.pdf (Accessed: 18th of May 2018).

[41] Gorringe, L.J., Kee, G.S., Saleh, M.F., et al. 'Use of the channel fill level in defining a design space for twin screw wet granulation', *International Journal of Pharmaceutics*, 2017. 519(1–2): pp. 165-177.

[42] Kandpal, L.M., Tewari, J., Gopinathan, N., et al. 'Quality assessment of pharmaceutical tablet samples using Fourier transform near infrared spectroscopy and multivariate analysis', *Infrared Physics & Technology*, 2017. 85: pp. 300-306.

[43] Pharmaceutical Technology Editors. (2018). 'Vertex Receives FDA Approval for Continuously Manufactured Drug Product' [online], PharmTech. Available at: http://www.pharmtech.com/vertex-receives-fda-approval-continuously-manufactured-drug-product (Accessed: 18th of May 2018).

[44] Palmer, E. (2015). 'Vertex, J&J, GSK, Novartis all working on continuous manufacturing facilities' [online], Fierce Pharma. Available at: https://www.fiercepharma.com/supply-chain/vertex-j-j-gsk-novartis-all-working-on-continuous-manufacturing-facilities (Accessed: 18th of May 2018).

[45] ERC for Structured Organic Particulate Systems. (2015). 'FDA Approves Tablet Production on Continuous Manufacturing Line' [online], Engineering Research Centers. Available at: http://erc-assoc.org/content/fda-approves-tablet-production-continuous-manufacturing-line-0 (Accessed: 11th of July 2018).

[46] Brennan, Z. (2016). 'FDA Allows First Switch From Batch to Continuous Manufacturing for HIV Drug' [online], Regulatory Affairs Professionals Society. Available at: https://www.raps.org/regulatory-focus%E2%84%A2/news-articles/2016/4/fda-allows-first-switch-from-batch-to-continuous-manufacturing-for-hiv-drug (Accessed: 17th of July 2018).

[47] Grote, S., Kleinebudde, P. 'Roll Compaction/Dry Granulation of Dibasic Calcium Phosphate Anhydrous – Does the Morphology of the Raw Material Influence the Tabletability of Dry Granules?', *Journal of Pharmaceutical Sciences*, 2018. 107(4): pp. 1104-1111 .

[48] DiProspero, D. (2018). 'Continuous OSD Manufacturing - A Product & Patient Perspective' [online], ISPE.org. Available at: https://ispe.org/pharmaceutical-engineering/ispeak/continuous-osd-manufacturing-product-patient-perspective (Accessed: 5th of February 2019).

[49] RCPE: Research Center for Pharmaceutical Engineering - Process and Manufacturing Science. (2017). 'Homepage' [online]. Available at: http://www.rcpe.at (Accessed: 27th of July 2017).

[50] CMAC-MIT. (2018). '3rd Symposium on Continuous Manufacturing: Implementation, Integration and Regulatory Approaches' [online]. Available at: https://www.iscmp2018.org/agenda/ (Accessed: 27th of July 2017).

[51] ISPE. (2018) '2018 Continuous Manufacturing Workshop' [online]. Available at: https://ispe.org/conferences/2018-continuous-manufacturing-workshop (Accessed: 27th of July 2017).

[52] CCP. (2018). 'Summit 2019 - Commercializing Continuous Processing in Pharma' [online]. Available at: http://continuous-processing-pharma.com/ (Accessed: 27th of July 2017).

[53] Ervasti, T., Simonaho, S.-P., Ketolainen, J., et al. 'Continuous manufacturing of extended release tablets via powder mixing and direct compression', *International Journal of Pharmaceutics*, 2015. 495(1): pp. 290-301.

[54] Jivraj, M., Martini, L.G., Thomson, C.M. 'An overview of the different excipients useful for the direct compression of tablets', *Pharmaceutical Science & Technology Today*, 2000. 3(2): pp. 58-63.

[55] Lipsanen, T., Antikainen, O., Räikkönen, H., et al. 'Novel description of a design space for fluidised bed granulation', *International Journal of Pharmaceutics*, 2007. 345(1-2): pp. 101-107.

[56] Kleinebudde, P. 'Roll compaction/dry granulation: pharmaceutical applications', *European Journal of Pharmaceutics and Biopharmaceutics*, 2004. 58(2): pp. 317-326.

[57] Van Melkebeke, B., Vermeulen, B., Vervaet, C., Remon, J.P. 'Melt granulation using a twin-screw extruder: A case study', *International Journal of Pharmaceutics*, 2006. 326(1): pp. 89-93.

[58] Vercruysse, J., Córdoba Díaz, D., Peeters, E., et al. 'Continuous twin screw granulation: Influence of process variables on granule and tablet quality', *European Journal of Pharmaceutics and Biopharmaceutics*, 2012. 82(1): pp. 205-211.

[59] Meier, R., Thommes, N., Rasenack, N., et al. 'Granule size distributions after twin-screw granulation – Do not forget the feeding systems', *European Journal of Pharmaceutics and Biopharmaceutics*, 2016. 106: pp. 59-69.

[60] Coperion K-Tron. (2018). 'Product Information: Feeders' [online]. Available at: https://www.coperion.com/en/products-services/process-equipment/feeders/ (Accessed: 1st of June 2018).

[61] Blackshields, C.A., Crean, A.M. 'Continuous powder feeding for pharmaceutical solid dosage form manufacture: a short review', *Pharmaceutical Development and Technology*, 2018. 23(6): pp. 554-560.

[62] Brabender Technology (2018). 'Product Information: Gravimetric and Volumetric Feeders' [online]. Available at: https://www.brabender-technologie.com/en/products/ (Accessed: 1st of June 2018).

[63] Gao, Y. (2012). 'Modeling and analysis of continuous powder blending (Doctoral Dissertation)', Graduate School-New Brunswick, Rutgers University, USA. Available at: https://rucore.libraries.rutgers.edu/rutgers-lib/38761/PDF/1/play/ (Accessed: 1st of June 2018).

[64] Munson Machinery Co., Inc. (2018). 'Product Information: Rotary Continuous Mixers' [online]. Available at: http://www.munsonmachinery.com/Rotary-Continuous-Mixers/ (Accessed: 1st of June 2018).

[65] Pernenkil, L. (2008). 'Continuous Blending of Dry Pharmaceutical Powders (Doctoral Dissertation)', Department of Chemical Engineering. 2008, Massachusetts Institute of Technology, USA. Available at: https://rucore.libraries.rutgers.edu/rutgers-lib/38761/PDF/1/play/ (Accessed: 1st of June 2018).

[66] Shanmugam, S. 'Granulation techniques and technologies: Recent progresses', *BioImpacts*, 2015. 5(1): pp. 55-63.

[67] Amidon, G.E., Houghton, M.E. 'The Effect of Moisture on the Mechanical and Powder Flow Properties of Microcrystalline Cellulose', *Pharmaceutical Research*, 1995. 12(6): pp. 923-929.

[68] Sun, C.C. 'Mechanism of moisture induced variations in true density and compaction properties of microcrystalline cellulose', *International Journal of Pharmaceutics*, 2008. 346(1): pp. 93-101.

[69] Gotthardt, S., Knoch, A., Lee, G. 'Continuous wet granulation using fluidized-bed techniques I. Examination of powder mixing kinetics and preliminary granulation experiments', *European Journal of Pharmaceutics and Biopharmaceutics*, 1999. 48(3): pp. 189-197.

[70] Gohel, M., Parikh, R., Baldaniya, L., et al. (2007) 'Fluidized Bed Systems: A Review' [online], Pharmainfo.net. Available at: https://www.researchgate.net/publication/260025445 (Accessed: 25th of July 2018).

[71] Mangal, H., Kirsolak, M., Kleinebudde, P. 'Roll compaction/dry granulation: Suitability of different binders', *International Journal of Pharmaceutics*, 2016. 503(1): pp. 213-219.

[72] Malkowska, S., Khan, K.A. 'Effect of Re-Compression on the Properties of Tablets Prepared by Dry Granulation', *Drug Development and Industrial Pharmacy*, 1983. 9(3): pp. 331-347.

[73] Mu, B. Thompson, M.R. 'Examining the mechanics of granulation with a hot melt binder in a twin-screw extruder', *Chemical Engineering Science*, 2012. 81: pp. 46-56.

[74] Mašić, I., Ilić, I., Dreu, R., et al. 'Melt granulation in fluidized bed: a comparative study of spray-on versus in situ procedure', *Drug Development and Industrial Pharmacy*, 2014. 40(1): pp. 23-32.

[75] Makkawi, Y.T., Ocone, R. (2011). 'Mass Transfer in Fluidized Bed Drying of Moist Particulate' in Prof El-Amin, M. (ed.). *Mass Transfer in Multiphase Systems and its Applications*. 1st Edition. London, United Kingdom: InTech Open.

[76] Kreimer, M., Aigner, I., Sacher, S., et al. 'Mechanical strength of microspheres produced by drying of acoustically levitated suspension droplets', *Powder Technology*, 2018. 325: pp. 247-260.

[77] Conder, E.W., Cosbie, A.S., Gaertner, J., et al. 'The Pharmaceutical Drying Unit Operation: An Industry Perspective on Advancing the Science and Development Approach for Scale-Up and Technology Transfer', *Organic Process Research & Development*, 2017. 21(3): pp. 420-429.

[78] Parikh, D.M. (2014). 'Solids drying: basics and applications' [online], Chemical Engineering. Available at: http://www.chemengonline.com/solids-drying-basics-and-applications/?printmode=1 (Accessed: 3rd of August 2018).

[79] Randel, E., Schak, J., Islam, A. (2013). 'Fluid-bed dryers: Static versus vibrating' [online], Powder and Bulk Engineering. Available at: https://www.powderbulk.com/enews/2013/whitepaper/GEA.pdf (Accessed: 25th of July 2018).

[80] Mortier, S.T., Gernaey, K.V., De Beer, T., Nopens, I. 'Analysing drying unit performance in a continuous pharmaceutical manufacturing line by means of mass – Energy balances', *European Journal of Pharmaceutics and Biopharmaceutics*, 2014. 86(3): pp. 532-543.

[81] Vercruysse, J., Peeters, E., Fonteyne, M., et al. 'Use of a continuous twin screw granulation and drying system during formulation development and process optimization', *European Journal of Pharmaceutics and Biopharmaceutics*, 2015. 89: pp. 239-247.

[82] Jacob, M., Boeber, R., Pila, R., Pritzke, H., Inventor; Glatt Ingenieurtechnik GmbH, Assignee. (2014). 'Patent US 2016/0074827 A1: Fluidizing Device', United States Patent Application Publication.

[83] Jacob, M., Boeber, R., Pila, R., Pritzke, H., Inventor; Glatt Ingenieurtechnik GmbH, Assignee. (2014). 'Patent US 2016/0047599 A1: Rotary Dryer Star and Method for Treating Solid Particles', United States Patent Application Publication.

[84] Loh, Z.H., Samanta, A.K., Sia Heng, P.W. 'Overview of milling techniques for improving the solubility of poorly water-soluble drugs', *Asian Journal of Pharmaceutical Sciences*, 2015. 10(4): pp. 255-274.

[85] Nakach, M., Authelin, J.R., Chamayou, A,. Dodds, J. 'Comparison of various milling technologies for grinding pharmaceutical powders', *International Journal of Mineral Processing*, 2004. 74: pp. S173-S181.

[86] Monteyne, T., Vancoillie, J., Remon, J.P., et al. 'Continuous melt granulation: Influence of process and formulation parameters upon granule and tablet properties', *European Journal of Pharmaceutics and Biopharmaceutics*, 2016. 107: pp. 249-262.

[87] Wu, C.Y., Hancock, B.C., Mills, A., et al. 'Numerical and experimental investigation of capping mechanisms during pharmaceutical tablet compaction', *Powder Technology*, 2008. 181(2): pp. 121-129.

[88] Palmieri, G.F., Joiris, E., Bonacucina, G., et al. 'Differences between eccentric and rotary tablet machines in the evaluation of powder densification behaviour', *International Journal of Pharmaceutics*, 2005. 298(1): pp. 164-175.

[89] Denis, C., Hemati, M., Chulia, D., et al. 'A model of surface renewal with application to the coating of pharmaceutical tablets in rotary drums', *Powder Technology*, 2003. 130(1): pp. 174-180.

[90] Thompson, M.R. 'Twin screw granulation – review of current progress', *Drug Development and Industrial Pharmacy*, 2015. 41(8): pp. 1223-1231.

[91] Seem, T.C., Rowson, N.A., Ingram, A., et al. 'Twin screw granulation — A literature review', *Powder Technology*, 2015. 276: pp. 89-102.

[92] Meier, R., Moll, K.P., Krumme, M., Kleinebudde, P. 'Impact of fill-level in twin-screw granulation on critical quality attributes of granules and tablets', *European Journal of Pharmaceutics and Biopharmaceutics*, 2017. 115: pp. 102-112.

[93] Fonteyne, M., Vercruysse J., Díaz D.C., et al. 'Real-time assessment of critical quality attributes of a continuous granulation process', *Pharmaceutical Development and Technology*, 2013. 18(1): pp. 85-97.

[94] Liu, Y., Thompson, M.R., O'Donnel, K.P., Grasman, N.S. 'Effect of temperature on the wetting behavior of hydroxypropyl methylcellulose in a twin-screw granulator', *Powder Technology*, 2016. 302: pp. 63-74.

[95] Pauli, V., Elbaz, F., Kleinebudde, P., Krumme, M. 'Orthogonal redundant monitoring of a new continuous fluid-bed dryer for pharmaceutical processing by means of mass and energy balance calculations and spectroscopic techniques', *Journal of Pharmaceutical Sciences,* 2019. 108: pp. 2041-2055.

[96] Kestur, U., Desai, D. (2016). 'Excipients for Conventional Oral Solid Dosage Forms, in Koo, O.M.Y. (ed.). *Pharmaceutical Excipients: Functionality, and Applications in Research and Industry.* (1st Edition). Hoboken, New Jersey, USA: John Wiley & Sons, Inc.

[97] Lee, B.-J. (2008). 'Pharmaceutical preformulation: physicochemical properties of excipients and powders and tablet characterization', in Gad, S.C. (ed.). *Pharmaceutical Manufacturing Handbook: Production and Processes*. (1st Edition). Hoboken, New Jersey, USA: John Wiley & Sons, Inc.

[98] Medicines Complete. (2018). 'Handbook of pharmaceutical excipients' [online]. Available at: http://www.medicinescomplete.com/#/browse/excipients (Accessed: 21st of July 2018)..

[99] Li, J., Wu, Y. 'Lubricants in Pharmaceutical Solid Dosage Forms', *Lubricants*, 2014. 2: pp. 21-43.

[100] Moore, C.M.V. (2012). 'Quality by Design – FDA Lessons Learned and Challenges for International Harmonization' [PowerPoint presentation], International Conference on Drug Development, Austin, Texas, USA. Available at: https://www.fda.gov/downloads/aboutfda/centersoffices/officeofmedicalproductsandtobacco/cder/ucm341204.pdf (Accessed: 26th of July 2017).

[101] Maguire, J., Peng, D. (2015) 'How to Identify Critical Quality Attributes and Critical Process Parameters' [PowerPoint presentation], FDA/PQRI 2nd Conference, North Bethesda, Maryland, USA. Available at: http://pqri.org/wp-content/uploads/2015/10/01-How-to-identify-CQA-CPP-CMA-Final.pdf (Accessed: 12th of June 2017).

[102] Liu, H., Galbraith, S.C., Ricart, B., et al. 'Optimization of critical quality attributes in continuous twin-screw wet granulation via design space validated with pilot scale experimental data', *International Journal of Pharmaceutics*, 2017. 525(1): pp. 249-263.

[103] Novartis Pharma AG. (2017). 'Novartis Internal Documents', Basel Switzerland.

[104] ICH. (2005). 'ICH Harmonized Tripartite Guideline: Quality Risk Management Q9'. Available at: https://www.ich.org/fileadmin/Public_Web_Site/ICH_Products/Guidelines/Quality/Q9/Step4/Q9_Guideline.pdf (Accessed: 6th of August 2018).

[105] Eriksson, L., Johannson, E., Kettaneh-Wold, N., et al. (2008). *Design of Experiments - Principles and Applications*, 3rd Edition. Umea, Sweden: Umetrics Academy.

[106] International Electrotechnical Commission. (2006). 'International Standard IEC 61025 2.0: Fault tree analysis (FTA)', 2nd Edition.

[107] International Electrotechnical Commission. (2006). 'International Standard IEC 60812 2.0: Analysis techniques for system reliability – Procedure for failure mode and effects analysis (FMEA)', 2nd Edition.

[108] International Electrotechnical Commission. (2016). 'International Standard IEC 61882 2.0: Hazard and operability studies (HAZOP studies) - Application guide', 2nd Edition.

[109] Stamatis, D.H. (2003). *Failure Mode and Effect Analysis: FMEA from Theory to Execution*', 2nd Edition. Milwaukee, Wisconsin, USA: ASQ Quality Press.

[110] Siesler, H.W:, Ozaki, Y., Kawata, S., Heise, H.M. (eds). (2002). *Near-Infrared Spectroscopy: Principles, Instruments, Applications*, 1st Edition. Weinheim, Germany: WILEY-VCH Verlag GmbH.

[111] De Beer, T., Burggraeve, A., Fonteyne, M., et al. 'Near infrared and Raman spectroscopy for the in-process monitoring of pharmaceutical production processes', *International Journal of Pharmaceutics*, 2011. 417(1): pp. 32-47.

[112] Peters, J., Taute, W., Bartscher, K., et al. 'Design, development and method validation of a novel multi-resonance microwave sensor for moisture measurement', *Analytica Chimica Acta*, 2017. 961: pp. 119-127.

[113] Peters, J., Bartscher, K., Döscher, C., et al. 'In-line moisture monitoring in fluidized bed granulation using a novel multi-resonance microwave sensor', *Talanta*, 2017. 170: pp. 369-376.

[114] Li, M. Duncan, S. 'Dynamic Model Analysis of Batch Fluidized Bed Dryers. *Particle & Particle Systems Characterization*, 2008. 25: pp. 328-344.

[115] Henneberg, M., Heinrich, S., Ihlow, M., Mörl, L. 'Fluidized Bed Air Drying: Experimental Study and Model Development', *The Canadian Journal of Chemical Engineering*, 2003. 81(2): pp. 176-184.

[116] Inaba, H., Husain, S., Horibe, A., Haruki, N. 'Heat and Mass Transfer Analysis of Fluidized Bed Grain Drying', *Memoirs of the Faculty of Engineering Okayama University*, 2007. 41: pp. 52-62.

[117] Portoghese, F., Berruti, F., Briens, C. 'Continuous on-line measurement of solid moisture content during fluidized bed drying using triboelectric probes', *Powder Technology*, 2008. 181(2): pp. 169-177.

[118] Wang, H.G., Senior, P.R., Mann, R., Yang, W.Q. 'Online measurement and control of solids moisture in fluidised bed dryers', *Chemical Engineering Science*, 2009. 64(12): pp. 2893-2902.

[119] Mettler Toledo. (2018). 'Good Titration Practice in KF Titration' [online]. Available at: https://www.mt.com/dam/LabDiv/Campaigns/TestingLabs2013/moisture/package/gtp-karl-fischer-EN.pdf (Accessed: 6th of August 2018).

[120] Mettler Toledo. (2018). 'What is a moisture analyzer and how does it work?' [online]. Available at: https://www.mt.com/be/en/home/library/FAQ/laboratory-weighing/what-is-a-moisture-analyzer.html (Accessed: 6th of August 2018).

[121] Hansuld, E.M., Briens, L. 'A review of monitoring methods for pharmaceutical wet granulation', *International Journal of Pharmaceutics*, 2014. 472(1): pp. 192-201.

[122] Burggraeve, A., Van Den Kerkhof, T., Hellings, M., et al. 'Evaluation of in-line spatial filter velocimetry as PAT monitoring tool for particle growth during fluid bed granulation', *European Journal of Pharmaceutics and Biopharmaceutics*, 2010. 76(1): pp. 138-146.

[123] Burggraeve, A., Monteyne, T., Vervaet, C., et al. 'Process analytical tools for monitoring, understanding, and control of pharmaceutical fluidized bed granulation: A review', *European Journal of Pharmaceutics and Biopharmaceutics*, 2013. 83(1): pp. 2-15.

[124] Naidu, V.R., Deshpande, R.S., Syed, M.R., Wakte, P.S. 'Real-time imaging as an emerging process analytical technology tool for monitoring of fluid bed coating process', *Pharmaceutical Development and Technology*, 2017. 23(6): pp. 596-601.

[125] Hu, X., Cunningham, J.C., Winstead, D. 'Study growth kinetics in fluidized bed granulation with at-line FBRM', *International Journal of Pharmaceutics*, 2008. 347(1): pp. 54-61.

[126] Silva, A.F.T., Burggraeve, A., Denon, Q., et al. 'Particle sizing measurements in pharmaceutical applications: Comparison of in-process methods versus off-line methods', *European Journal of Pharmaceutics and Biopharmaceutics*, 2013. 85(3, Part B): pp. 1006-1018.

[127] Malvern Panalytical. (2018). 'Laser Diffraction (LD): Particle size distributions from nanometers to millimeters' [online]. Available at: https://www.malvernpanalytical.com/en/products/technology/light-scattering/laser-diffraction (Accessed: 6th of August 2018).

[128] Findlay, W.P., Peck, G.R., Morris, K.R. 'Determination of fluidized bed granulation end point using near-infrared spectroscopy and phenomenological analysis', *Journal of Pharmaceutical Sciences*, 2005. 94(3): pp. 604-612.

[129] Rosas, J.G., Blanco, M., González J.M., Alcalà M. 'Real-time determination of critical quality attributes using near-infrared spectroscopy: a contribution for Process Analytical Technology (PAT)', *Talanta*, 2012. 97: pp. 163-170.

[130] Otsuka, M., Mouri, Y., Matsuda, Y. 'Chemometric evaluation of pharmaceutical properties of antipyrine granules by near-infrared spectroscopy', *AAPS PharmSciTech*, 2003. 4(3): pp. 142-148.

[131] Retsch Technology. (2011). 'Particle Analyzer CAMSIZER XT: Particle Size and Particle Shape Analysis with dynamic image analysis' [online] Available at: http://www.horiba.com/fileadmin/uploads/Scientific/Documents/PSA/CAMSIZER_XT_flyer.pdf (Accessed: 6th of August 2018).

[132] United States Pharmacopoeia. (2018). 'General Chapter <786> Particle size distribution estimation by analytical sieving', USP 41. Rockville, Maryland, USA: United States Pharmacopeial Convention.

[133] Omar, C.S., Dhenge, R.M., Osborne, J.D. et al. 'Roller compaction: Effect of morphology and amorphous content of lactose powder on product quality', *International Journal of Pharmaceutics*, 2015. 496(1): pp. 63-74.

[134] European Medicines Agency. (2014). 'Guideline on the use of near infrared spectroscopy by the pharmaceutical industry and the data requirements for new submissions and variations – Revision 2'. Available at: https://www.ema.europa.eu/documents/scientific-guideline/guideline-use-near-infrared-spectroscopy-pharmaceutical-industry-data-requirements-new-submissions_en.pdf.

[135] (2018). 'Chapter 2.2.40. Near-infrared spectroscopy', European Pharmacopoeia 9.5. Strasbourg, France: Council of Europe.

[136] (2018). 'Chapter 5.21. Chemometric methods applied to analytical data', European Pharmacopoeia 9.5. Strasbourg, France: Council of Europe.

[137] (2015). 'General Chapter <1119> Near-Infrared Spectroscopy', United States Pharmacopoeia 38. Rockville, Maryland, USA: United States Pharmacopeial Convention.

[138] Roggo, Y., Chalus, P., Maurer, L., et al. 'A review of near infrared spectroscopy and chemometrics in pharmaceutical technologies', *Journal of Pharmaceutical and Biomedical Analysis*, 2007. 44(3): pp. 683-700.

[139] De Bleye, C., Chavez, P.F., Mantanus, J., et al. 'Critical review of near-infrared spectroscopy methods validations in pharmaceutical applications', *Journal of Pharmaceutical and Biomedical Analysis*, 2012. 69: pp. 125-132.

[140] Berntsson, O., Danielsson, L.-G., Lagerhom, B., Folestad, S. 'Quantitative in-line monitoring of powder blending by near infrared reflection spectroscopy', *Powder Technology*, 2002. 123(2): pp. 185-193.

[141] Blanco, M., Gozalez Baño, R., Bertran, E. 'Monitoring powder blending in pharmaceutical processes by use of near infrared spectroscopy', *Talanta*, 2002. 56(1): pp. 203-212.

[142] Burggraeve, A., Silva, A.F.T., Van Den Kerkhof, T., et al. 'Development of a fluid bed granulation process control strategy based on real-time process and product measurements', *Talanta*, 2012. 100: pp. 293-302.

[143] Hayashi, Y., Sato, T., Otsuka, M. 'Real-Time Monitoring of the Drying of Extruded Granules in a Fluidised Bed Using near Infrared Spectroscopy and Kinetic Evaluation of the Drying Process', *Journal of Near Infrared Spectroscopy*, 2013. 21(2): pp. 107-115.

[144] Chalus, P., Roggo, Y., Walter, S., Ulmschneider, M. 'Near-infrared determination of active substance content in intact low-dosage tablets', *Talanta*, 2005. 66(5): pp. 1294-1302.

[145] Goodwin, D.J., Van Den Ban, S., Denham, M., Barylski, I. 'Real time release testing of tablet content and content uniformity', *International Journal of Pharmaceutics*, 2018. 537(1-2): pp. 183-192.

[146] Dyrby, M., Engelsen, S.B., Nørgaard, L., et al. 'Chemometric Quantitation of the Active Substance (Containing C≡N) in a Pharmaceutical Tablet Using Near-Infrared (NIR) Transmittance and NIR FT-Raman Spectra', *Applied Spectroscopy*, 2002. 56(5): pp. 579-585.

[147] Nieuwmeyer, F.J., Damen, M., Gerich, A., et al. 'Granule Characterization During Fluid Bed Drying by Development of a Near Infrared Method to Determine Water Content and Median Granule Size', *Pharmaceutical Research*, 2007. 24(10): pp. 1854-1861.

[148] Malley, D., Martin, P.D., Ben-Dor, E. (2004). 'Application in analysis of soils' in Roberts C.A., Workman, J. Jr., Reeves, J.B. (eds.). *Near infrared spectroscopy in agriculture*. Madison, Wisconsin, USA: American Society of Agronomy, Crop Science Society of America, and Soil Science Society of America.

[149] Herkert, T., Prinz, H., Kovar, K.-A. 'One hundred percent online identity check of pharmaceutical products by near-infrared spectroscopy on the packaging line', *European Journal of Pharmaceutics and Biopharmaceutics*, 2001. 51(1): pp. 9-16.

[150] Järvinen, K., Hoehe, W., Järvinen, M., et al. 'In-line monitoring of the drug content of powder mixtures and tablets by near-infrared spectroscopy during the continuous direct compression tableting process', *European Journal of Pharmaceutical Sciences*, 2013. 48(4-5): pp. 680-688.

[151] Vargas, J.M., Nielsen, S., Cárdenas, V., et al. 'Process analytical technology in continuous manufacturing of a commercial pharmaceutical product', *International Journal of Pharmaceutics*, 2018. 538(1-2): pp. 167-178.

[152] Rantanen, J., Yliruusi, J. 'Determination of Particle Size in a Fluidized Bed Granulator With a Near Infrared Set-up', *Pharmacy and Pharmacology Communications*, 1998. 4(2): pp. 73-75.

[153] Tok, A.T., Goh, X., Ng, W.K., Tan, R.B. 'Monitoring Granulation Rate Processes Using Three PAT Tools in a Pilot-Scale Fluidized Bed', *AAPS PharmSciTech*, 2008. 9(4): pp. 1083-1091.

[154] Alcalà M., Blanco M., Bautista M., González J.M. 'On-line monitoring of a granulation process by NIR spectroscopy', *Journal of Pharmaceutical Sciences*, 2010. 99(1): pp. 336-345.

[155] Jørgensen, A.C., Luukkonen, P., Rantanen, J., et al. 'Comparison of torque measurements and near-infrared spectroscopy in characterization of a wet granulation process', *Journal of Pharmaceutical Sciences*, 2004. 93(9): pp. 2232-2243.

[156] Huang, J., Romero-Torres, S., Moshgbar, M. (2010) 'Practical Considerations in Data Pre-treatment for NIR and Raman Spectroscopy' [online], American Pharmaceutical Review. Available at: https://www.americanpharmaceuticalreview.com/Featured-Articles/116330-Practical-Considerations-in-Data-Pre-treatment-for-NIR-and-Raman-Spectroscopy/ (Accessed: 31st of January 2018).

[157] Rinnan, Å., Berg, F.V.D., Engelsen, S.B. 'Review of the most common pre-processing techniques for near-infrared spectra', *Trends in Analytical Chemistry*, 2009. 28(10): pp. 1201-1222.

[158] Massart, D.L., Vandeginste, B.G.M., Buydens, L.M.C. (eds.). (1998). *Handbook of Chemometrics and Qualimetrics: Part A*, Vol. 20. Amsterdam, The Netherlands: Elsevier Science B.V.

[159] Clavaud, M., Roggo, Y., Dégardin, K., et al. 'Global regression model for moisture content determination using near-infrared spectroscopy', *European Journal of Pharmaceutics and Biopharmaceutics*, 2017. 119: pp. 343-352.

[160] Hyvärinen, A., Karhunen, J., Oja, E. (2001). *Independent component analysis*, 1st Edition. New York, USA: John Wiley & Sons.

[161] Stone, J.V. (2004). *Independent component analysis: a tutorial introduction*, 1st Edition. Cambridge, Massachusetts, USA: MIT Press.

[162] Hyvärinen, A., Oja, E. 'Independent Component Analysis: Algorithms and Applications', *Neural Networks*, 2000. 13(4-5): pp. 411-430.

[163] Wold, S., Sjöström, M., Eriksson, L. 'PLS-regression: a basic tool of chemometrics', *Chemometrics and Intelligent Laboratory Systems*, 2001. 58(2): pp. 109-130.

[164] De Leersnyder, F., Peeters, E., Djalabi, H., et al. 'Development and validation of an in-line NIR spectroscopic method for continuous blend potency determination in the feed frame of a tablet press', *Journal of Pharmaceutical and Biomedical Analysis*, 2018. 151: pp. 274-283.

[165] Geladi, P. Kowalski, B.R. 'Partial least-squares regression: a tutorial', *Analytica Chimica Acta*, 1986. 185: pp. 1-17.

[166] MKS Umetrics. (2012). 'User Guide to SIMCA - Version 13'. Malmö, Sweden: MKS Umetrics AB.

[167] Eriksson, L., Byrne, T., Johannson, E., et al. (2013). *Multi- and Megavariate Data Analysis: Basic Principles and Applications*, 3rd Edition. Umea, Sweden: Umetrics Academy.

[168] Yang, Z., Nie, G., Pan, L., et al. 'Development and validation of near-infrared spectroscopy for the prediction of forage quality parameters in Lolium multiflorum', *PeerJ*, 2017. 5: pp. 1-20.

[169] Marlin, T.E. (2000). *Process Control - Designing Processes and Control Systems for Dynamic Performance*, 2nd Edition. Boston, USA: McGraw-Hill Science.

[170] Bersimis, S., Panaretos, J., Psarakis, S. 'Multivariate Statistical Process Control Charts and the Problem of Interpretation: A Short Overview and Some Applications in Industry', *Munich Personal RePEc Archive*, 2005. Paper No. 6397.

[171] Bersimis, S., Psarakis, S., Panaretos, J. 'Multivariate statistical process control charts: an overview', *Quality and Reliability Engineering International*, 2007. 23(5): pp. 517-543.

[172] Abujiya, M.A.R., Riaz, M., Lee, M.H. 'Enhanced Cumulative Sum Charts for Monitoring Process Dispersion', *PLOS ONE*, 2015. 10(4): pp. 1-22.

[173] Sibanda, T. Sibanda, N. 'The CUSUM chart method as a tool for continuous monitoring of clinical outcomes using routinely collected data', *Medical Research Methodology*, 2007. 7: p. 46.

[174] Rasmussen, H.T., Zheng, F. 'Use of Orthogonal Methods During Pharmaceutical Development: Case Studies', *chromatographyonline.com*, 2009. 27(4): pp. 16-21.

[175] Pharmaceutical Technology Editors. (2017). 'Understanding How Excipients Affect Drug Quality' [online]. Available at: http://www.pharmtech.com/understanding-how-excipients-affect-drug-quality-1 (Accessed: 17th of July 2017).

[176] Bhaskar, A., Barros, F.N., Singh, R. 'Development and implementation of an advanced model predictive control system into continuous pharmaceutical tablet compaction process', *International Journal of Pharmaceutics*, 2017. 534(1-2): pp. 159-178.

[177] Hattori, Y., Otsuka, M. 'Modeling of feed-forward control using the partial least squares regression method in the tablet compression process', *International Journal of Pharmaceutics*, 2017. 524(1-2): pp. 407-413.

[178] Matero, S., Van Den Berg, F., Poutiainen, S., et al. 'Towards Better Process Understanding: Chemometrics and Multivariate Measurements in Manufacturing of Solid Dosage Forms', *Journal of Pharmaceutical Sciences*, 2013. 102(5): pp. 1385-1403.

[179] Pauli, V., Roggo, Y., Pellegatti, L., et al. 'Process analytical technology for continuous manufacturing tableting processing: A case study', *Journal of Pharmaceutical and Biomedical Analysis*, 2019. 162: pp. 101-111.

[180] Pharma Technology. (2018). 'Product Information: Pharmatec Deduster/Polisher with Metal Check & 4 parameters IPC Tablets Tester'. Available at: http://www.pharmatec.be/products/dedusterpolisher-with-metal-check-4-parameters-ipc-tablets-tester (Accessed: 17th of October 2018).

[181] MadgeTech, Inc. (2015). 'Product User Guide to RHTemp1000IS, Rev4'. Available at: http://www.madgetech.com/pdf_files/productreferencecards/RHTemp1000IS_PIC.pdf (Accessed: 17th of October 2018).

[182] MadgeTech, Inc. (2014). 'Product User Guide to Temp1000IS, Rev12'. Available at: http://www.madgetech.com/pdf_files/productreferencecards/Temp1000IS_PIC.pdf (Accessed: 17th of October 2018).

[183] MadgeTech, Inc. (2015). 'RHTemp1000IS Data Sheet DOC1272009-00 REV 3'. Available at: http://www.madgetech.com/pdf_files/data_sheets/RHTemp1000IS_DS.pdf (Accessed: 10th of October 2018).

[184] Moran, M.J., Shapiro, H.N. (2006). *Fundamentals of Engineering Thermodynamics*, 5th Edition. West Sussex, England: John Wiley & Soncs, Inc.

[185] VDI – Gesellschaft Verfahrenstechnik und Chemieingenieurswesen (ed.). (2010). *VDI Heat Atlas,* 2nd Edition. Berlin, Germany: Springer-Verlag Berlin Heidelberg.

[186] Harvard University. (2017). 'A Summary of Error Propagation - Lecture of Physical Sciences 2' [online]. Available at: http://ipl.physics.harvard.edu/wp-uploads/2013/03/PS3_Error_Propagation_sp13.pdf (Accessed: 25th of July 2018).

[187] Pauli, V., Roggo, Y., Kleinebudde, P., Krumme, M. 'Real-Time Monitoring of Particle Size Distribution in a Continuous Granulation and Drying Process by Near Infrared Spectroscopy', *European Journal of Pharmaceutics and Biopharmaceutics*, 2019. 141: pp. 90-99.

[188] Kazmier, L.J. (2004). *Schaums Outline: Business Statistics*, 4th Edition. New York, USA: The McGraw-Hill Companies, Inc.

[189] Nelson, L.S. 'The Shewhart Control Chart – Tests for Special Causes', *Journal of Quality Technology*, 1984. 16(4): pp. 237-239.

[190] ICH. (2005). 'ICH Harmonized Tripartite Guideline Validation of Analytical Procedures: Text and Methodology Q2(R1)'. Available at: https://www.ich.org/fileadmin/Public_Web_Site/ICH_Products/Guidelines/Quality/Q2_R1/Step4/Q2_R1__Guideline.pdf.

8. Erklärung

Hiermit erkläre ich gemäß §5 Absatz 1 der Promotionsordnung der Mathematisch-Naturwissenschaftlichen Fakultät der Heinrich-Heine-Universität Düsseldorf des Eides Statt, dass die Dissertation von mir selbstständig und ohne unzulässige fremde Hilfe unter Beachtung der „Grundsätze zur Sicherung guter wissenschaftlicher Praxis an der Heinrich-Heine-Universität Düsseldorf“ erstellt worden ist und dass ich diese in der vorgelegten oder in ähnlicher Form noch bei keiner anderen Institution eingereicht habe.

_____

Ort, Datum und Unterschrift

Victoria Pauli

9. Acknowledgements

I want to thank my thesis supervisor, Prof. Dr. Dr. h.c. Peter Kleinebudde for taking me on as a PhD-student in his team and the great working atmosphere in the past three years. Thank you for patiently answering any questions, thank you for your fast and constructive review of papers and the thesis manuscript, thank you for the great discussions during our project meetings in Basel, and thank you for the joyful hours at Volta after the meetings. I learned a lot from you, professionally and personally the like!

Thank you to my mentor Prof. Dr. Jörg Breitkreutz for accepting to co-supervise the project and for your insightful comments and discussions during the PhD-student seminars in Dusseldorf.

I want to thank my Unit Head at Novartis, Dr. Markus Krumme for believing in me and my capabilities. Thank you for the countless discussions, and for continuously supplying me with new ideas regarding orthogonal process control or automated development approaches like the Sequencer. Thank you for reviewing my papers and thesis manuscript and for sharing your experiences. I learned a lot from you about continuous manufacturing and the pharmaceutical industry, and at least the same amount about airplane technology. Thank you also for fighting your way through the 'concrete-ceiling' for me, so I can stay a part of the CM-Unit in the future! I am looking forward to many new challenges to be solved!

Thank you to my managers at Novartis, Dr. Klaus-Peter Moll and Dr. Simon Ensslin, for always keeping your door open in case of questions or issues. Thank you for being problem solvers, for the productive discussions during our regular project meetings, and thank you for your trust in me and the resulting freedom I had as a PhD-Student in your team. Thank you Simon, for your effort to keep me in the team in the future! I am looking forward to continue working with you!

I want to thank Dr. Timo Schmidberger and Chloe Lang for introducing me into the topic of multivariate data analysis, NIRS calibration, and process control strategies. You always had an open ear and helpful answer for me. Timo, thank you for defining the initial outline of the project with me.

Thank you to 'Papa' Frantz Elbaz, for taking me on after Timo left the company, for introducing me to the world of QbD, for reviewing my papers and data analyses, for helping out wherever needed, for ordering tons of compressed air via SAP for me, and for the initiation of delicious QbD-PAT ice cream meetings in the summer.

Thank you to Dr. Yves Roggo for performing the NIRS-calibrations in Unscrambler and R for me, for supporting me in any PAT-related questions, for working on the papers with me, and for proofreading parts of the thesis!

Thank you to our scientists, Florence Desvignes and Samuel Fischer, for helping me in the lab during trials and any related issues, and for the joyful working environment, even in stressful situations! The same goes for Maud Duchesne, Ricardo Pereira, Hervé Bohrer, and Hans-Peter Bach. Thank you for your tremendous efforts during all my trials, I could not have done it without you!

Thank you to our automation engineers, especially to Philipp Heger for reviewing and implementing the LOD-Estimator into DeltaV, for helping with automation issues whenever

needed, and for your constant good mood. Thank you to Tibor Wengritzky and Hervé Notter for implementing the Sequencer and the DRS Ramp into DeltaV.

Thank you to Davina Sohier and the PHAD ARD team for performing reference HPLC analysis of granules and tablets.

Thank you to Julien Taillemite for being the solution to so many issues and questions! Thank you for always helping, for never being annoyed or saying no, and for asking 'what can I do?' when the GMP-documentation was about to get the best of me. Thank you!

Thanks to Roger Hiltbrunner for his helping hands in the lab during his time as an intern with us.

Thank you to Dr. Laurent Pellegatti and Dr. Quang Nguyen Trung, for solving many technical PAT-issues and Analytical-related questions throughout the years!

I furthermore want to thank everyone in the CM-Unit I have not mentioned by name, for always lending a helping hand and for such a great working atmosphere, professionally and personally! I enjoyed working with you as a PhD-Student and am looking forward to continue the great teamwork with all of you in the future.

A huge thank you goes to Glatt GmbH in Binzen, especially Dr. Adrian Kape, Xaver Knöpfle, and Dr. Jochen Thies, who offered me their lab space, resources, and equipment for numerous trials in the past three years. Thank you for the great collaboration and working atmosphere and for sharing your valuable experiences!

Thank you to Dr. Hans de Waard, who became sort of a mentor to me – always there to give advice, by asking the right questions over and over. I enjoy our recurring lunches and hope we will continue to do so in the future!

Thank you to all the other PhD-students in the groups of Prof. Dr. Dr. h.c. Peter Kleinebudde and Prof. Dr. Jörg Breitkreutz. Even though I was not around much in Dusseldorf, you always made me feel welcome and included when we met during conferences or the PhD seminars! I hope we will continue to meet in the future in the small world of the pharmaceutical industry!

Thank you to Dr. Adrian Schmidt, for lighting up the working days in the past years! We started off as desk-neighbors during our internships and continued the mutual journey during our PhDs. Thank you for the exchange in experience, the entertaining conversations, and the heated badminton matches Monday night.

Thank you to Philip Parmentier for being a worthy replacement of Adrian as desk-neighbor, for the conversations and jokes that made the workdays go by faster, and for teaching me about GMP-compliance and wing-night at Flanagans.

Furthermore, I want to thank my incredible R16-roomies Lotte, Nico, Benni, Flo, and Nassim for being my family far away from home! I could not have picked a better flat to start my life in Basel and am so grateful for all of you! You made life outside work amazing and I cannot wait for more weekends and trips to come! To the Clara-crew, thank you for the great parties and cozy dinner nights! Thanks to Zarek for disclosing the anti-infinity theory to me, it blew my mind! Thanks to Filipa and Julia and the rest of the girls for the gym-visits, the lunchbreaks, and the after work activities at the Rhine!

Danke an Bea mit Theo und Mirko, dass ich Teil eurer kleinen Familie sein darf! Die Kuchen- und Waffelsonntage, Gammel Abende und Wochenendausflüge sind Traditionen die wir unbedingt beibehalten sollten!

Danke an Sabine, für deine Freundschaft all die Jahre! Danke fürs Zuhören, gemeinsam Lachen und Weinen, Aufmuntern und Prosecco Trinken! Ich hoffe wir verlieren uns trotz der Entfernung nie aus den Augen!

Danke an Johannes für die Endspurt Unterstützung! Danke für deine Geduld, deine gute Laune, deine Zuversicht, deine Aufmerksamkeit, und deine unendliche Unternehmungslust! Ich freue mich auf viele gemeinsame Pläne in der Zukunft! 🐟

Von ganzem Herzen Danke ich meiner Familie! Vor allem meinen Eltern die mich immer in all meinen Vorhaben unterstützt und motiviert haben. Danke, dass ihr immer für mich da seid. Danke für das ‘zu Hause’, in das ich jederzeit gerne zurück komme. Danke, dass ihr mit uns auf den vielen schönen gemeinsamen Reisen die Welt entdeckt habt! Danke, dass ihr mir das Studium in München ermöglicht habt. Danke, dass ihr mir beigebracht habt mich durchzubeissen. Danke, dass ihr mir die Freiheit gegeben habt meine eigenen Erfahrungen zu machen und meine eigenen Entscheidungen zu treffen. Danke Mama, dass du mir beigebracht hast nicht jedes ‘Nein’ einfach so hinzunehmen, sondern für das einzustehen und zu kämpfen was ich will. Danke Papa, dass du mir beigebracht hast Probleme besonnen und systematisch zu lösen! Ohne Eure Unterstützung hätte ich es nicht geschafft. Danke!

10. Supplementary data

10.1. Criticality matrix rating

Table S 1: Criticality matrix rating for TSG and FBD. If a sound justification was presented that the probability for a certain variable to fluctuate during production is low, it was downgraded to not-critical. All remaining variables were defined as pCPPs or pCMAs that need to be investigated in detail for their criticality on CQAs LOD and PSD. Data was previously published in Publication 1 (see page v).

Category		Factor	Decision	Justification
Twin-Screw-Granulation	Environment	Room Temperature	--	*Controlled by room control (21 ± 6 °C); also: TSG and FBD have internal heating and cooling units that define the process temperature*
		Relative Humidity	**pCPP**	*controlled by room control but can vary depending on the weather by ±20% rH AND: defines dryer inlet humidity --> to be evaluated for criticality on drying behavior*
		Room Airflow	--	*assumed to be constant, qualified within a certain range (GMP)*
		Cooling Water Temperature for TSG	--	*assumed to be constant, qualified within a certain range (GMP)*
		Cooling Water Flow Rate from Building to TSG	--	*assumed to be constant, qualified within a certain range (GMP)*
		Vibrations	--	*constant level of vibration during production*
	Materials	Abrasiveness/ Corrosiveness (Wear & Tear on Equipment)	--	*constant on the same equipment, equipment is qualified and constantly serviced*
		Pre-blend Water Content (LOD)	**pCMA**	*can vary, depending on relative humidity & room temperature and between different batches of excipients & drug substance --> to be evaluated*
		Pre-blend Particle Size Distribution (PSD)	--	*in this trial only excipients from one batch were used, therefore assumed to be constant within the conducted experiments. For later development, influence of PSD should be evaluated*
		Pre-blend Blend Uniformity (BU)	--	*BU was confirmed once for conducted blending procedure before the trials (HPLC-analysis). The same blending procedure was used in all trials and same batches of excipients/drug substance, therefore assumed to be constant.*
		Pre-blend Flowability	--	*The same blending procedure was used in all trials and same batches of excipients/drug substance, therefore assumed to be constant.*
		Pre-blend Pour- & Tap Density	--	*The same blending procedure was used in all trials and same batches of excipients/drug substance, therefore assumed to be constant.*
		Pre-blend Water Uptake Capacity/ Wettability	--	*The same blending procedure was used in all trials and same batches of excipients/drug substance, therefore assumed to be constant.*
		Temperature of Water (Granulation Liquid)	--	*qualified within a certain range (GMP), kept at room temperature during granulation, also TSG has internal heating unit that defines the process temperature*
	Process Parameters	Screw Rotation Speed TSG	**pCPP**	*to be evaluated*
		Barrel Temperature TSG	**pCPP**	*to be evaluated*
		Transfer pressure from TSG to FBD	--	*assumed to be constant (controlled by FBD)*
		Powder Feed Rate	**pCPP**	*to be evaluated*
		Fill Level of Hopper	--	*constant within a certain +/- range (in this trial manual refill but later in production continuous refill from continuous blender)*

Table S 1 continues on the next page

Category		Factor	Decision	Justification
		Feeding Control Mode	--	*only important during manual refill = very short time point, later in production hopper will be refilled continuously --> not applicable*
		Feeding Mode (Volumetric/Gravimetric)	--	*constant (gravimetric feed control)*
		Agitator-/ Screw speed	--	*closely related to feeding rate --> feeding rate rated is rated pCPP and will be evaluated*
		Hopper Refill Frequency	--	*assumed to be constant (in this trial manual refill but later in production continuous refill from continuous blender)*
		Liquid Feed Rate	**pCPP**	*to be evaluated*
	Machine	Type of Granulator	--	*fixed*
		Screw Configuration	--	*fixed*
		Response Time	--	*constant with same equipment*
		Cooling Efficiency	--	*not critical in wet-granulation*
		Pipe diameter from TSG to FBD	--	*fixed*
		Metal composition (Screws and Barrel)	--	*fixed*
		Runtime	**pCPP**	*to be evaluated*
		Type of Powder Feeder	--	*fixed*
		Hopper Capacity	--	*fixed*
		Hopper Shape	--	*fixed*
		Feeding Screw Design	--	*fixed*
		Gear Box Speed	--	*fixed*
		Agitator Design	--	*fixed*
		Calibration Frequency Powder feeder & Liquid Feeder	--	*constant (performed before each trial/production)*
		Runtime	**pCPP**	*to be evaluated*
		Type of pump	--	*fixed*
		Volume of tubing (pump)	--	*fixed (pump is calibrated before production)*
		Runtime	**pCPP**	*to be evaluated*
	People	Operator	--	*only trained operators are allowed to work, pre-defined recipes (GMP)*
Fluid-Bed-Drying	Environment	Room Temperature	--	*Controlled by room control (21±6°C); also: TSG and FBD have internal heating and cooling units that define the process temperature*
		Relative Humidity	**pCPP**	*controlled by room control but can vary depending on the weather by ±20% rH: defines dryer inlet humidity, could potentially influence drying behavior --> to be evaluated*
	Materials	Wet Granules PSD	--	*critical for drying behavior, but closely related to dried granules --> will be evaluated on dried granulate (PSD measured after dryer)*
		Wet Granules Moisture Content	**pCMA**	*wet granule characteristics are assumed to change with changing L/S ratio, total material mass flow and screw speed and assumed to have potential critical influence on drying behavior. However, wet granules characteristics will not be analyzed in detail, instead potential influences*
		Wet Granules Density	**pCMA**	
		Wet Granules Morphology	**pCMA**	

Table S 1 continues on the next page

Category		Factor	Decision	Justification
		Wet Granules Stickiness	**pCMA**	*will be assessed by analyzing dried granules after the dryer for LOD and PSD*
		Wet Granules Temperature	**pCMA**	
	Process Parameters	Inlet Air Temperature	**pCPP**	*to be evaluated*
		Inlet Air Humidity	**pCPP**	*=relative humidity of environment--> will be evaluated*
		Drying Air Flow Rate	**pCPP**	*to be evaluated*
		Drying Time (Rotor Speed)	**pCPP**	*to be evaluated*
		Filter Blowing (Duration/ Interval/Pressure)	--	*interval is controlled by FBD, assumed to be constant*
		Preheating Conditions	--	*same conditions for each trial, assumed to be constant*
		Chamber Fill Mass (=Fluid-Bed Height)	**pCPP**	*to be evaluated (defined by total material mass flow and dryer rotation speed)*
		Discharge Air Pressure	--	*controlled by FBD, assumed to be constant*
	Machine	Type of Dryer	--	*fixed*
		Bottom Plate Porosity	--	*fixed*
		Exhaust Air Filter Cartridge Type/ Porosity	--	*fixed*
		Outlet Chute Diameter	--	*fixed*
		Dead Volume in the Chamber	--	*fixed*
		Runtime	**pCPP**	*to be evaluated*
	Peop le	Operator	--	*only trained operators are allowed to work with pre-defined recipes (GMP)*

10.2. Auto-DoE

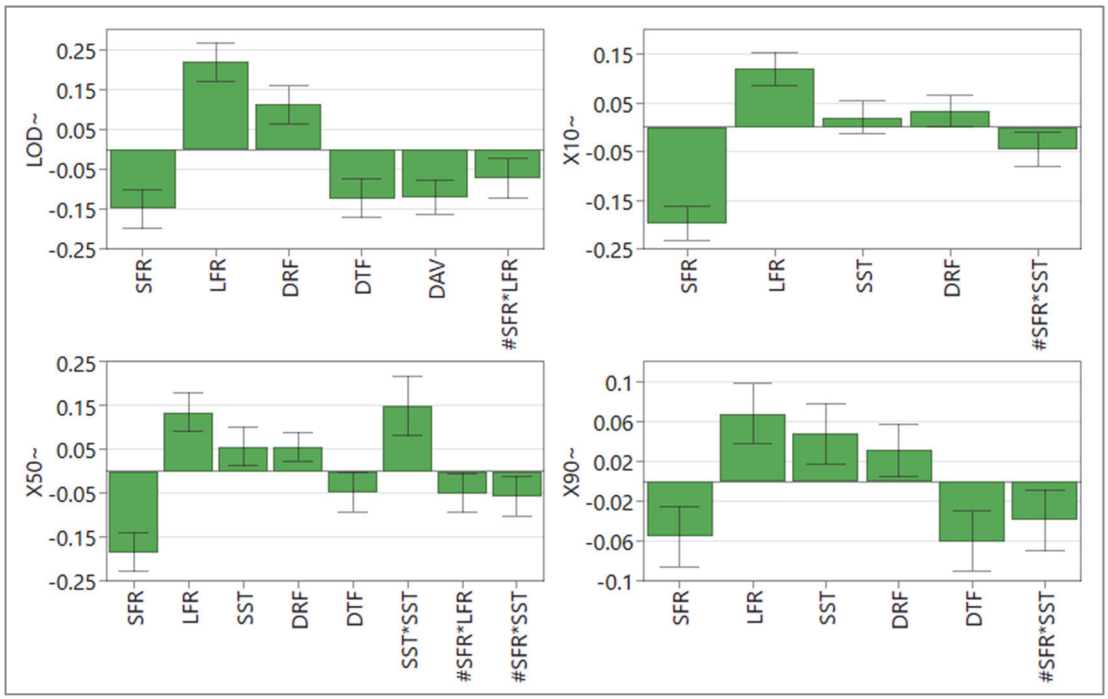

Figure S 1: Coefficient plot for LOD and PSD models based on auto-DoE results and IPC reference analytics.

Table S 2: Overview of performed trials during Auto DoE. The table is filled with the actually observed process values, instead of the setpoints (average process value observed during sample time). Run Order is arranged by blocks of the same drying temperature. Experiment 1 was excluded from the statistical analysis, due to a wrong air flow setting.

day	Exp. # / Run Order	Incl/ Excl /Test	Quantitative Factors												U*	time	responses			
			SFR		LFR		SS		DRS		DT		DAV		X_{IN}	t	LOD	X_{10}	X_{50}	X_{90}
			level[&]	kg/h	level[&]	kg/h	level[&]	rpm	level[&]	rph	level[&]	°C	level[&]	m^3/h	g/kg	h	%	µm	µm	µm
Day 1	heating/cooling		0		0		10		17		70		120		-	1.50			-	
	1	Excl	+	5.00	-	1.00	+	600	-	5	-	70.0	+	160.2	7.2	0.53	1.9	45	194	1031
	2	Incl	-	2.99	-	1.00	-	300	-	5	-	70.0	-	99.9	7.0	0.53	3.5	94	280	1099
	3	Incl	+	5.00	+	1.40	-	300	-	5	-	70.0	+	139.6	6.9	0.53	4.4	77	306	1566
	4	Incl	-	3.00	+	1.40	+	600	-	5	-	70.0	-	99.9	7.1	0.53	14.8	266	1218	2291
	heating/cooling		0		0		10		17		80		120		-	1.00			-	
	5	Incl	0	4.00	0	1.20	0	450	0	17	0	80.0	0	119.6	7.5	0.39	3.1	**117**	**372**	**1399**
	heating/cooling		0		0		10		17		90		120		-	1.00			-	
	6	Incl	+	4.99	-	1.00	-	300	-	5	+	90.0	-	100.0	7.5	0.53	1.5	59	181	765
	7	Incl	-	2.99	+	1.40	-	300	-	5	+	90.0	+	140.1	7.8	0.53	5.9	N/A	N/A	N/A
	8	Incl	-	3.01	-	1.00	+	600	-	5	+	90.0	+	140.3	7.6	0.53	1.1	128	421	1360
	9	Incl	+	4.98	+	1.40	+	600	-	5	+	90.0	-	99.8	7.6	0.53	3.2	80	256	1117
Day 2	heating/cooling		0		0		10		17		80		120		-	1.50			-	
	10	Incl	0	3.99	0	1.21	0	450	0	17	0	80.0	0	120.4	7.5	0.39	3.2	**100**	**299**	**1294**
	heating/cooling		0		0		10		17		70		120		-	1.00			-	
	11	Incl	-	3.01	-	1.00	-	300	+	29	-	70.0	+	140.0	7.2	0.37	4.0	133	414	1399
	12	Incl	+	4.98	+	1.40	-	305	+	29	-	70.0	-	100.3	7.7	0.37	8.3	102	396	1717
	13	Incl	+	4.98	-	1.00	+	600	+	29	-	70.0	-	99.8	7.4	0.37	5.1	48	294	1280
	14	Incl	-	3.00	+	1.40	+	600	+	29	-	70.0	+	140.1	8.0	0.37	13.7	496	1473	2392
	heating/cooling		0		0		10		17		80		120		-	1.0			-	
	15	Incl	0	4.00	0	1.20	0	450	0	17	0	80.0	0	119.8	7.5	0.39	3.2	**101**	**296**	**1195**
	16	Incl	X	3.99	X	1.20	X	450	X	11	X	80.0	X	120.3	8.3	0.42	3.0	**84**	**210**	**770**
	17	Incl	X	4.03	X	1.20	X	450	X	23	X	80.0	X	120.0	7.8	0.38	4.0	**97**	**272**	**1215**
	18	Incl	X	3.99	X	1.20	X	450	X	17	X	80.0	X	80.2	8.5	0.39	7.0	**88**	**262**	**1036**
	heating/cooling		0		0		10		17		90		120		-	1.00			-	
	19	Incl	+	4.98	+	1.40	+	600	+	29	+	90.0	+	139.9	8.3	0.37	2.5	56	199	846
	20	Incl	-	2.99	+	1.40	-	313	+	29	+	90.1	-	100.1	8.7	0.37	14.3	N/A	N/A	N/A
	21	Incl	-	3.07	-	1.00	+	589	+	29	+	90.1	-	100.9	8.2	0.37	4.9	148	450	1522
	22	Incl	+	4.99	-	1.00	-	300	+	29	+	90.0	+	139.9	7.6	0.37	1.6	98	322	1397
Day 3[%]	heating/cooling		0		0		10		17		80		120		-	1.50			-	
	T1	Test	~	4.49	~	1.30	~	550	~	11	0	80	~	130.0	7.3	0.42	2.7	98	269	1144
	T2	Test	~	2.70	~	1.05	~	400	~	20	0	80	0	120.2	7.5	0.38	4.2	156	437	1275
	T3	Test	~	4.81	~	1.10	+	600	~	24	0	80	~	134.8	7.4	0.38	2.3	67	242	1065

**uncontrolled factor: monitored during trials*

[&]+/-: trial with high or low factor setting; 0: center point setting; ~:setting inbetween the high & low factor ranges; X: additional trial to increase resolution; N/A: granules too coarse for CamSizer measurement.

[%] T1-T3: test experiments performed, not included in the statistical analysis of DoE-trials

10.3. NIRS for LOD

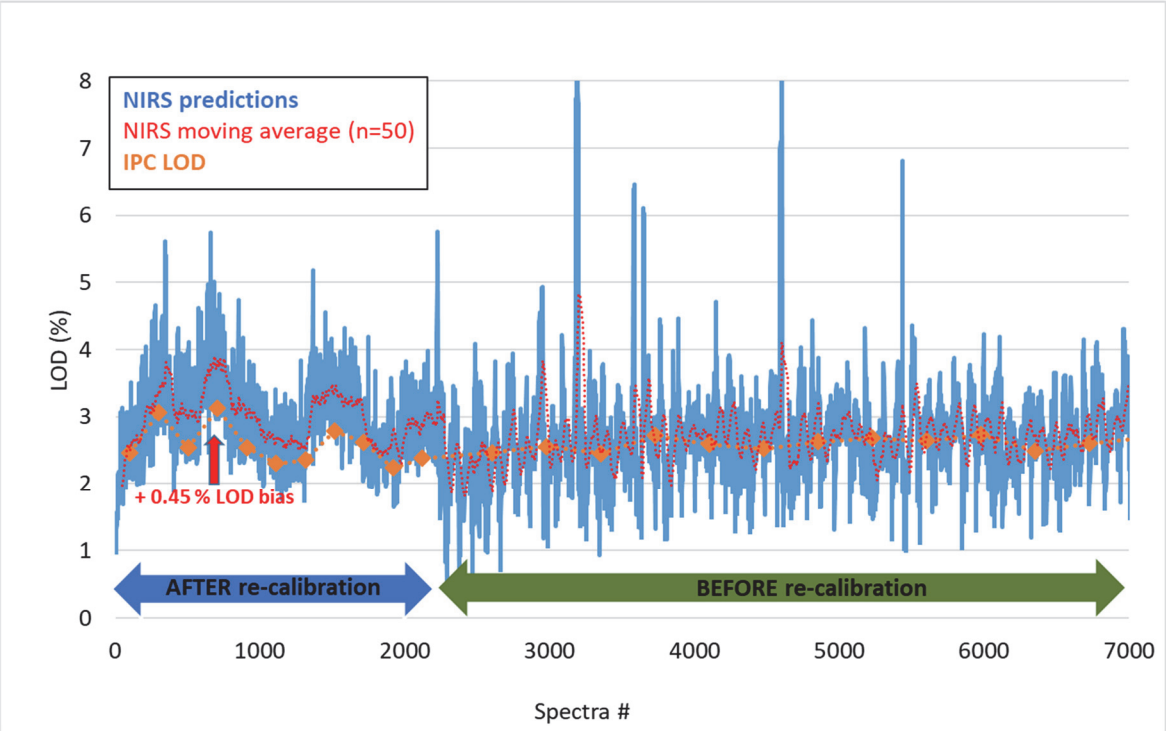

Figure S 2: Demonstration example of observed bias in NIRS LOD prediction after the NIRS reference standard was re-calibrated. The observed bias of + 45% LOD was subtracted from any NIRS predictions performed after reference re-calibration, to eliminate the observed bias. In the future, the method will be expanded, to include new data recorded with the re-calibrated reference standard.

10.4. MSPC for PAT data reconciliation

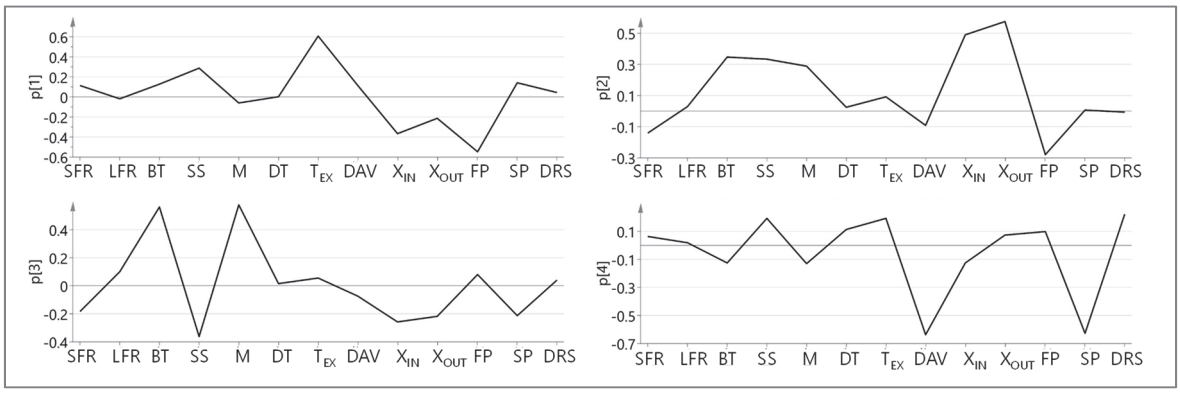

Figure S 3: Loading plots calibration I, PC 1-4. The 1st PC is mainly attributed to outlet temperature and filter pressure, the 2nd and 3rd PCs are mainliy attributed to humidity and granulation parameters, and the 4th PC to dryer airflow and sieve pressure.

Table S 3: Overview of conducted trials for DoE-based MSPC calibration

Run Order	SFR	LFR	DAV	Response: LOD
1	4.00	1.20	140	2.47
2	4.40	1.23	130	3.07
3	3.60	1.23	150	2.54
4	3.60	1.23	130	3.13
5	4.00	1.20	140	2.55
6	4.40	1.23	150	2.30
7	3.60	1.17	150	2.36
8	3.60	1.17	130	2.79
9	4.40	1.17	130	2.62
10	4.40	1.17	150	2.24
11	4.00	1.20	140	2.38

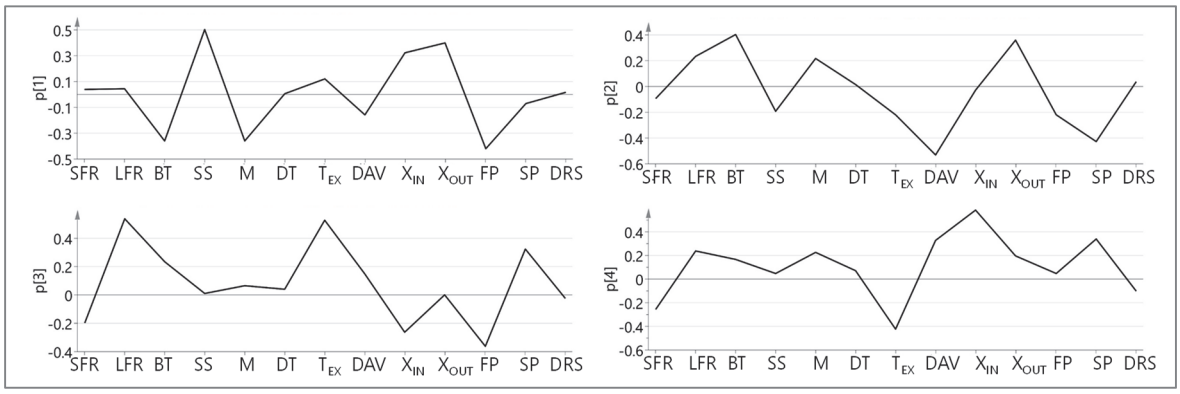

Figure S 4: Loading plots of calibration II, PC 1-4 (combination of initial calibration dataset and DoE-based MSPC calibration dataset). The 1st PC is attributed to variability in humidity and granulation parameters, the 2nd to airflow and humidity, the 3rd to feed rates, exhaust temperature and filter pressure, and the 4th to humidity and exhaust temperature.

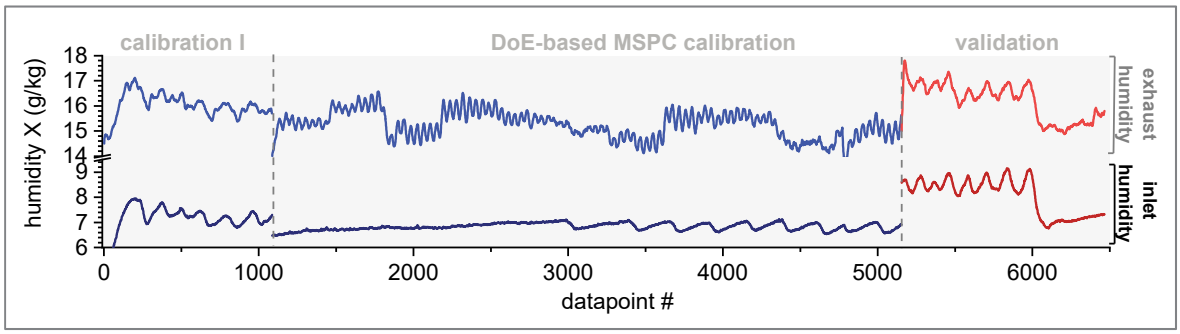

Figure S 5: Humidity comparison between calibration (blue) and validation (red) datasets. During the validation run, humidities were much higher than during the calibration runs.

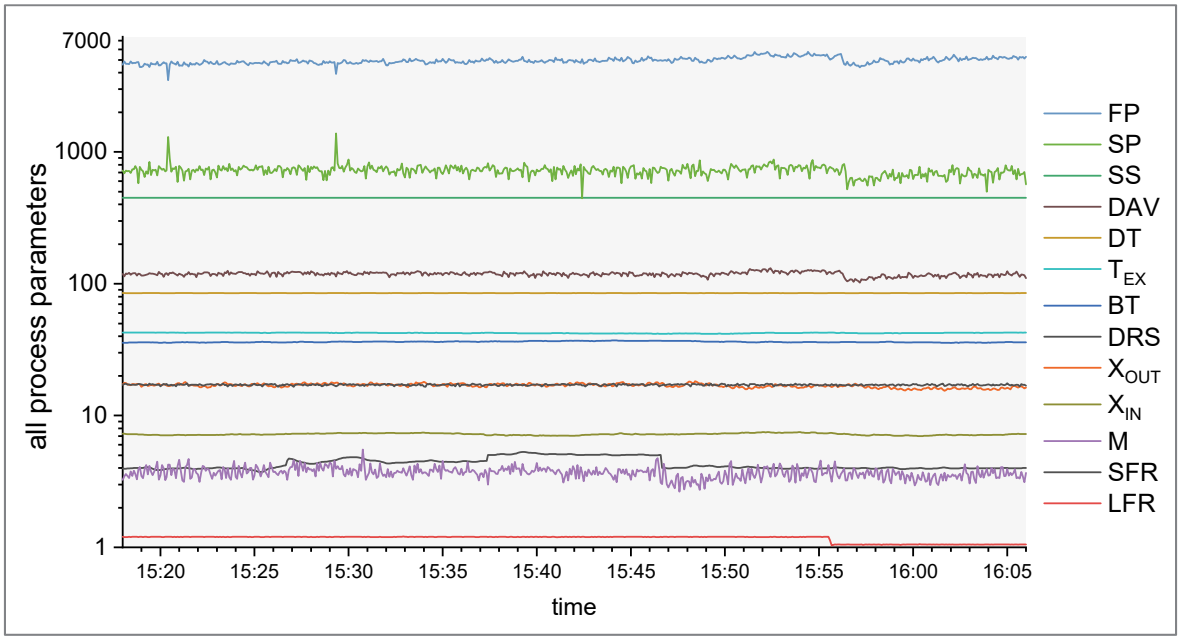

Figure S 6: Demonstration of moving average MSPC calibration approach with real process data: Overview of all included process parameters in the example..

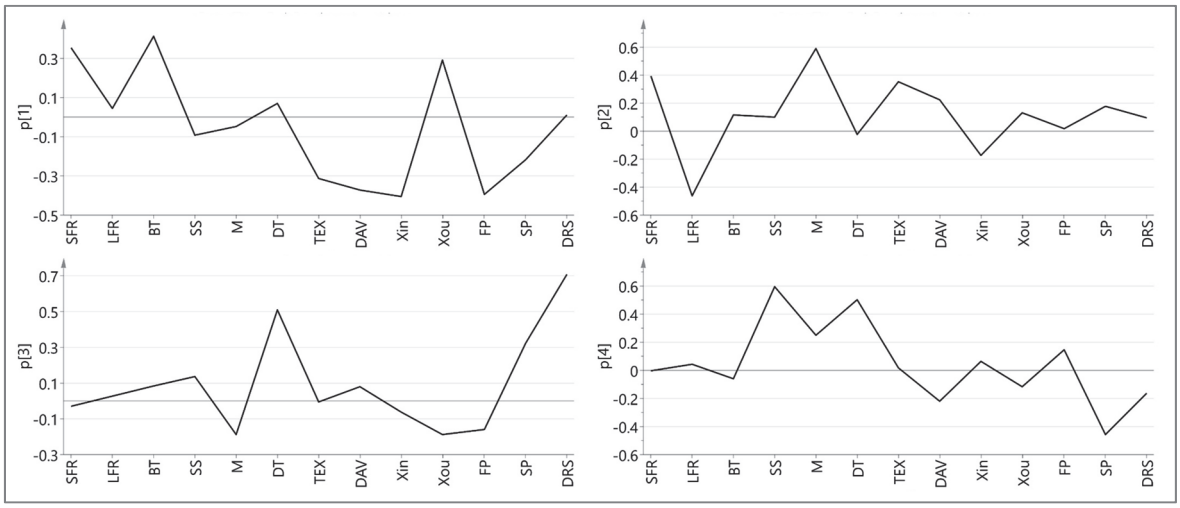

Figure S 7: Loading plot of "frozen" moving average calibration "c", PC 1-4.

10.5. Residence time distribution – summary of results

Table S 4: Summary of RTD assessment results trials (due to technical issues, NIRS 4 results are only available for trials #9 and #10).

			NIRS 1 (blender)			NIRS 2 (dryer)			NIRS 3 (Feed frame)			NIRS 4 tablets		
Trial #	**step**		**EPT5**	**EPT95**	**MRT**	**EPT5**	**EPT95**	**MRT**	**EPT5**	**EPT95**	**MRT**	**EPT5**	**EPT95**	**MRT**
1	100-130	sec	9	519	93	151	942	328	1119	2207	1517	N/A		
		min	0.2	8.7	1.5	2.5	15.7	5.5	18.7	36.8	25.3			
	130-70	sec	8	232	62	105	484	252	1070	2050	*1443*			
		min	0.1	3.9	1.0	1.8	8.1	4.2	17.8	34.2	24.0			
	70-100	sec	11	268	74	106	616	264	1027	1881	*1358*			
		min	0.2	4.5	1.2	1.8	10.3	4.4	17.1	31.4	22.6			
2	100-130	sec	16	421	104	59	712	196	1633	3243	2246			
		min	0.3	7.0	1.7	1.0	11.9	3.3	27.2	54.1	37.4			
	130-70	sec	20	320	94	134	1057	412	1817	3248	*2365*			
		min	0.3	5.3	1.6	2.2	17.6	6.9	30.3	54.1	39.4			
	70-100	sec	14	374	79	12	655	204	1867	2669	*2196*			
		min	0.2	6.2	1.3	0.2	10.9	3.4	31.1	44.5	36.6			
3	100-130	sec	18	737	291	117	951	308	1176	2284	1520			
		min	0.3	12.3	4.9	1.9	15.8	5.1	19.6	38.1	25.3			
	130-70	sec	7	254	59	123	1004	310	1014	1999	*1387*			
		min	0.1	4.2	1.0	2.1	16.7	5.2	16.9	33.3	23.1			
	70-100	sec	9	245	50	90	575	208	1038	2397	*1448*			
		min	0.2	4.1	0.8	1.5	9.6	3.5	17.3	39.9	24.1			

Table S 4 continues on the next page

			NIRS 1 (blender)			NIRS 2 (dryer)			NIRS 3 (Feed frame)			NIRS 4 tablets		
Trial #	**step**		**EPT5**	**EPT95**	**MRT**	**EPT5**	**EPT95**	**MRT**	**EPT5**	**EPT95**	**MRT**	**EPT5**	**EPT95**	**MRT**
4	100-130	sec	8	514	105	90	286	843	1103	2235	1470	N/A		
		min	0.1	8.6	1.7	1.5	4.8	14.0	18.4	37.2	24.5			
	130-70	sec	9	245	65	138	664	231	973	2069	1326			
		min	0.2	4.1	1.1	2.3	11.1	3.9	16.2	34.5	22.1			
	70-100	sec	9	232	64	155	791	346	982	1888	*1311*			
		min	0.1	3.9	1.1	2.6	13.2	5.8	16.4	31.5	21.9			
5	100-130	sec	6	137	57	505	998	754	862	1703	1152			
		min	0.1	2.3	1.0	8.4	16.6	12.6	14.4	28.4	19.2			
	130-70	sec	6	211	37	398	999	614	853	1725	1144			
		min	0.1	3.5	0.6	6.6	16.7	10.2	14.2	28.8	19.1			
	70-100	sec	8	265	119	271	1818	638	775	1792	1110			
		min	0.1	4.4	2.0	4.5	30.3	10.6	12.9	29.9	18.5			
6	100-130	sec	7	161	44	96	991	288	682	1487	1008			
		min	0.1	2.7	0.7	1.6	16.5	4.8	11.4	24.8	16.8			
	130-70	sec	8	248	76	76	536	272	639	1728	1032			
		min	0.1	4.1	1.3	1.3	8.9	4.5	10.7	28.8	17.2			
	70-100	sec	7	175	47	72	534	195	730	1373	984			
		min	0.1	2.9	0.8	1.2	8.9	3.2	12.2	22.9	16.4			

Table S 4 continues on the next page

			NIRS 1 (blender)			NIRS 2 (dryer)			NIRS 3 (Feed frame)			NIRS 4 tablets		
Trial #	**step**		**EPT5**	**EPT95**	**MRT**	**EPT5**	**EPT95**	**MRT**	**EPT5**	**EPT95**	**MRT**	**EPT5**	**EPT95**	**MRT**
7*	100-130	sec	7	295	70	33	1395	409	*145*	*2188*	*891*	N/A		
		min	0.1	4.9	1.2	0.6	23.2	6.8	*2.4*	*36.5*	*14.9*			
	130-70	sec	9	277	63	47	752	230	*599*	*1879*	*998*			
		min	0.1	4.6	1.1	0.8	12.5	3.8	*10.0*	*31.3*	*16.6*			
	70-100	sec	6	251	76	27	456	155	*514*	*1760*	*857*			
		min	0.1	4.2	1.3	0.5	7.6	2.6	*8.6*	*29.3*	*14.3*			
8	100-130	sec	7	561	128	335	857	565	1041	2132	1411			
		min	0.1	9.3	2.1	5.6	14.3	9.4	17.4	35.5	23.5			
	130-70	sec	8	345	77	455	1684	779	995	2164	1403			
		min	0.1	5.8	1.3	7.6	28.1	13.0	16.6	36.1	23.4			
	70-100	sec	7	677	122	409	1602	685	1098	1621	1796			
		min	0.1	11.3	2.0	6.8	26.7	11.4	18.3	27.0	29.9			
9	100-130	sec	9	191	58	221	771	371	679	1509	991	531	1587	852
		min	0.2	3.2	1.0	3.7	12.8	6.2	11.3	25.2	16.5	8.9	26.4	14.2
	130-70	sec	7	257	64	223	965	460	606	1419	920	511	1200	920
		min	0.1	4.3	1.1	3.7	16.1	7.7	10.1	23.7	15.3	8.5	20.0	15.3
	70-100	sec	7	257	64	68	720	342	1344	1913	1577	1331	1905	*1611*
		min	0.1	4.3	1.1	1.1	12.0	5.7	22.4	31.9	26.3	22.2	31.7	26.9
10	100-130	sec	8	223	77	61	783	234	993	1886	1309	889	1683	1191
		min	0.1	3.7	1.3	1.0	13.0	3.9	16.6	31.4	21.8	14.8	28.1	19.9
	130-70	sec	7	306	82	75	795	261	978	2053	*1351*	901	1849	1218
		min	0.1	5.1	1.4	1.2	13.3	4.4	16.3	34.2	22.5	15.0	30.8	20.3
	70-100	sec	6	299	81	92	480	215	982	2022	*1349*	919	1644	*1236*
		min	0.1	5.0	1.4	1.5	8.0	3.6	16.4	33.7	22.5	15.3	27.4	20.6

* NIRS probe fouling in NIRS 3 (potentially caused by very dry, electrostatic material)

10.6. Residence time distribution – LOD-dependent correction factor

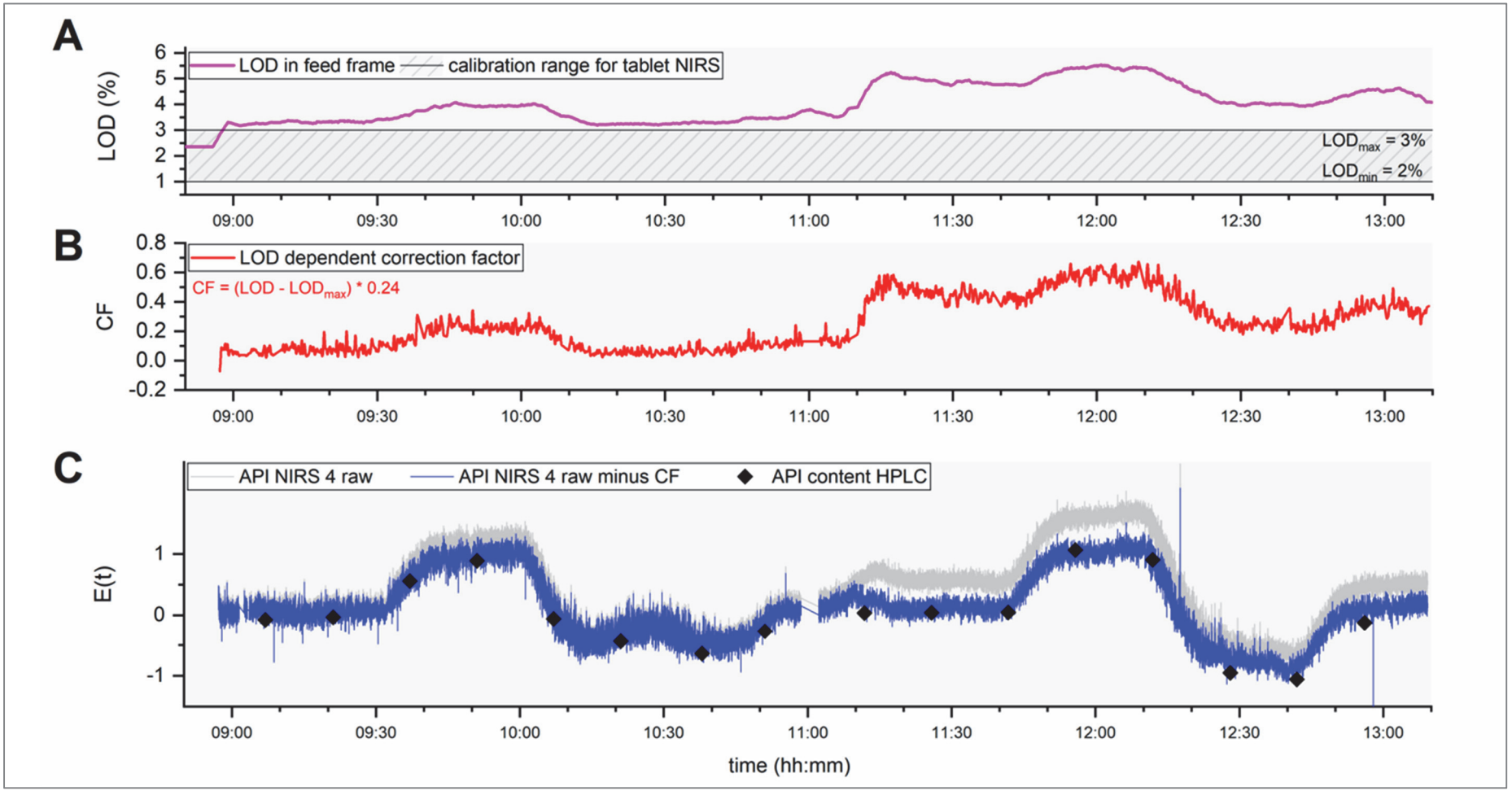

Figure S 8: Since the NIRS method for tablets API content was not robust towards variations in tablet LOD outside of the calibration range (2-3 % LOD), a LOD-dependent correction factor was applied (see B) according to CF = (LOD-LOD$_{max}$) * 0.24, where LOD$_{max}$ = 3% (based on the NIRS calibration range) and the term "0.24" was determined empirically to ascend the predictions at 100 % LC back to the target effect (i.e. F = 0). Corresponding LOD was monitored via NIRS 3 in the tablet press feed frame (see A), the development and validation of the related method is described in section 3.3.2.2, page 57 ff. The validity of CF was demonstrated by reference HPLC results (see C).